UNIVERSITÀ DEGLI STUDI DI GENOVA

SCUOLA POLITECNICA

DIME

Dipartimento di Ingegneria Meccanica, Energetica, Gestionale e dei Trasporti

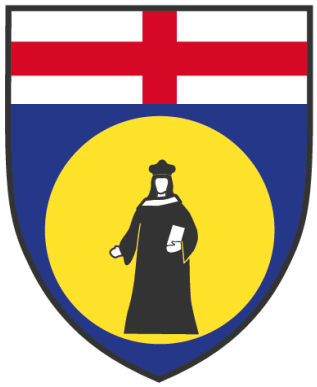

Ph.D. program

Engineering of modeling, machines, and systems for energy, the environment, and transportation

Flexible Heat and Power Generation: Market Opportunities for Combined Cycle Gas Turbines and Heat Pumps Coupling

Supervisor:

Chiar.mo Prof. Ing. Alessandro Sorce

Co-supervisor:

Chiar.mo Prof. Ing. Aristide Fausto Massardo

Student:

Alberto Vannoni

30th of May 2022

Flexible Heat and Power Generation: Market Opportunities for Combined Cycle Gas Turbine and Heat Pumps Coupling

Abstract

Climate pledges, besides the need for a secure, reliable, and affordable supply of energy, are posing the challenging target of an energy sector's carbon footprint reduction that does not jeopardize the access to energy itself, ensuring the demand satisfaction, consequently economic growth, the right to development of all countries, and the energy poverty reduction. From the policy point of view, the United Nations 2030 Sustainable Development Agenda is often considered as a reference, it states 17 general goals adopted by all the UN member states, the 7th and the 13th concern specifically the right to access clean and affordable energy and the climate action. Then, each country has implemented locally or regionally, specific policy instruments to support the shift from a fossil fuel-based economy to a climate-neutral one, a process commonly defined as energy transition.

Even if the implemented policy tools may differ from each other, the effects are somehow similar worldwide: massive renewable energy power generation capacity has been installed in the last decade, and even a larger amount is foreseen to be installed in the next years. Nevertheless, the stochasticity of the sources and the non-programmability, that characterized many renewable generators, pose serious challenges in the electricity grid management with an increased demand for efficiency and flexibility from traditional programmable power plants. Such power plants have shifted their traditional role from constant baseload generators to fluctuating backup capacity and service providers. Consequently, the operating hours have been reduced and the costs have increased because of the frequent start-ups, the lower efficiency in off-design, and the increased need for maintenance that flexible operation requires. Thus, despite the fact they turn out to be essential to grid management, dispatchable generators often face economic issues and their viability is no longer certain.

Besides the electricity sector, on which the attention is often focused, the transition toward a decarbonized economy is needed also in the other sectors. Among these, heating is one of the most relevant. Heating still largely relies on fossil sources, even if district heating networks, waste heat recovery, heat pumps, and other forms of coupling with less carbon-intense sectors are available technologies that can reduce the sector impact in the future.

This thesis aims to explore solutions coupling Combined Cycle Gas Turbine (CCGTs) power plants with Heat Pumps (HPs) in other to enhance the flexibility of power plants, pursuing the threefold target of an increased ability in providing services to the grid, reduced uncertainty about economic viability, and the supply of a reduced carbon intensity heating.

The Introduction and the first chapter describe in detail the motivations for this thesis, the context in which the investigated technologies are supposed to operate and review the existing literature. Chapter 2 focuses on the Combined Cycle Gas power plants, investigating

the effects of flexible operations on emissions and quantifying the benefits of inlet air conditioning as a measure for flexibility enhancement. Chapter 3 concerns heat pumps, a model developed for techno-economic analysis is presented alongside some results comparing different fluids and heat sources for different supply temperatures. Chapter 4 combines what is presented in the previous two chapters investigating solutions for CCGTs and HPs coupling.

Different coupling concepts have been explored for two main purposes, a flexibility increment, by inlet air conditioning, of those plants devoted only to power generation, and the coupling of the heat pump to a combined heat and power CCGTs. The power-oriented concept is based on an inlet air conditioning unit consisting of a heat pump, cold storage, and some heat exchangers. The unit operates heating, to increase the off-design efficiency, or cooling, to boost the net power output, and the gas turbine inlet air according to different operational modes. The combined heat and power concept uses a high-temperature heat pump that, integrated with the CCGT, harvests privileged heat sources (different options are investigated) increasing the maximum thermal output and the global efficiency. Warm storage is also included allowing flexible management of the coupled HP and CCGT.

Finally, Chapter 5 describes the market context in which power plants operate today. It focuses on the importance of recognizing the economic value of flexibility in the ancillary services market. A novel model of optimal dispatch for power generators and storage is presented, it schedules the power plant, or storage, operations optimizing not only the profits in traditional energy-only markets but the overall expected profits considering also the services markets and keeping into account the uncertainty of offers/bids acceptance.

Generazione Flessibile di Calore ed Elettricità: Opportunità di Mercato per l'accoppiamento di Cicli Combinati e Pompe di Calore

Sommario

Gli impegni di contenimento del cambiamento climatico, oltre alla necessità di una fornitura di energia sicura, affidabile ed economica, pongono l'obiettivo impegnativo di una riduzione delle emissioni di gas serra del settore energetico, garantendo comunque il soddisfacimento della domanda, e di conseguenza la crescita economica, il diritto allo sviluppo di tutti i paesi, e la riduzione della povertà energetica. Dal punto di vista politico, l'Agenda per lo Sviluppo Sostenibile 2030 delle Nazioni Unite è spesso considerata come un riferimento, essa stabilisce 17 obiettivi adottati da tutti gli stati membri dell'ONU, il 7° e il 13° riguardano specificamente il diritto all'accesso all'energia pulita ed economica e l'azione climatica. Ogni paese ha poi implementato a livello locale o regionale, strumenti specifici per sostenere il passaggio da un'economia basata sui combustibili fossili ad una neutralità climatica, un processo comunemente definito come transizione energetica.

Anche se gli strumenti politici implementati possono differire l'uno dall'altro gli effetti sono in qualche modo simili in tutto il mondo, una massiccia capacità da fonti rinnovabili è stata installata nell'ultimo decennio, e una quantità ancora maggiore è prevista essere installata nei prossimi anni. Tuttavia, la stocasticità delle fonti e la non programmabilità, che caratterizzano molti di questi generatori, pongono serie sfide nella gestione della rete elettrica con una maggiore richiesta di efficienza e flessibilità da parte delle tradizionali tecnologie programmabili. Tali centrali hanno modificato il loro ruolo tradizionale di generatori di carico base costante a fornitori di capacità di *backup* fluttuante e servizi. Di conseguenza, le ore di funzionamento si sono ridotte e i costi sono aumentati a causa dei frequenti avviamenti, della minore efficienza in *off-design* e della maggiore necessità di manutenzione che il funzionamento flessibile richiede. Così, nonostante si rivelino essenziali per la gestione della rete, i generatori programmabili devono spesso affrontare problemi economici e la loro redditività non è più certa.

Oltre al settore dell'elettricità, sul quale l'attenzione è spesso focalizzata, la transizione verso un'economia decarbonizzata è necessaria anche negli altri settori, tra i quali il riscaldamento è uno dei più rilevanti. Il riscaldamento si basa ancora in gran parte su fonti fossili, anche se le reti di teleriscaldamento, il recupero del calore di scarto, le pompe di calore e altre forme di accoppiamento con settori a minore intensità emissiva sono tecnologie disponibili che possono ridurre l'impatto del settore in futuro.

Questa tesi si propone di esplorare soluzioni di accoppiamento tra centrali turbogas a ciclo combinato (CCGT) e pompe di calore (HP) per aumentare la flessibilità delle centrali, perseguendo il triplice obiettivo di una maggiore capacità di fornire servizi alla rete, una ridotta incertezza sulla sostenibilità economica e la fornitura di riscaldamento a ridotta impatto ambientale.

L'introduzione e il primo capitolo descrivono in dettaglio le motivazioni di questa tesi, il contesto in cui si suppone che le tecnologie studiate operino, e riportano la letteratura esistente in materia. Il Capitolo 2 si concentra sulle centrali a gas a ciclo combinato, studiando gli effetti del funzionamento flessibile sulle emissioni e quantificando i benefici del condizionamento dell'aria in ingresso come misura per il miglioramento della flessibilità. Il Capitolo 3 riguarda le pompe di calore, un modello sviluppato per l'analisi tecno-economica viene presentato insieme ad alcuni risultati che confrontano diversi fluidi e fonti di calore per diverse temperature di utilizzo del calore. Il Capitolo 4 combina quanto presentato nei due capitoli precedenti, studiando soluzioni per l'accoppiamento di CCGT e HP.

Diverse soluzioni di accoppiamento sono state esplorate per due scopi principali, un aumento della flessibilità, tramite il condizionamento dell'aria in ingresso, di quegli impianti dedicati esclusivamente generazione di energia elettrica, e l'accoppiamento della pompa di calore a un CCGT cogenerativo. Il primo si basa su un'unità di condizionamento dell'aria, composta da una pompa di calore, un accumulo freddo e alcuni scambiatori di calore. L'unità funziona riscaldando, al fine di aumentare l'efficienza off-design, o raffreddando, per aumentare la potenza netta, l'aria in ingresso alla turbina a gas secondo diverse modalità operative. L’accoppiamento in impianti cogenerativi utilizza una pompa di calore ad alta temperatura che, integrata con il ciclo combinato, sfrutta fonti di calore privilegiate (diverse soluzioni impiantistiche sono considerate) aumentando la potenza termica massima e l'efficienza globale. Un accumulo a media temperatura è anche incluso, permettendo una gestione flessibile della pompa di calore e del ciclo combinato accoppiati.

Infine, il Capitolo 5 descrive il contesto di mercato in cui operano oggi le centrali elettriche. Si concentra sull'importanza di riconoscere il valore economico della flessibilità nel mercato dei servizi ancillari. Viene presentato un nuovo modello di dispacciamento ottimale per i generatori di energia e tecnologie di stoccaggio, che ottimizza non solo i profitti sui mercati tradizionali di sola energia ma i profitti complessivi attesi considerando anche i mercati dei servizi e tenendo conto dell'incertezza di accettazione delle offerte su questi ultimi.

Ringraziamenti

Una comunità in cui imparare, condividere, mettersi in gioco e crescere tessendo relazioni di qualità. È su questa base, probabilmente ancor più che per le indubbie competenze o l'ambiente internazionale e stimolante, che, quattro anni fa, ho sciolto le riserve e scelto di intraprendere questo viaggio con il TPG.

Sono felice di questa scelta e grato di sentirmi parte di questo gruppo. In questi anni tante facce, tante vite ed esperienze si sono incrociate al TPG, molti di quelli che mi hanno da subito accolto e coinvolto hanno ora hanno intrapreso altre strade, altri si sono uniti successivamente e rapidamente sono passati dall'essere accolti all'accogliere chi di anno in anno arrivava. Un bell'ingranaggio in cui le responsabilità umane e relazionali crescono di pari passo a quelle professionali.

Questi stessi anni verranno anche ricordati come quelli che, con l'innesco delle misure di contrasto alla pandemia, hanno definitivamente demolito in molti luoghi la dimensione collettiva e comunitaria del Lavoro ormai storicamente in declino. Sono però felice di constatare che, anche in assenza di quella dimensione comunitaria che ho vissuto nel corso del primo anno, in forme diverse le dinamiche che descrivo sopravvivono per merito di chi ha la premura di prendersene cura. Sperando di aver dato anche io il mio contributo nel prendersi cura, nell'animare e far crescere il TPG non mi resta che ringraziare tutti coloro con cui ho avuto occasione di percorrere qui un tratto di strada più o meno breve che sia.

Grazie ad Avinash, Eleonora e Carlo, con i quali quest'avventura è iniziata e dei quali è stato fondamentale il supporto e il confronto nelle più svariate situazioni.

Un ringraziamento particolare va ad Alessandro che con estrema pazienza ha saputo guidarmi, stimolando la mia curiosità scientifica, condividendo conoscenze e competenze; anche grazie a lui il dottorato è stata un'esperienza realmente formativa.

Infine voglio ringraziare tutte le persone con cui ho condiviso il breve ma intenso periodo presso la *Division of Heat and Power Technology* del *KTH Royal Institute of Technology* di Stoccolma, esperienza umana e professionale estremamente positiva e arricchente.

Index

Introduction

Energy is, from the industrial revolution onwards, one of the most essential goods on which many human activities rely. Energy is needed in different forms and for different purposes: for human wellness and basic needs (lighting, cooking, heating, and cooling), for industrial purposes and any kind of consumer goods production, for transport, and also is increasing the energy demand related to the services and internet data.

The primary energy consumption has increased continuously in the last decades, with the exception of some years characterized by economic recession or, in the case of 2020 by the COVID-19 global pandemic. The increasing trend in energy demand is clearly shown in Figure 1, which highlights how the global increase is mostly driven by those regions which have been recently developed or are still growing from an economic or demographic perspective.

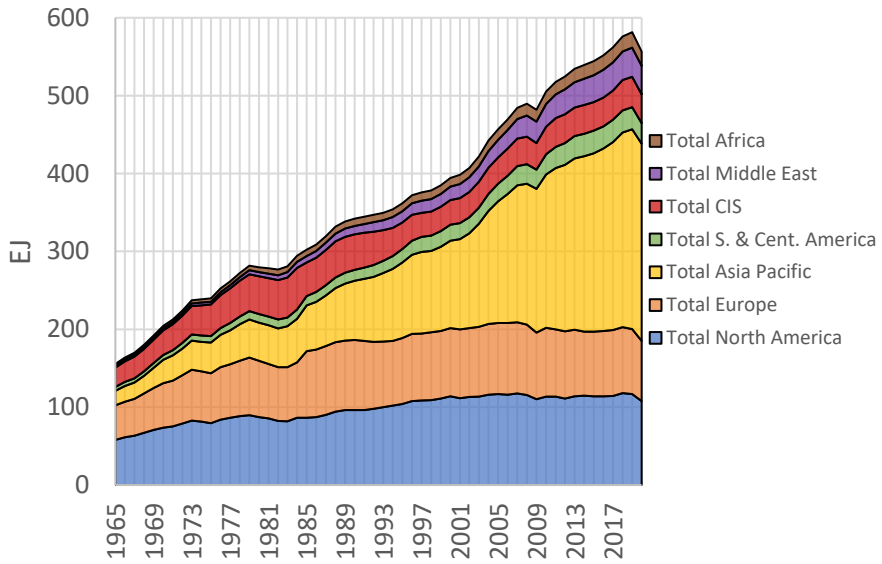

Figure 1: Word's primary energy consumption trend by region, elaboration of data reported by BP [1].

Although the growing sensitivity to the problem of climate change has drawn attention to the issue of energy, there is no target, adopted or under discussion, which concerns a limit or reduction in energy demand. Many policies have been enacted aiming to reduce the energy intensity (i.e., the average amount of energy required to produce a unit of GDP) or to improve the quality, from an environmental point of view, of the energy production mix.

This is because each country's wealth and human wellness are strongly related to energy consumption. Figure 2 and Figure 3 report how both the Gross Domestic Product (GDP) and the Human Developed Index (HDI) correlate with primary energy consumption. From this chart, it is easy to figure out how the global energy demand can increase when the most populated developing countries, such as China and India, will have grown further.

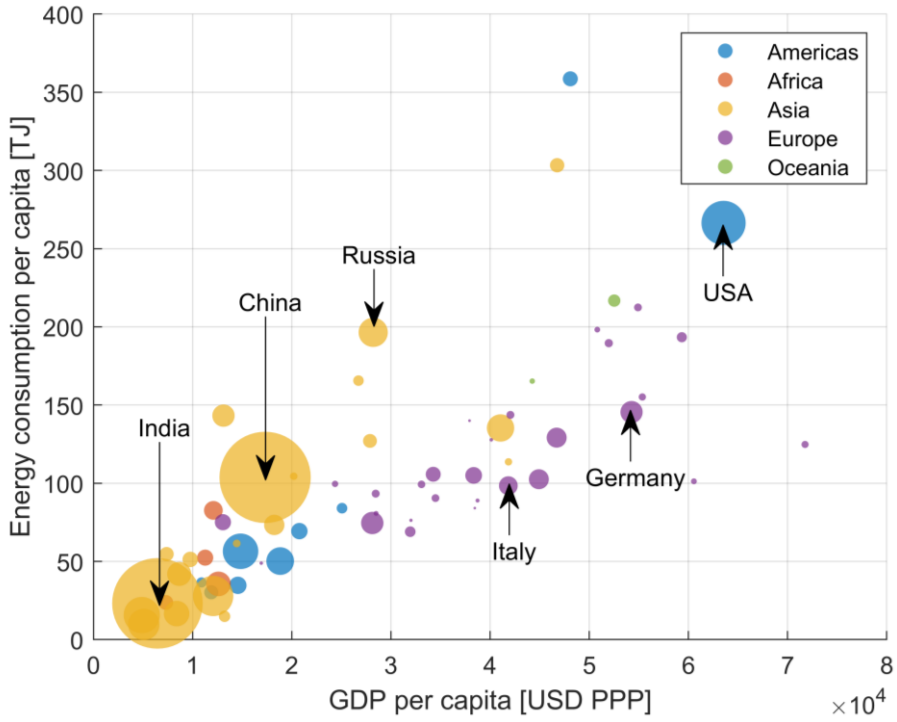

Figure 2: yearly energy consumption versus pro capita GDP, all the data are referred to 2020. The size of the markers is proportional to the country's population. elaboration of data reported by BP and the World Bank [1,2].

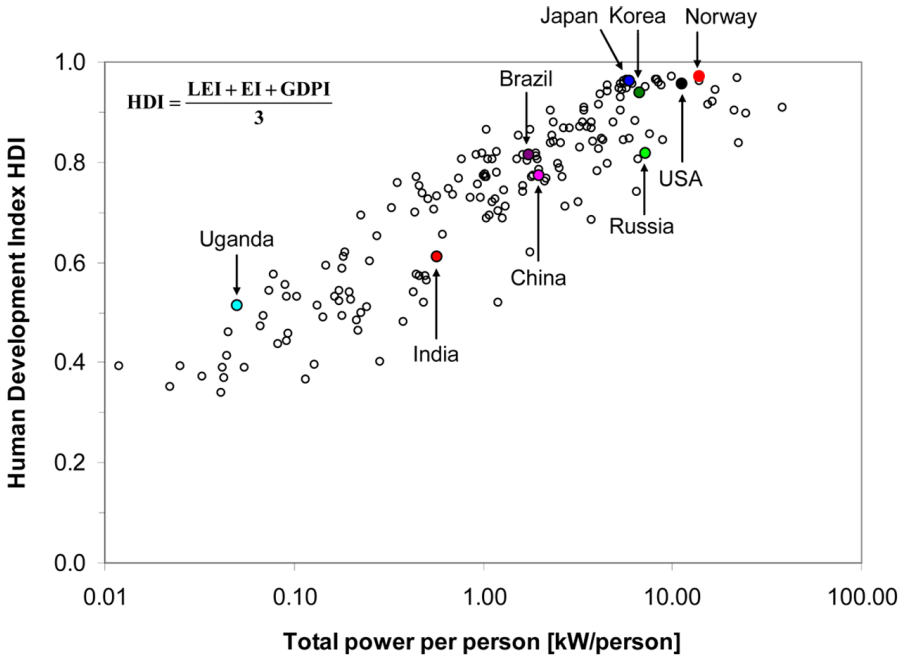

Figure 3: HDI correlation to energy consumption [3].

Nevertheless, climate change and its consequence are considered a severe issue that is expected to have relevant human and economic consequences and costs if not limited. An increase in extreme weather events, sea-level rise up, desertification, and others represent future scenarios which have to be kept under serious consideration.

It was previously told that human wellness and economic growth strongly depend on energy access and its availability, however, the energy sector is responsible for most of the Greenhouse Gases (GHGs) emissions, i.e., emissions of those gasses presenting relevant climate change potential. And this poses a dilemma to the governments and policymakers between the worldwide right to develop, the right to an adequate living standard without social limitation, which is defined as energy equity, and environmental sustainability.

Energy equity concerns what is related to the affordability and availability of energy, 761 million people did not have access to the electricity grid in 2019 mainly in sub-Saharan African countries [2,4]. But affordability represents an issue also within developed countries, the Italian observatory on energy poverty reported in 2019 that 8.8% of Italian families are in energy poverty conditions [5] and equally considerable values are reported also at the European level [6]. Energy equity may be posed in conflict with environmental sustainability since often the cheapest energy sources are those implying considerable environmental local pollution or high carbon dioxide or other GHG emissions.

This dilemma could be solved by investing money and resources in cleaning up the energy mix and with policies oriented toward charging these costs according to social equity criteria. Nevertheless, this effort should be carefully oriented because there is a risk of posing a serious threat to the security of the energy system jeopardizing the security of supply. As a matter of fact, policies that do not consider this aspect sufficiently may cause an excessive dependence on abroad for fuel or electricity supply or a huge quantity of Renewable Energy Sources (RES) capacity within an inadequate grid, which may cause high price volatility or even the incapacity to meet the peaks of the electricity demand causing outages and blackouts. The Global Energy Institute of the US chamber of commerce assesses an energy security index on the basis of 37 measures in 9 categories: global fuels; fuel imports; energy expenditures; price and market volatility; energy use intensity; electric power sector; transportation sector; environmental; and basic science and energy research and development [7].

The Energy Security issues make the previous dilemma a “trilemma”, as defined by the World Energy Council [8], which annually assesses how each country manages to respond to the three different competing demands of the trilemma. Energy Equity, Environmental Sustainability, and Energy Security are the three main challenges that engineering and technology are currently called to deal with. The need of committing to these challenges is worldwide shared and these targets are officially adopted by the UN member states in 2015 including them in the 2030 agenda for sustainable development, whose seventh and thirteenth goals are “Ensure access to affordable, reliable, sustainable and modern energy for all” and “Take urgent action to combat climate change and its impact” respectively [4].

This is the context in which this thesis has been developed, it aims to propose and evaluate technological solutions to meet the challenges described above in at least two key sectors: electricity and heating. In particular, power-to-heat and combined heat and power configurations are investigated to simultaneously respond to the needs of both sectors. Generally speaking, the focus has been on addressing, at the same time, the need for flexible and programmable power generation, and decarbonization of the heating sector. In detail many activities described in this thesis have been carried out within the PUMPHEAT project, an H2020 EU-funded project[1] coordinated by the University of Genova with a

[1] Grant Agreement No 764706.

variegate consortium of industrial and academic partners all across the European Union [9]. The project concluded in 2021 after four years of investigating optimal coupling between Combined Cycle Gas Turbines (CCGTs) and Heat Pumps (HPs).

Therefore, the topics targeted by this thesis are, on the one hand, the CCGT power plants in the current energy scenario, investigating the consequences of the flexibility requirements, and heat pumps as sustainable heat generators, also for high-temperature applications. On the other hand, optimal layouts coupling these two technologies are explored in order to enhance the benefits and limit the relative disadvantages.

The Table below schematically reports the research questions, posed by the energy context described in Chapter 1, that this thesis addresses. Motivations to each question are exhaustively described in Chapter 1, while the table indicates the section facing each question in detail. Sections not reported in the table introduce the state of the art and the methods and tools used in the research. An analogous table can be found in the Conclusion section, summarizing the answer to the research questions.

Table 1: Research Questions and related objectives

RQ 1	Is the flexibilization (i.e., increased number of start-ups and reduced operative hours) of Combined Cycle Gas Turbine Power plants reflected in increased pollutant emissions?	
Objectives	• Quantify the pollutant emissions due to Combined Cycle Gas Turbine's transients. • Assess how the real power plants' operations have changed with the increasing renewable penetration by means of numeric quantifiers (i.e., yearly fired hours, number of start-ups, stand still hours, the capacity factor). • Assess if flexibility is reflected in an increased environmental impact, even if compared to the institutional Environmental Impact Assessment (*Valutazione di Impatto Ambientale*).	
Methods	• Data collection and statistical analysis to quantify the operational profiles of real CCGT power plants. • Data collection and statistical analysis to quantify transients emissions by measured real data. • Environmental impact assessment of the Italian Combined Cycle Gas Turbine fleet, considering the real data of operation.	
Section	2.3	
Paper	Vannoni, A., Belotti, D., Sorce, A., & Massardo, A. (2021). *Analysis of the impact of Combined Cycle in the energy transition*. E3S Web of Conferences, 312, 1001. https://doi.org/10.1051/e3sconf/202131201001	[10]

RQ 2	Could the inlet air heating of a gas turbine improve its off-design efficiency, and is this reflected in relevant fuel-saving or emission reduction?	
Objective	• Quantify the economic and environmental benefits of gas turbine heating up to 45°C.	
Methods	• Fitting Gate-Cycle model outputs of a Combined Cycle Gas Turbine Power Plant, to effectively describe the influence of inlet temperature on the off-design performance. • Simulation for the whole Italian Combined Cycle Gas Turbine fleet of the optimized real operation considering the possibility of inlet heating.	
Section	2.4	
Paper	Vannoni A., Sorce a., Guedez R., Barberis, B., & Traverso A. (2021). *Combined Cycle Performance Gain Through Intake Conditioning*. Proceeding of Gas turbines in a carbon-neutral society 10th International Gas Turbine Conference 11-15 October 2021.	[11]
RQ 3	Are High-Temperature Heat Pumps a viable solution to provide low-carbon heating and couple the electric and heating sectors?	
Objectives	• Fluid comparison for High-Temperature Heat Pumps applications to waste heat recovery, considering different temperatures of source and supply. • Selected R600 as the best fluid for high-temperature applications, investigating the sensitivity of techno-economic performance to heat demand, economic indicators, and location.	
Methods	• Development of a techno-economic model for vapor compression Heat Pumps in MATLAB • Multi-Objective-Optimization targeting the minimization of the cost of investment and the maximization of the Coefficient Of Performance, for different fluids, heat sources, and supply temperatures. • Systematic run of the developed techno-economic model to investigate the sensitivity to time-usage opportunities, and gas and electricity retail prices. • Utilization of Eurostat open-access database to characterize each country according to the average opportunities for such applications	
Section	3.3	
Paper	Vannoni, A., Sorce, A., Traverso, A., & Aristide, F. M. (2021). *Techno-Economic Analysis of Power-to-Heat Systems*. EDP Sciences. https://doi.org/10.1051/e3sconf/202123803003	[12]

RQ 4	How do market and climate parameters affect opportunities for Heat Pumps coupled with Combined Cycle Gas Turbines that aim to condition inlet air for power modulation purposes?	
Objectives	• Investigate the impact of markets and climate indicators on the techno-economic performance of an inlet conditioning unit, consisting of a heat pump and low-temperature thermal energy storage. • Explore the viability of the proposed concept in different markets. • Provide an easy and fast to assess tool to roughly assess the profitability of retrofitting a Combined Cycle Gas Turbine power plant.	
Methods	• Climate, electricity, and gas markets analysis in order to characterize the European and US market bidding zone according to the potentialities for the proposed concept. Unsupervised kNN clustering to select a relevant statistical sample representing the different market and climatic scenarios. • Use of a Mixed Integer Linear Programming model of optimal dispatch to explore how the inlet conditioning unit exploits different operational modes in different locations to maximize the operational profits.	
Section	4.1	
Paper	Vannoni, A, Garcia, Guedez, R, & Sorce, A. (2022) *Combined Cycle, Heat Pump, And Thermal Storage Integration: Techno-Economic Sensitivity To Market And Climatic Conditions Based On A European And United States Assessment*. Proceedings of the ASME Turbo Expo 2022: Turbomachinery Technical Conference and Exposition. Rotterdam, The Netherlands. June 13–17, 2022.	[13]
RQ 5	How Heat Pumps could be coupled to Combined Cycle Power Plants, devoted to the simultaneous generation of heat and power, in order to maximize the market viability and reduce the uncertainty of techno-economic performances?	
Objectives	• Identify the best heat source within a Combined Cycle Gas Turbine power plant to be exploited by a High-Temperature Heat Pump designed to increase the thermal output and provide additional flexibility. • Identify the best Heat Pump arrangement, Series or Parallel. • Explore the influence of the minimum temperature required at the stack on the optimal coupled layout. • Exploiting the condensing flue gas as the Heat Pump's heat source, perform a sensitivity analysis of the thermodynamic, economic, and environmental key performance indicators through comparison against a heat-only boiler. • Exploiting the flue gas condensing as the heat pump's heat source, investigating the uncertainty of the thermodynamic, economic, and environmental key performance indicators through comparison against a heat-only boiler.	

Methods	• Layout performance comparison based on mass and energy balance equations on each plant's component. • Data-driven modeling of the electricity price and thermal demand, parametric and sensitivity analysis varying the average electricity price the cost of investment, the interest rate, and the carbon dioxide allowance cost. • Montecarlo simulation considering, as input, gas and electricity price distributions fitted on the historical data and keeping into consideration the hour of the day and distinguishing between weekdays and holidays.	
Section	4.2	
Papers	Vannoni, A., Giugno, A., & Sorce, A. (2021). *Integration Of A Flue Gas Condensing Heat Pump Within A Combined Cycle: Thermodynamic, Environmental And Market Assessment*. Applied Thermal Engineering, 184, 116276. https://doi.org/10.1016/j.applthermaleng.2020.116276.	[14]
	Vannoni, A., Giugno, A., & Sorce, A. (2021). *Thermo-Economic Assessment Under Electrical Market Uncertainties of a Combined Cycle Gas Turbine Integrated With a Flue Gas-Condensing Heat Pump*. ASME. J. Eng. Gas Turbines Power. April 2021; 143(4): 041003. https://doi.org/10.1115/1.4049769	[15]
RQ 6	How the economic value of flexibility is awarded in the markets and how it can be assessed by a techno-economic analysis?	
Objectives	• Quantify the contribution of flexibility economic value, awarded on the electricity ancillary services markets, to the overall power plants' profits • Develop a novel methodology to quantify the economic value of flexibility of power generators, storage, or retrofitting of these by new concepts	
Methods	• Statistical analysis of the market historical data • Novel Mixed Integer Linear Programming model of optimal dispatch considering both the Day-Ahead-Market and the Ancillary-Services-Markets and the related uncertainties • Machine learning classification and probability prediction of offers/bids acceptance on the Ancillary-Services-Markets	
Sections	5.2 and 5.3	
Paper	Vannoni, A, Garcia, JA, Mantilla, W, Guedez, R, & Sorce, A. (2021) *Ancillary Services Potential for Flexible Combined Cycles*. Proceedings of the ASME Turbo Expo 2021: Turbomachinery Technical Conference and Exposition. Volume 4: Controls, Diagnostics, and Instrumentation; Cycle Innovations; Cycle Innovations: Energy Storage; Education; Electric Power. Virtual, Online. June 7–11, 2021. https://doi.org/10.1115/GT2021-59587	[13]

1. The current energy context: climate pledges and future scenarios

In the last decade of the last century, with the increase in economic and industrial development, consequently accompanied by the growth of energy consumption, awareness of related environmental issues has also spread. Climate change, as a consequence of Greenhouse Gasses (GHG) emissions, is recognized as the major environmental issue dependent on the energy sector; among the GHG, carbon dioxide, even if it has not the highest Global Warming Potential (GWP), is considered particularly critic since its emission is intrinsic of any fossil energy source exploited by combustion which are the energy sources on which the development has been based on since the industrial revolution. So the increasing sensibility and concern on this topic have led in 1992 to the United Nations Framework Convention on Climate Change (UNFCCC), established to combat "dangerous human interference with the climate system". The Kyoto protocol is the following milestone within the climate pledge history, it was signed in 1997 and entered into force in 2005 after the Russian ratification. Then a second commitment period was agreed to in 2012 to extend the agreement to 2020, known as the Doha Amendment to the Kyoto Protocol [16].

More recently, in December 2015, 189 parties out 197 of Conference of Parties signed in Paris, at the 21st UNFCCC Conference of Parties, an agreement committing to the long-term goal of keeping the increase in global average temperature to well below 2°C above pre-industrial levels, aiming to limit the increase to 1.5°C [17]. The agreement entered into force in November 2016 when 55 countries, representing at least 55% of global emissions, deposited their instruments of ratification.

The current status of CO_2 emissions is well synthesized by Table 1.1 which reports the data for those countries (and the European Union) emitting more than 1 billion carbon dioxide tons and representing more than 65% world's emissions, data are referred to 2019 in order to exclude the COVID-19 crisis whose effects have still to stabilize. The table reports both the absolute value of emitted mass but also the value normalized on the population, the absolute value is important since describes how much the policies stated, or under consideration, in that countries could be relevant on a global scale. The value per capita is interesting since it highlights the demographic factor on the absolute value and shows how it is correlated to economic development pointing out as the energy equity, the right to develop, and the climate justice are all issues that should be considered to carry out an effective and equal fight to climate changes. The relative trends over a 5-years period may give an idea of the relevance of each emitter in the future.

Table 1.1: CO_2 emission by countries with a yearly value above 1 Gt [18].

	Emissions	Relative Change 2014-2019	Emissions per capita	Relative Change 2014-2019
China	10.49 Gt	+5.05%	7.32 t	+2.54%
USA	5.26 Gt	-4.83%	15.97 t	-7.84%
EU27	2.91 Gt	-4.16%	6.54 t	-4.78%
India	2.63 Gt	+20.13%	1.92 t	+13.91%
Russia	1.68 Gt	+3.5%	10.51 t	+2.65%
Japan	1.11 Gt	-12.49 %	8.72 t	-11.58%

Therefore, all around the globe, the energy policies aim to cut the emission of carbon dioxide, as the main responsible for climate change consequently the focus is often on those sectors presenting the highest carbon intensity. This section will give an overview of the commitments and the adopted policies by the six big emitters reported in Table 1.1.

China has nationally determined its action to achieve the peaking of carbon dioxide emissions around 2030, to low carbon intensity (i.e., carbon dioxide emission per unit of GDP) by 60-65% from the 2005 level, and to increase the share of non-fossil fuel in primary energy consumption up to 20%. Thus, a reduction of coal in the energy mix, a further increase of RES capacity for power generation, and wider adoption of carbon emission trading pilots launched in 2011 in 7 provinces are expected [19,20].

The United States after Paris agreement rejoining in April 2021 is setting an economy-wide target of reducing its net greenhouse gas emissions by 50-52 percent below 2005 levels in 2030, defining a sector-by-sector pathway for Electricity, Transportation, Buildings, Industry, and Agriculture [21].

European Union sets the target of cutting emissions by at least 55% from 1990 levels by 2030 and of 32% share of energy from Renewable Energy Sources (RES) in the Union's gross final consumption of energy by 2030, with the possibility to increase it where there are further substantial costs reductions in the production of RES [22], beyond the horizon of 2030 the target is the climate neutrality in 2050 [23]. In December 2020 the EU communicated its own Nationally Determined Contribution of its member states [24]. In July 2021 the EU commission Adopted a package of proposals known as “fit for 55”, referring to the declared target of emission cutting, in order to make the EU's climate, energy, land use, transport, and taxation policies fit for it. This package poses energy efficiency, RES implementation, and the European Emission Trading (EU-ETS) revision as priorities [25,26]. Moreover, the EU requires the member states to develop a National Energy and Climate Plan (NECP) outlining how the country intends to address the Union’s targets of energy efficiency, renewable energy sources, GHG emission reduction, interconnection, research, and innovation [27].

India also pledges a reduction of its GDP carbon intensity by 33 to 35% by 2030 from the 2005 level, mainly planning to implement non-fossil fuel (nuclear and RES) generation capacity and create an additional carbon sink of 2.5 to 3 Gt of CO_2 equivalent [28]. Moreover, in November 2021, at the COP26 in Glasgow (UK), the Indian prime minister announced the target of hitting net zero emission by 2070 [29], however in Glasgow over 40 countries pledged to quit coal at COP26 [30], but India was not among them and today coal meets 44% of India’s primary energy demand [31].

Russia mainly claims, as climate action, its forest as a carbon sink, within its National Determined Contribution, due as a Paris Agreement signer, Russia declared a target for "limiting greenhouse gas emissions, which provides for a reduction in greenhouse gas emissions by 2030 to 70 percent relative to the 1990 level, taking into account the maximum possible absorptive capacity of forests and other ecosystems and subject to the sustainable and balanced social-economic development of the Russian Federation" [32]. It should be noted that 1990 as a reference year makes the target softer given the substantial post-Soviet era de-industrialization.

Japan also declared its long-term target to achieve the net-zero emission by 2050, aiming to reduce its GHGs emission to 0.76 CO_2 equivalent Gt (-46% from the 2013 level) by 2030 [33].

Globally, electricity and heat generation account (according to 2019 data) for 43.75% of total CO_2 emissions [34], for the Industry and Buildings end-sectors. So the focus of the aforementioned policies addressed to the emission cut are often focused on these, and for this reason, they are described in-depth within the two following subsections.

1.1. Current electrical supply context: climate policies and market fundamentals

Within the international context described in the previous section, electricity production is one of the sectors which has been affected firstly by the energy transition. Many countries all around the globe have already implemented strong policies oriented to the sector's decarbonization and further targets are set to be more and more challenging. China announced to bring its wind and solar PV power generation capacity to 1,200 GW by 2030 [20], currently, the capacity from these two sources amounts to 535 GW representing 9.5% (727.6 GWh) of the total electricity generation. The USA recently declared the goal to reach 100% carbon pollution-free electricity by 2035, but some states had already set a target, such as California which imposes that by 2030 the 60% of the electricity retail sales must be served by renewable resources [35]. The EU required the member states to set specific targets on the electricity system decarbonization within the National Energy and Climate Plans (NECPs), as a matter of example in the electricity sector France, Italy and Germany set respectively 40%, 55%, and 65% of RES generation share by 2030 [36–38].

In order to meet all these targets in the electricity sector by the deadline the adopted policy instruments include the promotion and the subsiding of large amounts of RES capacity [39], carbon pricing systems implementation [40], the promotion of the coal to gas shifting as a lower carbon-intensive dispatchable source [41,42]; as a consequence also the electricity grid transportation capacity improvement and storage technologies implementations are needed.

In 2017, the EU had the largest share of renewable energy subsidies, due to its 78 billion USD subsidy for power generation (Figure 1.1 left). The EU accounts for 62 % of total renewable power generation subsidies in 2017, while Japan and China accounted for 15 % and 12 %, respectively. The EU accounted for an estimated 86 % of offshore wind power subsidies in 2017, 52 % of solar PV subsidies, and 57 % of onshore wind subsidies. Globally, solar PV is estimated to have received the largest share (48 %) of renewable power generation support, with 60.8 billion USD in 2017. The next largest recipient was the onshore wind which received 31.6 billion USD (25 %), followed by biomass with USD 21.9 billion (17 %) and with offshore wind receiving 6.6 billion USD (5 %) [43].

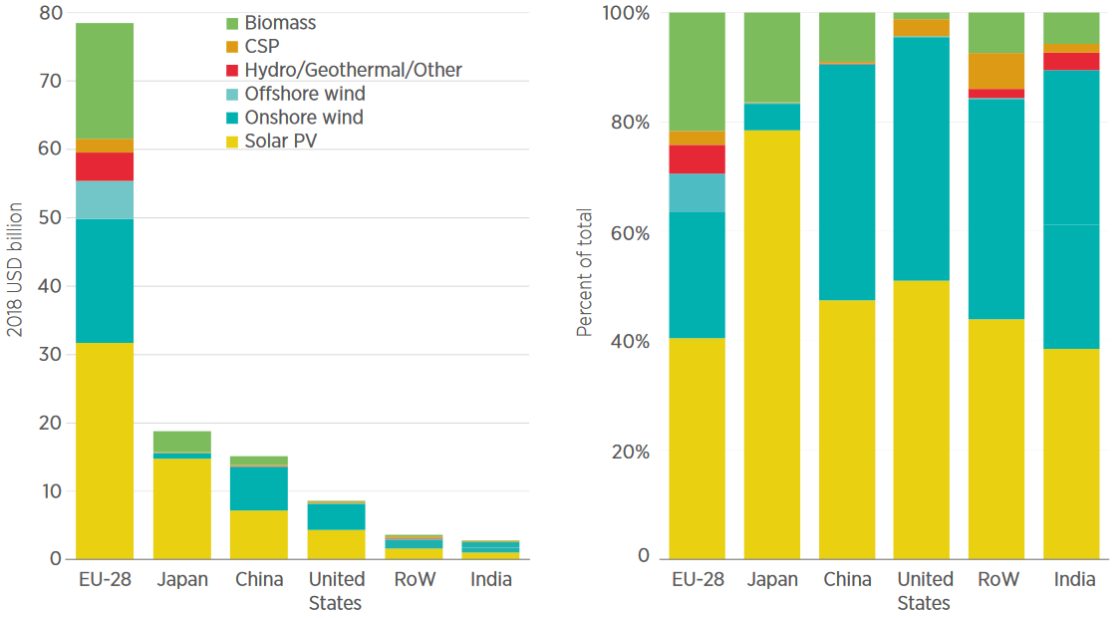

Figure 1.1: Global subsiding for RES power generation [43]. RoW=Rest of the World.

Focusing on the renewable power generation technologies receiving support by country/region (Figure 1.1 right) reveals that in 2017, Japan had the highest share (77 %) of support going to solar PV (which is also the highest share for one technology). This reflects the overwhelming dominance of solar PV in recent deployment [44]. Of the EU's USD 78 billion subsidies for renewable power generation in 2017, 40 % supported solar PV, 23 % supported onshore wind, 22 % went to bioenergy power generation, 7 % to offshore wind, 5 % to "hydropower, geothermal, and others" and 3 % to CSP. In China, India, and the rest of the world, onshore wind received large shares of the total renewable power generation subsidy.

Italian case results to be particularly interesting from this point of view since Italy has strongly subsidized Solar PV at the beginning of the 2010s and in a few years, a lot of capacity has been installed. In 2008 the solar PV installed capacity was 0.43 GW and it raised rapidly until 18.89 GW in 2015, then the trend stabilized and in 2021 the installed capacity of solar PV is 22.2 GW. This sudden change within the Italian energy mix had relevant consequences on the national electricity markets and it required facing more complicated grid management strategies, the Italian authority ARERA reports that the RES subsidizing in Italy costs 11.5 billion euros annually (6.2 B€ only considering solar PV subsidies) [45]. On the other hand, it should not be neglected how the massive solar PV installation, together with good hydro potential, has allowed Italy to reach a relevant goal such as 37.6% of RES share in the electricity generation in 2020 [46], the third-highest share among the 10 biggest economies by GDP, after Canada and Germany.

Carbon emissions cost, as described in the instruction the climate change, demonstrated to be a consequence of GHG emission, mainly carbon dioxide emission, has an environmental, social, and economic cost. However, this cost is externalized by the producers and the consumers. Carbon pricing is an increasingly used policy tool that can play a key role in incentivizing low-carbon activities by internalizing the emission cost. So the common feature of all the carbon pricing policies is a price that should be paid for each ton of emitted carbon dioxide. The price is commonly applied to all carbon-intensive

activities such as power generation, transport, and many industry sectors such as cement or iron and steel. The aim of this section is to explore and focus on how carbon pricing affects power generation and the electricity sectors.

There are two main policy approaches to carbon pricing, carbon tax and emission trading, also known as cap-and-trade. The carbon tax is a tax fixed by the policymaker (i.e., the government) which should be paid by the emitters for each unit of emitted carbon. The advantage of the carbon tax is that the price is fixed there is no uncertainty about it, nevertheless, there is no certainty about the outcome: the price may be too low causing an insufficient response in the emitted quantity or it may be too high achieving a further reduction than expected but introducing excessive distortions into the market. In contrast, the cap and trade systems are based on fixing the outcomes, so it is fixed a ceiling beyond which the companies are not allowed to emit, even if the allowance is not bought from others that want to sell it, so the allowances price is established by the demand and the supply for them and there is no certainty about it.

The difference between the two approaches is well exemplified by Figure 1.2 which describes how the aim of a quantity reduction is pursued by the carbon tax (left) and cap and trade (right). The carbon tax shifts upward the supply curve of the product (from red to green), in fact, it represents an extra cost to be paid, however, the achieved reduction ΔQ depends on the shape of the original supply (red) and demand (blue) curve. On the left is illustrated how the cap and trade works, the outcome is fixed by the cap value but the extra cost (Δprice), depends on the market features. The lower the cap the higher the price to pay for emitting beyond the cap.

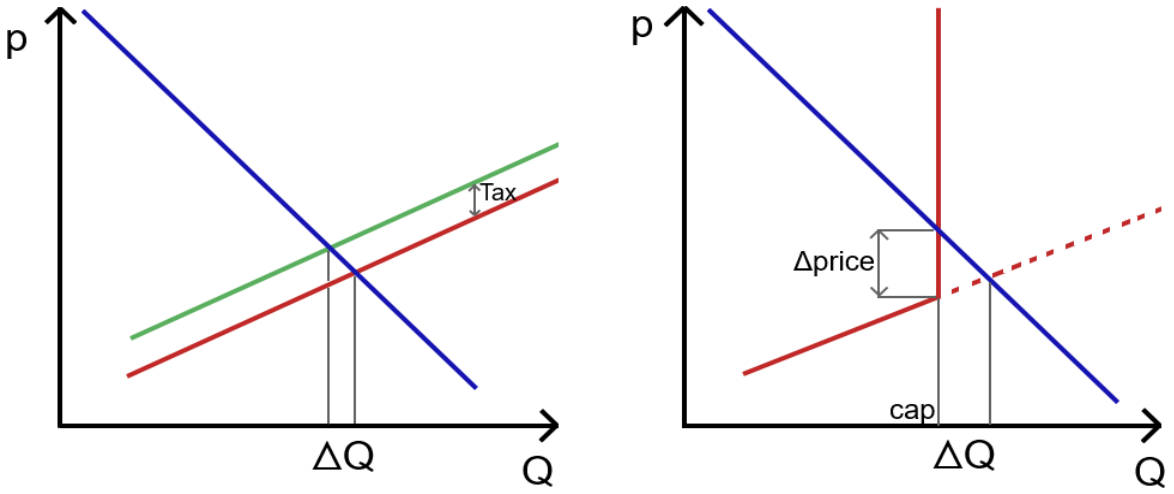

Figure 1.2: Carbon tax, left, and Cap and Trade (Emission Trading), right, economic approach comparison.

Figure 1.3 reports the current state of carbon pricing around the globe as in the World Bank annual report [47]. In 2021 21.5% of global GHG emissions are covered by the carbon pricing instruments in operation, the China national Emission Trading System (ETS) launched in February 2021 became the world's largest carbon market. Cap and trading systems are prevalent covering 8.73 $GtCO_2e$ (equivalent CO_2 gigatons), while carbon taxes globally address an amount of emission equal to 2.99 $GtCO_2e$. Overall 21.5% of global GHG emissions are covered, moreover, additional carbon pricing systems implementation is already scheduled, including an ETS in Ontario and some USA states (Washington, Connecticut, Massachusetts, Rhode Island, Washington DC) and a carbon tax in Indonesia

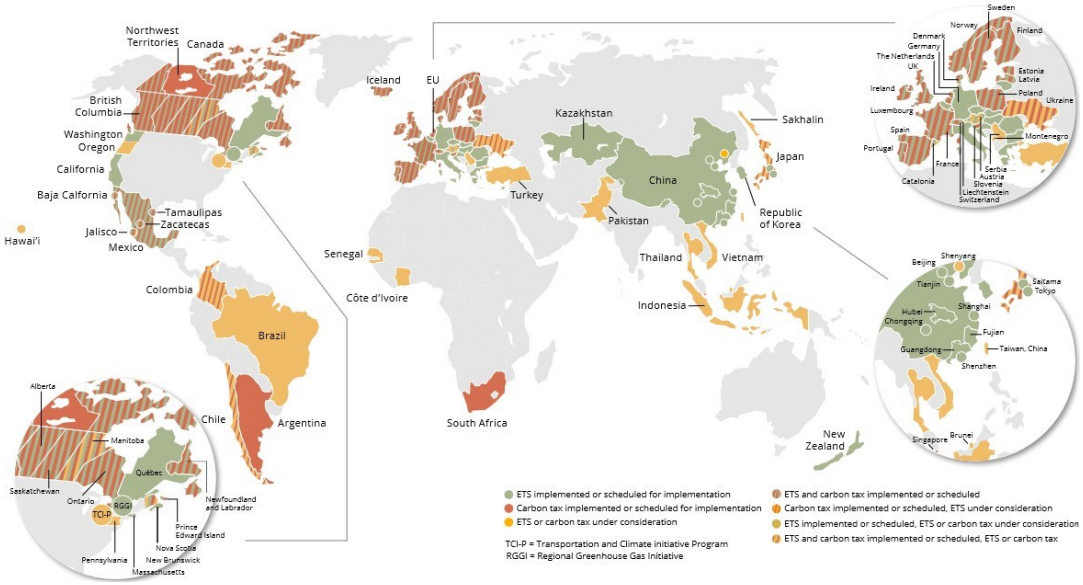

Figure 1.3: State of carbon pricing in 2021 [47].

From the fossil fuel-based power generator's point of view, there is not so much difference between the two carbon pricing systems, apart from the potential volatility of carbon price within an ETS market. The carbon price represents, in both cases, an extra cost to pay proportionally dependent on the amount of the emitted CO_2, so of the burned fuel. A parameter often used to assess the viability of fossil fuel-based power generators is the spread between the cost of generating electricity and the potential revenues on the electricity market, so the generator's theoretical gross economic margin. This is commonly known as Spark Spread (SS) [48], for natural gas-fired generators, or as Dark Spread for coal-fired generators. Equation 1.1 reports Spark Spread's definition.

$$SS = pr_{el} - \frac{pr_{gas}}{\eta_{el}} \tag{1.1}$$

By introducing a carbon pricing system, the Spark Spread no longer describes the profitability of the generator, since the amount paid for carbon emissions would have to be subtracted from the Spark Spread to obtain an estimate of the gross economic margin. Then the utilized parameter is the Clean Spark Spread, or Clean Dark Spread for coal-fired generators [49], defined as in equation 1.2.

$$CSS = pr_{el} - \frac{pr_{gas} + pr_{CO_2} \cdot \mathrm{e}}{\eta_{el}} \tag{1.2}$$

where p_{CO_2} is the carbon price and e is the emission factor, i.e., the ratio between the emitted ton and the energy potential of the burned fuel.

The difference between the Clean Dark Spread and the Clean Spark Spread is sometimes known as the Climate Spread or Bed Spread [50] and it describes the economic benefit of using a more carbon-intense energy source such as coal rather than natural gas. Coal is normally cheaper than gas and, even if the cycle efficiency is normally lower, it allows for the production of cheaper electricity (positive Climate Spread). However the ratio e/η_{el} is much higher, since the use of coal is more carbon-intense, and an high enough pr_{CO_2} can impose a convenience of gas with respect of coal (negative Climate Spread) driving a coal-to-gas shifting and a consequence carbon-intensity reduction [51,52].

$$CS = \frac{pr_{gas}}{\eta_{el\,gas}} - \frac{pr_{coal}}{\eta_{el\,coal}} + pr_{CO_2}\left(\left(\frac{e}{\eta_{el}}\right)_{gas} - \left(\frac{e}{\eta_{el}}\right)_{coal}\right) \tag{1.3}$$

Since the early 2000s, the promotion of coal to gas switching has been indicated by the scientific community as a mid-term solution to reduce the carbon system's carbon intensity and mitigate the damages of the fossil fuel-based economy during the transition to a decarbonized future [53]. Then the policy implementation follows some years later [41], sometimes driven by the twofold target of GHG emission cut and air quality improvement, especially in China [54]. In North America, the switching has been driven also by the shale gas revolution, due to the rise of modern hydraulic fracturing [55]. In the last years, the implemented switching led to an effective decrement in carbon intensity, especially in those countries which strongly relied on coal in the past, such as the United Kingdom [56]. Nowadays the shift from coal to gas is a debated issue, on one hand substituting a coal-based generator with a natural gas-based of the same size would lead to an objective benefit, on the other hand, environmentalist associations, green parties, and others claim no new fossil fuel-based power plant. Often is proposed to phase out the coal immediately and use the existing gas turbine generators to support the energy transition until they would be essential, then switch them off at the end of their lifespan. For the same reasons, Knittel et al. argue that the drop in the price of natural gas has an ambiguous effect on global carbon emissions because of three countervailing effects: coal-to-gas switching in the US electric power sector, an increase in the relative cost of US renewable energy sources, and an increase in US coal exports [57].

Before illustrating the security and adequacy issues of electrical supply, the following subsection describes the basics feature of electricity markets which are common to the most developed countries, then it will be carried out on the Italian electricity market since Italy will be considered as the scenario for some of the case studies presented in this thesis.

1.1.1. Electricity market fundamentals

Electricity delivered from generators to the consumers through the grid implies two different levels: transmission and distribution. Transmission relies on long distances and high voltage connections, while distribution concerns e delimited local area.

This subsection aims to describe how the electricity trade is regulated and how the physical levels (generation, transmission, distribution, and consumption) are reflected in the regulatory plan. Generally speaking, the generation itself is more and more regulated by the market, during the last century it was centrally controlled but by the 90s the liberalization occurred all around the world. In Europe, in 1998 the European Commission directive signed a milestone [58,59]. The targets of liberalization processes are lower costs, higher efficiency, and more consumer choice. Since the networks are a natural monopoly[2], there remains one single entity responsible for the operation. So the market mechanism will not function properly and sector regulators are needed to regulate access to the electricity network and network use. The regulator will set the access conditions, supervise the performance of the network companies and set the tariffs. Retailing electricity to the users could be also liberalized.

[2] A natural monopoly occurs when the most efficient number of firms in the industry is one. It typically has very high fixed costs meaning that it is impractical to have more than one firm producing the good. In this case transmission grid is a natural monopoly, since having two, or more, grids is obviously not the best solution: even if it would increase the competition, and so the efficiency, the costs would overcome benefits.

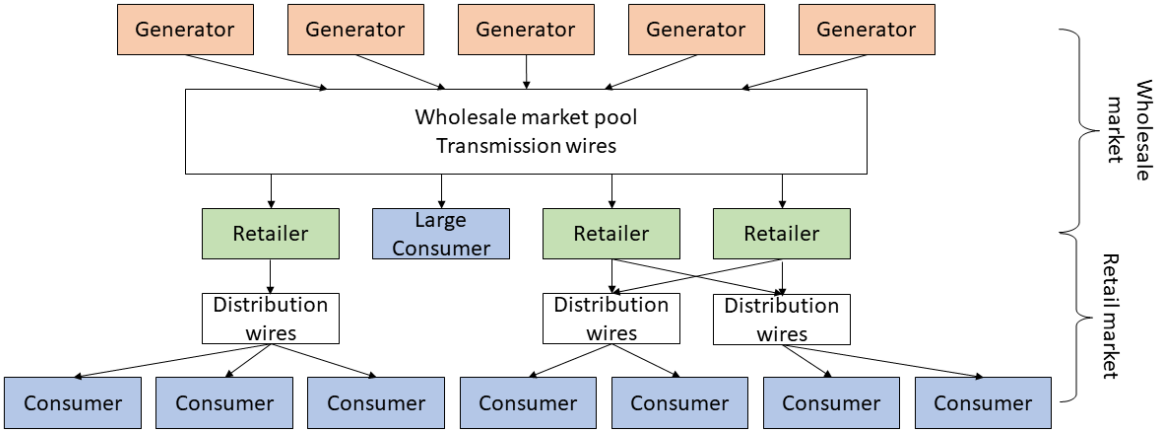

Figure 1.4: Electricity sales flow, from the generator to the consumers.

This thesis focus on the generator's point of view, and the aim of this chapter is not to provide an exhaustive description of all that concerns the electricity market but to illustrate the fundamentals which need to be introduced before reporting the addressed case studies in order to fully understand them. For these reasons, this chapter hereby considers the wholesale market only.

In a market we have two main players, within the wholesale market of electricity one is the consumer or the retailer, and the other is the producer. The latter provides the supply and the other the demand. What brings these two together is the price, the price matches supply and demand.

Consumers are retailers, households, companies, or other entities who consume a product, in this case, electricity. However, electricity has a price. All the consumers want electricity but the question is how much they are willing to pay for it. This concept is known in general as "willingness to pay". It represents the value that consumers attach to the consumption of electricity. This willingness to pay depends on both the price and the scarcity of the product. Linking the two together produces the demand curve, Figure 1.5. On the horizontal axis, we have the quantity of electricity that is purchased. On the vertical axis, we have the costs or the price. We arrange demand according to the consumer's willingness to pay, as reflected in the red line, so the highest willingness to pay to the left and the lower willingness to pay to the right. A certain price, the price here pr*, reflects a specific price in the market. Consumers who are willing to pay more than this price are on the left-hand side of Q*. There are also consumers who have a willingness to pay that is lower than the price pr*, when the market price is pr*, they will not be willing to purchase electricity. So here the Q* represents the quantity bid by consumers who are willing to pay more than the price pr* for electricity.

A producer is somebody who supplies electricity to the market. So, typically, this is the generator, but it can also be a kind of intermediary like a trader or a retailer. Producer behavior depends heavily on two factors: Production costs and the number of companies competing in the same market. Focusing on the first, ideally, producers are willing to sell electricity in the market whenever their production costs are lower than the price they receive in the market. It is important to note here that the production costs are the marginal costs of operating the generator. These are the costs of producing one additional unit of electricity. If the production cost for producing this additional unit of electricity is lower than the market price, generators are willing to produce and sell their electricity.

This is the supply curve, the green line, for electricity producers. A supply curve in the electricity market represents which producers offer electricity to the market at which price. On the horizontal axis, we have again the quantity here intended as the quantity of electricity generated or generation capacity. On the left are arranged the generators with the lowest marginal production costs. To the right, we have fossil fuel-based generators. Their marginal costs contain a large component of fuel costs, so their electricity is typically much more expensive to generate.

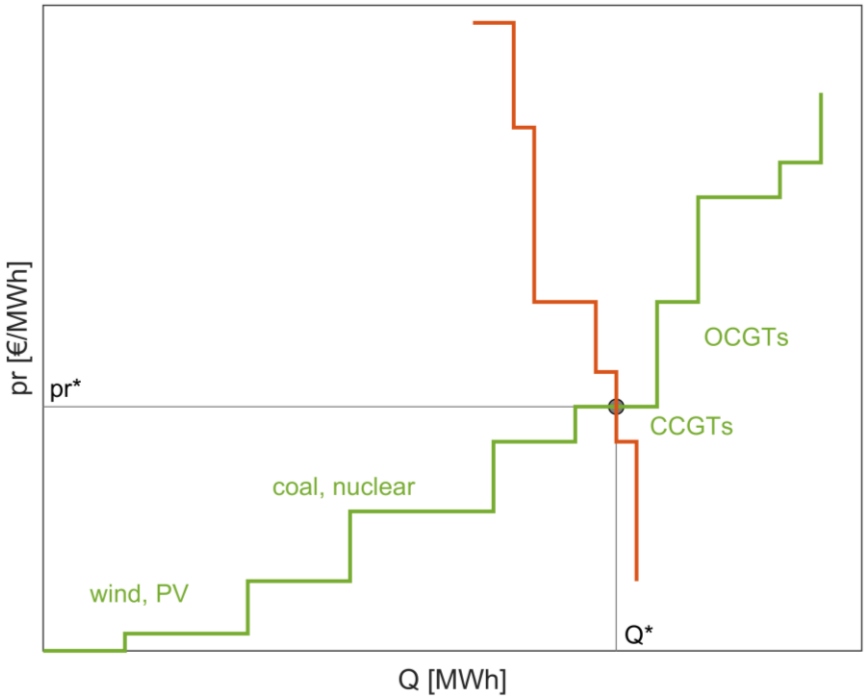

Figure 1.5: Exemplified demand (red) and supply (green) curves.

So this decides how much electricity is produced and consumed (Q*) and at which price (pr*). However it should be pointed out how what is described above represents an oversimplification, real market should consider at the least the two following issues:

- Electricity is a non-storable commodity, so generation and consumption should be balanced at each time. Both the supply and the demand curves are time-dependent since the demand varies with time but also the availability of the primary source, e.g., wind or solar, or its cost, e.g., fuels price, is not constant. So the market equilibrium (the clearing price pr* and the clearing quantity Q*) changes continuously.
- The grid may result to be congested. The ideal equilibrium may imply most of the power generation within a geographical zone whereas the marginal cost could be lower, e.g., relevant RES availability, but then the grid capacity could be inadequate to transfer such power where the energy is required to be consumed.

For these reasons, the market has to be discretized temporarily and spatially. Typically the main market closes one day ahead of the real-time and the temporary discretization is hourly or quarter-hourly, this market is called Day-Ahead Market (DAM). The spatial discretization consists of bidding zones (more common in Europe) or grid nodes (more common in North America), many countries have only a national bidding zone, while subnational bidding zones are adopted for instance in Italy, Denmark, Sweden, and Norway.

On the DAM, for each time interval and bidding zone (or grid nodes), each market player makes an offer (generators) or a bid (consumers/retailers) building the specific supply and demand curves.

This market is typically open for some weeks before the real-time to the day ahead, then closer to the real-time other markets address the purpose of strictly compliance between demand and supply, in fact, some discrepancies may occur between the day-ahead demand forecast and the actual demand, these markets are commonly known as intraday markets (IDM) and typically close some hours ahead of the real-time.

DAM and IDM can be referred to as energy-only markets since electricity is traded with the only scope of satisfying the demand for electric energy. Nevertheless, there are other markets in which the electricity is sold as a service to the grid. These services, commonly defined as ancillary services, are needed for maintaining the secure and stable operation of the power system or recovering system security, ensuring power supply, and meeting voltage, frequency quality, and other requirements. Ancillary services provision can be regulated differently but is widespread, especially for some of those, a market-based regulation. In this market, Ancillary Services Market (ASM), the consumer (who requires services) is the Transmission System Operator (TSO)[3] that buys services selecting the best offers among those power plants that are able and available to increase or reduce their supply of power. This market runs in real time.

1.1.1.1. Italian Electricity Market Focus

This section describes the Italian electricity market structure, in order to give a detailed knowledge of the market context in which some of the techno-economic assessments presented in this thesis are carried out. The Italian electricity grid is divided into six geographical zones in Italy: northern Italy (NORD), central-northern Italy (CNOR), central-southern Italy (CSUD), southern Italy (SUD), Sicily (SICI), and Sardinia (SARD), in addition to which must be accounted a constrained zone (ROSN), which is a portion of the national transmission grid, wherein the maximum generation capacity is higher than the grid's transmission capacity.[4]

The two main markets are the Forward Electricity Market (FEM) and the Spot Market. The Spot Market is managed by *Gestore dei Mercati Energetici* (GME), a public company

[3] A transmission system operator (TSO) is an organization committed to transporting energy in the form of natural gas or electrical power on a national or regional level, using fixed infrastructure. In the United States, the organization categories are similar, being an independent system operator (ISO) and regional transmission organization (RTO). The roles of the TSO in a wholesale electricity market include managing the security of the power system in real time and co-ordination of supply and demand for electricity that avoids fluctuations in frequency or interruptions of supply. The TSO service is normally specified in rules or codes established as part of the electricity market. To minimize the probability of grid instability and failure, regional or national transmission system operators are interconnected. The TSOs function may be owned by the transmission grid company, or may be entirely independent. TSOs are often wholly or partly owned by state or national governments.

[4] This subdivision was in force until 31st of December 2020. From 1st of January 2021 the subdivision is slightly different, without the ROSN constrained zone and with the new CALAB geographical zone including the administrative region of Calabria. Nevertheless the former zone configuration is here reported since the most of data presented in these thesis are from periods antecedents the 2021.

vested with the economic management of the Electricity Market. On the FEM buyers and sellers define their economic and energetic transactions independently from the GME, the contracts are subscribed days, months, or years before the delivery of the electricity without any obliged reference to standardized contracts. The energy transactions resulting from this market are communicated properly to the GME and the TSO (Terna) and are taken into consideration in order to define the Day-Ahead Market closure [60]

Anyhow, almost the whole amount of the electricity is bought or purchased on the four main sections of the spot market [61], schematized by Figure 1.6 and whose timing is reported in Figure 1.7:

- Day-Ahead Market (DAM), *Mercato del Giorno Prima*, is where generators can present offers to sell energy and both retailers and big consumers, can present bids to purchase energy for each hour of the following day. GME accepts offers/bids by price merit order, taking into account the transmission limits between zones notified by the TSO. Accepted supply offers are remunerated at the zonal clearing price. Accepted demand bids are remunerated at the National Single Price (PUN), *Prezzo Unico Nazionale*, an average of zonal prices in the DAM, weighted for total purchases. Participation in this market is optional [60].

- Intra-Day Market (IDM), *Mercato Infragiornaliero*, is the venue for the trading of electricity supply offers and demand bids, in respect of each hour of the next day, which modify the injection and withdrawal schedules resulting from the DAM. This market takes place in 7 different sessions. GME accepts offers/bids submitted into the IDM by price merit order, taking into account the zonal transmission limits remaining after the DAM. Accepted offers/bids are remunerated at the zonal clearing price. Participation in this market is optional [60].

- Ancillary Services Market (ASM), *Mercato dei Servizi di Dispacciamento*, is the venue for the trading of supply offers and demand bids in respect of ancillary services. The TSO uses this market to acquire resources for relieving intrazonal congestions and procuring an adequate reserve margin. On the ASM, offers/bids are accepted by economic merit order, taking into account the need for ensuring the correct operation of the system. Offers/bids are presented within a single market session, the one that opens and closes at D-1, and then selected in 6 different sessions. The awarded quantity is valued at the offered price (Pay as bid). Participation in the ASM is mandatory but restricted to units that are authorized to supply ancillary services [60]. Since 2017 this market is also open to small consumers and non-programmable RES generators [62].

- Balancing Market (BM), *Mercato di Bilanciamento*, consists of 6 sessions. The first session of the BM takes into consideration the offers/bids that participants had submitted in the previous ASM session. On the BM the TSO accepts energy demand bids and supply offers in order to provide its service of secondary control and to balance energy injections and withdrawals into/from the grid in real-time The awarded quantity is valued at the offered price (Pay as bid) [60].

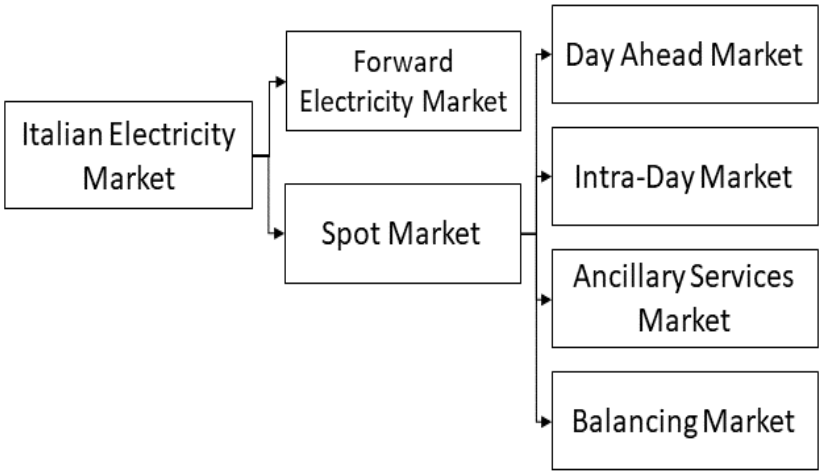

Figure 1.6: Italian electricity market structure.

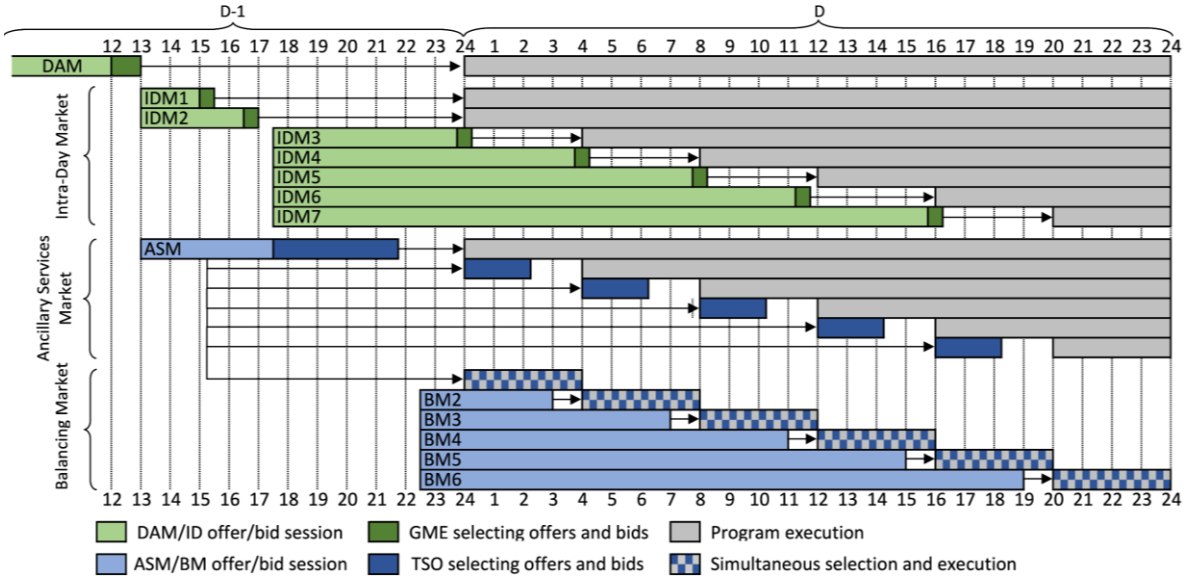

Figure 1.7: Italian spot electricity market timing.

1.1.2. Electricity grid adequacy

As stated in the Introduction, the energy security is one of the three pillars of the energy trilemma, at the macroscopical level the energy security deals mostly with the availability at a reasonable price, this topic began pivotal in the EU at the end of 2021 with a progressive increase of natural gas price up to the historical maximum [63], natural gas is essential for heating purpose in many countries, but natural gas-fired power plants are often the marginal technology on the electricity market, consequently, they fix the electricity price, first on the wholesale market, then on the retail market for final consumers.

Nevertheless, within the electricity sector, energy security is commonly intended as grid operational security, resource (generator) availability, and system balancing. Recent events have underscored the criticality of some electrical systems' security, and, within exceptional circumstances, curtailment, rolling outages of electricity, generic grid disservices, or simply non-optimal resource dispatch occurred. In August 2020 in California, an exceptional

heatwave was followed by a considerable demand for electricity, on the other hand, high temperatures cause a decrement in the natural gas fleet capacity and efficiency, making it non-viable to operate. As a consequence, the system operator had to curtail the load [64]. Something similar under exceptional weather conditions happened in Texas in February 2021 following a severe winter storm [65,66]. Natural gas production in Texas fell by almost 45% in a few days due to freeze-offs, which occur when water and other liquids in the raw natural gas stream freeze at the wellhead or in natural gas gathering lines near-production activities [67]. Other sources of electricity – nuclear, coal, and wind – also suffered from supply disruptions but these were smaller than the loss of generating capacity from gas power plants. Within the same days because of the increasing use of electrical heating devices, the demand reached unprecedented highs and the state faced an overall outage of 30 GW. The gap between production and demand forced the non-profit grid manager, the Electric Reliability Council of Texas (ERCOT), to cut off supply to millions of customers or face the system's collapse that by some accounts was minutes away [68,69]. Other significant events happened recently also in Grain Britain in August 2019 [70] and within the National Electricity Market in Australia [71].

RES penetrations have introduced two major issues of concern for operational security. The first concerns the variability and uncertainty proper of the inherent nature, non-programable and stochastic, of some sources such as wind and solar. This is in other words the afore-described issue of resource adequacy but it can impact power system parameters such as frequency and voltage. The second concern relates to how most of the renewables generators interface with the grid: through electronic inverters rather than synchronous generators driven by the turbine’s shafts, so the physical effect of rotational inertia cannot be used to damp the frequency oscillation of the grid [72].

Adequacy strongly relies on the concept of expected available capacity, i.e., the probability that the installed capacity will be available when needed to meet the energy demand, of course, it is much lower than 1 for RES because of the stochasticity of the source previously mentioned. Nevertheless, also other generators have a probability lower than 1 of being available during the peak of demand. California and Texas outage events reported above followed a decrement of the gas generators' capacity, due to exceptionally high temperatures or the freeze-off of gas supply lines. Despite these exceptional circumstances, the whole installed capacity cannot be available 24/7 because of the generator’s maintenance needs. However, the probability for these generators is much higher than wind and solar PV, and are defined as programmable generators since they can schedule their generation without relevant external constraints. It’s important to remark that not all RES are non-programmable: hydro and geothermal are an example of renewable programmable sources. Moreover, adequacy concerns also the grid, many sources, even renewables such as wind, are located far from the users. Thus, not only the available generation must be enough to meet the demand but also the grid capacity is required to be adequate to transfer the amount of generating energy.

For these reasons, besides the growing RES penetration, the grid has to be developed, implementing new connections to avoid congestion, especially within countries that for their morphological and geographic nature historically developed a poor interconnected grid [73]. On the other side, to mitigate the risk of a capacity outage, storage technologies should be implemented to improve the reliability of the power supply [74]. Furthermore is pursued also the demand response which consists of flatting the peak demand [75]. Some market designs include the possibility, by a price signal to the end-users, to promote the shift of

programmable demand (i.e., electric vehicles charging, heating spaces with relevant thermal inertia) from high peak price and demand period to off-peak. In other words, the target is to make the demand curve, presented in Figure 1.5 more elastic[5].

Adequacy is commonly assessed by some parameters [76–79]:

- Expected Energy Not Served (EENS): consists of the amount of energy demand exceeding the available capacity;
- Loss of Load Expectation (LOLE): is the number of hours of the years during which the demand is higher than the available sources;
- Loss Of Load Probability (LOLP): represents the probability that the forecasted LOLE hours actually occur.

ENTSO-E[6] runs a simulation model based on data provided by the Transmission System Operators (TSOs) for demand, supply, and the power grid for each of the European electricity market bidding zone [80]. The assessment, whose outcomes are schematized in Figure 1.8, points out that some portions of the grid pose criticisms from the adequacy point of view peripheral zones and islands are those with the highest LOLE because of their position which does not allow easy interconnection with the others. A LOLE equal to 3 h is often taken as a threshold value to declare the adequacy of an electricity system.

[5] Demand elasticity refers to how sensitive demand for a good is compared to changes in other economic factors, such as price. The demand for electricity is traditionally considered as almost inelastic so a change in price on the wholesale market does not significantly impact the overall demand since most of consumers pays fixed tariffs which are correlated to the average value of electricity on the wholesale market but not sensitive to the hourly fluctuations.

[6] ENTSO-E is the European association for the cooperation of transmission system operators (TSOs) for electricity.

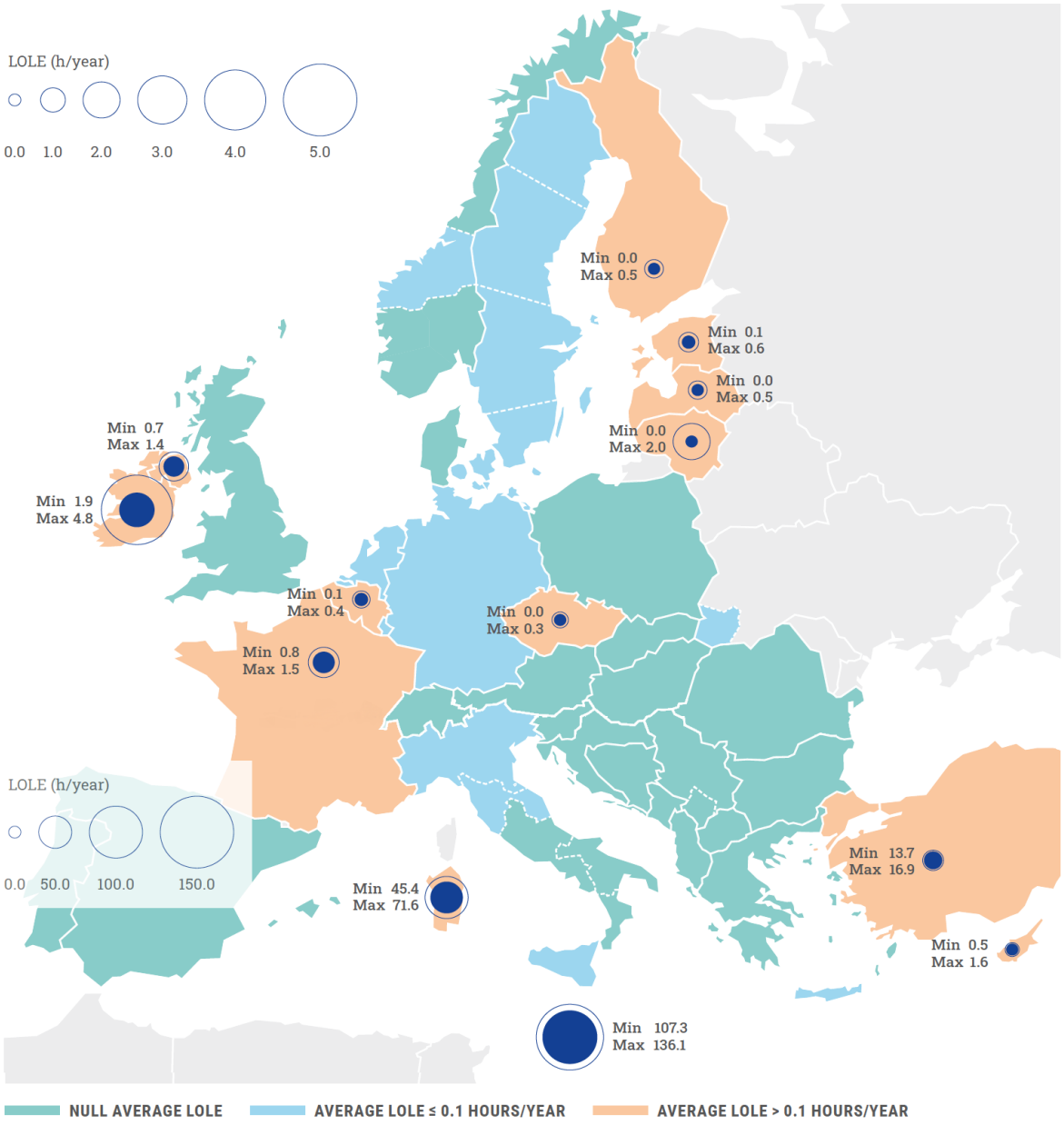

Figure 1.8: ENTSO-E mid-term adequacy forecast for 2025 [80].

The second challenge which the RES penetration pose depends on the physics of the connection between the sources and the grid, the rotating parts of the synchronous machines inherently provide inertia to the system. This is the case of all those sources which relies on alternators driven by a mechanical shaft, typically a turbine or an ICE shaft: gas turbines, steam turbine (including those driven by nuclear power plants), hydro, geothermal, and so on. While the growing RES technologies, typically wind and solar PV, are defined as Inverter Based Sources (IBR) since they are connected to the grid by means of an electronic inverter. The consequence is that in the case of disturbances and supply/demand imbalances, the inertia that naturally mitigates the system's reaction in the short term (up to 5s) and provides time to the controllers and the operator to take actions is significantly reduced, and the resulting rate of change of frequency is much higher in systems with low inertia [81–83].

The following equation (1.4) describes the physical dependency of frequency on power for synchronous machines [84]:

$$I\dot{\omega}(t) \doteq P_s(t) + P_{ns}(t) - P_{load}(t) - P_{loss}(t) \tag{1.4}$$

where I is the overall inertia of the synchronous machines, ω is the average frequency of the system, while at the equation's second member there is a simplified power balance including the synchronous and non-synchronous generators, the demand load, and grid losses.

Within a hypothetical system based exclusively on IBRs equation (1.4) comes to (1.5):

$$0 = P_{ns}(t) - P_{load}(t) - P_{loss}(t) \tag{1.5}$$

so there is no more physical dependency of power on frequency. Nevertheless, such a scenario is not realistic, even if many countries pledge for a 100% RES electricity system toward the horizon of 2050 or 2070, at the least medium and large systems will always rely on large hydropower plants or other RES synchronous machines.

1.1.3. Final remarks about the electricity sector

What Section 1.1 has outlined allows drawing some conclusions pointing out some final remarks about the context within this thesis has been carried out.

The carbon intensity reduction will be a priority for the next decades, then a huge amount of RES-based generators are foreseen to be installed, most of them are expected to be from non-programmable technologies such as on-shore, and off-shore, wind turbines, solar PV, and concentrating solar power plants. However, this poses serious challenges to the security of the electricity system and its adequacy.

Demand response, storage implementation, and grid improvements may help in managing the system, but today it's difficult to think about a large electricity system without programmable synchronous generators, able to provide reliable generation scheduling, spinning reserve, frequency control, and other essential services to the grid. Under this perspective, Combined Cycle Gas Turbines (CCGTs) represent the most efficient way to exploit the fossil fuel potential, so the less carbon-intensive way to guarantee the security of supply. In the future, power-to-fuel could be an interesting storage solution, but today the immaturity of some combustion technologies, the low round-trip efficiency, and the lack of infrastructure to transport the synthetic low (or free) carbon fuel make it difficult to apply.

Alternatively to CCGTs, Open Cycle Gas Turbines (OCGTs) are foreseen to play this role in supporting the transition toward RES-based electricity systems. In fact, they do have not a Heat Recovery Steam Generator (HRSG) and the other steam bottoming cycle components presenting relevant thermal inertias. Consequently, OCGTs are characterized by lower investment costs (from 40 to 50% of CCGTs [85]), shorter start-ups and higher ramp-up rates [MW/min]. Nevertheless, the OCGTs' efficiency is lower, typically about 35%, as a consequence, the fuel cost is increased and the capacity factor reduced, and it is reflected in the Levelized Cost of Electricity three times higher [86]. Although the LCOE does not take into account the economic benefits of flexibility (assessed in Chapter 5) the difference is considerable.

It could be observed that as the transition proceeds also the CCGTs' capacity factor is expected to decrease and so the difference in LCOE could be lower in the future and the

cycle efficiency play a lesser role if compared to the operational flexibility. Nevertheless, there is a relevant already existing capacity from CCGTs that may support the electricity system in the future, and retrofitting options enhancing their operation[7] are particularly interesting at this stage.

Then CCGTs are expected to operate flexibly and shift their historical role from providing base-load power to providing fluctuating backup power to control and stabilize the grid, operating fewer hours, and performing more start-ups/shutdown cycles in order to prioritize the RES dispatch and cut the GHG emissions [87]. Nevertheless, such an extremely flexible operation may have an economic and environmental impact. the economic impact of the extreme flexibilization of traditional programmable generators, such as CCGTs, is known and investigated by many authors. The intermittent operation and the fluctuating load are reflected in increased maintenance costs and lifetime consumption. But flexibilization may also have environmental consequences since increased pollutants emissions, such as carbon monoxide and nitrogen oxides (CO, NO_x), are associated with transients (e.g., start-ups and shutdowns). Despite the operative hours reduction, the balance of the overall emitted pollutant mass is uncertain. Section 2.3 carries out a complete assessment based on real data of operation and emissions.

The regulatory framework is more and more market-based for both the energy and the services needed by the grid. As explained by section 1.1.1 the dispatching selection criterium is the offers economic merit order, since the RES operates with low or null marginal cost [86] it becomes challenging for CCGTs or other programmable power plans to enter the market. The CSS, i.e., the profit margin of a CCGT power plant on the market, turns out to be a pivotal parameter. As reported by Section 5.1, within the negative, null, or not long-term reliable CSS the traditional business-oriented power generation for the energy market is compromised.

As a consequence, the investment in programmable capacity is often discouraged within this market context, and often dismission and mothballing of existing plants occur [88,89], posing a serious threat to the security of supply. To avoid this risk many countries have implemented policies to support the programmable capacity able to provide services to the grid. One of the most popular is the capacity market. The capacity market is a market-based tool employing which the needed capacity is supplied to the TSOs [90,91]. The capacity market has been implemented in the United Kingdom, Poland, Ireland, France, and Italy, and is at the moment under implementation in Belgium. Out of Europe, it is used in some electricity markets in Australia and North America. Other policies and market tools designed for the same purpose are the capacity subscription and the strategic reserve capacity [92,93].

All these instruments should be carefully implemented in order to support just the capacity which is essential for the pursued adequacy level. An oversubsidizing of this kind of capacity may lead to the paradoxical result of slowing down the energy transition towards a decarbonized economy.

[7] From the flexibility enhancement point of view, CCGTs, unlike OCGTs, present an interesting invariability of efficiency on inlet air temperature that could be exploited by inlet conditioning devices as proposed in Section 4.1.

1.2. Current Heating supply context: decarbonization strategies

The heating share of global final energy consumption was about 50% in 2021 [94], then the sector decarbonization is very important within the energy transition scenario. While cooling is highly coupled with the electricity sector, since electricity is the main source to drive the air conditioning and chiller devices, heating is often defined as a sector hard to decarbonize because most of the heat today relies directly on fossil sources and it is often decentrally generated by small units. So the shift to decarbonized technologies is complicated since the owner of the dislocated small units must be persuaded to adopt an alternative low (or free) carbon technology, within a market-based economy these alternatives are supposed to be cheaper to be adopted on a large scale. The German trend of RES implementation can give an idea about how different are the results achieved within the electricity and the heating sectors, comparable developments can be observed in other industrialized countries. In 2016 the share of renewables in gross power generation was nearly 32% in Germany, up from around 3% in the early 1990s. In contrast, concerning final energy demand for heating and cooling the RES share was only around 13% in 2016, up from 2% in 1990 [95]

The strategies mostly adopted to reduce the environmental impact of heating are:

- Sector coupling and heating electrification
- Efficient heat generation, distribution, and use, including condensing boilers, solar collectors, Combined Heat and Power (CHP) generation, waste heat recovery, and District Heating Networks (DHNs) for distribution

According to the IEA to reach carbon neutrality by 2050 the share of heat pumps, low-carbon district heating, and renewables-based heating must exceed 80% of sales in 2030. Figure 1.9 points out how after years of slow but steady decline, the share of coal, oil, and natural gas boilers in global heating equipment sales fell under 50% [94].

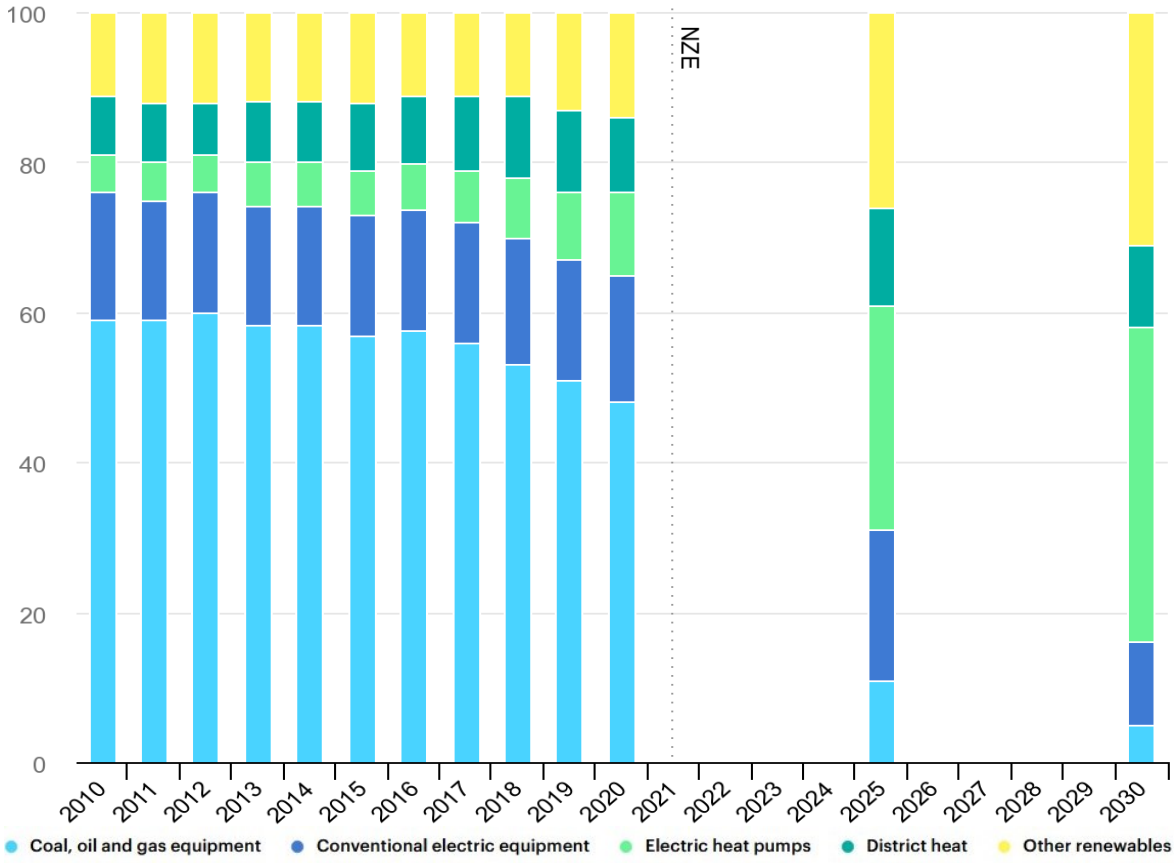

Figure 1.9: Heating technologies sold globally for residential and service buildings 2010-2030, 2025, and 2030 values are simulated according to the scenario towards the 2050 carbon neutrality [94].

1.2.1. Heating sector's coupling

Generally speaking, it is common to refer to "sector coupling" to indicate the interconnection of the sector, which has traditionally relied on other sources (such as heating or transport), to the power sector. It may be defined also as "power to heat" or heat electrification. The process is considered to be essential for a deep decarbonization of heating [96,97].

Moreover, power to heat technologies may provide elasticity to the electrical demand [98,99], this is today a debated issue since if not properly managed the massive electrification of the heating systems may increase the demand for electricity within some time of the day since the need for heating is almost simultaneous for most of the residential buildings. It would require a lot of power capacity to be installed, but then this capacity may be unused when there is no demand for heating (during low demand hours or warm seasons), and it may be reflected in the risk of not paying back the new capacity investment or in very high electricity price during the peak demand hours. But if the power to heat system is carefully implemented and managed, including energy storage[8] or exploiting the building

[8] Thermal Energy Storage (TES) are commonly simpler and cheaper of batteries and other electro-chemical devices to store electrical energy. So TES application are growing for demand side management purpose. More commonly the storage time is in the order of hours or few days, but

thermal inertia as storage itself, and the market has an effective design able to provide proper price signals to the final user, the heating sector coupling may be beneficial also for a deep RES penetration in the electricity generation. Section 1.1 outlined how the growing penetration of renewable energy sources, mostly non-programmable and inverter-based, requires more and more demand for services and demand response, under this perspective poly-generation technologies, smart grids, and advanced power management strategies could give a substantial contribution to the decarbonization of bot electricity and heating sectors [100].

The complete array of technologies available to convert the electricity to heat has been well revied by Bloess et al. [96], but heat pumps are the most promising, and their widespread it's giving a real chance for a relevant coupling of the heating sector [101,102], heat pumps are presented and described into details by the Chapter 3 of this thesis while this section aim just to briefly introduce the sector coupling concept.

The benefits of heating electrification in terms of carbon intensity are of course correlated to the average carbon intensity of the power generation. If all current fossil-fueled heat generation technologies were replaced by heat pumps overnight the combined emissions of the heat and power sector would be reduced but the benefit quantification depends on the local electricity grid. If the heat is generated by and heat pump with a COP of 2-3, reasonable for air sourced HP in a cold climate (ref. Chapter 3), and the heat pump is fed with the electricity of a coal-based power plant with a 30-35% efficiency, then the results are comparable or even worse than what a condensing gas boiler emits to supply the same amount of heat. The Joint Research Center of the European Union assesses that the benefits would be about a decrease in carbon dioxide emission by 16% on average in the EU but reports heterogeneous results among the member states. The biggest potential is found in FR, a strongly nuclear-based electricity system, with 65%, and the lowest potential in PL and EE, coal-based economies, with 4%. Without additional "clean" capacity additions the additional electricity demand for heating will be mainly generated by dispatchable sources which usually have a higher emission rate than the average electricity generation mix and the environmental potential of heating electrification may be reduced.

1.2.2. Waste heat recovery

Many purposes for which large amounts of heat are required, especially in the industry sector[9], need it at high-temperature levels. When the heat has utilized its potential at some level and the temperature falls below the value required by the specific application, unless the heat can be supplied to other users at a lower thermal level at the site, it will be wasted and dumped into the environment. The interest in recovering such waste has been strong for decades [103] but in the last year, the growing fuel prices and the effort in reducing global GHG emissions boost the research and the applications. Additionally, in the last years, the exponential growth of demand for data centers cooling has been observed, the cooling medium exits the data center at a warm temperature with a relevant heat potential if the vastity of the source is considered [104].

---

seasonal thermal energy storage are also investigate as a further step for decarbonize the residential heating sector [237].

[9] Most heat demanding industries include, but are not limited to, cement, ceramic, iron and steel, refineries, glassmaking, chemicals, paper and pulp and food and drink.

The waste potential is normally divided between the high-temperature waste heat recovery (>400 °C)[10], medium-range (100-400 °C), and low-temperature (>100 °C). Usually, most of the waste heat in the high-temperature range comes from direct combustion processes, in the medium range from the exhaust of combustion units, and in the low-temperature range from parts, products, and the equipment of process units [105]. The waste can be exploited for three different purposes. (i) Heating purpose, so the heat is redirected to the new user, if required, improving its thermal level by heat pumps. (ii) Mechanical or electrical purpose, utilizing the technology which best suits the waste temperature, the heat can be recovered in form of mechanical and electrical energy. Organic Rankine Cycles (ORC) are a fast-developing technology that meets this demand [106]. (iii) For refrigeration or cryogenic purpose exploiting adsorption refrigerators. The highest is the temperature the easiest is the recovery for all the aforementioned purposes, e.g. the influence on the heat pumps performance is well described by the Chapter 3, while Chapter 2 mentions how the waste of heat is reduced in a Combined Cycle Gas Turbine (CCGT) with respect to an Open Cycle Gas Turbine (OCGT) and how the thermodynamic cycle differs to get higher temperature out of the turbine and facilitate the heat recovery through the Heat Recovery Steam Generator (HRSG).

Jouhara et al. [107] reviewed all the available technologies for waste heat to heat and waste heat to power recovery, highlighting that the selection of heat recovery methods and techniques largely depends on key factors such as the quality, quantity, and the nature of heat source in terms of suitability and effectiveness. However, it is also shown that heat pumps best suits medium and large amounts of low-temperature waste heat recovery, as it gives the capability to upgrade waste heat to a higher temperature and quality. Since heat pumps intrinsically imply the heating sector coupling, the use of this technology for low-temperature waste heat recovery is particularly interesting because it may allow combining the benefits presented by the previous subsection with a deep energy efficiency improvement which would follow a systematic recovery and exploitation of low-temperature heat sources.

In order to quantify the described potential Forman et al. [108] systematically applied a novel top-down approach for the estimation of waste heat in the most common sectors of end-use (transportation, industrial, commercial and residential) including electricity generation on a global scale. The results pointed out that 72% of the global primary consumption is wasted, and transportation and electricity reported the highest values (81% and 61% respectively). Moreover, on average 63% of wasted heat is classified as low-temperature, within the electricity sector the low-temperature share reaches 88%[11].

1.2.3. District Heating Networks

The waste heat recovery potentialities have been explained by the previous subsection, however, these wasted resources are often far from the residential areas [109,110]. Moreover, the integration of flexible and clean energy sources into the energy mix could be challenging at the individual building level in urban dense areas. For this reason the centralizing of the heat generation is generally considered auspicial, furthermore, a centralization would reduce the number of stakeholders that newly designed policies would involve, and it will make easier their implementation. Centralizing the heat generation also implies developing networks to transfer that amount of heat from the generator to the user,

[10] Sometimes 300 °C is proposed as threshold value.

[11] Waste heat in the electricity sector is mostly discharged as exhaust or effluents, 80% [108].

such networks are commonly defined ad District Heating Networks (DHN)[12] which is a technology implemented since the 1870s than could today play a pivotal role in the sector decarbonization [111].

China, Russia, and Europe are responsible for more than 90% of global DHN production, and therefore critically influence the current average carbon intensity of district heating. The International Energy Agency has defined the DHNs as an important part of heating sector decarbonization but today the sector is classified as "not on track" to reach the 2050 targets [112]. The combined share of renewable sources and electricity in global district heat supplies together should rise from 8% today to about 35% in the current decade, China DHN carbon intensity is the highest, 29% higher than the world average. Moreover, the share of DHN on the overall heating demand is almost constant since 2000, although building area has increased by 65% over the same period. It means that DHN adoption for new buildings does not increase despite the effort in reducing GHG emissions. The countries with the highest growth rate are China and Korea, with +7% each in 2020, In Northern China especially DHN is considered essential to improve the air quality during the heating season [113].

Usually, DHNs rely on a combination of several generators together, most of them are fossil fuel-based today. In particular, cogeneration plants (e.g., Combined Cycle, Internal Combustion Engine, and Steam power plant) are usually adopted to cover the base of the thermal load while Heat-Only Boilers (HOBs), whose Levelized Cost of Heating (LCOH) is normally higher, cover demand peaks or supply back-up generation. Thermal Energy Storages (TES) are commonly integrated within the networks as well for effective demand management. Even centralized heat generation, using larger combustion units with higher energy efficiency and more advanced control over air pollution is a benefit itself the DHN potentialities are not limited to this.

Many networks have successfully integrated renewable energy sources. RES with the highest potential to be employed in district heating systems are solar thermal, geothermal, and bioenergy. Bioenergy currently accounts for the largest share of renewable district heat supplies, especially for use as a conversion fuel in old plants or areas with high biofuel availability (e.g., biomass-rich mountain areas) [112]. Copenhagen covers 95% of the demand by bioenergy (biomass and waste) [114], while Silkeborg, Denmark, has a relevant percentage of demand covered by solar thermal production, up to 20%, with 110 MW_{th} installed capacity [115,116].

DHN technology has been improved for more than a century since its first application, Lund et al. [117] reviewed the development of the networks concerning the supply temperature, piping insulation, energy sources, management strategies, and ability to be used also as a cooling network. Based on these features they identify four different DHN generations, as illustrated in Figure 1.10. The division into four generations is widely accepted and used, even if the concept for the fifth generation has been presented such as a network operating at ambient temperature and using distributed heat pumps [118]. In the end, low-temperature DHNs are appreciated for their low carbon intensity potential achievable through RES integration, heat losses reduction and the potential for large heat pumps efficient operations [119].

[12] Others acronyms are also common such as DH or DHC for those network used also for cooling supply.

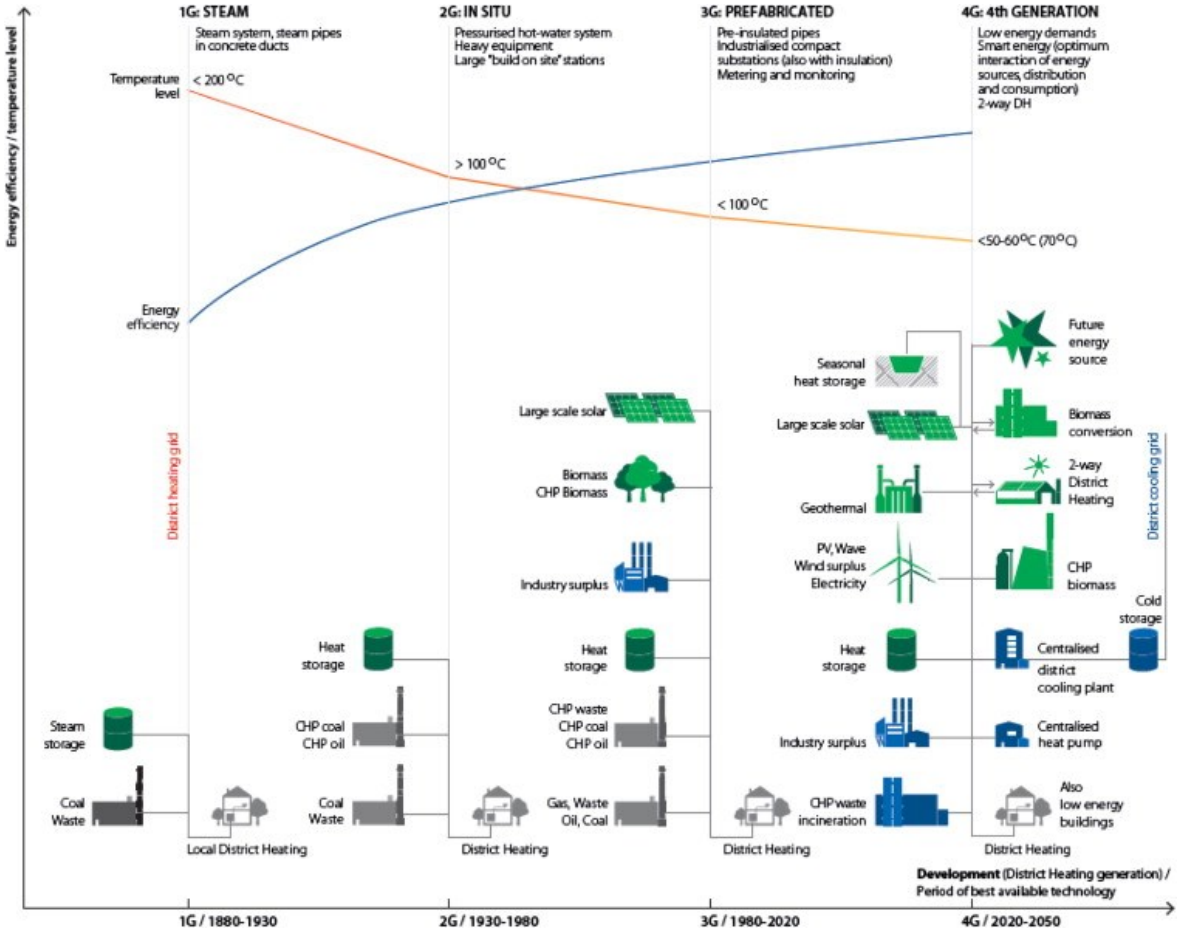

Figure 1.10: Illustration of the concept of DHN generation [117].

1.3. Concluding remarks

This chapter has described the current context of energy, focusing on the heat and electricity sectors that are addressed by this thesis. What characterizes the energy today and is expected to characterize it in the future is the pledge for GHG emission reduction. Then science and engineering are required to provide cost-efficient and low-carbon solutions for generating heat and power.

Power generation is probably the most addressed sector by decarbonization policies, and some electricity systems have increased their share of renewable energy sources up to considerable levels. Nevertheless, this poses serious challenges, which should be solved in order to low further the average carbon intensity rate. Major issues concern the management of a system highly penetrated by inverter-based and non-programmable generators. Section 1.1 explains that synchronous generators are currently essential, at the least to provide inertia, frequency response, and other services to the grid, ensuring the security of supply and allowing further RES capacity installation. Heating is commonly considered harder to decarbonize than power, but Section 1.2 points out how heat pumps and district heating networks have a key role to play in the energy transition.

This summarizes the motivation of the present thesis. Among the available dispatchable energy generator technologies existing CCGTs and maybe new highly flexible OCGTs are supposed to support the manage the electricity system, balancing the load, and regulating the

frequency. The Firsts are characterized by high costs of investment, so even if are considered the best available technology in terms of fuel energetic potential, no relevant amount of new capacity from these generators is expected to be installed in the next year, especially in developed countries. The latter are cheaper and characterized by high operational flexibility, but less efficiency and so reporting higher specific emission rates. Relying on existing CCGTs is the best solution in terms of cost-effectiveness, while OCGTs may play a more relevant role in the last stage of transition when most existing CCGTs would have expired their lifetime and the reduced use of fossil fuel generators will not allow the viability of new expensive fossil fuel generators, especially if not flexible as OCGTs.

Since Combined Cycle Gas Turbines has still a role to play, their efficiency should be maximized in order to reduce their variable cost and carbon footprint. As described in Chapter 2, CCGT inlet air conditioning can be an effective way to achieve an improvement in both efficiency and flexibility, highest global efficiency rates are obtained using CCGTs as Combined Heat and Power generators. Heat pumps and CCGT coupling offer an interesting perspective for both these applications, then different coupling layouts will be explored in the following chapter with the aim to provide a flexible generator for low-carbon intense heat and power able to provide services to the grid, which could be viable within the current and future energy markets.

2. Combined Cycle Gas Turbine: an overview of Power Oriented and Combined Heat and Power applications

As the first chapter has highlighted the key role of CCGTs, the second chapter faces in detail this technology. Section 2.1 presents the state of the art and provides the basic principles for understanding the following section and chapters. It focuses on the Heat Recovery Steam Generator layout, the emissions, the technology development of the core element: the Gas Turbine, and the influence of the intake temperature. Then Section 2.1 describes how CCGTs are applied to CHP purposes. The last two sections (2.2 and 2.3) report two studies carried out in order to assess the environmental impact of a CCGT under the flexible conditions under which it is required to operate nowadays and the potential benefit of inlet heating conditioning for off-design efficiency enhancement.

2.1. Technology: state of the art

Gas turbines' exhausts have a relevant energetic and exergetic potential which is dumped into the environment by common open cycle machines (OCGT). However coupling steam cycles to gas cycles most of this potential can be recovered, within the most common and widespread layout the gas turbine exhaust, by means of a Heat Recovery Steam Generator (HRSG), generates the steam feeding a steam turbine which generates extra power improving the efficiency. So the gas cycle and the steam cycle are commonly referred to as the topping and the bottoming cycle respectively.

Coupling the two cycles into a Combined Cycle Gas Turbine (CCGT) achieves much higher efficiency[13] with respect to an OCGT or a conventional power plant driven by a steam turbine. The CCGTs widespread revolutionized the power generation industry in the late 80s and 90s leading to the oil phase-out first and more recently the coal. The CCGT technology rapidly spread also because of the possibility of retrofitting existing power plants, replacing the old steam generator with a gas turbine and an HRSG. Some CCGT, classified as "fired" implies a second combustion process between the topping and the bottoming cycle [120]. This thesis focuses on the most common unfired CCGT where the only combustion is the one that takes place in the gas turbine's combustion chamber.

To maximize heat recovery efficiency, the bottoming cycle works on different pressure levels. Three pressure levels with a reheat, schematized in Figure 2.1, are today considered the standard layout for industrial applications. Finally, it's common to combine more than one[14] GT and its own HRSG to the steam turbine (or steam turbines for multiple levels CCGTs), it is reflected in advantages in terms of steam turbine efficiency [120], flexibility, and off-design management improvement [121].

---

[13] The modern CCGT are able to reach peak efficiency within the order of 60%, the Chubu Electric Nishi-Nagoya power plant powered by a GE's 7HA.01 gas turbine claims for the world highest efficiency ever with 63.08% [238]. Table 5.1 at page 21 reports the annual average efficiency of CCGT power plant installed in Italy.

[14] Typically two, it's common to refer to this layout as "2+1 CCGT".

Combining the gas turbine to a bottoming cycle implies some difference in the gas cycle optimization. The GT compressor's pressure ratio, β, reaches considerable levels for an OCGT, since the higher it is the lower the exhaust temperature and the heat dumped into the environment; β is limited to 20-30 to keep the specific work higher than a minimum acceptable value. In a CCGT a higher temperature at the gas turbine outlet is appreciable since it enhances both the power and the efficiency of the bottoming cycle. Thus optimal β values for a CCGT are lower and limited within the 15-20 range.

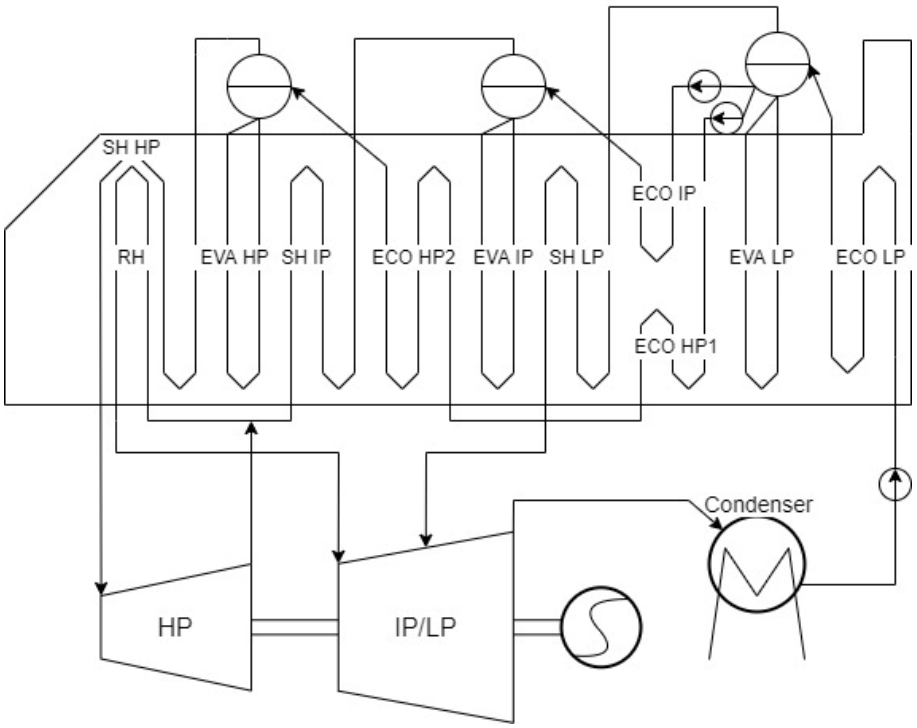

Figure 2.1: Three pressure levels with reheat CCGT's HRSG and bottoming cycle.

The combustion process involving natural gas and ambient air takes place in the combustion chamber. Excess air ratios are normally much higher than other combustion technologies since the temperature of gasses at the turbine inlet should be kept low enough to guarantee a reasonable lifetime for the turbine. So a relevant amount of air does not take part in the combustion but it's used for dilution (secondary air) and turbine cooling purposes. In addition to the carbon dioxide issue, largely discussed in the previous chapter, other pollutants are generated by the combustion processes: e.g., nitrogen oxides (NO_x), sulfur oxides (SO_x), carbon monoxide (CO), and particulate matter (PM). Ammonia (NH_3) can be emitted if a $DeNO_X$ Selective Catalytic Reduction (SCR) is installed, as ammonia is used in the process a part of it is conveyed in the flue gases These pollutants are hereby referred to as "local pollutants", in contrast to those GHGs (e.g., carbon dioxide) which have not an impact on the local environment but pose a global threat for their global warming potential.

Focusing on local pollutants, a CCGT power plant emits mainly NO_x and CO, while SO_x and PM are not relevant because there is no sulfur within the natural gas and the combustion of a gaseous fuel does not produce PM. However, the emission rate of the former two pollutants is strongly dependent on the gas turbine operating conditions: the NO_x formation is favored by high combustion temperatures, thus it results to be maximized at full-load operating conditions, while the CO is due to an incomplete combustion process at low

temperatures so it is most emitted during partial-load operating or start-ups [122]. During start-up due to the not even flow distribution, both CO and NO_x are generated The environmental impact of a CCGT power plant is fully assessed by Section 2.3.

Concerning the core element of a CCGT, the gas turbine (GT), the historical development is summarized in order to introduce some nomenclature, hereby used in the thesis. During the 20th century, especially within the second half GTs technology deeply developed [123] but a significant milestone is represented by the first F-class machine (GE 7F) installation by GE at Virginia Power's Chesterfield No. 7 Station in 1990 with an efficiency of 45.2% at ISO with a TIT of 1260°C and a total power output of 214 MW in the combined cycle mode (Note, in a simple cycle mode, this unit was rated at 150 MW and 34.5% efficiency) [124]. Almost all the CCGT powerplants built later are driven by an F-class turbine or following. Since that day the cycle efficiency has been improved significantly, even beyond the limit of 60%.

Historically, gas turbines have been divided into classes defined by power output, operating temperatures, and pressure ratio. With advances in materials and cooling technologies, gas turbines have been able to operate at higher temperatures with better performance. When a manufacturer made significant enough improvements to increase power and efficiency, a new class of turbine was defined. From the F-class onward the definition became murkier, last developed F-class turbines perform significantly better than the first prototypes. Today's classes can be generically divided into three areas based on size, efficiency, and OEM. Focusing on size, Class D and E turbines are typically in the 75 to 110 MW range. Models include GE's 7E.03, Siemens' SGT6-2000E, and Mitsubishi Hitachi's H-100, among others. F-class turbines are typically in the 170-230 MW range. Examples are GE's 7F.03-.05, Siemen's SGT6-5000F, Ansaldo AE94.3A, GT26, and Mitsubishi Hitachi's M501F. Finally, advanced class turbines (G, H, and J) are typically in the 275-350 MW range [125]. These include Mitsubishi Hitachi's M501J and M501G machines, Siemens' SGT6-8000H, Ansaldo's GT36, and GE's 7HA.01 and .02 models. As indicated by Figure 2.2, in the mid of 2000s the sales growth of advanced class turbines begins until around 2015 they overtook the F-class as the market leader product.

Nevertheless, despite the availability of advanced classes, F-class turbines maintain a relevant market share since sizes greater than 500 MW may be not needed or the site would require significant and costly transmission upgrades to enable the larger units. Additionally, the F-class already installed fleet is a good test case for refit operations finalized to the efficiency enhancement. For these reasons the studies presented in this thesis consider F-class turbines.

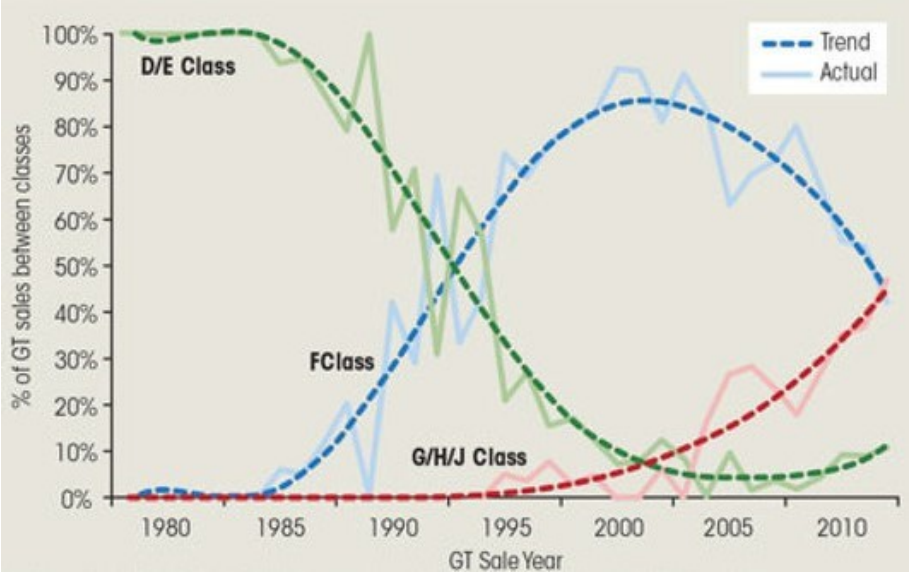

Figure 2.2: Gas Turbine classes market share, historical trend [126].

2.1.1. Influence of Air Inlet Temperature

The dependence of GT performance on atmospheric conditions (i.e., temperature, relative humidity, and pressure) is well known and documented in the literature, while less information is available concerning the effect of temperature on the complete Combined Cycle. Tiwari and al. [127] claim that the combined cycle loses its efficiency by about 0.04% for every 1°C rise in ambient temperature. Sorce et al. [128] performed a full numeric assessment by means of a Gate-Cycle model developed by the gas turbine OEM Ansaldo Energia, which can be reasonably extended to a generic F-class CCGT.

The change of GT inlet temperature affects the power output and the efficiency of the gas turbine for three reasons:

- The changes of intake air density, in such a constant volume engine, influence the mass flow and thus the gas turbine power output;
- The specific power consumed by the compressor increases proportionally to the air intake temperature;
- The increase of the intake temperature leads to pressure ratio reduction which, in a machine operated at constant Turbine Inlet Temperature (TIT), results in Turbine Outlet Temperature (TOT) increase, and thus GT efficiency reduction.

However, increasing TOT improves bottoming cycle performance (ref Section 2.1). Therefore, an increase in air temperature has a slight positive effect on the combined cycle efficiency by compensating for the reduced efficiency of GT [129]. As a result, the efficiency variation is almost flat at high temperatures, losing just 0.25% at 5°C, when decreasing temperatures. On the other hand, the impact of the increasing temperature on the power is mainly linear with an effect of 0.32% per 1°C [128]. The main outcomes of this article are well synthesized by Figure 2.3 which describes how the ambient temperature affects the power output and the efficiency at various turbine loads (i.e., different IGV opening ratios).

The model on which Figure 2.3 has been drawn considers a Water-Cooled Condenser (WCC), which temperature is constant at 15°C, otherwise if the condenser is Air Cooled (ACC) the ambient temperature has a twofold effect. On one hand, it results in the phenomena pointed out above, but moreover, it affects directly the bottoming cycle utilizing the condenser temperature. Therefore for CCGT with ACC, an increase in ambient temperature would lead to a decrement in efficiency, since the bottoming cycle's backpressure rises with a direct influence on the recoverable power.

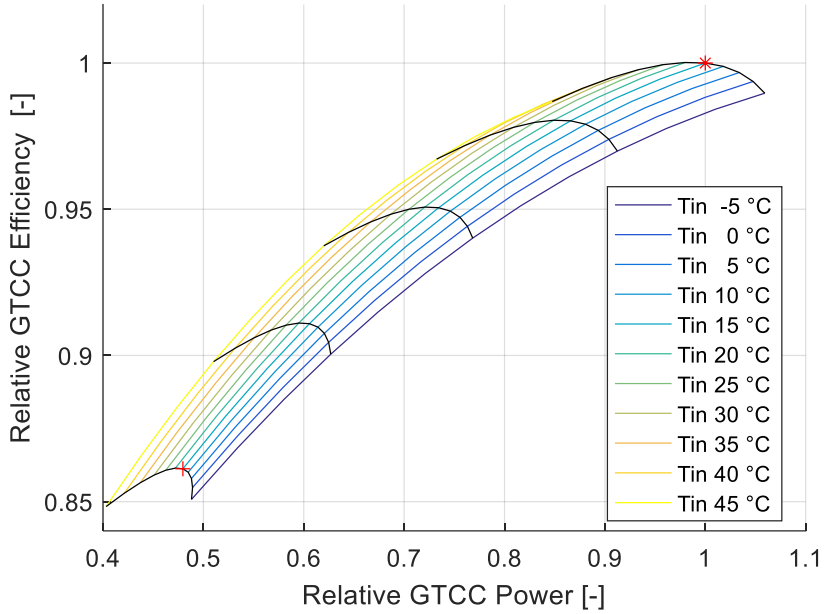

Figure 2.3: Off-design average F-Class based CCGT Performance with GT intake Temperature as parameter (colored); Black line (40%, 55%, 70%, 85%,100% of the GT percentage load [128].

2.2. CHP Applications

The opportunity of combining power and heat generation is well known for decades and not limited to the gas-fired power plant. It could be generally extended to all those combustion processes oriented to the power generation, through different layout solutions a fraction of this heat can be directly dedicated to the fulfillment of thermal demand. Is it also possible to exploit this potential to satisfy also cooling requests, this practice is defined as tri-generation and it is out of the scope of this thesis. Nowadays, within the policy and market context described in Chapter 1, the interest in Combined Cycle power plants operating in Combined Heat and Power (CHP) mode are increasing. The electricity market, especially if highly RES-penetrated, could be not viable enough to pay the investment back (ref. Section 1.1.1 and Chapter 5) but CCGTs-CHP are considered more economically sustainable thanks to the revenues from the heat production, which price is considered to be more stable and profitable [130]. So cogeneration brings potential advantages to the plant owner in terms of the viability of the investment, but its spread is positive also from the transmission system operator's point of view. In fact, even in less profitable conditions over the electricity market, such plants are usually maintained operative in order to satisfy the thermal demand, creating a useful backup capacity for grid resilience.

CHP power plants are usually installed close to an industrial site to satisfy high-temperature process steam demand, or close to a residential area to provide low-temperature heat, via District Heating Networks (DHNs). The co-production of electricity and heat in the CHP plants allows a reduction of carbon dioxide emissions compared to separated generations. Moreover, since centralized heat generation implies larger units, higher energy efficiency can be achieved [111].

A Power Oriented (PO) power plant, i.e., devoted only to the power generation, produces power supplying pressured steam to a turbine, and the condensation power is pure lost power, the condensing temperature is too low to allow further exploitations. This can also be applied to a CCGT's bottoming cycle. While CHP power plants utilize heat power coming out from the steam turbine, supplying the steam to the thermal user which can be can be either a DHN or an industrial manufacturing process. In industrial power plants typically more than one pressure level for process steam is needed. So the back-pressure control to provide the proper amount of steam at the required temperature is more complicated but the basic concept is the same: a fraction of steam will provide heat rather than flowing in the turbine and generating power [131].

Looking at specifically the CCGT-CHP applications Lee et al. [132] and Jarre et al. [133] provide some examples of how the steam is extracted from the bottoming cycle for the heating generation purpose. The steam is normally extracted at an intermediate pressure, at the IP pressure discharge, or during the IP expansion. Figure 2.4 schematizes the layout for a generic CCGT-CHP with three pressure levels and reheat. The HP steam generated by the HRSG expands through the HP steam turbine, which outlet at the intermediate pressure level is redirected to the HRSG, mixed with the steam from the IP steam drum, and superheated. The superheated IP steam flow through the IP steam turbine and then mixes with the LP steam from the HRSG. At this point it can be directed to the LP steam turbine or a fraction can be used within the DHN Heat Exchanger (DHN-HX). Then, the steam condensates within the conventional bottoming cycle condenser (cooled by air or by water depending on the specific power plant) or within the DHN-HX. The two condensate flows are mixed before entering again the HRSG. The fraction of steam extracted and delivered to the DHN-HX depends on the plant's operation mode and it can be variated in order to cope with the thermal demand. Generally, a minimum amount of steam is however forced to flow through the LP turbine in order to cool down the blades and the rotor [134]. More sophisticated techniques of extraction can also be adopted, for example, the so-called "3GT" CCGT of the Moncalieri power plant in Turin (Italy) uses two steam extractions. Lower pressure steam is extracted at the IP ST discharge and it heats up the DHN water from the returning temperature (70 °C for this specific case) to an intermediate level. A second extraction is performed at a higher pressure so the steam has a higher temperature and it is used within a second stage of the DHN-HX to heat the preheated water up to the supply temperature (here 120°) [134].

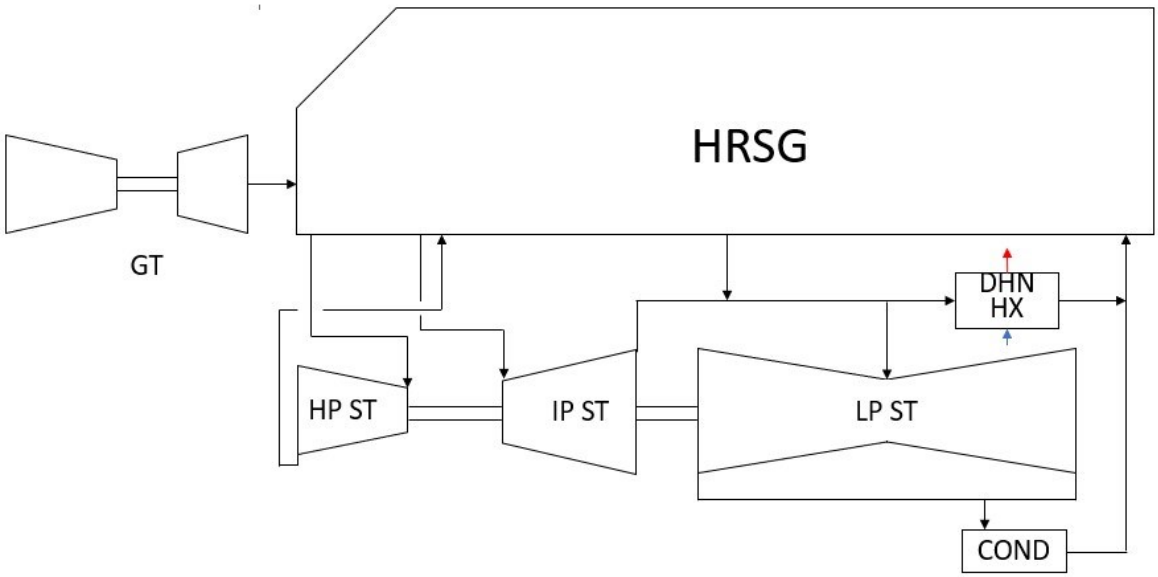

Figure 2.4: Generic scheme for a CCGT-CHP.

Extracting steam from the bottoming cycle and redirecting it to the DHN-HX implies a cost in terms of power lost and turbine efficiency since a lower amount of steam flowing through the LP steam turbine will generate, of course, less power moreover the turbine operating condition will be further away from the design point performing worse. The Power-Heat diagram, also known as Iron Diagram, such that in Figure 2.5 is commonly used to report a CCGT-CHP operational range. It shows how progressively extracting steam, and keeping constant the gas turbine load, the thermal power output increases while the power output decreases. Has previously illustrated, there is a limit in steam extraction highlighted in the figure by the red line. It is important to remark how this limits the operational range of the power plant, the thermal output is not independent of the GT load, indeed the maximum thermal output is available only at full-load conditions. Analogously if the lowest adoptable GT load is fixed by the carbon monoxide emission, the lowest electrical output depends on the thermal load. Labels in the figure report the global efficiency of the plant as defined by equation (2.1) where LHV is the lower heating value of the fuel and the numerator expresses the overall useful plant's output.

$$\eta_{global} = \frac{P_{el} + P_{th}}{LHV \cdot \dot{m}_{fuel}} \tag{2.1}$$

Increasing the thermal power output the global efficiency increases, since to be converted into electric power the steam energetic potential must be multiplied by an efficiency factor (i.e., the product of the turbine's isentropic efficiency, the turbine's mechanical efficiency, and the generator's electrical efficiency). Otherwise, if the steam is otherwise used for heating purposes its potential can be considered pure, it will be transferred to the user entirely (at the least neglecting thermal losses within the piping and the DHN-HX).

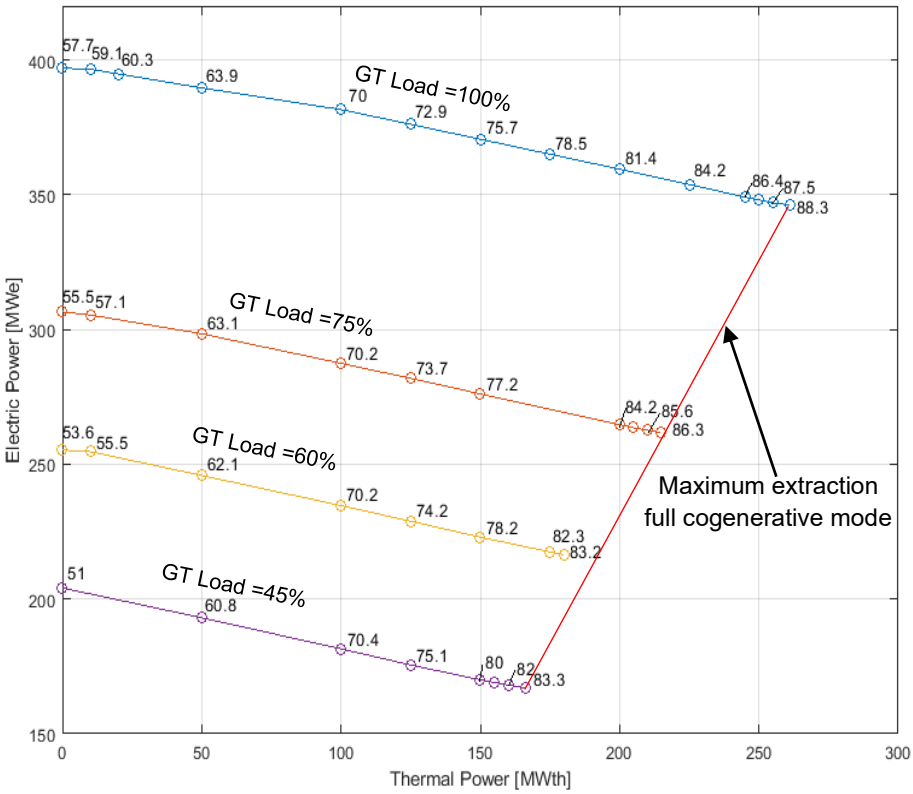

Figure 2.5: Power-Heat Diagram, Iron Diagram, for an F-class CCGT. Global efficiency is reported by labels, while the red line highlights the extraction limit.

Thus, most CHP plants rely on the concept that to provide a thermal output an amount of power has to be sacrificed for that purpose. The concept is not far from that normally applied to power-to-heat systems, known as Coefficient of Performance (COP). The COP (ref. Chapter 3) expresses the ratio between the thermal power and the electrical power which is needed to generate it. As COP for power to heat, for CHP plants is defined the Z factor, equation (2.2). The Z reciprocal is sometimes adopted and known as the power loss factor [135].

$$Z = \frac{\Delta P_{th}}{\Delta P_{el}} \tag{2.2}$$

Where the ΔP is intended to be positive and negative for thermal and electrical power respectively. Z is then analogous to the COP at all and, even if less used, is in this thesis preferred to the power loss factor since it allows immediately comparing CHP and power-to-heat technologies. The main difference between the COP and Z is that the denominator term of Z represented a missed generation, while on the COP it is an electrical consumption. Figure 2.6 shows that the Z factor is not constant on the Iron Diagram, it depends on the operating condition. Very high values are achievable at GT full load and low thermal output because a steam extraction will cause only slightly off-design operation of the LS steam turbine. As a rule of thumb, the far we are from the nominal condition the more the heat production will cost in terms of electricity. In other words, the power loss factor can be visualized as the inverse of the slope of iso-GT load lines on the Iron diagram.

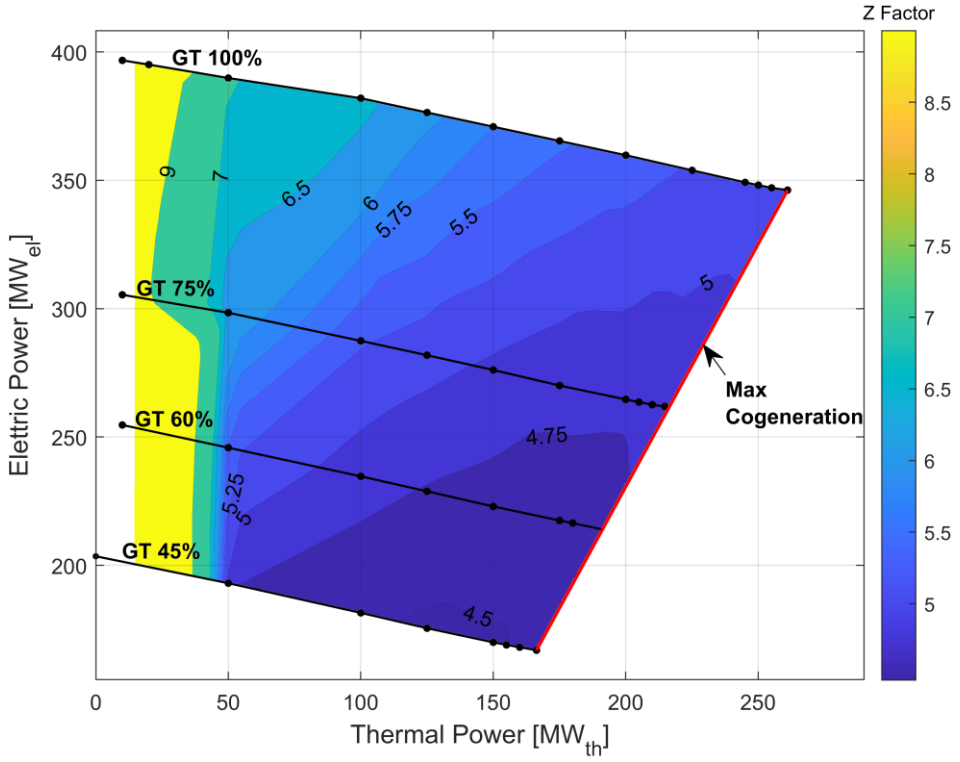

Figure 2.6: Z factor contour on the Power-Heat (Iron) Diagram. Calculation outputs on Moncalieri power plant (Italy) second CCGT.

Concerning a real CCGT-CHP power plant operation, Figure 2.7 shows that not all the Iron diagram operational area is equally exploited. Within the area bounded by red lines, the plant does not operate for the following precautionary reason. Electric generation is defined by the market and variation in the amount of energy delivered to the grid, scheduled or required, causes the application of economic penalties. Thermal production is defined by the DHN users. In case of reductions/anomalies of thermal demand, gas turbine load and steam extraction should increase/decrease to balance the thermal demand keeping the electric generation constant. However in the red area, the gas turbine is already at its minimum load, therefore there is no way of compensation apart increase/decrease the electric output causing unbalances [134]. Moreover, is possible to observe how the intermediate loads are less adopted and the plant is mostly operated at minimum or maximum load. Generally, if the market price for electricity is higher than the plant's marginal cost the power output is maximized to increase the sold electricity and the profits, otherwise is better to turn off the plant and avoid economic losses. Nevertheless, sometimes the off-peak price period is short enough that shutting down and starting up would imply higher losses or, in the case of a CHP plant, it must be on to fulfill the thermal demand. Under these conditions, the plant operates aiming to minimize fuel consumption and the lowest limit is defined by the maximum allowed concentration of carbon monoxide and by the operative logic just illustrated in this paragraph.

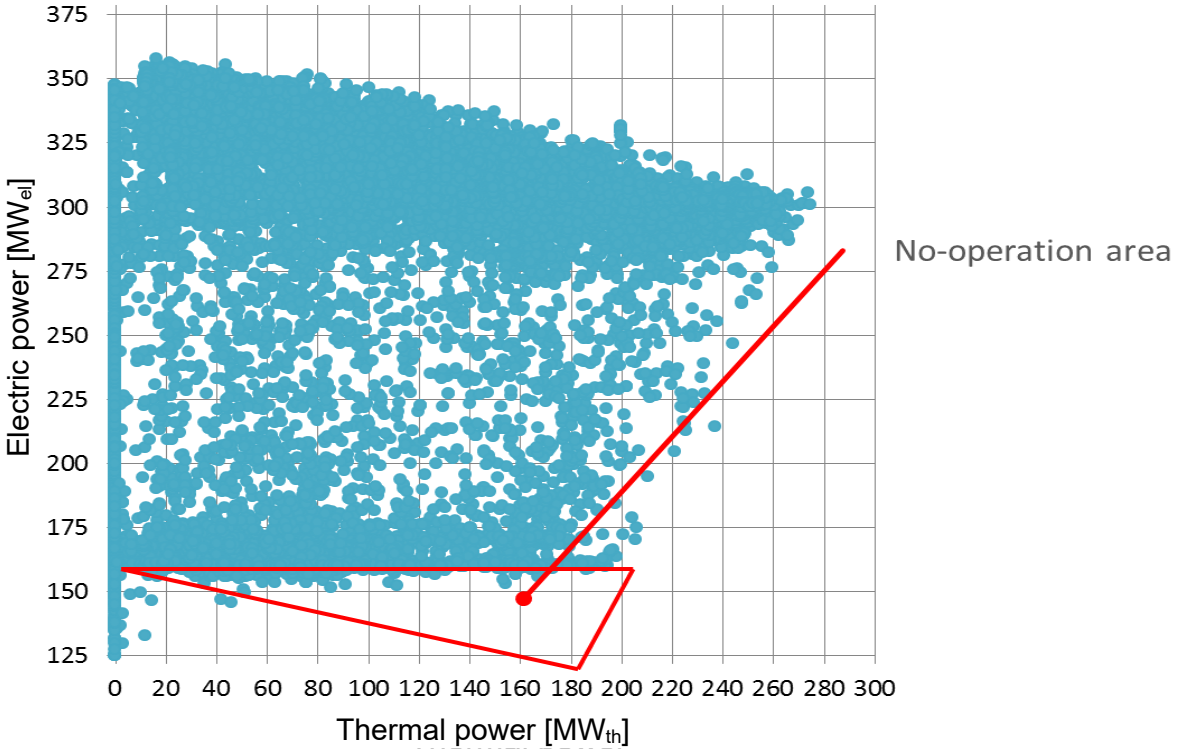

Figure 2.7: Real operating conditions of one year on the Power-Heat (Iron) diagram [134].

2.3. Environmental Impact Assessment of Flexible Operations

Because of their dispatchability and their high efficiency in exploiting the fossil fuel energetic potential, CCGT power plants are today required to provide reliable power supply and frequency regulation (ref. Chapter 1). So they have shifted from their historical duty of supplying an almost constant baseload power throughout the year, providing fluctuating backup power to control and stabilize the grid. This flexibility is reflected in a strong reduction in their yearly operative hours and a drastic increase in start-ups [136]. At the same time, Section 2.1 states that the pollutant emissions strongly rely on the operative condition, and transients (mainly start-ups and shutdowns) reports significantly different emission value if compared to normal operation.

Therefore, the shift of the CCGTs' role observed in the last decades has an influence on the actual plant's environmental impact [137–139]. If a decrease in operating hours is obviously reflected in lower pollutant emissions, the increased occurrence of start-ups could reduce this positive effect by increasing the overall emitted pollutants' mass. To assess the sign of this balance it is needed to properly quantify the emissions even during the start-ups. This value is affected by many parameters such as the residual temperature of the HRSG[15] [138] and of the steam turbine rotor [140] that influences the start-up duration [141]. Also the gas turbine manufacturer, the power plant management itself, or the presence of flue gas post-treatment technologies, (such as the Selective Catalytic Reduction, SCR, or the CO

[15] Steam drums are the most critical components in the HRSG.

catalyzer for the mitigation of nitrogen oxides and carbon monoxide respectively) could affect the quantity of pollutant emitted during the transients.

Some studies have been already carried out aiming at assessing start-up emissions, even for other technologies. Gonzalez-Salazar et al. [138] collected information from manufacturers, academic research, and also from power plant operators, reporting a comparison of the current and future values of specific emission factor at hot and cold starts for different technologies, according to them the emissions during a CCGT start-up are expected to be in the range of 0.02-0.9 kg/MW for NO_x and 0.1-1.8 kg/MW for CO. Suess D.T. et al. [141] reported the monitoring campaign of start-ups emissions of three General Electric gas turbines, during 18 months of operation. The study highlights a strong dependency of the emitted mass of pollutant on the transient duration showing how the emission rate [kg/min] is almost constant while the time required to start the power plant up is strongly correlated to the standstill hours since the last shutdown. Geng Z. et al. [142] developed a NO_x emission model based on CCGT data collected by the Chinese government, assuming a startup duration time between 1 h and 2 h, and an emission curve whose emission rate increases from 0 up to 0.6 kg/min. Finally, Bass R.J. et al. [143] presented experimentally measured data of NO_x emitted by an 800 MW CCGT plant monitored for 4 months, showing how the average pollutant concentration is higher for hot start-ups than cold because of relevant peak (>250 mg/m^3) during the first minutes till the parallel condition is reached.

The scope of this section is to quantify the mass of pollutants (NO_x and CO) due to a CCGT start-up, or shutdown, and the related variability, identifying the most significant variables and the effectiveness of the post-treatment technique during the transients. In order to accomplish this task, real data of the Italian CCGT fleet during 10 years of operation are analyzed, as described in the following section. Finally, employing these data, it is assessed how an increase in CCGT operational flexibility reflects in the local environmental impact with respect to the quantity estimated during the Environmental Impact Assessment (EIA), the Italian *Valutazione di Impatto Ambientale* (VIA).

2.3.1. Real CCGT operational profile

First, the flexibility increase needs to be quantified, the number of annual fired hours and start-ups are effective parameters to describe the CCGT operating. As reported in Figure 2.8, obtained processing GME market data [144] for 2018 and 2019, in recent years (2020 was not considered since the COVID-19 pandemic causes a strong decrease in demand for electricity), CCGTs generally operate according to four different profiles in all Italian market zones. This chart allows the clustering of power plants on the basis of the annual number of start-ups (SUs) and Fired Hours (FH) so on how flexibly they operate. It is possible to identify four clusters:

- Continuous: less than 50 SU and more than 4000 FH annually
- Mid-Continuous: approximately 60 FH for each SU on average
- Mid-Range: approximately 30 FH for each SU on average
- Peaker: more than 200 SUs annually and less than 10 FH per SU

The scatter plot reports, by means of different marker colors, the grid zone to which the power plant belongs (ref Section 1.1.1.1 on page 17).

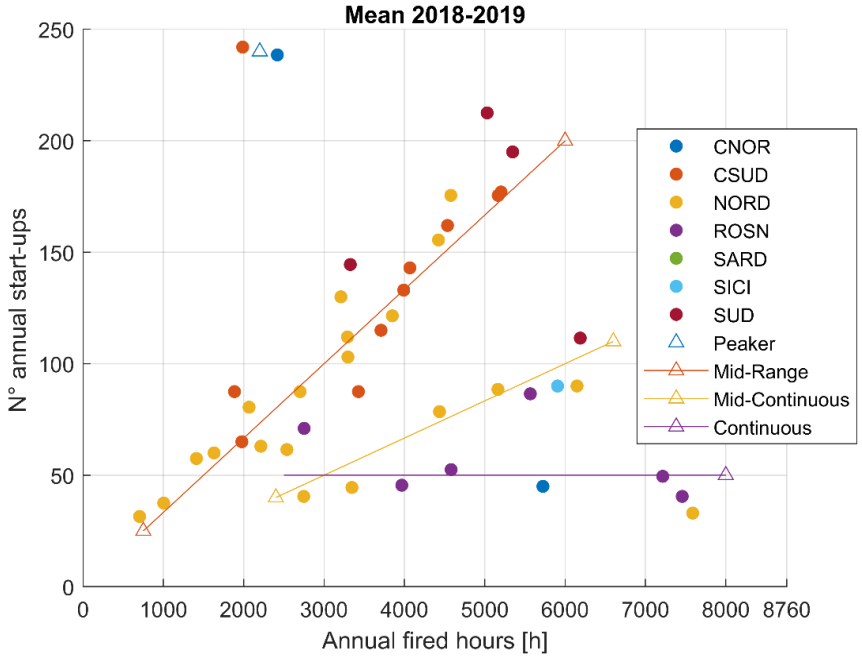

Figure 2.8: Italian CCGTs' operational profiles.

Most of CCGTs operate as Mid-Range, especially for CSUD and NORD zones, which present the largest number of installed CCGTs, while the Continuous power plants belong mainly to the ROSN zone. More flexible profiles (i.e., peakers or mid-range), imply severe consequences on the plant's lifetime since during the start-up the steam turbine's rotor undergoes strong thermomechanical stresses [140]. Moreover, the transients (start-ups and shutdowns) have a stronger impact on the overall pollutant mass emitted during the years.

2.3.2. Emission quantification from real CCGT public data

Italian power plants are limited in the pollutants they are allowed to emit during normal operation: the *Autorizzazione Integrata Ambientale* (AIA) poses a threshold, *Valore Limite di Emissione* (VLE), to the maximum concentration of nitrogen oxides and carbon monoxide in the exhaust. The environmental impact assessment (*Valutazione di Impatto Ambientale*) is carried out considering the power plant working continuously (8760 h/yr) at the VLE, and neglecting the transient contribution. This approach was highly conservative in the past, but nowadays, it could be strongly misleading. In fact, on one hand, it overestimates the pollutant mass emitted during the real normal operating hours (since actually, the annual fired hours are less and the power plant's operator maintains a safety margin on the emission threshold during normal operation), but, on the other hand, it doesn't consider the increasing number of transients at all, potentially underestimating the associated emissions.

Normal Operation FH pollutants emission is monitored continuously by the plant manager and remotely by the public control system to ensure the respect of the VLE. On the other side, during the transients, identified by a GT load lower than the minimum environmental load (i.e the load at which the normal operation begins), it is often not technically possible to observe the VLE limits, so the plant's manager is allowed to exceed them, but he has also the duty to monitor the flue gases composition and to communicate to the authority the overall pollutants' mass emitted during those transients within a yearly

report. These reports are available on the Ecological Transition Ministry's website [145] and are used to build the dataset as described in the following section.

2.3.2.1. The Dataset

The analysis is carried out considering only the Power Oriented (PO) power plants (i.e., exclusively devoted to power generation), since those that are devoted to the combined generation of heat and power, CHP, have to fulfill the local thermal demand, so are less affected by the flexibilization imposed by the power market. Today in Italy are currently active 45 CCGT-PO units in 31 power plants sites, of these 28 are 1 GT +1 ST unit, 17 are 2+1, thus the overall number of gas turbines operating in CCGT power plants is 61, Table 2.1 shows how those machines are distributed among the market zones in to which the grid is divided. All the turbines considered are F-class with 645-715 MW thermal power input.

More details about the power plant included in this analysis can be found in Appendix A, Table A.2.

Table 2.1: Italian CCGTs-PO.

	n. sites	Public report	Detailed transients monitoring	n. CCGT units	n. GT
NORD	13	10	6	22	30
CNORD	2	0	0	2	2
CSUD	7	7	5	10	13
SUD	4	4	2	4	6
ROSN	4	4	0	6	8
SICI	1	0	0	1	2
SARD	0	0	0	0	0
Total	31	25	13	45	61

As shown in Table 2.1, 13 power plants attach to the report, required by the AIA, a detailed monitoring of all the GTs' transients occurred during the year. These detailed monitoring data have been collected together into a dataset in order to properly assess the environmental impact of the start-ups Figure 2.9 reports the composition of the dataset showing the number of transient and GT monitored for each type: GT model, owner company, year, and whether a CO catalyzer has been installed or not.

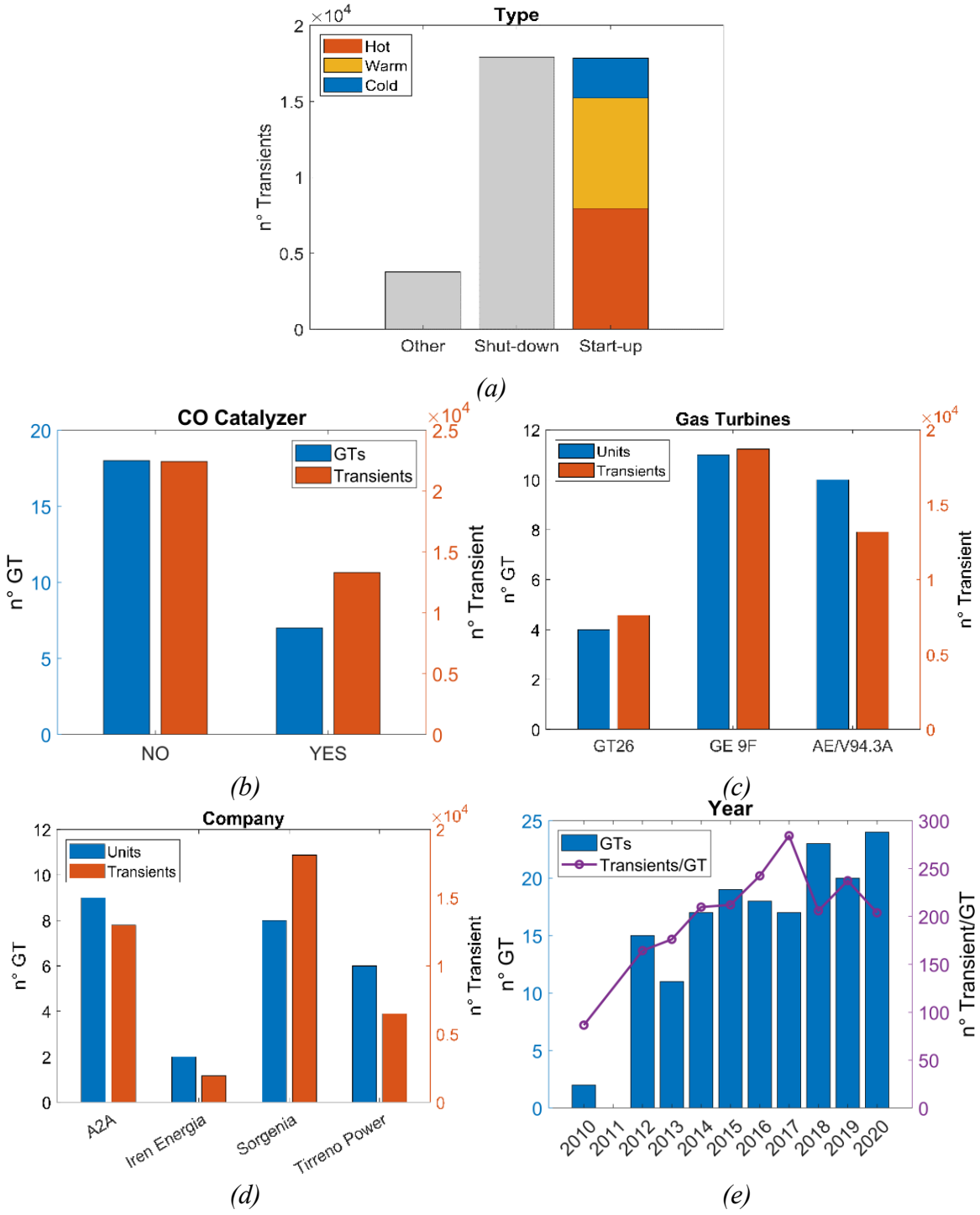

Figure 2.9: Dataset composition according to transient type (a), CO catalyzer (b), Gas turbine (c), Owner (d), and year (e). Blue bars, red bars, and the purple line indicate the number of GT, the number of monitored transients, and the number of transients for GT on average.

Each transient is defined as a start-up, shutdown, or other (failure start-ups, aborted shutdowns, or fluctuations below the minimum environmental load). Start-ups are defined as cold, warm, and hot, generally corresponding to more than 48, 48 or less than 48, or less than 12-8 Stand Still (SS) hours respectively, however, the most report does not specify a definition for cold, warm and hot, thus it could be not homogeneous among the considered gas turbines. This analysis and the figures from b to e only consider start-ups and shutdowns, looking at these it can be appreciated how the dataset is sufficiently large, dozens of thousands of data, to include the variability due to different plant management strategies, turbine manufacturers, and ambient conditions. Besides, a relevant number of transients of the gas turbine with and without CO catalyzer, respectively 7 and 18, were monitored allowing assessing the effectiveness of this device during the transients. In Figure 2.9e, the trend of the number of transients per GT over the years is highlighted: after a continuous growth up to 2017 the average number of transients appears to be stable at around 220 per year equal to ca 110 SUs per year on average.

2.3.2.2. Emission during the start-up and shutdown

Table 2.2 and Figure 2.10 highlight the duration and the mass of pollutants emitted during the transient, data demonstrated to be sparse on such a large dataset, however, some consideration can be drawn. Generally, hot start-ups are shorter, usually, around 40 minutes, than warmer (66 minutes) and cold (93 minutes) because of the residual temperature of the rotor and the drum, the warmer they are the shorter is the time to bring the bottoming cycle's components in temperature to start the steam turbine ramp-up without compromising the plant's lifetime excessively [140]. However, some fast warm and cold SUs (around 40 minutes) appear in the database. That could be the case when the second GT of a 2+1 CCGT is started up the steam cycle is already in temperature so a shorter time is required even for a formally colder start-up, so on average 2+1 power plant could have better performance but this difference is here not investigated.

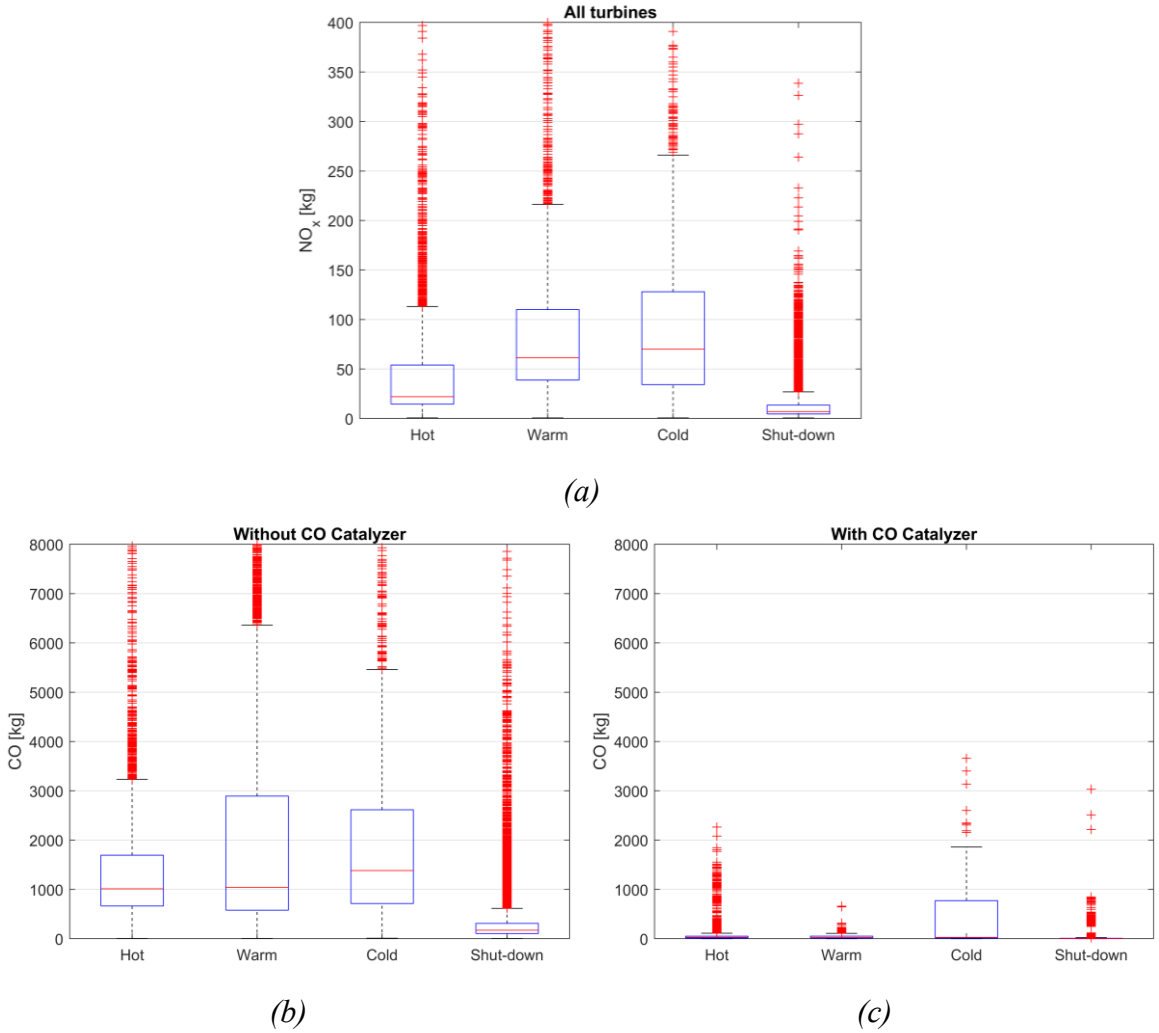

Figure 2.10: Transients pollutant mass emissions [kg/transient] (a) NO_x, (b) CO without CO catalyzer (c) CO with CO catalyzer.

The emitted mass demonstrates to be strongly correlated to the transient duration, so it can be stated that the faster the start-up, the lower the associated emission. It can be noticed that emission during transients is characterized by outliers that make the distribution positively skewed with a mean value that is always higher than the median and which often exceeds the 75th percentile of the distribution.

Looking in general at the analyzed transients, since they occur at low temperatures, the CO emissions tend to be prevalent, between 23 and 34 times the NO_x ones in absence of a CO catalyzer. On the other hand, the presence of a CO catalyzer allows to cut the carbon monoxide emissions by more than 95 % during hot and warm SUs, and about 86% during cold SUs. The adoption of such a secondary technique brings the CO emission in the same order of magnitude as the NO_x (0.5-3 times).

On average the NO_x emission appears to be more affected by the starting condition of the machine with a warm SU and cold SU emitting respectively 1.67 and 2.54 more than a warm SU on average. A ratio that is reduced to 1.15 and 1.71 when looking at the CO emission without a CO catalyzer.

Table 2.2: Duration and mass emission of transients

			All plants		w/o CO cat.	w CO cat.
	Max SS hours		**Duration [min/SU]**	**NO_x [kg/SU]**	**CO [kg/SU]**	**CO [kg/SU]**
Hot SU	8-12	Mean	52	42.43	1474.3	74.7
		Median	40	22.00	1012.5	27.4
		IQ	29	39.5	1030.7	39.7
		5th Percentile	17	8.70	143.5	2.66
		95th Percentile	123	125.55	4130.6	266.0
Warm SU	48	Mean	77	71.2	2196.3	36.1
		Median	66	61.39	1040.8	24.1
		IQ	41	71.20	2314.4	38.2
		5th Percentile	33	16.38	267.5	0.05
		95th Percentile	151	412.24	7895.4	84.6
Cold SU	>48	Mean	118	108.11	2524.0	341.9
		Median	93	70.00	1382.8	27.8
		IQ	90	93.73	1901.4	760.9
		5th Percentile	39	17.21	172.0	0.05
		95th Percentile	242	271.93	9747.3	1341.2
Shutdown	-	Mean	16	13.12	420.3	23.8
		Median	15	7.00	172.2	4.6
		IQ	6	8.95	204.7	8.1
		5th Percentile	8	2.32	19.3	0.05
		95th Percentile	28	37.88	1790.9	37.1

2.3.2.3. Emission normal operating fired hours

Looking at the publicly available information in the AIA for the power plants included in this analysis the VLE is in the range of 24 mg/Nm^3 to 50 mg/Nm^3, and the modal value is 30 mg/Nm^3 both for NO_x (72%) and CO (82% of the GTs of Table 3) on an hourly basis, equal to 55.63 kg/h for F-class machines as the ones under assessment in this work. This number can be compared with the actual data published annually in the reports by the CCGT operators. In fact, each report provides the amount of annual fired hours and the pollutant mass emitted during this period of normal operation. Processing these data, the values reported in Table 2.3 are obtained.

Table 2.3: Normal operating hours emissions of the 25 power plant sites publishing yearly reports.

	All	w CO cat.	w/o CO cat.
	NO_x	CO	
Mean [kg/h]	29.86	4.40	3.11
Median [kg/h]	30.46	2.89	2.91
IQR [kg/h]	11.67	2.70	3.57
5th Percentile [kg/h]	10.64	0.75	0.89
95th Percentile [kg/h]	41.70	6.69	11.71
VLE [kg/h]	55.63	55.63	55.63
Mean/VLE [%]	53.7	7.9	5.6

It must be noted how on average the CCGT emits just 53.7% of the amount of allowed emission per hour of NO_x and just between 5.6% and 7.9% of the CO during normal operating hours since carbon monoxide becomes relevant just to the low load condition.

It is very interesting to remark that there is almost no difference in CO emissions between those units having a CO catalyzer and those that have not. In fact, the main reason for which a CO catalyzer is installed is to lower the Minimum Environmental Load, MEL, (i.e., the minimum load which allows to fully respect the carbon monoxide VLE). A lower MEL is reflected in many benefits such as the ability in saving fuel, and so in cutting CO_2 emissions, and can also be reflected in the ability to provide reserve capacity and services to the grid. however it does not follow directly a decrease in CO emission during normal operating hours: at intermediate and full load the catalyzer could reduce the CO but small quantities are in the flue gas, while probably it works more frequently at the minimum load emitting almost the VLE as well as without catalyzer.

2.3.3. Environmental impact assessment's outcomes

This section proposes an approach to properly assess the environmental impact considering the real flexible operating profiles. Since a real power plant performs many start-ups hot, warm, and cold, the mean value of all the start-ups' data presented in Section 2 has been assumed as the representative of the average Italian CCGT for the pollutant mass emitted during the start-up. Moreover, the average value of shutdowns has been added, obtaining for each average SU/SD cycle 90.02 kg of NO_x, 136.9 kg, and 2405.5 kg of CO for a turbine with and without CO catalyzer respectively. For the normal operating emissions, average data presented in section 2.3.2.3 have been used analogously.

In the next figures, iso-emission black dashed lines, are superimposed on the CCGT operating profile in order to highlight the impact of the different management strategies. The plotted iso-emission lines correspond to different percentages of the mass considered by the VIA so that it is easy to check whether this assessment overestimates or underestimates the real emission of the pollutant.

Figure 2.11 shows how ISO emissions lines for NO_x are very steep, as 1 SU/SD cycle is equivalent to 3 fired hours, then the assessment carried out according to the VIA approach always overestimates the real power plants' NO_x emission, those continuous power plants operating more than 7000 h/yr emits only the 45% of what has been estimated by the VIA.

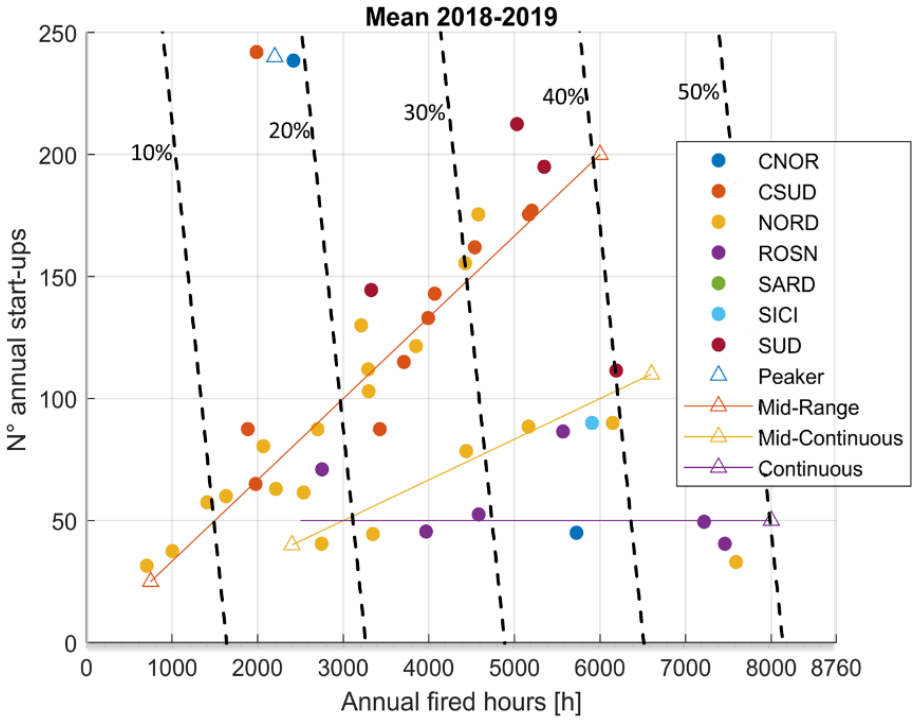

Figure 2.11: NO_x annual emission black dashed lines: percentage ratio of annual emission against annual VIA emission.

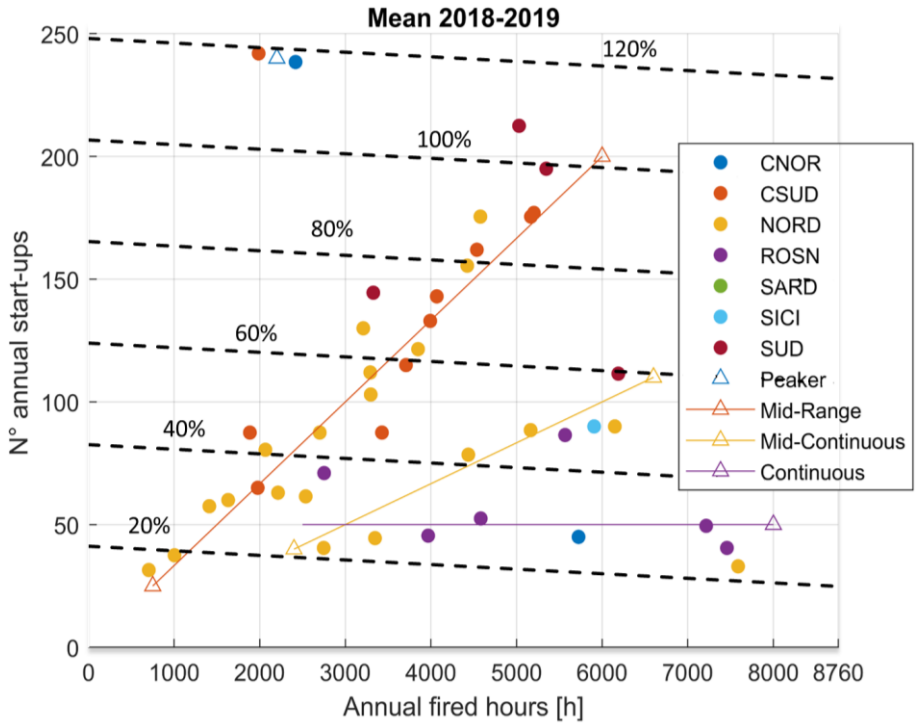

Figure 2.12: CO annual emission without CO catalyzer: black dashed lines: percentage ratio of annual emission against annual VIA emission.

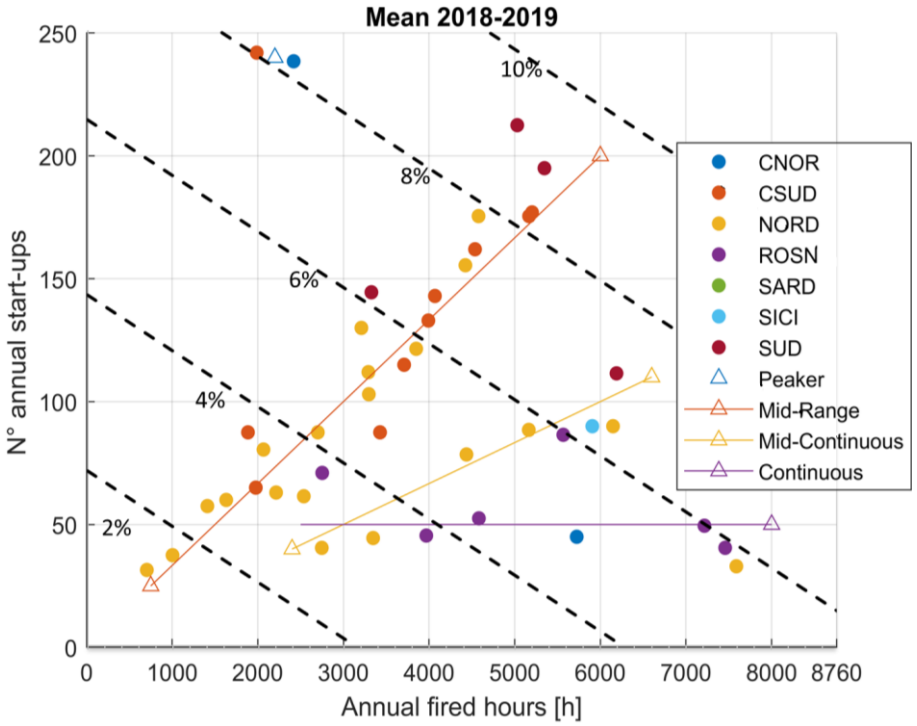

Figure 2.13: CO annual emission with CO cat: Italian CCGTs' operational profiles; black dashed lines: percentage ratio of annual emission against annual VIA emission.

Furthermore, it should be noted how the iso-emissions are almost flat since most of the CO is emitted during the start-ups, 1 SU/SD cycle is equivalent to 546 fired hours in terms of emitted mass. So carbon monoxide could be critical for those CCGTs working with frequent SU. Figure 2.12 highlights how, if most of the CCGTs (<110 SU) emit less than 50% of the CO that has been estimated by the VIA, the peakers (i.e., those CCGTs performing more than 200 SU/SD cycles per year) are expected to emit more.

Nevertheless, according to Figure 2.13, the peakers are expected to emit less than 10% of what is estimated by the VIA if they installed a CO catalyzer. As seen in the previous subsections, this device has no impact on the normal operating hours' emission, but it could drastically cut the start-ups' emission of CO since in this case a SU/SD is equivalent to 44 fired hours in terms of emissions, so those devices can be effectively used to eliminate the impact of a more frequent start-up even in the future energy transition.

The final outcomes can be summarized as follow. Looking at the annual pollutant emission, the CO one could be negatively affected by the flexible operation of CCGTs, since most of the pollutant mass is emitted during the start-ups (a start-up is equivalent to 546 fired hours). For those CCGTs performing more than 200 start-ups per year the mass of CO emitted could exceed the quantity assessed during the institutional environmental impact assessment (VIA). It must be stressed that this does not imply a severe environmental problem since the CO is not a critical pollutant from the air quality point of view (no values exceed the quality value across Europe), however, this must be considered performing the VIA process under more realistic assumptions. For such a high number of SU, in any case, the CO catalyzer is demonstrated to be an effective solution to mitigate the startups' emissions and it should be taken into account when the yearly start-up number approaches 200.

It has not been possible to assess the effectiveness of post-treatment technologies for NO_x mitigation as well, since none of the CCGTs included in the analysis have installed a Selective Catalytic Reactor, anyway NOx emissions are not negatively affected by frequent SUs and SDs, since the majority are emitted during normal operating hours, and the Environmental Impact Assessment is very conservative in estimating the annual mass NO_x emissions, since all the Italian CCGTs emit (less than the 50%), a value that is expected to decrease with the reduction of operative hours envisaged with the future energy transition.

Finally, besides being able to reduce the carbon footprint of the programmable power plant thanks to the high efficiency and the use of lower (natural gas) or neutral carbon footprint fuels, the Combined Cycles can support the energy transition without increasing their environmental impact at the local scale.

2.4. Inlet air conditioning for off-design operations

The extreme hourly variability of electricity prices on the market can limit the benefits of an optimal dispatch of a CCGT generator. The profits realized during the price peak hours can be compromised by losses during low price periods (typically during central hours, because of the peak in solar PV generation, or during the nighttime, because of the lower demand). Indeed if the off-peak period duration is quite short, it might be better to keep the GT operating at minimum load limiting the fuel consumption and the losses in order to avoid frequent start-ups and shutdowns which can even be more expensive or reflected in an increased environmental impact (ref. Section 2.3). However, losses during off-price periods can be relevant jeopardizing the overall economic viability of the power plant.

It seems there is not any strong correlation between the main operating parameters (i.e., Load Factor, Fired Hours, number and frequency of start-ups) of the operating clusters presented in Section 2.3.1 and the Off-Design Fired Hours (ODFH). ODFH are defined with the respect to the MEL-Full Load range[16] of the capacity evaluated at the real ambient temperature as:

$$\mathrm{ODFH} = \mathrm{FH}(0.38 \leq \mathrm{CCGT\%} \leq 0.9)/\mathrm{FH} \tag{2.3}$$

Table 2.4: Operating parameters of Italian CCGTs-PO for each operating profile.

	Load Factor [%]	**FH [h]**	**Annual SU**	**ODFH [%]**
Continuous	54.3	6226	49	52.0
Mid-Continuous	34.3	4467	67	66.5
Mid-Range	28.5	3524	128	63.8
Peaker	29.7	4329	231	60.7

However, all the operating profile clusters have on average more than the 50% of ODFH. Moreover, Figure 2.14 shows clearly how the production evolved in the last years with the CCGTs that spend nowadays more percentage of their time at partial load (about 70% of the time against the 60% in two 2018). Figure 2.15 shows the detailed operating hours distribution, of all the CCGT included in this analysis, according to the GT load. The hypothesis is that such intermediate load is mainly due to the more extensive production as grid supporter and Ancillary Services providers, which intensified in 2020 because of the high RES/load ratio.

[16] The following equation assumes the 0.38-0.9 range, consistent with the analysis presented by this section.

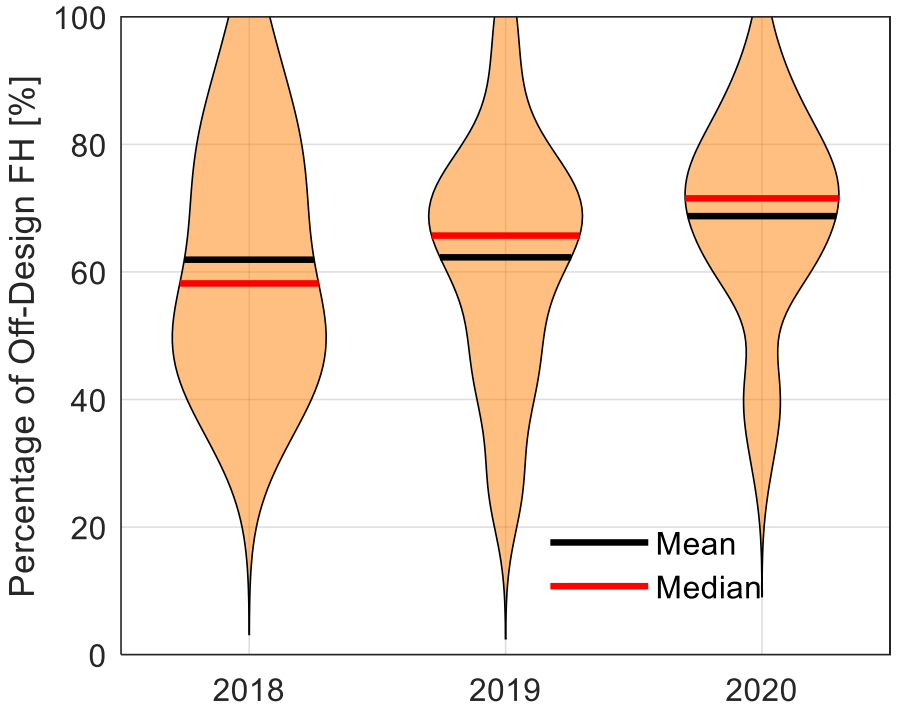

Figure 2.14: Italian CCGT: Percentage of Operating Hours in Off-Design.

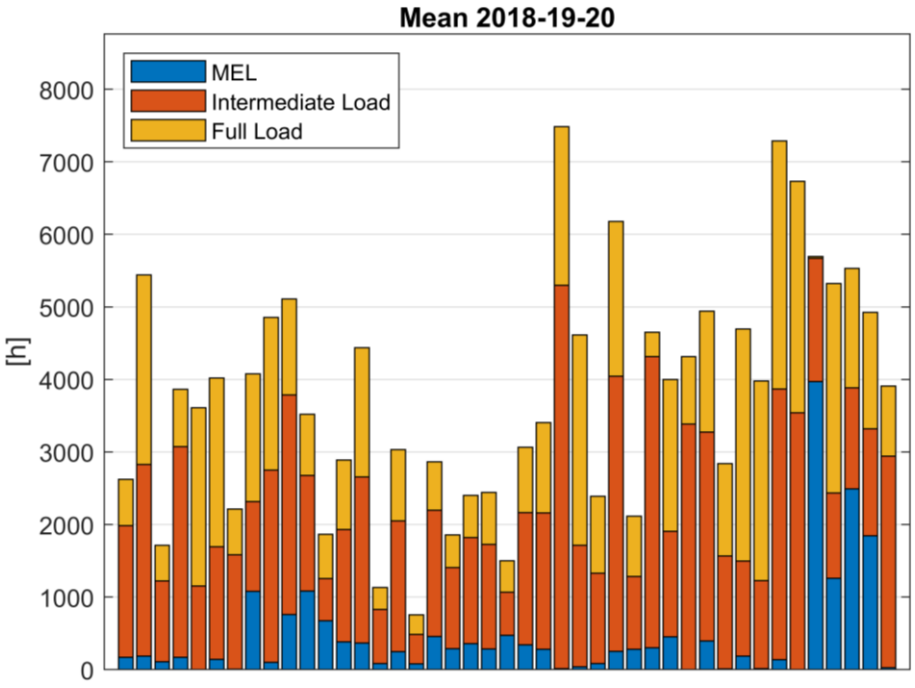

Figure 2.15: Italian CCGT: Operating Hours Distribution.

Section 2.1.1 explained the influence that the inlet temperature has on the CCGT performance in terms of power output and efficiency. It was assessed that Combined Cycle efficiency has low sensitivity to the ambient temperature, losing the 2% at 45°C when increasing temperatures and losing just the 0.25% at 5°C [128]. On the other hand, increasing the temperature reduces the off-design degree of the CCGT since the GT operates with a more open Inlet Guide Vane angle, of IGV resulting in overall higher efficiency.

This can be visualized in Figure 2.16 where is shown on the same chart of Figure 2.3 the potential benefit of inlet heating, as a matter of example, 85% of the CCGT load can be reached at 100% of GT load by increasing the intake temperature from 15° to 40°C (green segment in the figure). The efficiency benefit for this specific case is highlighted in green.

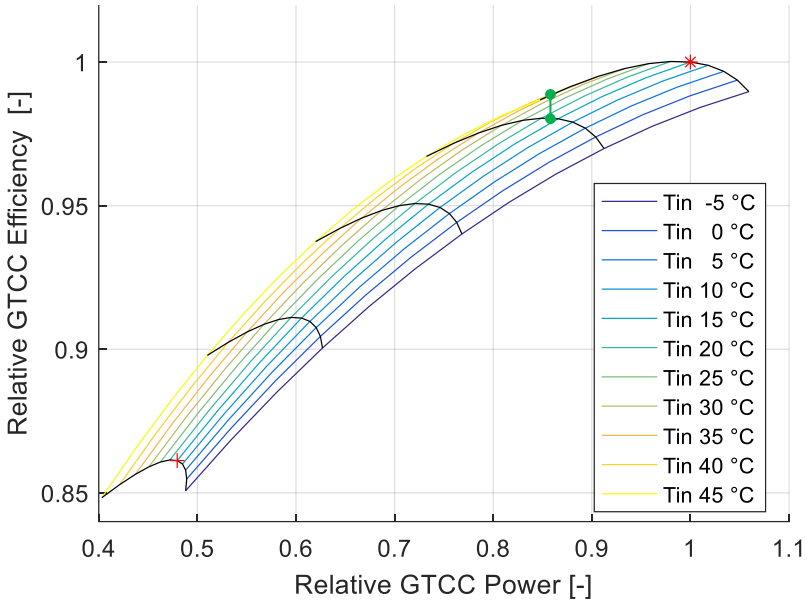

Figure 2.16: Effect of heating up the inlet air from 15°C to 40°C for CCGT operating at 85% load.

2.4.1. Analysis methodology

Different methods can be adopted to perform the intake heating: the heat can be recovered from the bottoming cycle by exploiting the flue gas thermal content or by extracting low-pressure steam or even by a heat pump dedicated to this purpose. The analysis presented in this section limits the increase in temperature to 20 K, a quantity that can be covered by the flue gas maintaining the temperature at the chimney above the 80°C for all the ambient and GT load conditions, so no reduction of the power or efficiency in necessary to feat up the system. Moreover, the impact of the pressure drops of the heat exchanger located at the intake and the CCGT discharge was neglected.

To assess on a large scale the inlet heating potentialities the analysis is carried out on the whole CCGT-PO plants which have been considered in the previous section. Table 2.5 reports the same power plants as in Table 2.1 adding the overall capacity installed for each zone. A detailed list can be found in Appendix A, Table A.2.The tool used to quantify the effect of the inlet temperature on power and efficiency is the previously cited Gate-Cycle model, developed for an F-class CCGT with 3 pressure levels and reheat [128].

All the CCGTs are assumed to adopt a water-cooled condenser (WCC), however, it is possible to neglect the difference between the two condensers because the inlet heating has potential benefits also for those CCGTs with an ACC. Although an ambient temperature increase would be reflected in an efficiency decrement with an ACC, that's not the case of inlet heating which conditionate only the intake air, while the bottoming cycle is not affected since still cooled by ambient air, so the behavior and the potential are not so far from the WCC case.

Table 2.5: Italian CCGTs-PO zonal distribution.

	n. sites	**n. CCGT units**	**n. GT**	**Overall zonal capacity**
NORD	13	22	30	10,394 MW
CNORD	2	2	2	756 MW
CSUD	7	10	13	4,077 MW
SUD	4	4	6	2,713 MW
ROSN	4	6	8	3,275 MW
SICI	1	1	2	780 MW
SARD	0	0	0	0 MW
Total	**31**	**45**	**61**	**22 GW**

Even if, in theory, a temperature change could be used to control the CCGT also close to full load, this cannot be performed in reality, so the intake heating is performed just in off-design conditions, defined as CCGT load lower than 90%. On the other side, the minimum environmental percentage load was set equal to 38% to exclude start-ups and shutdowns from the analysis.

Then the efficiency gain potential is maximized by performing an optimization of this parameter on an hourly basis for each power plant, imposing the production of the same absolute power, a limit of the intake temperature to 45°C, or a limit of the temperature increase of 20K. The calculation has been performed over three years (2018, 2019, and 2020), covering also the pandemic period, where the reduced load experienced by the grid can be seen as a hint of a future period of higher RES/load ratio that is envisaged due to RES capacity growth. So the input data to the model are:

- the actual power generation of each power plant
- the cost paid by the plant for burning the fuel, so the natural gas cost (including taxes and levies) and the CO_2 emission allowance cost
- the local ambient temperature

Concerning the power generation of the Italian CCGT fleet, it has been computed from the market results data published by the *Gestore dei Mercati Energetici* (GME) [144]. Summing up, for each time interval (1 hour), the energy sold and bought by each CCGT on all the market sections (Day-Ahead Market, Intra-day Market, Ancillary Service Market, Balance Market, ref Section 1.1.1.1) is possible to obtain a close estimation of the actual power plants power generation. Small errors may occur since the result of this data processing is a scheduling from which the actual generation could have moved away because of grid or plant unbalances, moreover it is a mean of one hour during which real data could have been non-constant.

The gas price was retrieved by adding to the Day-Ahead gas market price, *MGP-MGAS negoziazione continua*, available on the GME's website [144], and the average taxes and levies reported by the Italian authority ARERA [146]. Finally, it has been reported on the LHV basis considering a ratio equal to 1.1 between the LHV and HHV of natural gas. The CO_2 price was set constant equal to 21 €/ton, the three years average on the EU-ETS [147].

Each power plant location was considered, and the ambient temperature time series is estimated by means of hourly geospatial data of the temperature at 2 m of height from the soil available on the ERA5 dataset with a resolution of 9 km [148]. The results obtained were tested for 4 specific power plants and found in good agreement.

2.4.2. Results

The results of the use of an intake heating system during off-design hours are ordered and presented as a function of the different years and divided by operating profiles. The percentage of reduction of carbon dioxide emissions, Figure 2.17(a) is almost constant along the year and the use and it is equal to the enhancement of the average efficiency, that in all the conditions is increasing by a range of 0.5-0.8% This slight increase is having a larger impact on the CCGTs operated for a long time that can avoid up to 10 tonCO_2/(MW·year) equal to 4000 tons/year of CO_2 for an average 400 MWe CCGT. Finally, it can be noticed that the absolute amount of the avoided CO_2 is directly related to the number of Fired Hours, of the different operating profiles, while variations along the years are related to the increase of the percentage Off-Design Fired Hours Figure 2.18(a) straightforwardly confirm that the amount of saving achievable with the intake heating reflects the percentage of unburnt fuel, and so the overall increase of efficiency.

More important, in Figure 2.18(b) the absolute savings follows a trend similar to the one driven by the number of fired hours of the different operating profiles, but the weight of the gas cost brings a reduction of benefit in the last two years, with the continuous CCGTs that goes from 1449 €/(MW·year) equal to 579,700 €/year for a 400 MWe CCGT in 2018 to 873 €/(MW·year) equal to 350,000 €/year with the gas cost that went below 10 €/MWh with the minimum due to the pandemic crisis.

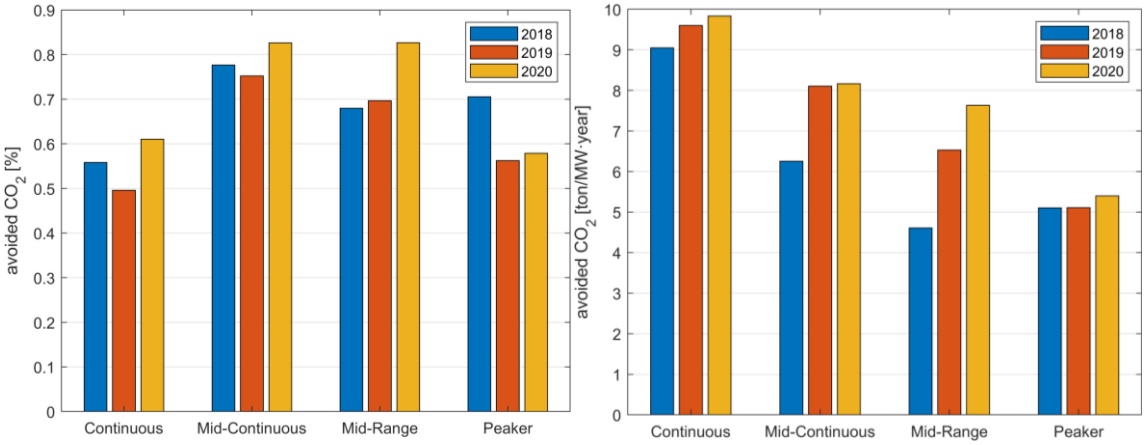

Figure 2.17: Intake Heating environmental impact: Percentage (a) and absolute (b) avoided carbon dioxide as a function of the different years and operating profiles.

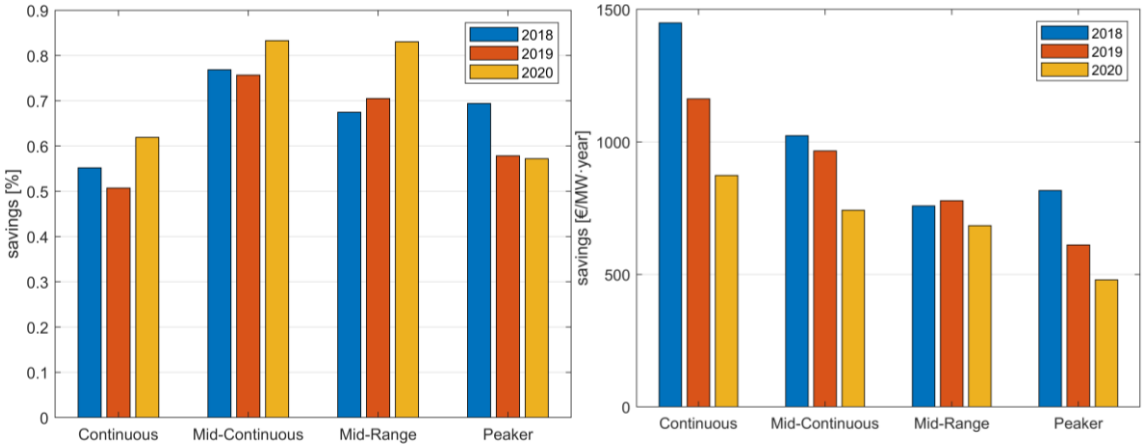

(a) *(b)*

Figure 2.18: Intake heating economic impact: percentage (a) and absolute (b) fuel savings as a function of the different years and operating profiles.

For the other operating profiles, a good estimation of the yearly savings was found around 800 €/(MW·year) equal to 320,000 €/year for 400 MWe CCGT. The Peaker units have a lower economic performance, so the solution may be adopted just if an anti-icing system is already in place.

Even if the percentage impact of the intake heading results in a mere 0.8%, an investment in this technology must be evaluated against the last figure. For 2021, the rising cost of CO_2 ETS allowances that characterized the 2021 reaching values up to 80 €/tons, 3-4 times of what was considered here and the price of gas skyrocketed, even more, price in the order of 100 €/MWh or more have been recorded on the European markets, bringing up the savings in the order of some millions euro per year for a 400 MWe Continuous CCGTs and around 500,000 euros per year for the others operating profiles, making this solution interesting and possibly self-sustaining considering an investment cost of 840,000€[17].

[17] Private communication from the manufacturer

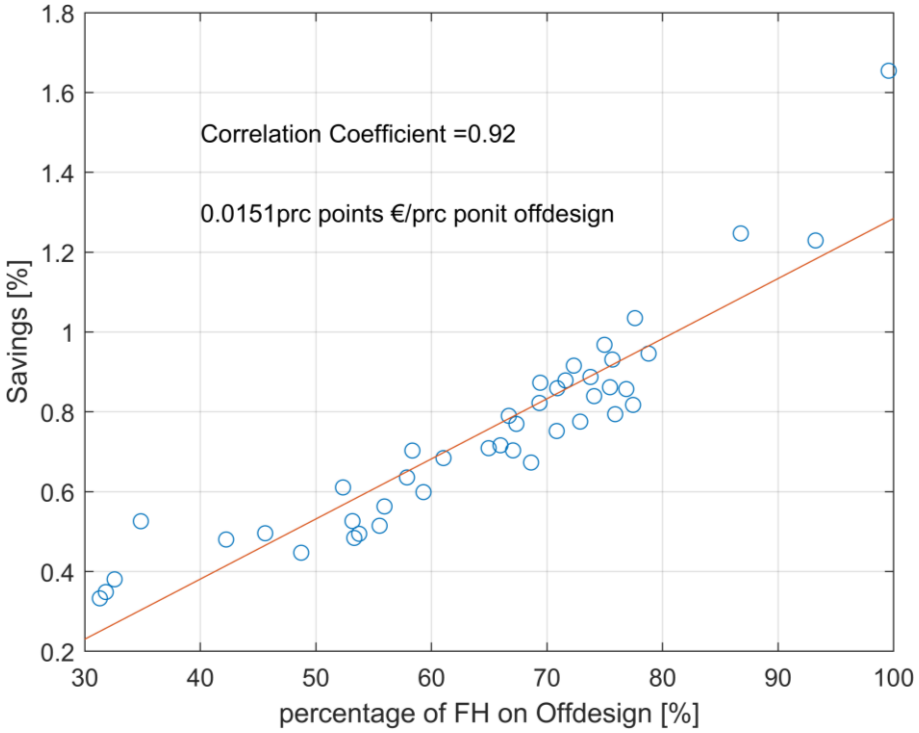

Figure 2.19: Effect of the average off-design hours over the percentage of savings for the single CCGT, average 2018-2020.

Figure 2.19 allows evaluating the impact of the operational profile, of course, the impact of the proposed solution is correlated with the time it is used. The higher the percentage of off-design hours the higher the benefits.

Besides the operational profiles, the second parameter that influences the increase in efficiency is the ambient temperature, synthesized in Figure 2.20 as the average temperature registered. The slight negative correlation can be exploited and is related to two main effects:

- The constraint of 45°C limits the use of the intake heating technique on the hot side, reducing then the positive effect of intake heating.
- Low average ambient temperature corresponds to higher inlet heating potentialities since the increase in temperature is associated with an increase in efficiency when operating in the 20°C-30°C range.

Based on that, it is expected to have a marginal increase (0.02 percentage points/°C of ambient temperature) in the benefit of the proposed solution when applying the solution further to the northern region (or to colder climates out of Italy). Moreover, since the installation of anti-icing systems is a practice more common within cold climates, it would be easier to extend their use with an efficiency enhancement logic as a first zero-cost application, even if the potential of the solution could not be completely exploited.

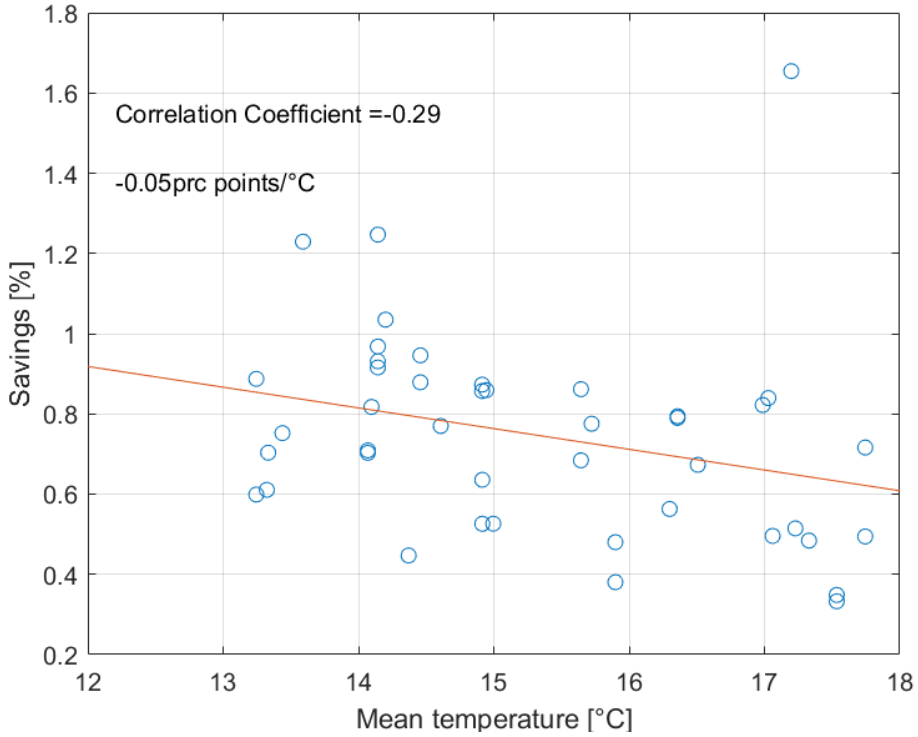

Figure 2.20: Effect of the average ambient temperature over the percentage of savings for the single CCGT, average 2018-2020.

2.5. Concluding remarks

The statistical analysis of the data presented in this chapter has quantified the operational flexibility required for modern CCGTs. Most of the Italian plants perform between 50 and 200 start-ups per year and operate less than 5000 h, 60-70% of these in off-design conditions. More in detail, four different operational profiles have been identified: Continuous, Mid-Continuous, Mid-Range, and Peakers.

Emissions of nitrogen oxides and carbon monoxide strongly rely on the start-up transients, on average during each start-up and shutdown cycle are emitted 90 kg of NO_x, and 2406kg of CO (137 kg if a CO catalyzer is installed). Therefore each start-up (plus the following shutdown) accounts for emission as 3 fired hours considering the NO_x, 546 or 44 fired hours considering the CO depending if the catalyzer is installed or not. However, the institutional Environmental Impact Assessment (VIA) is conservative and overestimates the real emissions except for the carbon monoxide emitted by those plants performing more than 200 start-ups per year. It highlights how the installation of a CO catalyzer should be considered especially by those power plants operating according to the Peaker profile.

Section 2.4 highlights how, for a CCGT, the power output is dependent on the inlet temperature, while the efficiency is not, and so how inlet air temperature conditioning can be exploited to improve the off-design performance. An investigation carried out on the Italian CCGT fleet quantifies the economic and environmental benefits. Economic and fuel savings between 0.5% and 0.8% can be achieved by heating the GT inlet air during the off-design operating hours. The concept exploits the reduction of the CCGT's power output and the invariability of efficiency as the inlet air temperature increases. Figure 2.15 well describes this behavior.

3. Heat pumps: state of art and High-Temperature applications

Section 1.2 introduces the potential key role of heat pumps in future energy systems as a strategic technology for sector coupling implementation. It highlights how the electrification of heating can contribute to the economy's carbon intensity reduction and, if managed properly, increase the electricity demand response supporting the operations of a highly RES-penetrated grid.

Heat Pumps (HPs) are for sure the most widespread and reliable and efficient technology for power to heat application, without any relevant competitors on large scale. Indeed today, researching in heating sector coupling and a comprehensive approach to heating decarbonization implies researching on HPs.

This chapter is dedicated to this technology, the first section is a general overview, providing the fundamentals and presenting the main applications. Then is presented the mathematical tool, developed in MATLAB, for assessing the thermodynamic and the economic performance of regenerated vapor compression heat pumps. This tool is then applied to the analysis presented in Section 3.3.

3.1. Introduction to heat pumps: fundamentals and applications

Heat pumps are designed in order to "pump" the heat, so allowing the transfer from a lower temperature source to a sink at a higher temperature, which results to be impossible spontaneously according to the Clausius statement of the Second Law of Thermodynamics:

"It is impossible to construct a device which operates on a cycle and produces no other effect than the transfer of heat from a cooler body to a hotter body."

However, heat pumps allow this transfer providing an energy input to the system. Here it occurs the first differentiation some heat pumps provide the energy input as mechanical work[18] compressing the working fluid vapor, so are referred to as Vapor Compression Heat Pumps (VCHPs), alternative the energy can be provided as low-temperature heat these pumps are based on an adsorption-desorption thermodynamic cycle and are known as Adsorption Heat Pumps (AHPs).

Although adsorption-desorption cycles are mostly applied for refrigeration purposes, they can also be used for heating applications. The AHPs' advantages, if compared against a the VCHP, are mainly the absence of noise and vibrations, due to the mechanical motor and compressor of VCHPs, the possibility to rely on a 100% RES sources, such as low-temperature heat provided by solar thermal collectors, and the absence of working fluid with an ozone depletion or global warming potentials (ODP and GWP respectively). In addition, the usually requires less maintenance because of the absence of moving components for the

[18] Some authors distinguish between mechanical driven and electrical driven heat pumps. Here this difference is omitted since the electrical power needs to be converted into mechanical to drive the compressor and supply work to the system.

fluid circulation. Nevertheless, AHPs have been pointed out as expensive, and too big and heavy compared to VCHPs [149]. For this reason, VCHPs are much more widespread and today cover almost the totality of the market, Pinheiro et al. [150] reviewed the AHPs discussing crucial aspects like operating conditions, working pairs, performances, adsorbent bed forms, adsorbent heat exchanger geometries, and cycle features. However, this category of heat pumps is out of the scope of this thesis and hereby vapor compression heat pumps are simply referred to as Heat Pumps (HP) which this section introduces.

3.1.1. Standard Thermodynamic Cycle and Components

The heat transfer from the low-temperature environment, defined as "source", to the high-temperature user, defined as "sink", is accomplished by circulating a heat transfer fluid, commonly referred to as refrigerant or working fluid. The working fluid received the heat from the source evaporating within a low-temperature heat exchanger, then it is compressed to rise in temperature and release the heat to the sink. So the standard thermodynamic cycle consists of four stages pointed out as follows with reference to the scheme in Figure 3.1 and the diagrams in Figure 3.2:

- Compression (1→2): the vaporized working fluid is compressed from the low-pressure level (evaporator pressure) to the high-pressure level (condenser pressure)
- Condensation (2→5): The superheated compressed vapor (2) is cooled down until the saturation temperature (3), then it condensates until (4) and reaches the liquid subcooled conditions (5). This stage can conceptually be divided into four steps but it is normally performed by a single heat exchanger.
- Expansion (5→6): the liquid expands through a dedicated device. The expansion usually takes place without any enthalpy variation. The expansion is two-phases since a fraction of liquid
- Evaporation (6→1): the evaporation is completed within the dedicated exchanger in which the heat flows from the source to the working fluid. The condition (1) is normally of superheated vapor as a safety measure to avoid the presence of liquid in the compressor

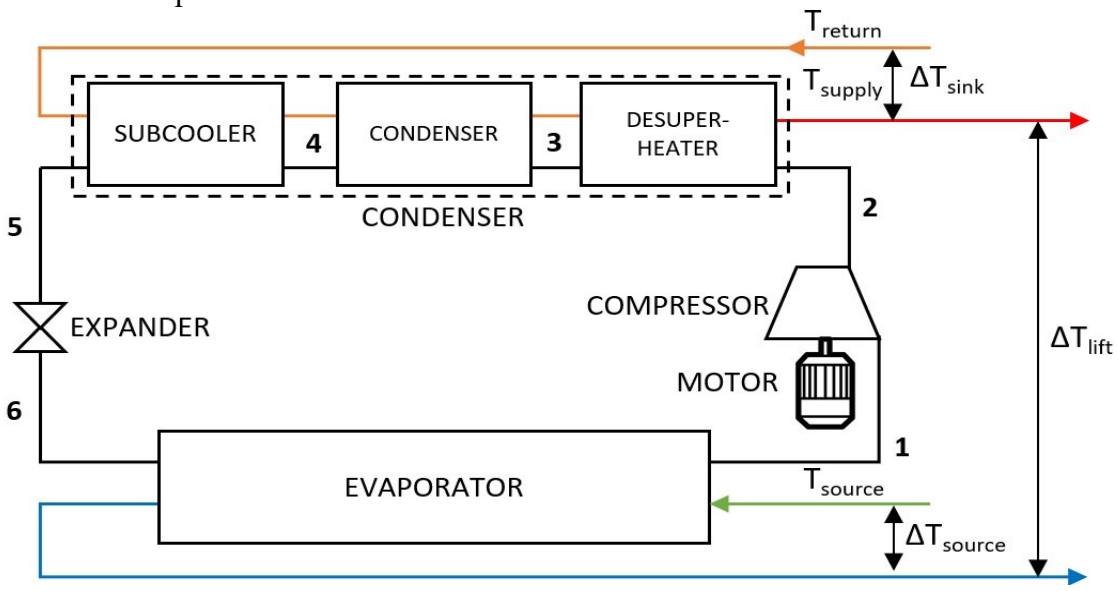

Figure 3.1: Standard layout for a vapor compression heat pump.

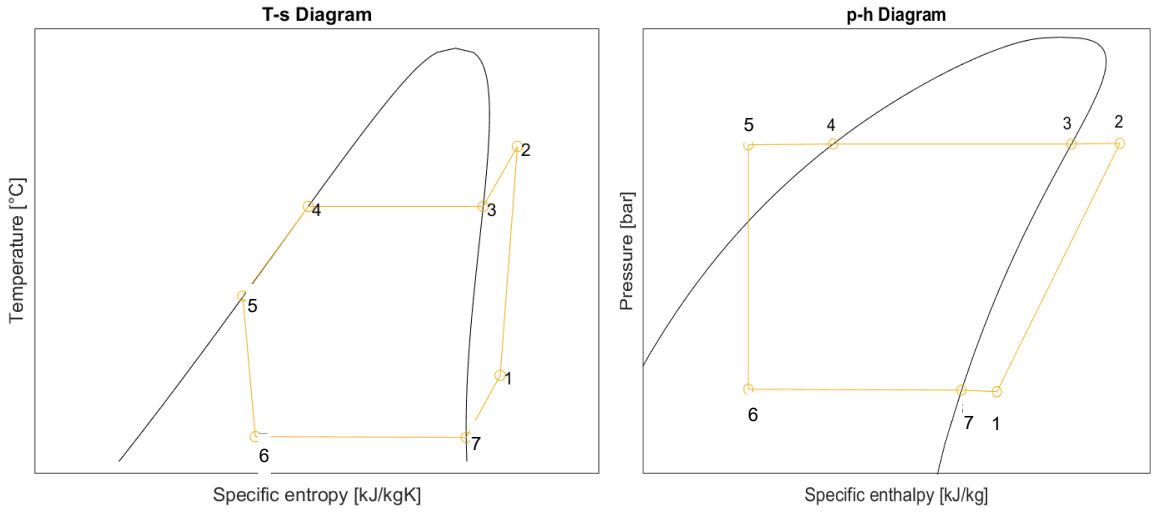

(a) *(b)*

Figure 3.2: Standard vapor compression heat pump cycle on the Temperature-specific entropy plan, T-s (a) and pressure-specific enthalpy plan, p-h (b). Diagrams are relative to R600 working fluid.

As a result, an amount of heat Q_{EVA} is absorbed by the working fluid which has a temperature lower than the source temperature. The source temperature is cooled down by the temperature difference $\Delta T_{source.}$ Work is provided to the system within the compression. An amount of heat Q_{COND} is delivered to the sink, the sink heat transfer fluid is heated up from T_{return} to T_{supply}. The difference between these two temperatures is defined as ΔT_{source}. A key operational parameter is then the difference between the source and the sink, so how much the thermal level of the heat source has to be raised, is defined as ΔT_{lift}.

The aforementioned four stages allow identifying four essential components the compressor, the expander, and two heat exchangers (the evaporator and the condenser). Several other components may be used in heat pumps based on different designs (e.g., four-way valves, solenoid valves, regenerators, control valves, water pumps, electrical fans, auxiliary heaters, and water pipes).

3.1.1.1. The Compressor

The compressors used in HPs belong to four different types: centrifugal, screw, piston, or scroll. Centrifugal compressors are preferred in industrial applications where there is a large flow of refrigerant in circulation. They are also preferred in applications where it is mandatory to avoid any contamination of the compressed gas with other fluids such as oil, in fact, does not require lubrication on the gas side because the shafts are cantilevered and the friction is reduced by the axial compactness. It is also characterized by a low cost of realization.

Screw compressors allow high compression ratios with medium or low fluid flow rates. These compressors are not very suitable for low power applications, because for smaller rotors the intrinsic loss to the rotors becomes much more significant. Generally needing abundant lubrication in order to contain friction and ensure a good seal over time, they are therefore required to be coupled to large oil separators. The gas compression process along a rotating screw coupling is carried out by means of a continuous sweeping movement, therefore the pulsation effect of the flow rate is almost null. As a result, this family of

machines is significantly more silent, generating less vibration and having efficiency advantages over their main competitors, the piston-type positive displacement compressors.

The alternative volumetric piston type is popular for small and medium-sized systems, as it is a very mature technology it is preferred for its simplicity and good efficiency. It is characterized by low flow rates but allows reaching very high compression ratios. It needs lubrication and therefore also an oil separator, dry models are available but they have strong limitations on compression ratios and delicate maintenance. In order to regulate it is possible to act on the number of activated cylinders or the rotating speed. The characteristic curve (β vs $\dot{m}$) varies considerably with the number of revolutions, the influence of which is greater at low compression ratios or high flow rates; another parameter of influence is the volumetric efficiency which depends on the compression ratio and the dead volume [151].

$$\eta_{vol} = 1 - \mu\left(\beta^{\frac{1}{k}} - 1\right) \tag{3.1}$$

Where μ is the clearance ratio, indeed the ratio of clearance volume to swept volume.

Scroll compressors are composed of two spirals, one fixed and the other in orbital motion. Their use in heat pump systems is greatly increasing, they are known to operate producing less noise and vibrations than many other compressors. They are widely used in domestic applications together with piston compressors. The advancement of scroll compressors represents the most relevant recent innovation regarding the compression phase in reverse cycles. They ensure efficiency of about 10% higher than a standard reciprocating compressor. The higher efficiency can be explained as follows: first of all, the suction and discharge processes take place in separate parts of the machine, which means that no heat is transferred to the gas entering the suction, which would cause it to expand and reduce the capacity of the gas suctioned. Secondly, the compression process is carried out at an angle of 540°, which is much slower than that of reciprocating compressors where compression takes place at an angle of 180°. Also for this reason, torque fluctuations in a scroll are about 10% of those in a reciprocating compressor on average. A further advantage of this device is the elimination of suction and discharge valves, which in the reciprocating compressor represent a significant source of loss. These reasons at the base of the recent wide diffusion of this type of compressor for small and medium-size applications [152].

3.1.1.2. The Expander

The device in which the expansion took place can be generally defined as an expander. In the most of cases, it is an expansion valve, performing a pressure reduction without any work exchange. So the process can be considered as iso-enthalpic expansion. Commonly, copper capillary tubes are used as a cost-efficient device able to perform this easy thermodynamic transformation without any particular issue.

Some researchers have investigated new expanders, such as microturbines, in order to exploit the expansion to generate some power that could compensate for the amount required by the compressor. However, designing an efficient and reliable two-phase expander implies severe issues which could jeopardize the overall benefits of such devices [153,154]. However, their diffusion on the market is almost negligible.

3.1.1.3. The Heat Exchangers

Generally speaking, a heat exchanger is a device designed to transfer heat between two, or more fluids. Many different types have been developed, this section aims to report those which are most used with the HPs' architecture and/or whose modeling is described in Section 3.2, flat plate, shell and tubes, and suction line heat exchangers.

A flat plate heat exchanger consists of a set of parallel and connected plates. Each plate presents four inlet and outlet ports and seals that direct fluid through alternating flow paths. The fluid path is the channel between two adjacent flat plates, the overall design imposes that two fluids flow alternatively through the channels so that each plate has the hot fluid on one side and the cold fluid on the other, and heat is exchanged via conduction in the plates. Within the fluid, also convection contributes to heat exchange, and specific plate design or sealing technologies can increase the turbulence in the channel and so the convective exchange with a positive contribution to the overall heat transfer coefficient but also increases the overall pressure drop. Typical categories of plate corrugations are washboard, zigzag, chevron or herringbone, protrusions and depressions washboard with secondary corrugations, and oblique washboard. Chevron-type plate heat exchangers are probably the most used [155].

Shell and tubes are made up of a series of tubes in a shell, the shell has an inlet and an outlet, and one fluid flows through the shell exchanging heat with the other one which flows in the tubes. Then the heat is transferred via the tubes' wall. Some baffles are placed in the shell in order to prevent the first fluid's backflow and ensure that it can contact all the tubes within the shell maximizing the heat exchanger effectiveness. Key design parameters are the number, the dimension and the distance among the tubes, the shell shape, the size beside the number, and the position of baffles [156].

The suction line heat exchangers can be adopted in the regenerated HPs cycles (ref. Subsection 3.1.3.2 and 3.1.3.1), especially for residential heating or comparable applications in terms of size and design temperatures. They are usually assembled according to a double-pipe counterflow arrangement [157]. As regenerators, gas-to-liquid flat plate heat exchangers are also adopted [158].

Independently on the exchanger typology, besides the pressure drop, an important parameter to assess the heat exchanger performance is the overall heat transfer coefficient (U) which quantifies the heat exchanger's ability in transferring the heat. The heat exchange is influenced by the exchange area A, and the mean temperature difference between the two fluids. If the overall heat transfer coefficient increases, the exchange process becomes more efficient increasing the heat flow. Otherwise keeping constant the ΔT_{LM} and $\dot{Q}$, the heat exchanger can be down-sized with an economic benefit.

$$\dot{Q} = UA\Delta T_{LM} \tag{3.2}$$

3.1.2. The Coefficient of Performance

The HP efficiency is commonly assessed in terms of Coefficient of Performance (COP), which is the ratio of the heat provided to the sink and the work needed to run the heat pump. It can also be expressed in terms of thermal flow and power.

$$COP = \frac{Q_{COND}}{W} = \frac{\dot{Q}_{COND}}{P_{motor}} \tag{3.3}$$

Neglecting the compressor adiabatic efficiency, as well the motor electric and mechanical efficiency, as the energy is conserved

$$COP = \frac{Q_{COND}}{W} = \frac{Q_{EVA} + W}{W} = \frac{Q_{EVA}}{W} + 1 = \frac{Q_{COND}}{Q_{COND} - Q_{EVA}} \tag{3.4}$$

Considering an ideal heat pump that operates an inverse Carnot cycle (i.e., isentropic compression and expansion, isothermal and isobaric heat exchange both at source and sink), is possible to express the maximum achievable COP as an exclusive function of the source and sink temperature (more precisely on the evaporator and condenser temperature.

$$COP_{Carnot} = \frac{Q_{COND}}{W} = \frac{Q_{COND}}{Q_{COND} - Q_{EVA}} = \frac{T_{COND}}{T_{COND} - T_{EVA}} \approx \frac{T_{COND}}{\Delta T_{lift}} \tag{3.5}$$

Equation (3.5) states that there is a performance limit beyond which is impossible to operate even for an ideal machine. So an HP can only approach the COP_{Carnot}, the most efficient the HP the closer the actual COP is to COP_{Carnot}. Therefore also the COP of real HPs is limited by ΔT_{lift}, while it increases for higher temperature of the sink. Nevertheless, it should be remarked that in Equation (3.5) temperatures are expressed in K, so within the range of typical application ΔT_{lift} has much more influence on the COP. Indeed, by keeping constant T_{COND}, and doubling the ΔT_{lift} the maximum achievable COP will decrease by 50%. On the other hand as an example, keeping constant ΔT_{lift}, and increasing T_{COND} from 50°C (323 K) to 100°C (373 K) the theoretical COP increases by 15%. Moreover, for real fluids, the higher the condensing temperature, the lower the fraction of heat exchange that takes place at a constant temperature. This will increases the distance between the real cycle and the ideal Carnot cycle, mitigating or even deleting the theoretical benefits of a higher temperature sink.

3.1.3. Classification

The potential role of HPs has focused the attention and many efforts in researching its development, efficiency improvement, and application in different contexts. This has led to a relevant variety of designs for Vapor Compression Heat Pumps. This section proposes a classification based on three different criteria: cycle design, heat source, and end-use. Table 3.1 on page 71 summarizes the classification criteria hereby proposed.

3.1.3.1. Cycles

Section 3.1.1 has outlined the basic operating principle of a standard VCHP. However, a relevant amount of different variants have been studied and investigated, most of which have not been successfully implemented on the market. A comprehensive review of the cycle design is out of the scope of this chapter, some concepts are hereby presented at glance in order to classify the heat pump technologies.

The first alternative layout introduced is the regenerative HP cycle, already cited within the subsection describing the heat exchangers' features (Subsection 3.1.1.3). Figure 3.3 and Figure 3.4 show the HP scheme and the thermodynamics diagram respectively. The T-s diagram of Figure 3.4(a) is not correct from a formal point of view since the specific entropy of the source and sink heat transfer fluids is reported with the same value on the horizontal axis of the heat pump working fluid. However, such a representation well highlights the temperature levels and the pinch point temperature differences in both the condenser and evaporator.

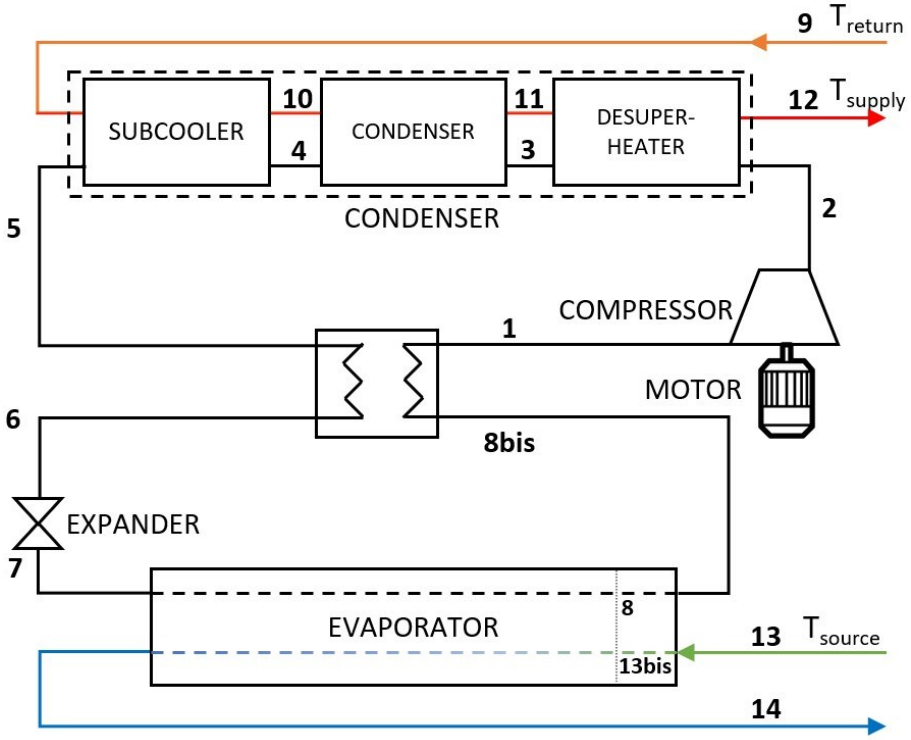

Figure 3.3: Regenerative layout for a vapor compression heat pump.

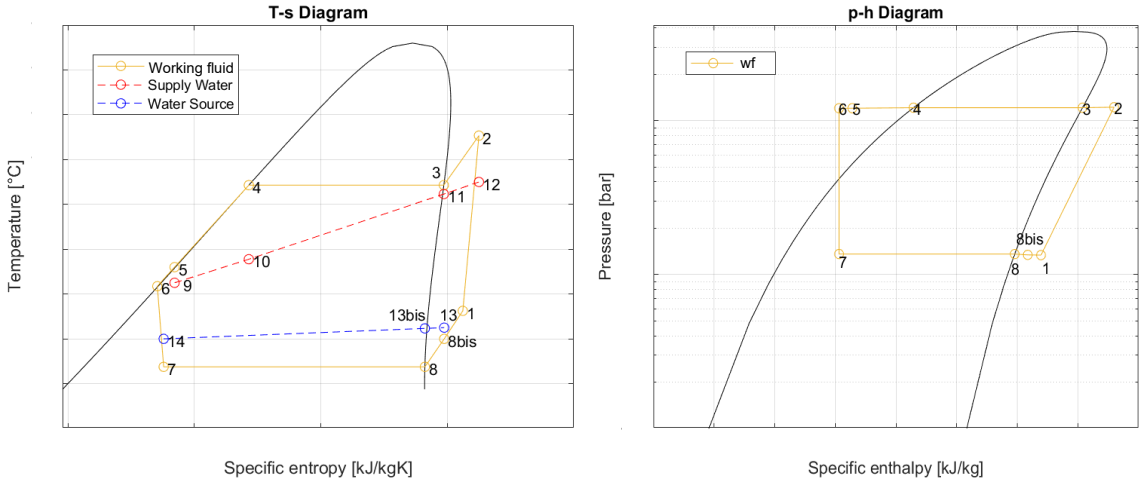

(a) *(b)*

Figure 3.4: Regenerative vapor compression heat pump cycle on the T-s (a) and p-h (b) plans.

The regenerative cycle includes an additional heat exchanger, cooling down further the subcooled liquid (5→6), which has delivered its heat potential to the sink, for the purpose of heating the vapor exiting the evaporator (8bis→1). The scheme shows how the superheating of low-pressure vapor can also start in the evaporator. Point 8 is relative to the saturated vapor condition, point 13bis is defined as the condition of the source heat transfer fluid, once the amount of heat, needed by the transformation 8→8bis, has been released to the working fluid[19]. The χ parameter quantifies the amount of vapor superheating performed by the evaporator on the overall superheating.

$$\chi = \frac{T_{8bis} - T_8}{T_1 - T_8} \cdot 100 = \frac{\Delta T_{SHbis}}{\Delta T_{SH}} \cdot 100 \tag{3.6}$$

So χ=100% implies a standard layout, without a regenerator. χ=0% implies that the evaporator outlet condition on the working fluid side, 8bis, coincides with the saturated vapor condition 8 and the vapor superheating is performed exclusively in the regenerator.

Another interesting variant in heat pump cycles is represented by cycles using an ejector-expander, these are characterized by the fact that compression is not carried out entirely by the compressor but also in part by an ejector. The idea behind these cycles is to eliminate one of the sources of loss and convert it into useful work. This is expansion through the lamination valve, normally operated by a capillary tube or valve. An expansion process operated in this way is highly dissipative and causes large thermodynamic losses, energy is totally lost in friction. Converting this loss into useful work provides a dual benefit, increased capacity at the evaporator and a reduction in the energy required by the compressor. An ejector-expander heat pump allows efficient use of low-temperature heat sources. Depending on the aerodynamics, geometry, and mechanical design of the ejector, many theoretical studies have shown how the COP can be increased by up to 21% compared to that of a conventional heat pump [159].

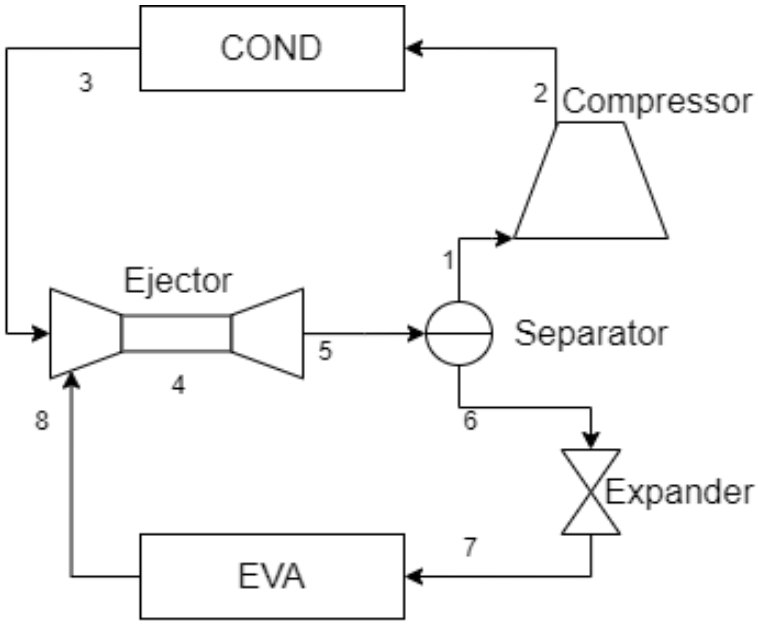

Figure 3.5: Ejector-expander layout for a vapor compression heat pump.

[19] Analogously have been defined the points 10 and 11 for the sink heat transfer fluid.

The general operation is simple, the condensed fluid enters the ejector. This device expands the primary fluid and draws the incoming flow rate from the evaporator, it performs mixing and exploiting the expansion energy of the primary fluid it operates partial recompression of the total flow rate, thus charging itself part of the work that the compressor should perform on the fluid. From here the two-phase fluid goes to a separator that divides the liquid part from the vapor part. The liquid goes to an expansion valve where it undergoes a minor pressure drop and after which it goes to the evaporator, the vapor is sent to the compressor and then to the condenser. From here the cycle starts again.

With relevant ΔT_{lift} values, due to high temperature of supply or too low source temperature (e.g., air during winter in severely cold climates), standards HP presents the following issues:

- Insufficient heat output as the required heat may increases
- High compressor discharge temperature, caused by the low suction pressure and high-pressure ratio across the compressor.
- Low COP (ref. Subsection 0)
- Oversized capacity if the source temperature (e.g., ambient air) increases

Two or multi-stage compressor systems address these problems. Cascade cycle, the two-stage cycle with intercooling, and the two-stage cycle with economizing demonstrated to be the most feasible designs [160,161]. While the cascade cycle consists of two independently operated single-stage refrigeration systems, the latter two designs are classified as compound HPs presenting two or more compression stages connected in series. Both concepts, by means of compression ratio reduction for each single stage, aim at increasing the compression efficiency and reducing the discharge temperature with positive effects on COP and operation management.

A further classification of the cycle can be carried out according to the operating pressure. Standard HPs (subcritical) operate below the critical pressure and working fluids with a low critical temperature (T_{crit}) are disadvantageous because they limit the operating temperature range: heat cannot be delivered at temperatures greater than the critical temperature. Further, at temperatures less than but near T_{crit}, the enthalpy of vaporization is reduced. This leads to a reduction in heating capacity and poor performance of the system. Thus a conventional heat pump should avoid operating at a heat rejection temperature near T_{crit}.

However some HPs operate beyond the critical level, and they are classified as transcritical or supercritical, depending on the low-pressure level. The demand for heat is often for a non-constant temperature supply, so a supercritical condenser pressure well suits such applications, on the other hand, sources are usually at an almost constant temperature (e.g., air, ground, rivers, sea) and a constant temperature heat exchange is appreciable [162]. For this reason, transcritical cycles are more common than supercritical. Moreover, the heat source temperature is a key parameter imposing the choice between transcritical and supercritical. The most used fluid for super/transcritical application is the CO_2 (R744 according to the ASHRAE[20] nomenclature), with a critical temperature of 31.04°C which is a temperature between the source and the sink temperature for many HP applications, then a transcritical cycle must be designed. Otherwise, if the T_{source} is higher than T_{crit} it must be

[20] American Society of Heating, Refrigerating and Air-Conditioning Engineers.

supercritical. $T_{source}>T_{crit}$ may happen if the source temperature is at a higher temperature or if the critical temperature of the adopted fluid is very low. Some options are air (R729) or argon (R740) as working fluids presenting critical temperatures of -140.5°C and -122.4°C respectively in these cases the cycle is forced to be supercritical [163].

3.1.3.2. Source

A. David et al. reviewed and classified the HPs, focusing on large-size applications, according to their sources seven types of sources have been identified: sewage water, ambient water, industrial waste heat, ground, flue gas, district cooling, and solar heat storage [119]. However, these sources can be clustered together based on the components and the design required for the HP. Four main clusters are identified: Air Sourced Heat Pump (ASHP), Water Sourced Heat Pump (WSHP), Ground Sourced Heat Pump (GSHP), and Solar Assisted Heat Pump (SAHP).

The most important characteristics of a heat source are

- The temperature level: as pointed out above the temperature level of the heat sources is directly correlated to the COP. Moreover, low source temperature, implies high ΔT_{lift} may require multistage design
- The stability and the security: besides the temperature level also the stability and the amount of exploitable heat are important in order to ensure a long-term efficient operation
- Proximity to the demand: sometimes some sources can present good thermal level and stability are far away from the urban area or the site where the heat is required limiting the exploitability opportunity

For the ASHPs, ambient air is the most common source, however also flue gas sourced heat pumps can be classified as ASHPs since they require the same heat exchanger typology. Ambient air is probably the most available source, however, its temperature is highly variable, both on a daily and seasonal scale. Moreover, ambient air-sourced heat pumps perform worse when the demand for heat is expected to be higher since low ambient temperatures generally drive high thermal demand and low COP operation of this kind of HP. Other gaseous steams may be included in the same source cluster, because of the similarity of the evaporator, as for the aforementioned flue gasses. Flue gasses represent a waste of heat, therefore their exploitation is considered as a free medium/high-temperature heat source. However they rely on the presence of a combustion process, and the location of the site may be far from the heat demand, moreover, the combustion can also be non-continuous and/or non-synchronous with the demand for heat. The Evaporator usually adopts some fans to force the convective heat exchange on the source side, therefore the fan's electrical consumption should be taken into account in assessing the efficiency performance.

Water can be a good heat source for heat pumps because water has a significantly higher density and approximately four times greater specific heat capacity than air. It can contain considerably more energy per volume than air. Water can be available as a source in different forms, generally, it presents good temperature stability while the temperature level depends on the specific source. Ambient waters are rivers, lakes, and the sea, they are not available everywhere but they are characterized by high thermal inertia and so very good stability in temperature, commonly higher than the ambient temperature during the winter, on the other hand, sewage waters are wildly available in urban areas, are expected to be warmer than

ambient water but the exploitable heat is generally limited. Waste heat can also be available as warm water (or other liquid) mass flow and thus exploitable by a WSHP, the consideration drawn above about flue gases is valid as well. Among wasted heat sources can figure DHC return water, even if real applications exploiting this source have been implemented it cannot be suitable on large scale, since cooling and heating demand are normally inversely correlated. A flat plate or shell and tube heat exchanger is normally adopted as an evaporator for WSHPs.

The ground is probably the source most appreciate for its stability. GSHP can be coupled to the ground by means of a heat transfer fluid or let the working fluid directly evaporate within the ground heat exchanger. The latter solution can be more efficient but implies higher costs, a relevant amount of working fluid, and piping corrosion issues. Ground heat exchangers are generally divided into two categories. It can be placed in a horizontal trench around one to two meters deep, but it requires a significant amount of land area, moreover, because of the shallow burial depth, the temperature can present a seasonal variability. This solution implies low installation costs. Alternatively, it can also be placed vertically in boreholes at a depth of around 50 to 150 m. Vertical GSHPs are more feasible than horizontal in high-density housing areas, however high installation costs from borehole drilling can be the main obstacle [164].

Solar Assisted Heat Pumps (SAHPs) are appreciated for exploiting renewable sources such as the sun, however, this source often lacks stability, and is used within hybrid solutions with others. As for the GSHPs the working fluid can exploit the source directly or indirectly[21], with analog pros and cons [164].

WSHPs, indirect GSHPs, and SAHPs present similarities if the analysis is limited to the cycle components, excluding the auxiliaries and the source heat transfer fluid. Therefore they are sometimes considered a unique cluster.

3.1.3.3. End-Use

Heat pumps can provide three main functions: space heating, and hot water heating in the residential and commercial sectors In addition, they can be used in the industrial sector for drying, food preparation, or paper manufacturing, among other uses. A common nomenclature for heat pumps is X-to-Y HP, where X indicates the source and Y is the sink. According to this air-to-air HPs are ASHPs heating up the air, for example for space heating purposes, water-to-water HPs are WSHPs heating water, and so on.

The kind of sink drives the condenser design, as the source determines the evaporator. HPs designed for air (or generally gaseous fluid) heating should consider fans to force the convective heat exchange on the condenser coil sink side.

The temperatures the heat pumps need to operate at are defined by the requirements of each application, 70-80°C is often considered a threshold value to classify the HP as a High-Temperature Heat Pump (HTHP). HTHPs require specific working fluid to work safely, keeping the higher cycle pressure and the components cost within a reasonable limit, avoiding too high compressor discharge temperature which can imply oil degradation, and maintaining a sufficient distance from the T_{crit}.

[21] The use of an heat transfer fluid, typically water, is more common. Often a low temperature thermal energy storage is included [239].

3.1.3.4. HPs set arrangement

The last classification criterium here proposed actually does not concern the HP itself but how a set of HPs can be arranged together. More than one HP are required to operate together to address two possible requests:

- Large and fluctuating power requirement
- Relevant difference between the source and the sink temperature

Very large capacity installations typically consist of two or more HPs in parallel, it allows limiting the size of each component making suitable those available on the market so avoiding an expensive *ad hoc* designing and manufacturing. HPs arranged in parallels operate among the same source and sink, they are usually identic in the cycle.

HPs series arrangement can be an alternative to multistage HPs. The concepts are not so far, both the solutions do not perform the lift of the working fluid temperature in a single stage. While multistage HPs require a specific design, outlined by Subsection 3.1.3.1, HPs arranged in series work independently and are the sink heat transfer fluid that is heated up in two stages. The source heat transfer fluid can be exploited in series as well if its mass flow is limited. So the HP operates on different thermal levels and their design (working fluid, heat exchangers, compressor, and others) is different.

Table 3.1: Heat pumps' classification resume.

<table>
<tr><td rowspan="3">Cycle Based Classification</td><td rowspan="2">Standard</td><td>Ejector Expansion</td><td rowspan="2">Single Stage</td></tr>
<tr><td rowspan="2">Traditional Compression</td></tr>
<tr><td>Regenerative</td><td>Multi Stage</td></tr>
<tr><td rowspan="4">Source-Based Classification</td><td colspan="3">Air Sourced Heat Pumps</td></tr>
<tr><td colspan="3">Water Sourced Heat Pumps</td></tr>
<tr><td colspan="3">Ground Sourced Heat Pumps</td></tr>
<tr><td colspan="3">Solar Assisted Heat Pumps</td></tr>
<tr><td rowspan="4">End-Use-Based Classification</td><td rowspan="2">Air Heating</td><td colspan="2">Standard</td></tr>
<tr><td colspan="2">High-Temperature Heat Pump</td></tr>
<tr><td rowspan="2">Water Heating</td><td colspan="2">Standard</td></tr>
<tr><td colspan="2">High-Temperature Heat Pump</td></tr>
<tr><td rowspan="2">Arrangement-Based Classification</td><td colspan="3">Series</td></tr>
<tr><td colspan="3">Parallels</td></tr>
</table>

3.1.4. Working fluids

Heat pumps are considered an environmental-friendly technology because of the role they are called to play in the energy transition towards a decarbonized scenario. However, working fluid leakages may have an impact in terms of contribution to ozone depletion or global warming. Then the choice of working fluid is driven, besides the HP's performance maximization, by the aim of minimizing the environmental impact. The two main parameters used for the environmental impact assessments are the Ozone Depletion Potential (ODP) and the Global Warming Potential (GWP), they express the respective potential as a ratio to the standard substance's potential. For the ODP the standard is assumed to be the trichlorofluoromethane (R11), while the carbon dioxide (CO_2 or R744) is the reference for the GWP.

In addition to environmental considerations, there are many technical aspects to take into account when choosing the working fluid. Firstly, the working fluid must adapt to the operating temperatures, guaranteeing reasonable pressures and a suitable distance from the critical pressure for most subcritical applications. Secondly, the maximum temperature reached at the outlet of the compressor is also an important factor, in order to avoid problems related to the degradation of the lubricating oil. Moreover, it should not be forgotten that the pressure level also influences the pressure drop in the exchangers and the value of the overall heat transfer coefficient. Also to be considered are the volumetric capacities necessary for the operation of the cycle to be realized, these influence the dimensions of the compressor and the exchangers or the relative investment costs. Another cost, even if minor, that is influenced by the volume of fluid in circulation, is that of the working fluid itself and its recharge. This may not be a problem in the case of economic substances such as natural fluids but may not be negligible in the case of more expensive fluids. Finally, the choice of fluid imposes considerations about its flammability, toxicity, and corrosiveness, which can be a problem for the safety standards required by some applications.

Chlorofluorocarbons (CFCs) were widely used and appreciated for their properties (both from the performance and safety perspective) in the last century, but because of their relevant ODP, they have been progressively phased out in the 90s as an effect of the Montreal Protocol, agreed on 16 September 1987, and entered into force on 1 January 1989 [165]. Hydrochlorofluorocarbons (HCFCs) have been adopted as transitional CFCs replacements, but they present a positive, even if minor, ODP and their phasing-out has been implemented some decades later. The following generation of HP working fluid and refrigerants are Hydrofluorocarbons (HFCs), among which the widespread R134a or the R410a mixture was considered ideal for R22 replacement. HFCs pose no harm to the ozone layer because, unlike CFCs and HCFCs, they do not contain chlorine. They are, however, greenhouse gases, with a high global warming potential (GWP), comparable to that of CFCs and HCFCs. The rising awareness about climate change and the pledges for GHG emission reduction led to the Kigali Amendment to the Montreal Protocol, which came into force On 1 January 2019 [166]. Under the Kigali Amendment countries promised to reduce the use of hydrofluorocarbons (HFCs) by more than 80% over the next 30 years. However, many countries have adopted stricter policies for years, including Switzerland and Denmark. In Denmark, the use of R134a in quantities greater than 10 kg has been banned since 2006 [167], while Switzerland has adopted a similar strategy, banning the placing on the market of stationary units using HFCs with capacities greater than 600 kW as of December 2013 [109].

Regarding the future, manufacturers are at a crossroads between two possible paths and it is not yet clear which one is the best, as each option has advantages and disadvantages. If

it is true that natural fluids such as ammonia, carbon dioxide, and hydrocarbons are established, some heat pump manufacturers are considering the use of a new family of refrigerants, the hydrofluoroolefins, also known as HFOs, these are slightly flammable fluids, whose ignition conditions, however, are not normal working conditions for standard applications. HFOs are also known as the fourth generation of refrigerants, they are similar to HFCs since they contain hydrogen, fluorine, and carbon, but in contrast to HFCs, they have a low GWP [168].

There is limited literature on hydrofluoroolefins if compared with other fluids. They appear to be applicable to large heat pumps, and generally have lower efficiencies than HFCs. However, their thermodynamic properties are very similar and this would allow the replacement of the working fluid in existing pumps with minimal plant modifications. However, these fluids are often criticized because of the toxic substances that in case of leakage into the environment are released as a result of their degradation [169].

On the other hand, as regards natural fluids, ammonia (R717), although toxic and flammable, has reached a certain level of popularity and technological maturity since it was wildly adopted since the half of the XIX century. HPs that adopt it can achieve similar performance, in some cases even better, than those that use HFCs. However, for HTHPs applications it implies considerable pressures and poses critical issues also in terms of maximum cycle temperature [170]. Another natural refrigerant used is CO_2 (R744), an inert fluid and completely safe for health, that is able to provide remarkable performance but is disadvantaged by the high operating pressures and thus by its expensive components. CO_2 HP operates transcritically or supercritically. Finally, hydrocarbons are the only natural fluids along with ammonia to have a stable presence on the market, they are non-toxic but highly flammable. Propane (R290) is particularly attractive as a substitute for R22 [171], while isobutane (R600a) and even more butane (R600) are interesting for HTHP applications [172].

Table 3.2 reports some of the most relevant fluids adopted for refrigeration and HP purposes, at least one fluid for each mentioned category (CFCs, HCFCs, HFCs, naturals, and HFOs) have been reported. This list is for an illustrative purpose only and is not intended to be complete or definitive

Table 3.2: Most notable working fluid features for each category.

	Molecular Formula	**ASHRAE Name**	**ODP**	**GWP**	**P_{crit} [bar]**	**T_{crit} [°C]**	**Type**
Dichlorodifluoromethane	CCl_2F_2	R12	1	10,000	41.36	11.97	CFC
Chlorodifluoromethane	HCF_2Cl	R22	0.05	1,700	49	96.1	HCFC
Tetrafluoroethane	CH_3	R134a	0	1,430	40.6	101.0	HFC
Forane 410A	mixture	R410a	0	2,088	47.7	70.2	HFC
Ammonia	NH_3	R717	0	0	113.5	132	Nat.
Carbon dioxide	CO_2	R744	0	1	73.8	31	Nat.
Propane	C_3H_8	R290	0	3	42.5	96.7	Nat.
Butane	C_4H_{10}	R600	0	3	38.0	152	Nat.
Isobutane	C_4H_{10}	R600a	0	3	36.3	134.7	Nat.
Tetrafluoropropene	CH_2	R1234yf	0	4	33.8	94.7	HFO
Trans-1,3,3,3-Tetrafluoroprop-1-ene	CF_3CH	R1234zeE	0	7	36.4	109.4	HFO

3.1.5. Economic aspects

The cost of a heat pump is vital in determining its use. The installation and economic viability of heat pumps rely heavily on different aspects, including climate conditions, locations, local policies, and market prices [85,173]. Heat pumps may be more expensive than other heating or cooling devices. Better system performance, environmental characteristics, and operating costs may compensate for this drawback.

Wang et al. [164] report a scheme to preliminary assess the Capital Expenditure (CAPEX) and the Operational Expenditure (OPEX), highlighting how they depend on the HP typology, the source, and the location. Ommen et al. [170] applied to the HPs the method proposed by Bejan [174] for assessing the CAPEX for each specific application.

3.2. Mathematical model for thermodynamic design and economic assessment

A mathematical model was developed in MATLAB in order to assess the performance of HPs both as stand-alone devices for power-to-heat purposes (the results of a techno-economic analysis of power-to-heat systems are reported in Section 3.3) and the CCGT-HP coupled layouts assessed in Chapter 4.

The model is developed in MATLAB, using a python wrapper to access the open sources CoolProp libraries [175]. A standard one stage vapor compressor architecture is considered, and the possibility of internal regeneration is also taken into account as illustrated in Figure 3.3. Figure 3.3 reports numbers that identify the fluid status, the same numbers are used in the equations' nomenclature of the next section.

3.2.1. HP Modelling and Thermodynamic Cycle Design

First, all the inputs to the model are hereby listed:

- The HP capacity (Q_{COND}), the power delivered to the sink from the condenser
- The supply temperature (T_{12}), the temperature at which the heat transfer fluid, commonly water, is heated up
- The source temperature (T_{13}), the temperature at which the heat source is available
- The temperature difference at the sink ($\Delta T_{sink}= T_{12} -T_9$), the return heat transfer fluid temperature, commonly it is correlated to the supply temperature
- The temperature difference for the source fluid ($\Delta T_{source}= T_{13}-T_{14}$), this parameter describes the source heat abundancy, alternatively, the source fluid mass flow can be provided as an input and the ΔT_{source} value is derived from the computed heat transferred to the evaporator (Q_{EVA})[22]
- The working fluid
- The pinch point temperature difference required at each heat exchanger (ΔT_{HXpp})

[22] The equations from (3.7-3.32) presented in this section are relative to model requiring ΔT_{source} as input. If Q_{EVA} is provided as an input the core of the model remain unaltered but the equations concerning T_{14} and the source fluid mass flow requires to be implemented differently but the applied energy balance are the same.

- The superheating required at the compressor suction (ΔT_{SH})
- The χ, as defined by equation 3.6
- Compressor efficiency

The cycle computation is based on a nested iterative logic starting from point 8, i.e., the saturation point after evaporation. Equations (3.7-3.32) describe the energy balance applied to each HP component, besides the iterative logic described, alternatively, Figure 3.6 provides a full schematic visualization of the iterative computational cycles.

First, the compressor suction conditions are computed, requiring to define status 8

$$T_8 = \begin{cases} T_{13} - \Delta T_{EVA\,pp} - \Delta T_{SHbis}, & \Delta T_{SHbis} > \Delta T_{source} \\ T_{14} - \Delta T_{EVA\,pp}, & \Delta T_{SHbis} \leq \Delta T_{source} \end{cases} \quad (3.7)$$

By equation (3.7) T_8 is selected as the maximum temperature complying with the pinch point temperature difference requirement at the evaporator ($\Delta T_{EVA\ pp}$), then and $T_{8bis}=T_8+\Delta T_{SHbis}$. Recalling equation (3.6), ΔT_{SHbis} is deduced from χ

$$\Delta T_{SHbis} = \Delta T_{SH} \cdot \frac{\chi}{100} \quad (3.8)$$

So the status 1

$$T_1 = T_8 + \Delta T_{SH} \quad (3.9)$$

$$p_1 = p_8 - \Delta p_{1\rightarrow 8bis} - \Delta p_{8bis\rightarrow 8} \quad (3.10)$$

$$h_1 = f(p_1, T_1) \quad (3.11)$$

To take into account the influence of compressor efficiency, the isentropic conditions at point 2, i.e., the compressor discharge, are assessed. A first attempt value of p_2 is guessed.

$$h_{2s} = f(p_{2s} = p_2, s_{2s} = s_1) \quad (3.12)$$

where the s subscript refers to the iso-entropic conditions.

$$h_2 = h_1 + \frac{h_{2s} - h_1}{\eta_{comp}} \quad (3.13)$$

Status 3 is defined as the saturation point at pressure p_3

$$p_3 = p_2 - \Delta p_{3\rightarrow 2} \quad (3.14)$$

$$h_3,\ T_3 = f(p_3,\ q_3 = 1) \quad (3.15)$$

Then is possible to compute the heat exchanged in the desuperheater section and thus the temperature T_{11}

$$Q_{DSH} = \frac{(h_2 - h_3)}{\dot{m}_{wf}} \quad (3.16)$$

$$T_{11} = T_{12} - \frac{Q_{DSH}}{\dot{m}_{HTF} \cdot c_{p_{HTF}}} \quad (3.17)^{23}$$

From T_{11} is possible to determine the minimum value of T_3 complying both with the pinch point temperature difference requirement at the condenser and the superheater, then a new best value for p_2

$$T_{3_{new}} = max\left(T_{11} + \Delta T_{COND\ pp}, T_1 + \Delta T_{SH\ pp}\right) \quad (3.18)$$

$$p_{2_{new}} = f\left(T_{3_{new}},\ q_3 = 1\right) + \Delta p_{3\to2}$$

Then the new value of the discharge pressure is iterated to equation (3.12) until T_3 converges. It should be highlighted that equations (3.16 and 3.17) require the working fluid mass flow. Firstly this value is guessed then another iteration cycle guarantees a proper value.

After the first cycle reaches the conversion is possible to define the status 4, i.e., the saturated liquid after condensation

$$p_4 = p_3 - \Delta p_{3\to4} \quad (3.19)$$

$$h_4,\ T_4 = f(p_3,\ q_4 = 0) \quad (3.20)$$

T_{10} can be deduced analogously to T_{11} by means of T_{11} itself and the heat exchanged in the condensing section. Then the heat exchanged in the subcooler section is imposed by T_9

$$Q_{cond} = \frac{(h_3 - h_4)}{\dot{m}_{wf}} \quad (3.21)$$

$$T_{10} = T_{11} - \frac{Q_{cond}}{\dot{m}_{wf} \cdot c_{p_{HTF}}} \quad (3.22)$$

$$Q_{SC} = \dot{m}_{wf} \cdot c_{p_{HTF}} \cdot (T_{10} - T_9) \quad (3.23)$$

Concerning the status 5, pressure is equal to p_4 minus the pressure loss, and the temperature is imposed by the subcooler and regenerating superheater (SH) constraints, the other properties follow

$$T_5 = max\left(T_9 + \Delta T_{COND\ pp}, T_1 + \Delta T_{SH\ pp}\right) \quad (3.24)$$

$$h_5,\ s_5 = f(p_5 = p_4 - \Delta p_{4\to5},\ T_5) \quad (3.25)$$

Since at the superheater's cold side both inlet and outlet conditions are imposed, status 6 is computed based on the heat exchanged in the superheater.

$$Q_{SH} = \dot{m}_{wf} \cdot (h_1 - h_{8bis}) \quad (3.26)$$

$$h_6 = h_5 - \frac{Q_{SH}}{\dot{m}_{wf}} \quad (3.27)$$

---

[23] The heat transfer fluid mass flow is known since both ΔT_{sink} and the HP capacity are provided as input.

$$T_6, s_6 = f(p_6 = p_5 - \Delta p_{5\to6},\ h_6) \tag{3.28}$$

At this point, the respect of the $\Delta T_{SH\ pp}$ should be verified, and in case the requirement is not met the discharge pressure p_2 should be revised upward iterating until its convergence.

$$p_{2_{new}} = \begin{cases} f\left(T_{5_{new}} = T_1 + \Delta T_{SH\ pp},\ s_5\right), & T_5 - T_1 < \Delta T_{SH\ pp}\ and\ T_5 - T_1 \geq T_6 - T_{8bis} \\ f\left(T_{6_{new}} = T_{8bis} + \Delta T_{SH\ pp},\ s_6\right), & T_6 - T_{8bis} < \Delta T_{SH\ pp}\ and\ T_5 - T_1 < T_6 - T_{8bis} \end{cases} \tag{3.29}$$

Then, once the discharge pressure value has converged the cycle computation carries on with the status 7, i.e., the evaporator inlet, the expansion is assumed to be iso-enthalpic, and the pressure is equal to the pressure in 8 plus the evaporator pressure drop, so that

$$T_7, q_7 = f(h_7 = h_6, p_7 + \Delta p_{7\to8}) \tag{3.30}$$

Since all the points of the cycle are now defined is possible to calculate a proper working fluid mass flow rate that matches the input HP capacity

$$\dot{m}_{wf_{new}} = \frac{Capacity}{(h_2 - h_5)}. \tag{3.31}$$

The code iterates from 3.12 to 3.31 until the working fluid mass flow rate convergence. Finally, the source fluid mass flow depends on heat extracted by the evaporator

$$\dot{m}_{source_{new}} = \frac{(h_{8bis} - h_7) \cdot \dot{m}_{wf}}{(T_{13} - T_{14}) \cdot c_{p_{source}}}. \tag{3.32}$$

Then is possible to calculate some important key performance indicators such as the coefficient of performance (COP) or the volumetric heat capacity (VHC)

$$COP = \frac{Capacity}{P_{el}} = \frac{Capacity}{(h_2 - h_5) \cdot \dot{m}_{wf}} \cdot \eta_{motor} \tag{3.33}$$

$$VHC = \frac{Capacity}{\dot{v}_{wf_1}} = \frac{Capacity}{\dot{m}_{wf} \cdot v_1} \tag{3.34}$$

For all the pressure drop computation is assumed a simplified procedure as in equation (3.35)

$$\Delta p_{i\to i+1} = 0.05 \cdot p_i \tag{3.35}$$

Figure 3.6, on the next page, reports a schematic and synthetic visualization of the above equations, the yellow box highlights the first iterative cycle, setting a proper discharge pressure so that the temperature T_3 complies with the condenser temperature difference. The orange box identifies the second iteration which adjusts, if needed, the pressure level so that also the regenerative superheater pinch point temperature difference is respected. Finally, the blue box is relative to the iteration carried out until the working fluid mass flow convergence. Blue variables represent those that are imposed, while red ones are the input to the model.

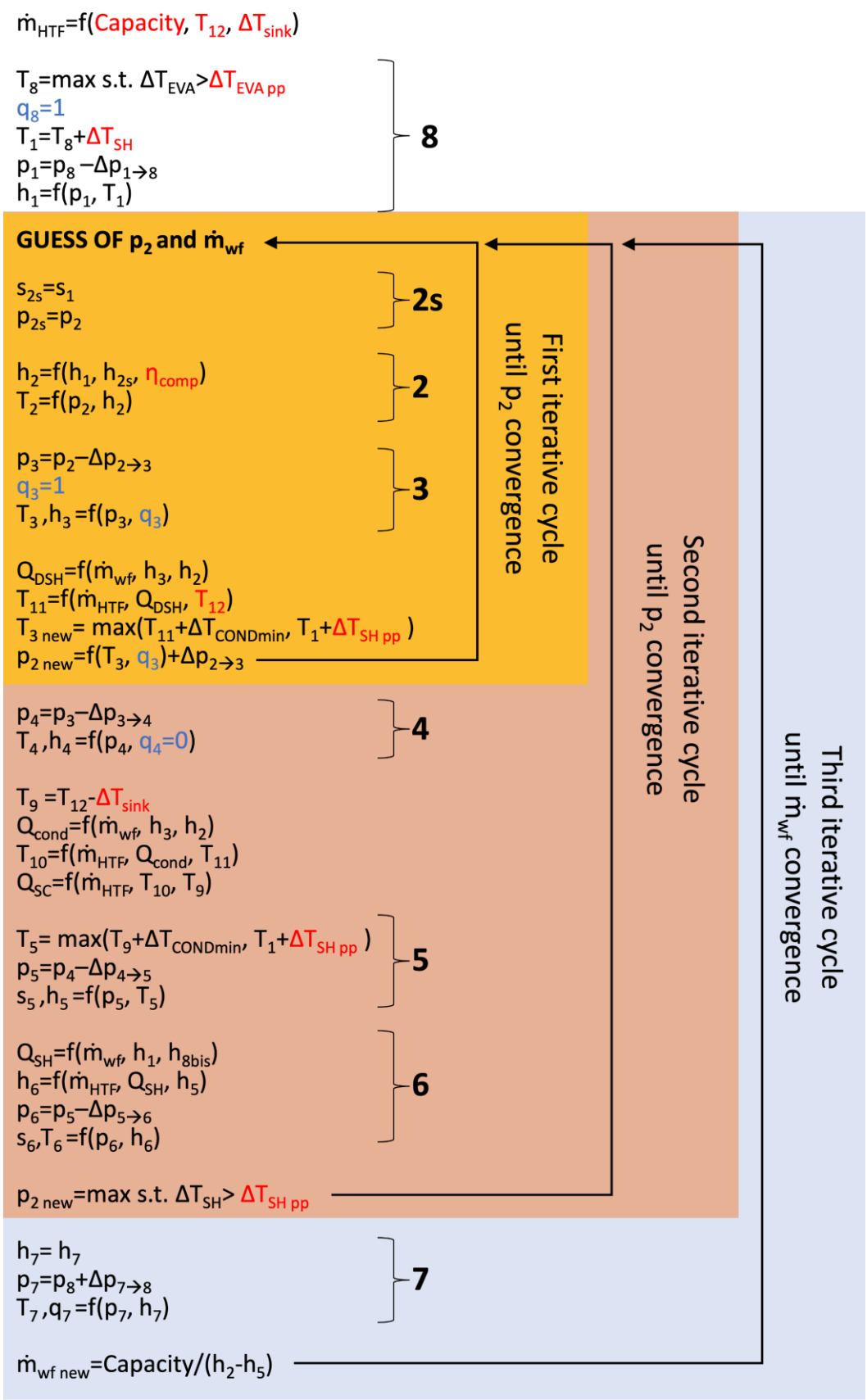

Figure 3.6: Nested iterative logic for the thermodynamic HP cycle computation.

3.2.2. Economic Assessment

According to the method presented by Bejan et al. [174], the total cost of investment (TCI) required by the heat pump is assessed based on the individual components Purchased Equipment Cost (PEC). The TCI, in this case, is equal to 4.16 times the sum of all components' PEC, this accounts for additional costs related to new investment at an existing facility.

The thermodynamic model, described in the previous subsection, selects the best cycle according to the boundary conditions, maximizing the evaporator pressure and minimizing the condenser pressure, thus maximizing the COP. After this model is used to design the cycle, the size of each component can be determined. Thus specific cost functions assess the component's PEC.

3.2.2.1. Heat Exchangers PEC assessment

Concerning the heat exchangers the described model gives as an output the exchanged thermal power which depends on the needed area devoted to the heat exchange. This parameter is the main one influencing the heat exchanger besides the heat exchanger typology (e.g., shell and tubes, plates, finned tubes) and the design pressure.

First, the heat exchanger typology is imposed for all the heat exchangers. The condenser (including the desuperheater, the condensing section, and the subcooler), and the regenerator is selected to be Chevron-type plates heat exchangers, while the evaporator selection depends on the heat source. For ASHP finned tube evaporator coil is adopted, while shell and tubes are for WSHP or GSHP. For those HPs exploiting high-temperature heat sources, such as waste heat from industrial processes or power plant thermal cascades, a Chevron plates evaporator is selected.

The Logarithmic Mean Temperature Difference (LMTD) across the heat exchanger is used to calculate the surface needed, according to equation (3.36) the area is directly proportional to the heat rate, and inverse to the global heat exchange coefficient U [W/m^{2}K] and the LMDT.

$$\mathrm{A} = \frac{\dot{Q}}{\mathrm{U} \cdot \mathrm{LMTD}} \tag{3.36}$$

$$\mathrm{LMDT} = \frac{\Delta \mathrm{T}_1 - \Delta \mathrm{T}_2}{\ln\left(\frac{\Delta \mathrm{T}_1}{\Delta \mathrm{T}_2}\right)} \tag{3.37}$$

where the subscripts 1 and 2 refer to the two heat exchanger sides, so that for a counter flow heat exchanger:

$$\Delta \mathrm{T}_1 = \mathrm{T}_{hot_{out}} - \mathrm{T}_{cold_{in}} \tag{3.38}$$

$$\Delta \mathrm{T}_2 = \mathrm{T}_{hot_{in}} - \mathrm{T}_{cold_{out}} \tag{3.39}$$

Equation (3.36) highlights the importance of the global heat transfer coefficient U, the purpose of this thesis is not to focus on an accurate estimation of U. Many studies, both numerical and experimental have investigated the dependence of U on many parameters. The aim is to develop a flexible and fast-to-run tool for a preliminary techno-economic assessment of HPs for stand-alone power-to-heat purposes and CCGT coupling.

The HP manufacturer of the PUMPHEAT project provided values for the global heat transfer coefficient for butane (R600) working fluid and Chevron plate heat exchangers. For other heat exchangers, the VDI Heat Atlas is taken as a reference [176]. Reference values (reported in Table 3.3) differ each from the others mainly for the exchanger typology and the phase on both sides (e.g., liquid-to-liquid, liquid-to-gas, gas-to-gas, condensation, or evaporation implies relevant differences in the heat exchange phenomena) and are associated with reference conditions, pressure and temperature for single-phase heat exchangers, pressure and temperature difference for two-phase ones. Table 3.3 includes "Evaporator bis", as in Figure 3.3, which refers to the last section of the evaporator devoted to the working fluid superheating from status 8 to 8bis.

U is the sum of the three main thermal resistances, due to the convection heat transfer on the hot and cold sides, and the conductivity of the heat exchanger wall. To take into account the working fluid's ability in transferring heat, and the influence of working conditions on the heat transfer, the reference values of U are corrected based on a simplified calculation in order to adjust the changed thermal resistance.

$$\mathrm{U} = \frac{1}{K_{hot} + K_{HX} + K_{cold}} \tag{3.40}$$

$$\mathrm{K}_{hot/cold} = \frac{1}{h} \tag{3.41}$$

$$\mathrm{K}_{HX} = \frac{t}{k} \tag{3.42}$$

The thermal resistance adjustment is carried out on the basis of calculations on simplified geometries, marked by * in equation (3.43), ref subscript is relative to the reference conditions in Table 3.3.

$$\mathrm{K} = K_{ref} \cdot \frac{K^*}{K^*_{ref}} \tag{3.43}$$

Then, the heat exchanger cost is assessed by employing the cost functions reported in Table 3.3, using the heat exchanger area as the input parameter. The area depends on the logarithmic temperature difference, the heat exchanged, and the overall heat transfer coefficient. The last is assessed at the working condition for the actual working fluid from the reference values (Table 3.3) and equations (3.40-3.43). Finally, the last factor having an impact on the heat exchanger PEC is the operating pressure, Turton et al. [177] reported how the operative pressure influence the cost function adopted for the finned tube evaporator, while for the other heat exchangers the pressure difference, from the nominal value for which the adopted cost functions are designed, influence on the other heat exchangers was the final cost according to the formula reported by Seader et al. [178].

For K* and $\mathrm{K}^*_{\mathrm{ref}}$ assessment the following correlations are adopted. Considering the same Reynolds number, corresponding to a moderately turbulent flow, both for actual and reference conditions.

- **Single-phase fluid:**

Martin's [179] methodology for Nusselt number assessment in a Chevron plate channel is

$$Nu = 0.122 \cdot Pr^{\frac{1}{3}} \cdot \left(\xi \cdot Re^2 \cdot \sin(2\varphi)\right)^{0.374} \tag{3.44}$$

$$h^* = \frac{Nu\ k}{L} \tag{3.45}$$

Where φ is the plate's area enlargement factor (i.e., the ratio between the actual plate area and its projection, it describes the dimensions of corrugations), k is the thermal conductivity and L is the characteristic length.

- **Condensing fluid:**

For this purpose film condensation on a vertical squared (1 m x 1 m) flat plate is assumed, and the correlation for the considered Reynolds number was proposed by Labuntsov [180].

$$h^* = \frac{Re\ k_{liq}}{8750 + 58\ Pr^{-0.5}(\ Re^{0.75} - 253)} \left(\frac{g}{v_{liq}^2}\right)^{\frac{1}{3}} \tag{3.46}$$

- **Evaporating fluid:**

The same flat plate geometry is adopted also for the evaporating fluids, the heat exchange is modelized under the film boiling assumption [181]. Firstly, the heat is assessed according to the following correlations, where D and C_{film} are geometrical coefficients equal to 1 under these assumptions:

$$a = \mathrm{g}\ k_{vap}^3\ \rho_{vap}\ (\rho_{liq} - \rho_{vap})\ \left[H_{lv} + 0.4\ c_{p_{vap}}(T_{flat\ plate} - T_{sat})\right] \tag{3.47}$$

$$b = \mu_{vap}\ D\ (T_{flat\ plate} - T_{sat}) \tag{3.48}$$

$$Q_{film\ boiling} = C_{film} \left(\frac{a}{b}\right)^{\frac{1}{4}} (T_{flat\ plate} - T_{sat}) \tag{3.49}$$

$$h^* = \frac{Q_{film\ boiling}}{A\ (T_{flat\ plate} - T_{sat})} \tag{3.50}$$

Table 3.3: heat exchangers' global heat transfer coefficients and cost functions.

	Typology	U_{ref} [W/m^{2}K]	P_{ref} [bara]	T_{ref} [°C]	ΔT_{ref} [K]	Cost Function
Evaporator	Finned tubes	300	7.4		4	[177]
	Shell and tubes	600	7.4		4	[182]
	Chevron plates	2500	7.4		4	[170]
Evaporator bis	Finned tubes	45	7.4	65		[177]
	Shell and tubes	85	7.4	65		[182]
	Chevron plates	230	7.4	65		[170]
Condenser	Chevron plates	2500	21.8		15	[170]
Subcooler	Chevron plates	2850	21.7	107		
Desuperheater	Chevron plates	350	21.8	132		
Regenerative superheater hot side	Chevron plates	50	21.6	84		[170]
Regenerative superheater hot side			7.2	78		

3.2.2.2. Other Components PEC assessment

Apart from the heat exchangers, the compressor, and the electric motor are components with a relevant PEC affecting the TCI, the compressor is sized based on the volumetric mass flow at the suction side. The motor, whose efficiency is assumed 95%, is sized according to the required electric power. Both are outputs of the model described in Section 3.2.1, then the PEC is assessed according to the cost function reported by Ommen T. et al [170].

3.2.2.3. Model comparison against public data

To assess the model's ability in modeling the HP cycle and predicting the real performance, it is run for the same operating conditions as for the machines whose performance and operating data are reported by David et al. in the supplementary materials of their paper [119]. The database, summarized in Table 3.4includes data about 125 HPs, only 55 report all the data needed as model inputs (working fluid, capacity, supply temperature, source temperature, and source type), beside the COP value to compare against the model output. The source temperature difference at the evaporator is assumed to be 20 K and 10 K, for waste heat recovery applications and others respectively.

Table 3.4: Large vapor compressor heat pumps by source and fluids [119]

Heat Sources		**Water**		**Waste Heat**	
Refrigerant		**R717**	**R134a**	**R717**	**R134a**
Units [#]		14	64	12	12
Unit Capacity [MW]	min	1.2	0.8	1	1.5
	avg	2.45	14.8	1.5	9.3
	max	4.4	50	3	17
T source [°C]	min	0	3	18	12
	avg	10.7	15.5	31	31
	max	25	55	40	38
T supply [°C]	min	43	55	60	70
	avg	71.7	78.0	68	79.1
	max	90	90	81	90
COP [-]	min	2.85	2.65	3.9	3.1
	avg	3.8	3.15	4.86	4.1
	max	5.5	6	6.5	5.4
$\frac{\mathbf{COP}}{\mathbf{COP_{id}}}$ **[%]**	min	48.7	36.6	32.6	39.5
	avg	67.5	55.2	51.0	57.9
	max	85.5	75.6	69.2	75.9

Assuming that the design target of these HPs was an economic optimization, the superheating temperature at the compressor suction is the one that maximizes the economic performance for each of the 55 HPs. Then, HPs in the database are divided according to the DHN generation they can feed, based on the classification illustrated in Section 1.2. For each generation[24], is evaluated the average pinch point temperature difference at the heat exchangers (i.e., the pinch point temperature difference) that minimizes the COP deviation between the model output and the database value. It results in 2.4 K and 4.2 K for the 4th and 3rd generation respectively, and the COP deviation probability density is reported in the following figures.

[24] Only the 4th (T_{supply}<75°C) and the 3rd (75°C≤T_{supply}<105°C) generation are present in the database.

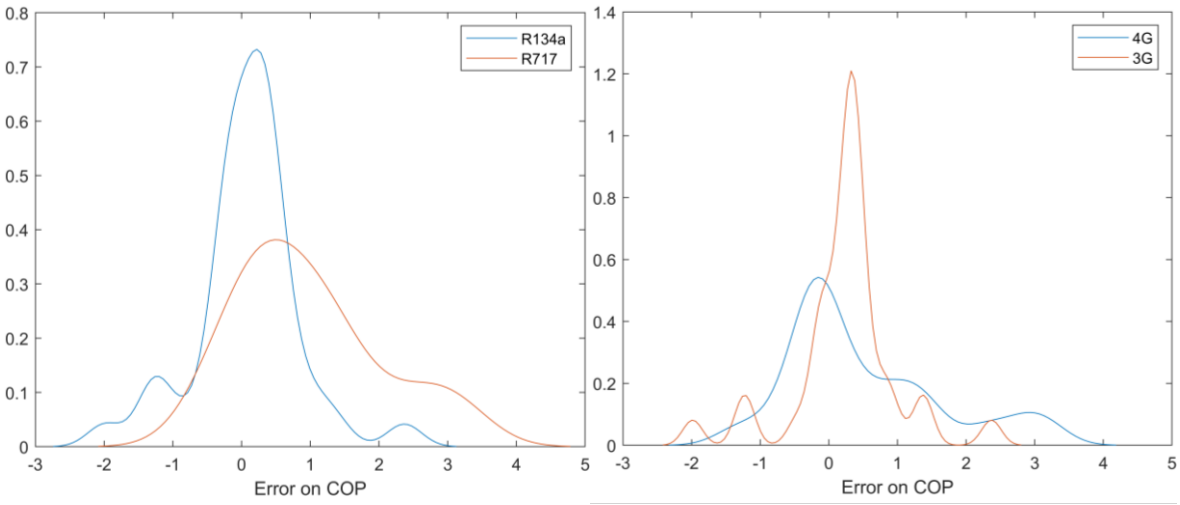

(b) *(c)*

Figure 3.7: COP deviation between model and database [119]*, for different fluids and DHN generation (supply temperature).*

Data for the 3rd DHN generation ($75°C \leq T_{supply} < 105°C$) and for R717 working fluid are much more sparse and for these reasons the model results to be less accurate in fitting the COP values.

3.3. Techno-economic analysis of HTHPs

The model described in Section 2.2 is here applied to a general techno-economic analysis of power-to-heat solutions for DHNs. The first subsection aims to compare how different fluids behave varying the supply temperature and the source temperature, exploring how much higher investment in HP's components is paid back in terms of better performance (i.e., higher COP) that are reflected in lower variable cost operating the heat pump.

The second subsection focuses on specific cases identified through the first analysis, investigating the sensitivity of techno-economic indicators to the thermal demand (HP capacity and working hours) and economic scenario (retail electricity and natural gas price). Within this analysis, the investigated HTHPs are benchmarked against an already Heat-Only-Boiler (HOB) assessing the technology viability against competitor technologies characterized by higher emissions.

3.3.1. Fluid comparison

The analysis here presented is based on a systematic process of multi-objective optimization (MOO) running the model described in Section 3.2. The MOO algorithm used for this purpose is the paretosearch function in MATLAB, the first object optimized is the minimization of the HP's total cost of investment (TCI) which represents almost the whole amount of fixed costs paid during the system lifespan. The second objective is the maximization of the COP on which relies the variable costs, i.e. the electricity needed for operating the HP. Higher investment is reflected in larger heat exchanger heat transfer surfaces and larger compressors able to deal with larger volumetric flows, then the possibility to design cycle with lower pressure lifts, less power required to the compressor for the same amount of heat discharged at the sink (higher COP).

The best trade-off between capital expenditure and the variable cost depends on the economic indicator which is targeted by the design (net present value, payback period, levelized cost of heat, or others) and on the assumptions about the interest rate and inflation rate. However, the multi-objective optimization output visualized as a Pareto front curve allows comparing the performance independently of a single KPI, assessing how much cost in terms of investment a reduction of variable cost. Reporting the COP on the x-axis and the specific CAPEX on the y-axis, the higher is the Pareto front slope more expensive is the increase in COP.

Figure 3.8, Figure 3.9, and Figure 3.10 report the described Pareto fronts for different HP applications comparing different fluids. The analysis considers three fluids presenting reduced environmental impact: Ammonia (R717) and two hydrocarbon fluids butane (R600) and propane (R290), whose performances are benchmarked against the standard R134a, today avoided because of its high Global Warming Potential (ref. Section 0). The heat source is supposed to be waste heat from an industrial process and the heat is supplied to a DHN, as pointed out in Chapter 1, these applications represent promising solutions to provide a low carbon heat supply, nevertheless often they are not competitive enough on the market if compared to traditional gas-fired boilers. The analysis here presented, as well in Section 3.3, investigates the HP technology readiness to replace traditional boilers to supply heat to a network when waste heat is available as a low-temperature source. In the current scenario.

Different scenarios are considered, the supply temperature is varied according to 2nd, 3rd, and 4th generation typical values (i.e., 120°C, 90°C, and 60°C respectively), heat sources are a low-temperature (30°C) and a medium temperature (70°C). The ΔT at the evaporator on the source side is imposed to 20 K, the investigated HP capacity is 3kW$_{th}$, a sensitivity analysis of this parameter is presented in Section 3.3.2. The other inputs to the model (the superheating degree at the compressor suction ΔT_{SH}, χ as defined by equation 3.6, and the pinch point temperature difference at the condenser $\Delta T_{COND\ pp}$, the subcooler $\Delta T_{SC\ pp}$, the regenerative superheater $\Delta T_{SH\ pp}$, and the evaporator $\Delta T_{EVA\ pp}$) are the optimization variables.

Not every fluid can feed 2nd generation DHNs supplying heat up to 120°C performing a subcritical cycle, for instance, R134a and R290 have critical temperatures of 101°C and 96.7°C respectively[25]. Moreover, the scenario with T_{supply}=60°C and T_{source}=70°C is not considered.

First, from Figure 3.8, Figure 3.9, and Figure 3.10, is possible to appreciate the dependence of the COP on the temperature lift. For those HPs feeding a 2nd generation DHN, the COP is limited to 4-4.5 and 2.5-3 for 30°C and 30°C T_{source} respectively. For 3rd generation DHN, the limits move to 6.5 and 3.5, while for T_{supply}=60°C and T_{source}=30°C it is between 4.5 and 5. While for CAPEX is much more relevant the source temperature, lower temperature implies lower pressure and so higher volumetric flow at the compressor suction

[25] N.B. The critical temperature is not the real limit, in facts for discharge pressures below the critical pressure is possible reach temperature above critical temperature since the fluid present the status of superheated vapor. Is not easy to establish a certain correlation between the fluid critical temperature and maximum feasible temperature of supply. The discharge pressure relies also on the temperature difference at the heat exchangers, and the superheating degrees at the discharge depends on the superheating imposed at the suction side. However the present analysis demonstrate that neither R134a nor R600 suit supply temperatures that characterize 2nd generation DHNs.

affecting the cost of this component. The fluid influence the final cost in two different ways, by the ability of the fluid in transferring heat, higher convection heat transfer coefficient for the same conditions, and by the density at the compressor suction side, higher volumetric mass flow requires bigger and more expensive compressors. In all the scenarios R600 results to be the most expensive fluid, followed by R134a, R290, and the cheapest ammonia (R717).

Despite the lower operative pressures which characterize the R600 cycle (if compared against R717), the HP cost results increased. The reason relies on the higher specific volume of butane requiring a larger compressor, the volumetric flow rate is even higher because of the considerable adopted superheating degrees. The R600 vapor saturation curve has a positive slope on the T-s diagram, it implies that the superheated vapor a the compressor suction approaches the saturation line during the compression. To avoid the condensation of a fraction of vapor within the compressor, larger superheating is adopted with severe consequences on the compressor's cost. This problem is more serious the higher the compression ratio is, consequently the costs increase a lot for HPs addressing considerable temperature lifts.

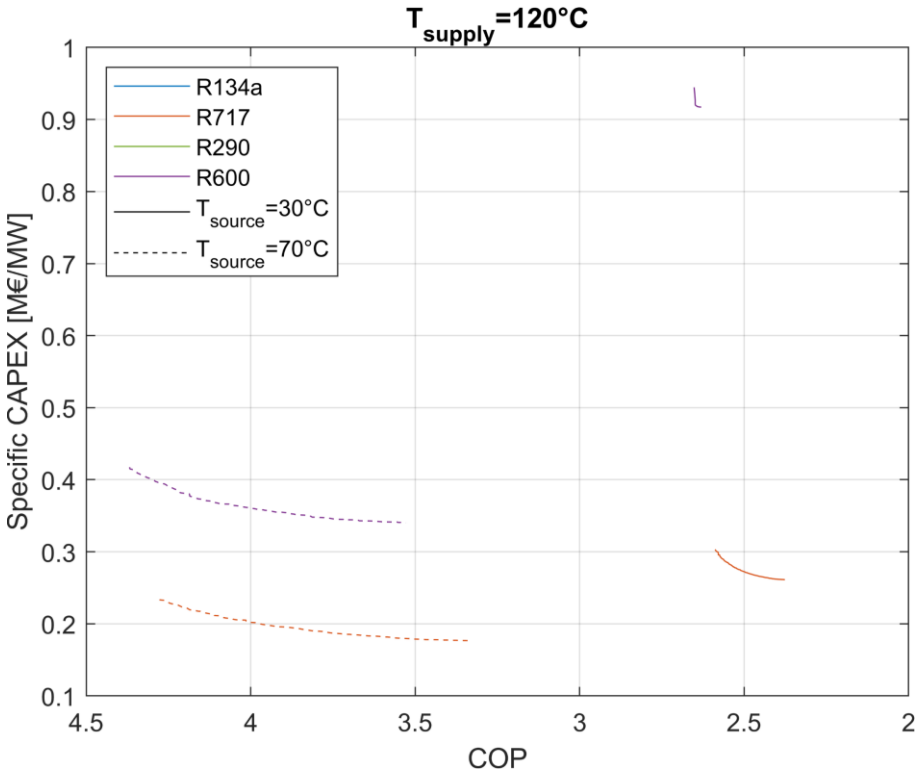

Figure 3.8: Pareto fronts analysis for different fluids as working fluid of an HP feeding a 2nd generation DHN, two different source temperature levels are considered, 30°C (continuous lines) and 70°C (dashed lines).

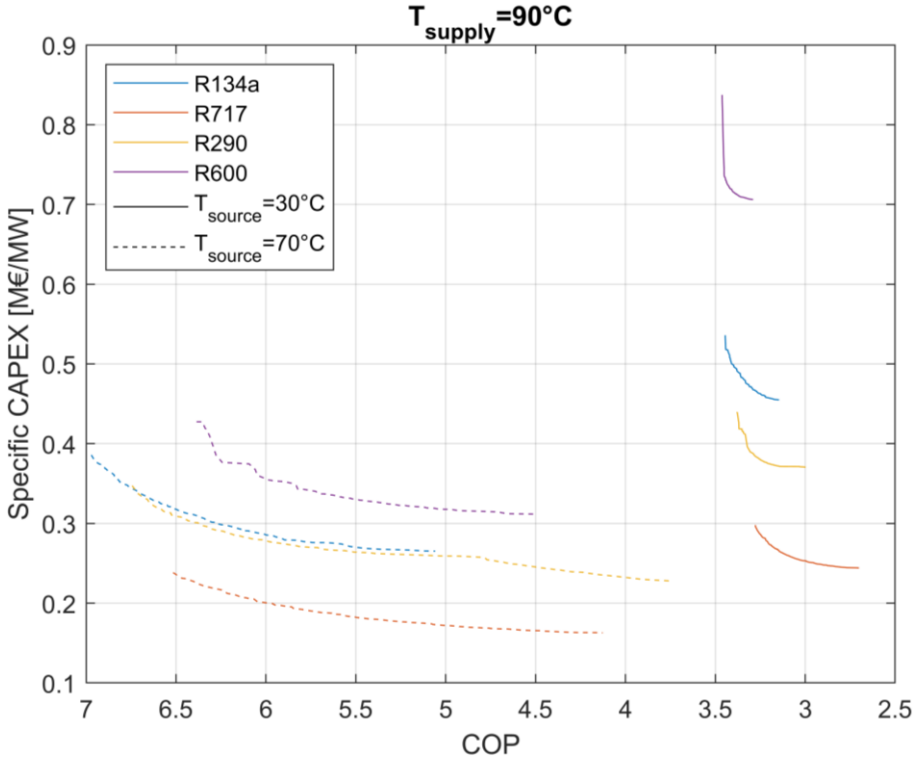

Figure 3.9: Pareto fronts analysis for different fluids as working fluid of an HP feeding a 3rd generation DHN, two different source temperature levels are considered, 30°C (continuous lines) and 70°C (dashed lines).

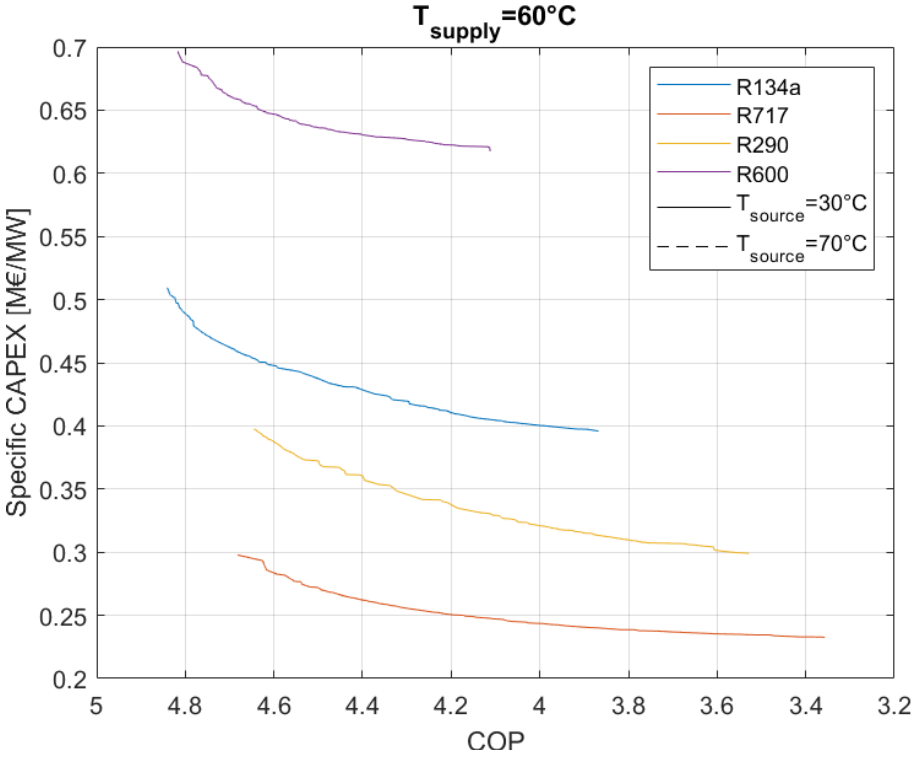

Figure 3.10: Pareto fronts analysis for different fluids as working fluid of an HP feeding a 4th generation DHN, two different source temperature levels are considered, 30°C (continuous lines) and 70°C (dashed lines).

CAPEX is almost independent of the supply temperature, the only variation that should be highlighted is the case of R600 HPs exploiting low-temperature heat sources, lowering the supply temperature from 120°C to 60°C the costs are reduced by 30%. Figure 3.11 (a, b, and c) report the Pareto fronts of the previous figures coloring the markers based on the superheating degree at the suction side. The R600 HPs' CAPEX reduction is justified by the fact that for high-temperature machines high superheating compressor's suction, and so at the discharge as well, allows delivering a relevant amount of heat in the desuperheating phase (2→3, according to the nomenclature of previous sections), then lower condensing temperatures, pressure, and, in the end, less power required to the compressor. On the other hand, HPs feeding new generation DHNs, adopt more moderate superheating, limiting the volumetric flow and the compressor cost. It is interesting to note that, unlikely the other fluids, R290 adopts lower superheating for the cheapest solutions, this is because in searching for cheaper solutions the pinch point temperature difference requirements at the heat exchangers are increased, this causes a shift in the condition setting the discharge pressure, equation (3.29), or the evaporating temperature, equation (3.7) and the suction pressure. Consequently, the correlation between higher superheating degrees and bigger compressors is no longer valid. This justify also the discontinuity in the trend slope of the R290, T_{supply}=90°C, and T_{source}=70°C (yellow dashed line in Figure 3.9).

In Figure 3.11 (d, e, and f) markers' color is set according to the discharge pressure. Looking at these charts it turns out that R600 is always characterized by low operating pressures, R717 implies very high-pressure levels, while R134 and R290 can be considered mid-range fluids under this point of view. For all the fluids, higher pressures are required for older DHN generations, additionally, the cheapest solutions adopt higher heat exchanger temperature differences to reduce the heat exchange surface and it implies higher pressure at the condenser on the working fluid side, although higher working pressure affects the heat exchanger cost, there is still an advantage in reducing the area.

Looking at the pressure level it turns out that R717 cycles supplying temperature at 120°C are characterized by pressure levels beyond the operative limits of plate heat exchangers. Moreover, also the temperature T_2 at the compressor discharge exceeds 180°C the threshold value beyond which operating the compressor is critical because of the oil degradation. As a consequence, R717 HPs are unfeasible to feed 2nd generation DHNs, independently of the source temperature level. Dealing with 3rd generation networks, R717 can be adopted but it is limited to the most expensive solutions (i.e., the left part of the Pareto front curve).

It is possible to conclude that for the 2nd DHNs the only adoptable working fluid, among the investigated, is butane (R600) which is characterized by high CAPEX from 0.3 to 1 M€/MW. Concerning medium temperature range, 3rd generation DHNs, ammonia (R717), despite its use is limited by high discharge pressure is the cheapest option, R290 implies higher CAPEX (+40%) but it allows better COP. However the best COP, up to 7, are reached only by the high GWP fluid R134a for high-temperature sources while the advantage is reduced looking at the low-temperature sources. Finally, feeding a 4th generation DHN ammonia (R717) is the best solution since it is cheaper than alternative fluids and the COP is comparable to the most efficient R134a. It is interesting to note how the gap in cost between butane (R600) and ammonia (R717) is reduced for such applications for the reasons previously explained.

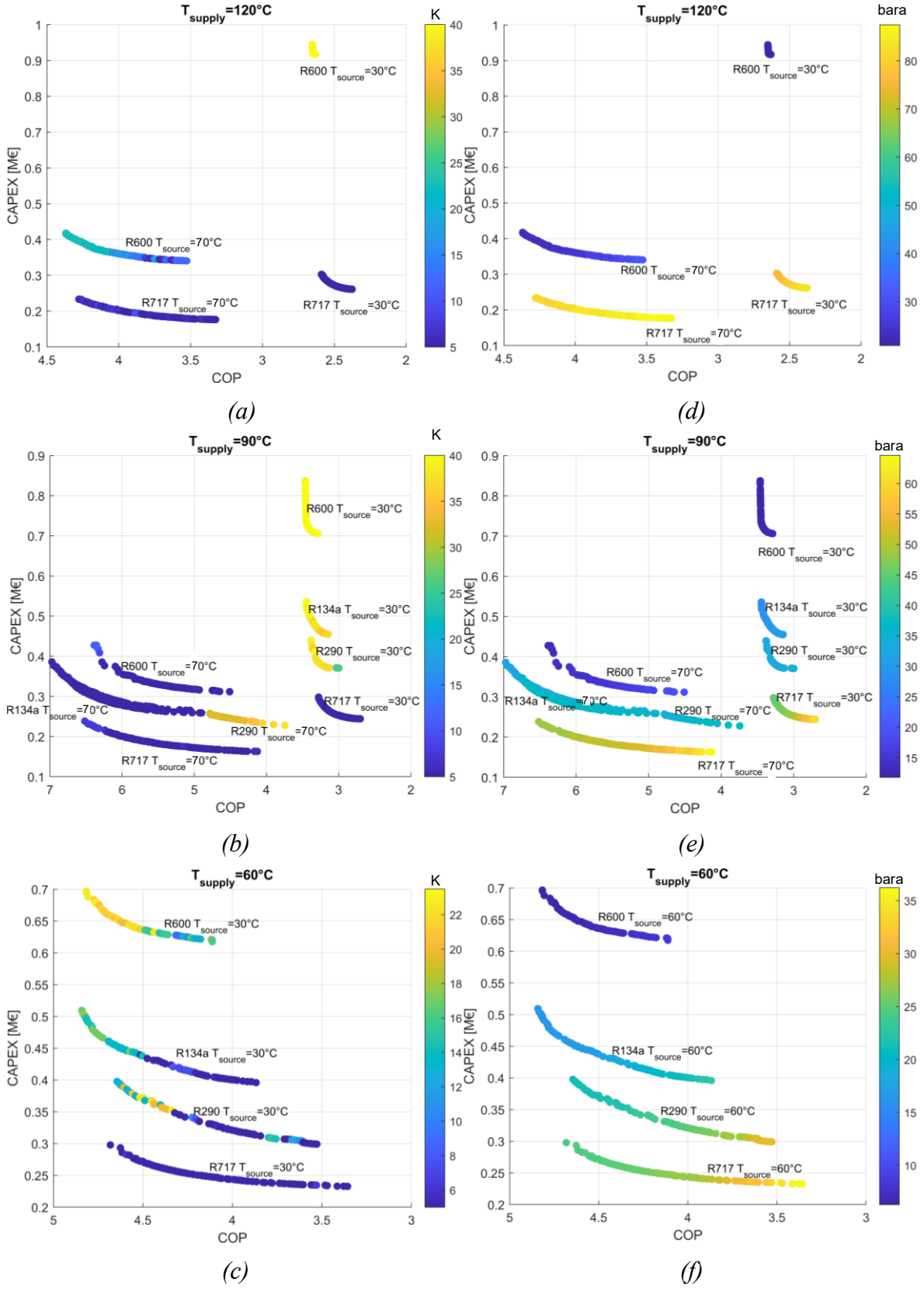

Figure 3.11: Pareto front analysis with markers color correlated to the superheating degree [K] ((a), (b), and (c)) and compressor discharge pressure [bara] ((d), (e), (f)).

3.3.2. R600 HTHPs techno-economic indicators sensitivity

The fluid comparison through the multi-objective optimization carried out in the previous section has highlighted how the techno-economic viability of HPs is more uncertain for high temperatures of supply. For such applications the range of working fluids is limited, the cheapest options often turn out to be unfeasible because of the too low critical temperature of the working fluid, or because of too high operative pressures, or oil degradation issues due to high temperature at compressor discharge. The difficulty in designing cheap, efficient, and reliable HTHPs is one of the reasons why is difficult to proceed with deep decarbonization of the heating sector. However, recently adopted fluids such as butane (R600), demonstrate their ability to supply heat up to 120°C and a spread of such a technology on a large scale would be a fundamental step to meeting the climate goals. For this purpose R600 HTHPs can perform cycles characterized by COP in the order of 4, keeping operating pressures within reasonable limits, and requiring an investment of about 400 k€/MW.

The present section investigates the sensitivity of the economic viability of R600 HPs for high-temperature applications, highlighting the influence of the economic context and HP usage. A supply temperature of 120°C is considered besides a source at 70°C. The return temperature at the sink is imposed at 70°C and the ΔT_{source} 20K.

3.3.2.1. Assumptions and key performance indicators

In order to estimate the profitability, the difference in net present value between the heat pump and an already existing natural gas-fired Heat Only Boiler, HOB, working in the same condition, is assessed. This approach allows comparing easily the heat pump as a low-carbon alternative to already existing traditional fossil fuel-based technologies. Moreover, since the comparison is on the same thermal demand the revenues from the heat supply are the same and in computing the difference no assumptions on the heat economic value are needed.

$$\Delta NPV = NPV_{HP} - NPV_{HOB} \tag{3.51}$$

$$NPV_j = -TCI_j + \sum_{k=1}^{n} \frac{Revenue_j - VC_j - O\&M_j}{\left(1 + i_{eff}\right)^k} \tag{3.52}$$

The TCI is assumed to be zero for the HOB since it was considered as already existing, while the HP cost is returned as an output by the techno-economic model described in Section 3.2. The Operating and Maintenance costs are composed of a fixed part, 1900 €/MWyr for the HOB and 2000 €/MWyr for the HP, and a variable component, 1 €/MWh for the HOB and computed as follows for the HP [183].

$$O\&M_{var_{HP}} = 2.7509 + 7 \cdot 10^{-5}(Capacity[kW]) \tag{3.53}$$

i_{eff} is the effective interest rate over the lifetime of the system, calculated as below, where i is the interest rate and i_L is the inflation rate, assumed equal to 7% and 2% respectively on a time horizon of 20 years (n in equation (3.52)).

$$i = \frac{1 + i}{1 + i_L} - 1 \tag{3.54}$$

The other variable costs (VC) [€], i.e., fuel and electricity consumption, depend on the efficiency of the two systems. In the HOB case, the fuel cost includes also the price of CO_2 emission allowance in the EU-ETS.

$$VC_{HP} = \frac{\dot{Q}}{COP} \cdot C_{el} \cdot \mathrm{OH} \tag{3.55}$$

$$VC_{HOB} = \frac{\dot{Q}}{\eta_{HOB}} \cdot \left(C_{gas} + e \cdot C_{CO_2}\right) \cdot \mathrm{OH} \tag{3.56}$$

Besides the ΔNPV also the Payback period (PBP) is monitored as an economic indicator, PBP is defined by the following equation, where CFR is the capital recovery factor:

$$PBP = \frac{TCI}{(VC_{HOB} - VC_{HP}) + (O\&M_{HOB} - O\&M_{HP}) \cdot \mathrm{CFR}} \tag{3.57}$$

$$\mathrm{CFR} = \frac{i \cdot (1+i)^n}{(1+i)^n - 1} \tag{3.58}$$

The cost of gas and electricity is assumed equal to the retail prices in the first semester of 2021[26] reported by Eurostat [184] including all taxes and levies, fitting the bands of consumption with a power function, the emission factor e is equal to 0.2014 ton/MWh according to the Italian government data for natural gas [185], while C_{CO_2} mean value on the plant's life time is assumed to be 60 €/ton. The Heat boiler efficiency has been modelled according to Satyavada and Baldi in order to take into account the increase of efficiency at lower return temperature thanks to the flue gas latent heat potential exploitation [186].

3.3.2.1. Sensitivity to thermal demand

The first sensitivity analysis is performed to investigate the influence of the thermal demand, the HP is supposed to feed a DHN as a baseload generator, as a consequence, the working hours are supposed to be operated at full load and the off-design behavior is neglected in this analysis. The electricity and gas price is assumed to be equal to the EU27 average for the first semester of 2021.

The HPs variable costs are lower than the HOBs since the COP is much more higher than the boiler efficiency compensating for the higher cost of electricity with respect to gas, additionally, HP does not pay the allowance for emitting CO_2, equations (3.55 and 3.56). It does not mean that the heating generated by means of an HP is free of emissions, it depends on the energy mix feeding the electricity network, which varies with the location and the time. However CO_2 emission allowance or carbon tax are usually paid by the electricity generator and then internalized in the retail price as well as other costs depending on the country's policy[27].

Because of the lower cost of heating the more the HP operates the easier is to pay the higher CAPEX back. While fixing the number of operating hours, increasing the capacity is worth only in a good economic scenario. Otherwise, it would increase the amount of CAPEX which is not possible to recover. Since the HP cost is not increasing linearly but, according to the economy of scale principles, a further increase in capacity cost less the bigger the HP is, the minimum amount of operative hours to reach a neutral ΔNPV slightly decreases with

[26] The most recent data at the time this thesis is essayed.

[27] Considering all tax and levies from Eurostat database ensure to include all the costs regardless to the location.

the HP size (red lines in the following figures). The present analysis establishes that the minimum operational hours for an HP to be more profitable than an already existing HOB is between 1200 and 2000 hours per year.

Figure 3.12 shows the contour of the optimized ΔNPV, the optimization variables are the same as in the MOO in the previous section (superheating at the compressor suction ΔT_{SH}, minimum temperature difference required at heat exchangers ΔT_{HXs}, and χ) the optimization is performed through the fmincon MATLAB function using the default algorithm sqp. χ is constrained to avoid finding meaningless optima implying too small HX to be designed, equations (3.59 and 3.60).

$$\Delta T_{SHbis} > 1 \tag{3.59}$$

$$\Delta T_{SH} - \Delta T_{SHbis} > 3 \tag{3.60}$$

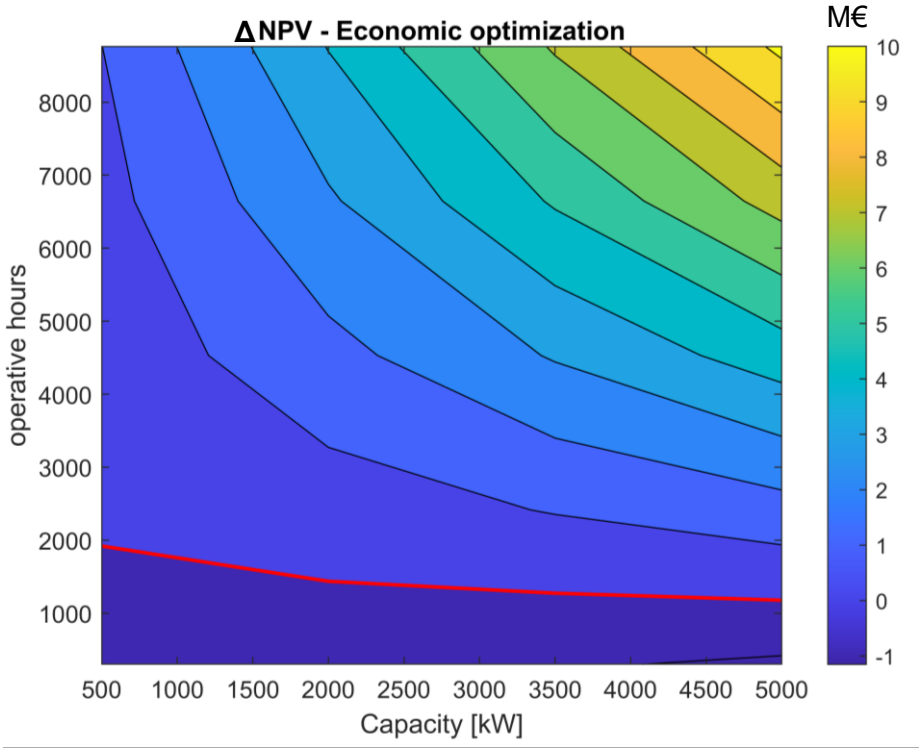

Figure 3.12: Optimized ΔNPV contour. Gas and electricity price are assumed according to the EU27 average in the 2021 first semester.

The comparison between the thermodynamic optimization of COP and the economic optimization of ΔNPV is highlighted in Figure 3.13 and Figure 3.14. the first reports the trend of ΔNPV if the optimization target is not the ΔNPV itself but the COP. The best achievable COP is independent of the thermal demand (operating hours and power), for the considered application is 4.56, corresponding to the extreme left points of the relative Pareto front shown in the previous section.

ΔNPV in Figure 3.12 is higher than in Figure 3.13 despite the lower COP, this is because an investment in the best possible machine is not fully compensated by the lower variable costs. From Figure 3.14 is possible to observe how a better machine is affordable if it is increased the amount of heat sold (i.e., higher capacity and more operative hours).

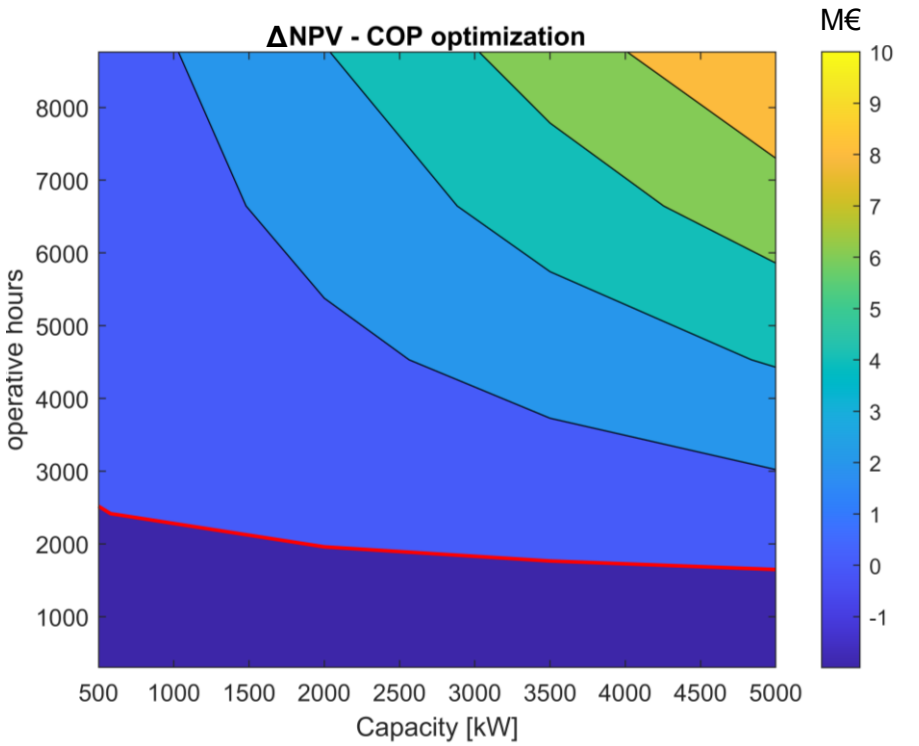

Figure 3.13: ΔNPV contour for optimized COP. Gas and electricity price are assumed according to the EU27 average in the 2021 first semester.

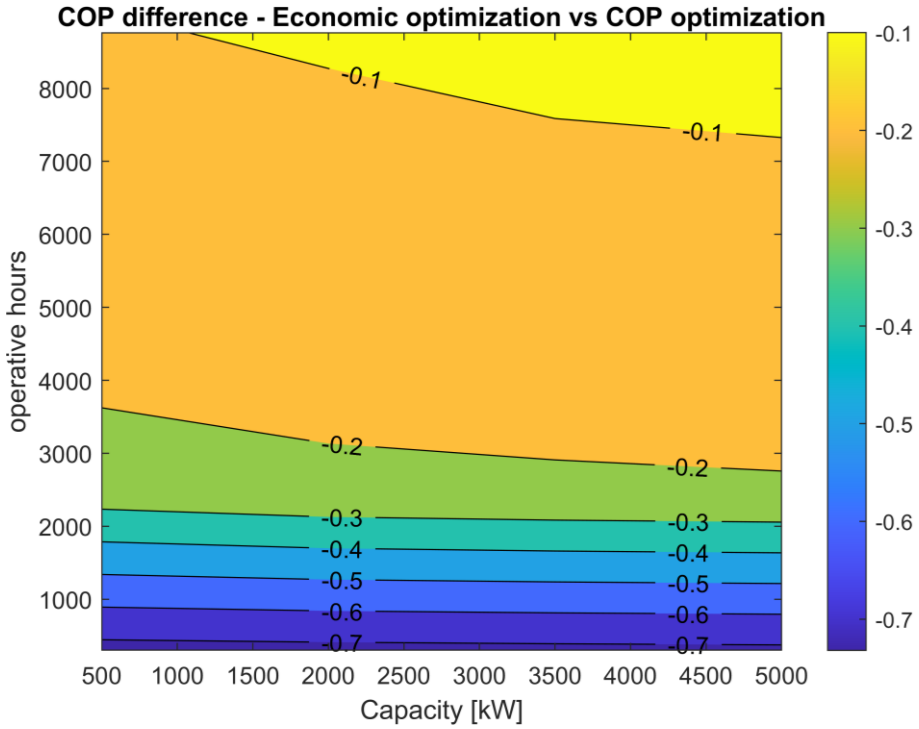

Figure 3.14: COP deviation from optimal COP for optimized ΔNPV. Gas and electricity price are assumed according to the EU27 average in the 2021 first semester. The optimal COP for Thermodynamic optimization is 4.56.

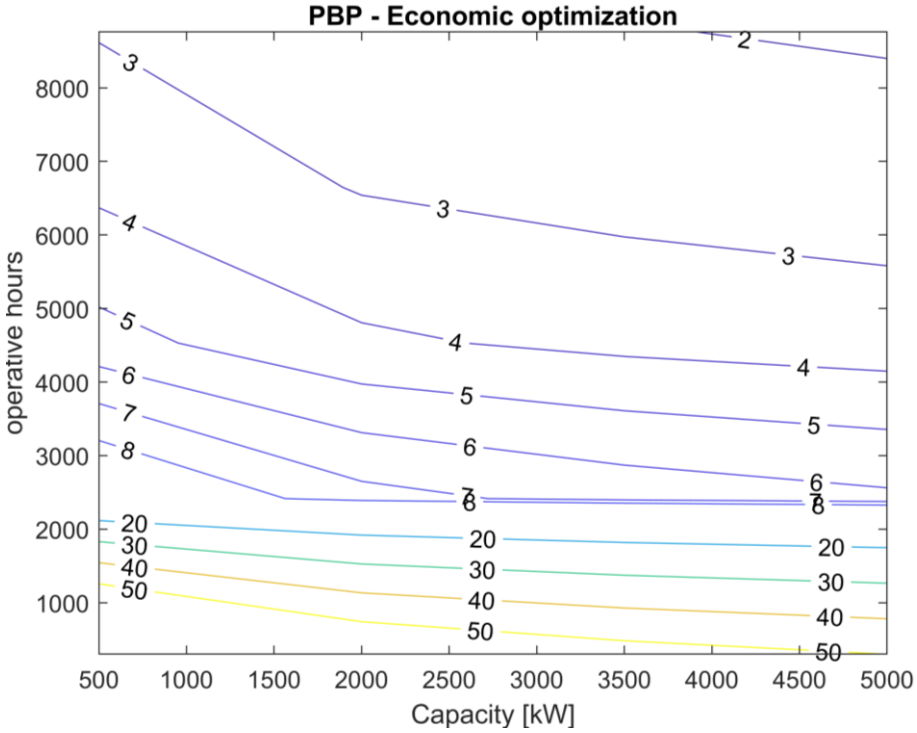

Figure 3.15: PBP [year] contour for optimized ΔNPV.

Figure 3.15 shows the PBP (as defined by equation 3.57) contour for the optimized ΔNPV, trends are similar to those concerning Figure 3.12 demonstrating the similarities between these two indicators. The PBP approaches and overcomes the estimated lifespan (20 years) for the same thermal demands corresponding to low or negative ΔNPV.

Finally, Figure 3.16 reports optimization variable trends, and the affordability of higher investment for larger HPs working several hours is confirmed. While the CAPEX reduction for lower COP HPs is mainly performed by increasing the heat exchangers' pinch point temperature difference and reducing the surface, partially also a slight decrement in suction superheating affects the investment.

Moreover, it turns out that the best way to perform the superheating is by means of the additional regenerative heat exchanger rather than an evaporator oversizing. In fact, the optimal value of χ is always 0.

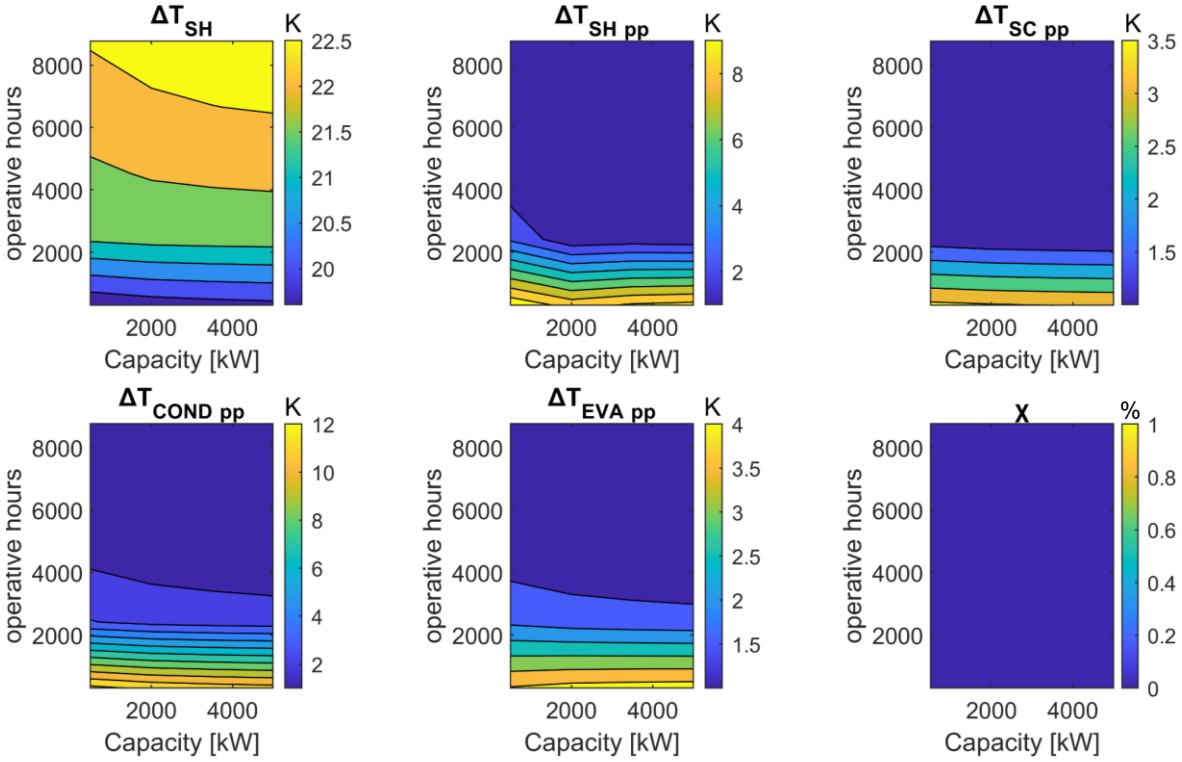

Figure 3.16: Economic optimization. Optimization variables trends with respect to the HP capacity and operating hours.

3.3.2.2. Sensitivity to the economic scenario

Secondly, the sensitivity to the economic context is explored, and the cost of the CO_2 emission allowance is maintained constant while the price of natural gas and the price of electricity are varied. Figure 3.17 shows the consequent variation in ΔNPV, axes report the prices of gas and the electricity the condition adopted in the previous section are denoted by the EU27 marker. ΔNPV is still the objective function of the optimization problem carried out on the same six optimization parameters. HP capacity and time usage are imposed to 3000 kW_{th} and 2000 h per year respectively.

The HP profitability with respect to the HOB is higher for high natural gas prices and low electricity prices. The dependency is strictly linear on both the parameters and all the variability can be described by the principal component X_1. The principal component is shown on the graph in Figure 3.17 (black continuous lines and labels), the 0 point is imposed on the EU27 average prices, so that positive X_1 corresponds to higher profitability as against the European average, and vice versa for negative X_1. On the figure are also plotted point markers indicating the single European country retail prices, it must be recalled that price data comes from the Eurostat database and are dependent on the yearly consumption, the price scaling function is a power function fitted on each single country data. Thus, the country's relative ΔNPV may be slightly assuming different capacity or time usage data.

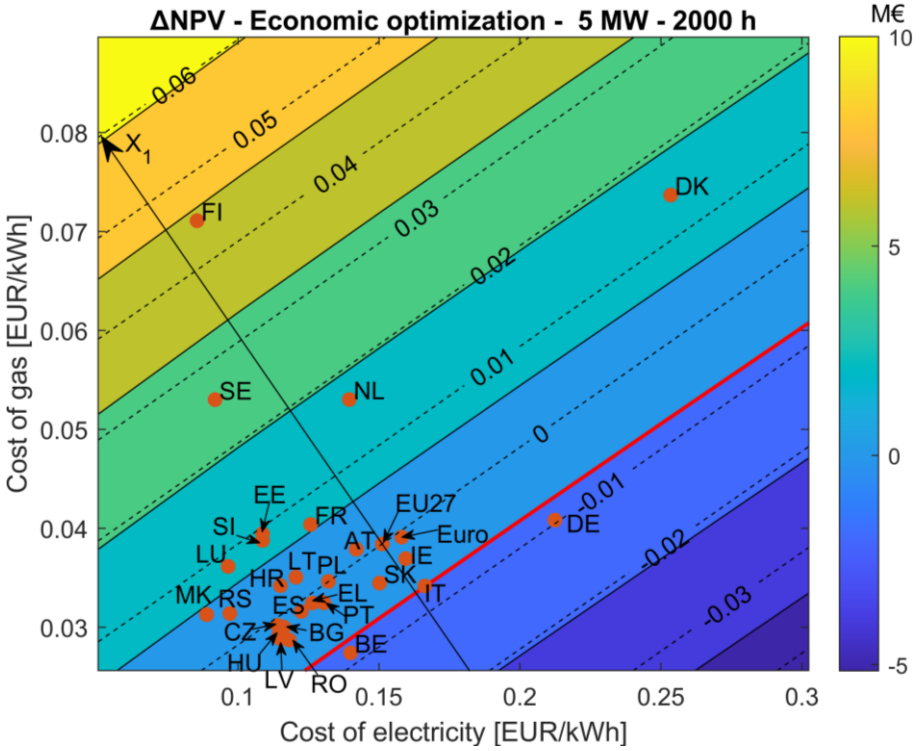

Figure 3.17: Sensitivity of ΔNPV to the price of gas and electricity.

Observing the optimization outputs, Figure 3.18, it is clear that the optimum design of the HP does not depend on the cost of gas, since it influences only the variable cost of the benchmarked solution, the HOB. The small variation in the optimal $\Delta T_{SH\ pp}$ can be considered a numeric instability of the optimization process. On the other hand, within high electricity price scenarios, it becomes more important to reduce the HP energy consumption since the same efficiency is reflected in higher variable costs, in such a situation the heat exchangers' pinch point temperature difference is reduced as well as the superheating at the suction side, optimum χ is still 0 as in the previous optimization.

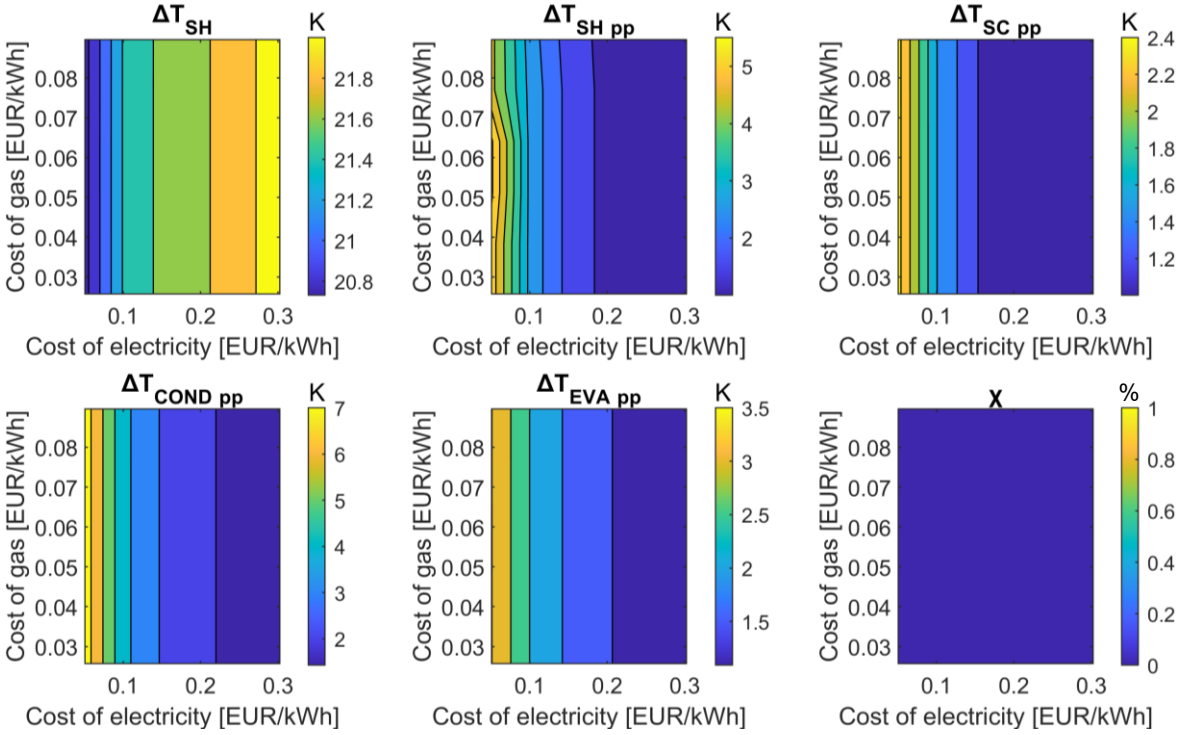

Figure 3.18: Economic optimization. Optimization variables trends with respect to the price of gas and electricity.

3.3.2.3. General investigation of market opportunities

Section 3.3.2.1 demonstrates that time usage is a crucial design datum to assess the viability of the HP. The opportunities to use an HP depend on the local thermal demand, which is reasonably correlated to the climate. Some specific applications devoted to local specific demand fulfillment may work more hours, but as a general rule, the location imposes an expected number of hours of heat demand.

Eurostat [187] reports the yearly time usage for many countries for ASHPs, WSHPs, and GSHPs. ASHPs operate fewer hours per year[28] because of their low efficiency, while WSHPs and GSHPs' time usage is comparable. GSHPs' time usage is taken as a reference because of the similarities to HPs exploiting waste heat as the heat source. In this way is possible to associate an expected time usage with each country already characterized by an economic scenario (the price of gas and electricity).

Figure 3.19 is drawn collecting together this information and plots for some countries the ΔNPV as a function of the capacity. Time usage is the expected number of working hours from the Eurostat database, electricity and gas price is varied according to the capacity, the time usage, and the single country price functions. Trends confirm the almost linear dependency on the installed capacity, in a profitable context the opportunity to install a larger HP is reflected in an increased advantage to the existing HOB, but if the conditions are not viable a larger HP would lead to larger losses.

[28] Heating hours are considered, excluding cooling hours of reversible machines.

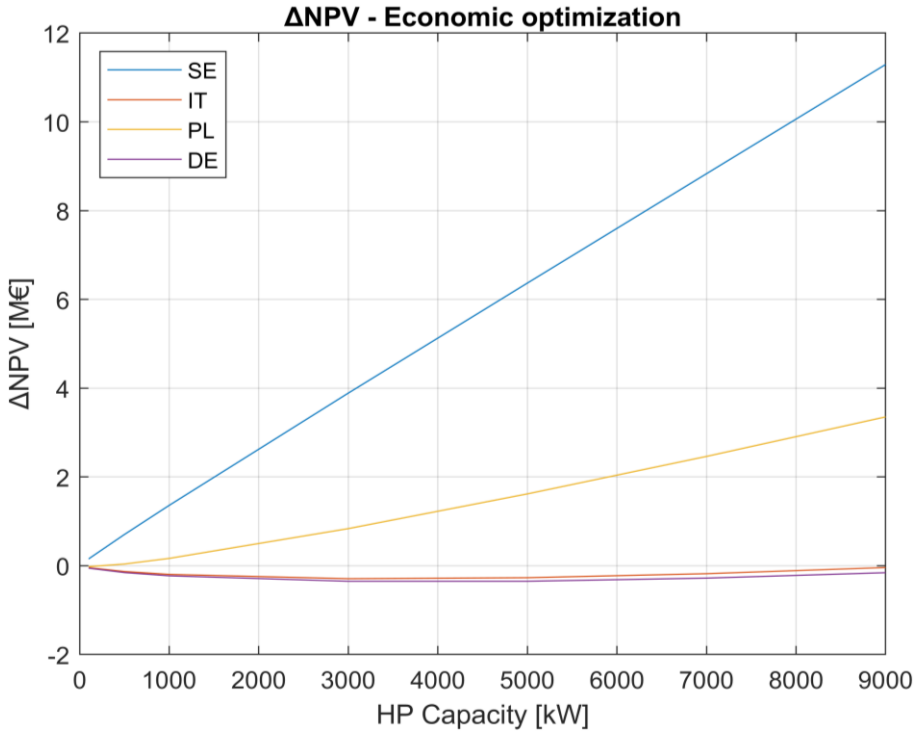

Figure 3.19: Optimal ΔNPV trend vs the HP capacity for different locations assuming each country's expected time usage and electricity and gas price function. Sweden 2470h, Italy 1680h, Poland 2393h, and Germany 1996h,

Linearities shown by this analysis are not trivial, in fact increasing the size of the heat pump the specific CAPEX decreases leading to a benefit as well as a decrease in paid electricity price. On the other hand, it also decreases the price of gas paid by the benchmarked gas-fired heat-only boiler (power functions are assumed to fit the trend of prices against the yearly consumption). These three effects sum together leading to the almost linear trend plotted in the figure.

Even if the visualization provided by the figure above allows to consider all the relevant parameters, price of gas, price of electricity, time usage (synthesized by the country), and HP size, it does not allow assessing an impact of a deviation from the expected time usage keeping constant the country's energy price. The following Figure 3.20 and Figure 3.21, relative to a 5 MW_{th} and 1 MW_{th} HP, propose contour plots with respect to the time usage and the economic scenario principal component X_1. Then, the x-axis is relative to the economic context, this variable demonstrates to describe the whole variability of the ΔNPV caused by electricity or natural gas price variations, while the y-axis is the time usage, fundamental input to an optimal design and viability of the HTHP investigated applications.

On the graph point markers show the position of each country, so to assess the viability of a new design the x-coordinate is constrained by the location, little variations may occur depending on the contracts with the energy retailers, while the position on the y-axis must be set according to the specific case study the marker is positioned to the expected average value according to the Eurostat database and it gives useful information about the viability of these HTHPs as a solution for the heating sector decarbonization on a large scale. Finally, defined the x and y coordinates of interest, the influence of the size can be assessed by looking at the two values reported in Figure 3.20 and Figure 3.21, since a linear correlation is demonstrated to be a good approximation, Figure 3.19, the values can be interpolated an extrapolated based on this hypothesis.

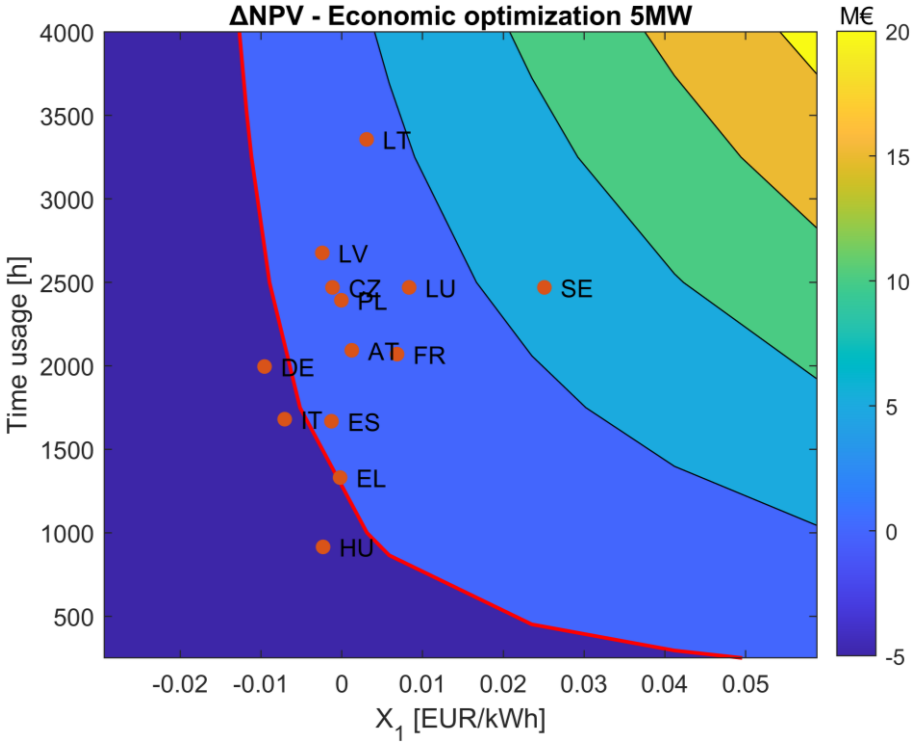

Figure 3.20: ΔNPV sensitivity to the economic scenario, x-axis, and time usage opportunity, y-axis, for 5 MW_{th} HP.

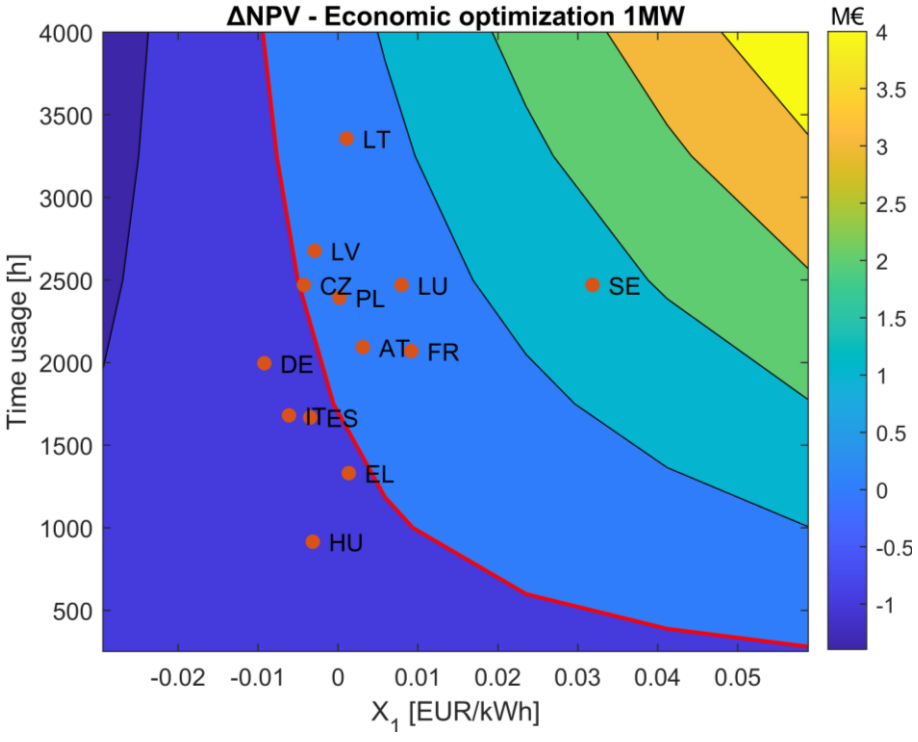

Figure 3.21: ΔNPV sensitivity to the economic scenario, x-axis, and time usage opportunity, y-axis, for 1 MW_{th} HP.

3.4. Concluding remarks

Chapter 3 focuses on heat pumps, especially high-temperature heat pump technologies as stand-alone generators recovering waste heat from other processes and feeding district heating networks. Such applications are essential to the deep decarbonization of the heating supply. However, HPs are often characterized by relevant investment costs, especially if compared to natural gas-fired boilers. A techno-economic model, developed in MATLAB is presented as a tool to assess the market viability power to heat systems.

The results are presented in sections 3.2 and 3.3, the fluid comparison highlights how ammonia (R717) is the preferable solution for low supply temperature since it implies reduced cost of investment and good thermodynamic performance. Butane (R600) is particularly suitable for high-temperature applications since it allows operating with moderate pressure at the compressor discharge. These two fluids have been investigated as low Global Warming Potential alternatives to R134a. R134a fluid represented a standard for years and demonstrates to achieve very high COP, even if compared against more recently employed working fluid. However, it cannot reach high temperatures of supply because of the relatively low critical temperature, so it is not suitable for retrofitting 2nd generation district heating networks characterized by supply temperatures up to 120°C.

Finally, the thermal demand, i.e., the size and the expected time usage, have an impact on the viability of such systems. As the size increases the specific CAPEX decreases, however also the cost of energy is not linear with the consumption both for a heat pump and the gas burn by a hypothetic competing boiler. these nonlinearities are canceled out by combining into the quasi-linear trends shown in Figure 3.19. Figure 3.20 and Figure 3.21 highlights the economic potential of different locations according to the expected time usage and the market context, demonstrating how these applications are particularly interesting for the Scandinavian and Baltic market but could be viable in many other European countries

4. CCGT-HP coupling

This chapter explores the possible coupling between CCGTs and HPs. Two main approaches to coupling are followed. The first is defined as Power Oriented, the power generation is the only plant's output and the HP is used to conditionate the intake air in order to enhance the flexibility. Alternatively, the HP is coupled to a CCGT-CHP integrating the CCGT's thermal generation and exploiting wasted heat from the cycle improving the overall efficiency.

Heat pumps are, up to date, not so flexible in modulating the load and performing immediate start-ups, for this reason the time intervals, considered in the analyses reported in this chapter, are no shorter than one hour, and only the Day-Ahead Market of electricity is taken into account whose reference time intervals are typically hourly and the scheduling known many hours in advance to the real-time.

Other studies must be carried out to fully assess the technical potentialities of the coupling layouts and their economic value, in services markets (ref Chapter 5), as flexibility enhancers. Besides the techno-economic analyses presented in this thesis the PUMPHEAT project studied the dynamic behavior of CCGTs and HPs coupling through dynamic modeling and a cyber-physical setup, implemented at the University of Genoa, to experimentally investigate the transient performance of such systems [158,188]

4.1. Power oriented applications

Chapter 1 highlighted how more and more flexibility is required to dispatchable power plants within an energy mix characterized by a relevant penetration of stochastic and/or Inverted Based Resources. Flexibility mainly consists of high ramp-up rates, the possibility of power augmentation to cope with high electricity demand, even with high ambient temperatures, high efficiency reflected in low marginal cost, even at partial loads, and low minimum environmental load. For the flexibility enhancement purpose, a wide range of solutions was investigated.

Compressed air injection can contribute both to the power augmentation within price/demand peak hours, and the ramp-up rate improvement [189,190]. However, to increase the power output, inlet cooling technologies are more common and have been installed on several GTs all around the globe, especially within hot climate locations. The literature reviewed inlet cooling several times, the concepts included, but are not limited to, evaporative coolers, fogger systems, wet compression, absorption, and mechanical chillers [191–193]. Additionally, cold storage contributes to further flexibility enhancement [194].

Finally, even less common, the opportunity of heating the inlet air was investigated to increase the off-design performance in terms of minimum load lowering and efficiency improvement [195,196]. Section 2.4 has investigated the potential benefits of inlet heating quantifying the saving (in terms of money and avoided CO_2 emissions) on the real operating conditions of the Italian CCGT fleet.

The benefit of an intake conditioning device turns out to be twofold. On one hand, heating up the GT's compressor intake can be beneficial within the off-design operating conditions, lowering the minimum load and increasing efficiency. On the other hand, cooling the GT intake is a well-known and widespread technology for power augmentation purposes. The

importance of avoiding the lack of generation capacity with hot temperatures is considered to be pivotal since under such conditions the electricity demand often rises as well because of the growing need for air conditioning and cooling. Nevertheless, to the author's best knowledge was not proposed any concept to simultaneously address the inlet cooling and heating.

Within the PUMP-HEAT H2020 Project, a solution focusing on the conditioning of the gas turbine intake was presented for the Power Oriented CCGT (CCGT-PO)[29]. This concept pursues both the power augmentation and the off-design efficiency enhancement by means of an Inlet conditioning Unit (ICU). The complete layout integrates, in an OEM independent approach, the CCGT with an Inlet Conditioning Unit (ICU) consisting of a Heat Pump (HP), a cold Thermal Energy Storage (TES), and two heat exchangers. The choice of the heat pump as cooling equipment is due to the possibility of charging the TES during periods of low electricity price reducing the minimum environmental load by means of inlet heating, or even acting, in a demand response scheme, as a smart load when the CCGT is off. The use of an air-cooled heat pump was made for sake of generality because it does not require specific sites condition for the installation. Additionally, two heat exchangers are included in the proposed ICU, the Gas Turbine's Heat Exchanger (GTHX) at the compressor's intake conditioning the inlet air and the Ambient Heat Exchanger (AmbHX) which is designed to ensure the heat exchange between the ambient and the heat transfer fluid which serves the heat pump or the TES

In particular, the Integrated Inlet Conditioning system, Figure 4.1(a), allows increasing the operational flexibility of CCGT in terms of power augmentation, useful during high electricity price periods (Peak Periods) to increase CCGT power output, and minimum Environmental Load reduction, off-design efficiency enhancement. A CCGT-ICU integrated power plant operates according to 5 operational modes:

- Continuous Cooling mode (Figure 4.1(b),), the GT inlet air is cooled down by the HP, and heat at the HP's condenser is dumped into the environment by means of AmbHX.
- TES discharging mode (Figure 4.1(c),), the GT inlet air is cooled down by the TES. The TES temperature is assumed constant at 5°C because of the properties of the phase change material CrodaTherm™ 5. The HP is switched off and does not require electricity.
- Continuous heating mode (Figure 4.1(d),), the GT inlet air is heated up by the HP, the ambient air is the HP's heat source, and thus the AmbHX is connected to the HP's evaporator.
- TES charging mode (Figure 4.1(e),), the TES is charged and the ambient air represents the HP's heat sink, thus the TES connected to the HP evaporator and the AmbHX to the condenser. This mode does not require the GT to be on, in this case, the electricity from the grid feeds HP.
- Heating and TES charging mode (Figure 4.1(f),), the TES is charged and the GT inlet air represents the HP's heat sink, thus the TES is connected to the HP evaporator and the AmbHX to the condenser.

[29] Devoted to power generation only.

- External Heating (Figure 4.1(g),), even if this is not an ICU mode, is here reported since it is included in the model of optimal dispatch. The Electric Heater (ELH) heats up the GT inlet air. All ICU components (HP and circulating pumps) are switched off.

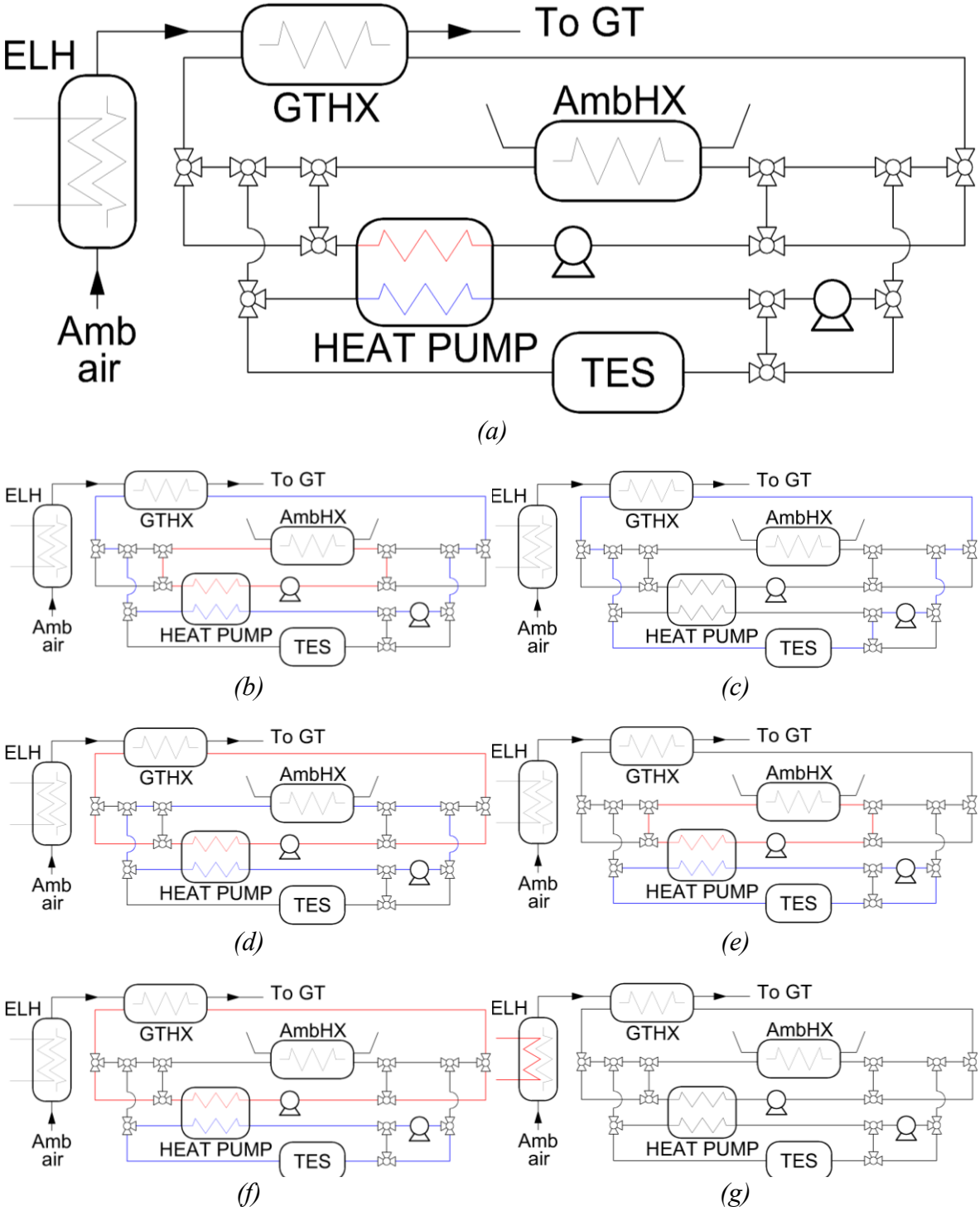

Figure 4.1:Integrated Inlet Conditioning Unit (ICU) for a CCGT intake.

The thermodynamic performances of the system were assessed by previous works. [128,197,198]:

1) Discharging the TES has the potential, starting from the summer condition (35°C), to increase power output up to 50 MW (+14%) while efficiency slightly increases by 0.1 percentage point (+0.17%); while using the HP for continuous cooling, once the TES is empty, results always in a power augmentation but an efficiency reduction.

2) The Minimum Environmental Load reduction, particularly useful during low electricity price periods, brings a decrease in fuel consumption, increasing turndown period sustainability with respect to an intraday shutdown/start-up cycle. Increasing inlet temperature up to 45°C, a load reduction of 30 MW (-16%) against an efficiency reduction of just 0.75 pt% (-1.5%) can be achieved with respect to MEL at ISO conditions. This results in a fuel consumption reduction which enables prolonged turndown periods (up to 15%), increasing the running hours and thus the chance of revenues in the ancillary service market. Concerning the analysis of pollutant emissions: despite the longer turn down period, CO_2 emissions are lower via inlet heating, even without taking into account the avoided SU/SD emissions.

3) The off-design efficiency enhancement, during intermediate load operation by the means of inlet heating was assessed, as well as the increase in part-load efficiency and annual average efficiency. The adoption of the HP in the Power Oriented configuration, as continuous heating, can bring about a 1.2% increase in average efficiency yearly; while using a Cold TES, decreasing the HP evaporator temperature, the global efficiency enhancement is reduced to 0.5%.

4.1.1. Market and Climate Impact on ICU Economic Viability

Within the PUMP-HEAT H2020 Project, it was developed a model of optimal dispatch for ICU integrated CCGT. The model determines the best hourly dispatch according to a Mixed Integer Linear Programming (MILP) optimization logic having as the objective function the equation (4.1) and considering a 24h horizon.

Table 4.1 reports the inputs and the optimized dispatching variables and the relative references. Besides, Table 4.2 reports the most important technical features of both the CCGT and the ICU. The full set of constraints, as well as a detailed description of the model, can be found in previous publications [197]. This was then used for the purpose of a worldwide investigation of the sensitivity on market and climate scenarios reported in this section.

$$max \sum_{j=1}^{n\ hours} El_j \cdot \left(P_j^{out} - P_j^{HP} - Q_j^{elh}\right) - C_{gas_j} \cdot \left(Q_j^{fuel}\right) - C_{hs}V_j^h - C_{ws} \cdot V_t^w - C_{CO2} \cdot e \cdot \left(Q_j^{fuel}\right) - O\&M_{var} \quad (4.1)$$

Table 4.1: Model Input and Output variables.

Optimized dispatching variables			
P_j^{out}	MWh		CCGT electricity production at time j
P_j^{HP}	MWh		HP electricity consumption at time j
Q_j^{elh}	MWh		Electric heater consumption at time j
Q_j^{fuel}	MWh		Fuel consumed at time j
CO_{2_j}	tonCO_2		CO_2 emitted at time j
V_j^h	-		Hot start-up binary variable at time j
V_j^w	-		Warm start-up binary variable at time j
Inputs to the objective function			
El_j	Geographically dependent	€/MWh	DAM electricity price at time j
C_{gas_j}		€/MWh	Gas price at time j
C_{CO2}		€/tonCO_2	Cost of CO_2 emissions
e	0.201 [185]	tonCO_2/ MWh	Emitted CO_2 on gas energetic potential
C_{hs}	10,450 [138,199]	€	Plant hot start-up cost
C_{ws}	14,800 [138,199]	€	Plant warm start-up cost
$O\&M_{var}$	3.15 [200]	€/MWh	Variable operating and maintenance cost
Other model inputs			
T_j^{amb}	Geographically dependent	°C	The ambient temperature at time j
$O\&M_{fix}$	10,500 [200]	€/MW	Fixed operating and maintenance cost

Table 4.2: CCGT and ICU technical features.

	Size	**Additional Features**	
GT	270 MW (400 MW in CC)	F-class	V94.3A4
HRSG	c.a. 400 MW_{th}	3 pressure levels and reheat	
HP	3.5 MW_{el}	COP_{design}=3.5, COP_{max}=5	R600
TES	10 MWh_{th} (±10MW_{th})	PCM: 15.1 ton	CrodaTherm™ 5
AmbHX	17.5 MW	Finned tube coil heat exchangers	
GTHX	17.5 MW		

4.1.1.1. Model of Optimal Dispatch

Several key performance indicators (KPIs) are monitored to fully assess the effectiveness from an economic, technical, and environmental point of view. The investment to be assessed is the ICU implementation, therefore all the KPIs are based on the difference in performance between a Business as Usual (BAU) scenario, simulating a standard CCGT, and an ICU scenario considering the ICU integration. The difference in profits, ΔOP, between the above-mentioned scenarios is used to compute the Net Present Value (NPV) and the Pay Back Period, (PBP).

$$NPV = \sum_{j=1}^{n} \frac{\Delta OP_j}{(1+i)^j} - CAPEX^{ICU} \tag{4.2}$$

$$PBP = \frac{\ln(\Delta OP) - \ln(\Delta OP - i \cdot CAPEX^{ICU})}{\ln(1+i)} \tag{4.3}$$

A lifespan of 20 years and a discount rate equal to 0.45 are considered, while $CAPEX^{ICU}$ is the cost of ICU initial investment, estimated at 6.3 M€ [12,201].

The considered technical indicators are the generated electricity difference, defined as in equations (4.4) and (4.5), and the Utilization Factors (UFs) of HP and TES respectively. The HP UF is defined as the averaged part-load operation of the HP for the hours it is used, while the TES UF is the ratio between the total energy discharged by the TES during the year, and the total energy discharged if the TES completed a full charge-discharge cycle once per day during the year.

$$\Delta el_{gen} = \frac{\left(el_{gen}^{ICU} - el_{gen}^{BAU}\right)}{el_{gen}^{BAU}} \cdot 100 \tag{4.4}$$

$$\Delta \mathrm{el}_{gen_{abs}} = \frac{\left|el_{gen}^{ICU} - el_{gen}^{BAU}\right|}{el_{gen}^{BAU}} \cdot 100 \tag{4.5}$$

The absolute difference in dispatched electricity, equation (4.5), highlights also the decrease in power generation (i.e., the decrease of the minimum environmental load obtainable by inlet heating) and so an increase in flexibility. Then equation (4.6) defines the difference in specific carbon dioxide emission [ton/MWh] assessing the environmental impact of the ICU integration.

$$\Delta CO_{2_{spec}} = \frac{\left(CO_{2_{spec}}^{ICU} - CO_{2_{spec}}^{BAU}\right)}{CO_{2_{spec}}^{BAU}} \cdot 100 \tag{4.6}$$

4.1.1.2. Statistical Sample Selection

The investigation focused on most of the European associations for the cooperation of transmission system operators (ENTSO-E) countries and the following USA system operators: California ISO (CAISO), New York ISO (NYISO), Electric Reliability Council of Texas (ERCOT), Midcontinent ISO (MISO) and ISO New England (ISO-NE). For each bidding zone, a specific location was selected and used as a reference for the meteorological data, Table 4.3 reports the complete list of considered bidding zone and the relative reference locations identified by the toponyms and by the geographical coordinates.

Table 4.3:Bidding zones and relative reference locations included in the analysis.

Country/ISO	Bidding zone	Reference location		
			Lat.	Long.
Sweden	SE1	Luleå	65.6	22.2
	SE2	Sundsvall	62.4	17.3
	SE3	Stockholm	59.4	18
	SE4	Malmö	59.6	13
Finland	FI	Helsinki	60.2	24.9
Denmark	DK1	Århus	56.2	10.2
	DK2	Copenhagen	55.7	12.5
Norway	NO1	Oslo	59.9	10.8
	NO2	Kristiansand	58.2	8
	NO3	Trondheim	63.4	10.4
	NO4	Tromsø	69.7	19
	NO5	Bergen	60.4	5.4
Estonia	EE	Tallinn	59.4	24.7
Latvia	LV	Vilnius	54.7	25.3
Lithuania	LT	Riga	56.9	24.1
United Kingdom	UK	Manchester	53.4	-2.2
Austria	AT	Vienna	48.2	16.3
Belgium	BE	Antwerp	51.2	4.4
Germany and Luxembourg	DELU	Düsseldorf	51.2	6.8
France	FR	Paris	48.9	2.3
Netherland	NL	Rotterdam	51.9	4.4
Spain	ES	Barcelona	41.4	2.11
Portugal	PT	Krakow	50.4	20
Poland	PL	Lisbon	38.6	-9.1
Greece	GR	Athens	38	23.7
Switzerland	CH	Zurich	47.4	8.5
Italy	CNOR	Florence	43.8	11.2
	CSUD	Naples	40.9	14.3
	NORD	Milan	45.5	9.2
	SARD	Sassari	40.7	8.5
	SICI	Palermo	38.1	13.3
	SUD	Taranto	40.5	17.2

Country/ISO	Bidding zone	Reference location		
			Lat.	Long.
CAISO	PGAE	San Francisco	37.8	-122.4
	SCE	Los Angeles	34	-118.1
	SDGE	San Diego	32.7	-117
	VEA	Pahrump	36.2	-116
ERCOT	LZ_AEN	Austin	30.25	-97.8
	LZ_CPS	San Antonio	29.5	-98.5
	LZ_HOUSTON	Houston	29.75	-95.3
	LZ_LCRA	San Marcos	29.9	-97.9
	LZ_NORTH	Abilene	32.4	-99.7
	LZ_RAYBN	Sherman	33.6	-96.6
	LZ_SOUTH	Corpus Cristi	27.8	-97.6
	LZ_WEST	Dallas	32.7	-96.8
ISO-NE	CONNECTICUT	New Haven	41.4	-72.9
	MAINE	Portland	47.7	-70.3
	NEMASSBOST	Boston	42.4	-71.1
	NEW HAMPSHIRE	Manchester	43	-71.4
	RHODEISLAND	Providence	41.8	-71.5
	SEMASS	New Bedford	41.7	-70.9
	VERMONT	Montpellier	44.3	-72.6
	WCMASS	Springfield	42.1	-72.6
MISO	ARKANSASHUB	Pine Bluff	34.2	-92
	ILLINOISHUB	St. Louis	38.7	-90.2
	INDIANAHU	Indianapolis	39.8	-86.2
	LOUISIANAHUB	New Orleans	29.9	-90.1
	MICHIGANHUB	Detroit	42.4	-83.2
	MINNHUB	Minneapolis	44.94	-93.3
	TEXASHUB	Beaumont	30.1	-94.1
	MSHUB	Jackson	32.3	-90.2
NYISO	CAPITL	Albany	42.65	-73.8
	CENTRL	Syracuse	43	-76.2
	DUNWOD	Yonkers	40.9	-73.9
	GENESE	Rochester	43.15	-77.6
	HUDVL	Poughkeepsie	41.7	73.9
	LONGIL	Long Island	40.85	-73
	MHVL	Utica	43.1	-75.2
	MILLWD	Millwood	41.1	-73.8
	NYC	New York City	40.8	-74.0
	NORTH	Plattsburgh	44.7	-73.5
	WEST	Buffalo	42.9	-78.8

Firstly a statistical analysis was performed in order to characterize the markets based on the last four complete years, from 2017 to 2020. For this purpose, 16 parameters are selected, describing the electricity, gas, and emission allowances prices, the ambient temperature, and the interaction between them. The raw data used and their sources are listed below, currency values are converted into euros using the average exchange rate for the reference year:

- Electricity market (Day-Ahead price) hourly data, available on the ENTSO-E Transparency Platform [202] and LCG consulting [203].
- The gas market historical daily series, the Dutch TTF, and the American Henry Hub were assumed as reference spot markets for Europe and USA respectively. The daily closing price on the spot market was assumed.
- The local hourly ambient temperature is estimated by means of hourly geospatial data of the temperature at 2 m of height from the soil available on the ERA5 dataset [148] with a resolution of 9 km.
- The carbon pricing policy and value for fossil fuel-based power generators, according to the price reported by the annual World Bank report typically refers to the value during the month of April [40].

The 16 parameters hereby defined, equations (4.7)-(4.21), plus the ambient temperature) aim to describe each market by quantifying different features often treated as qualitative, such as the relationship between the electricity market and the gas or the local climate, the local climate itself, or the daily electricity price curve shape.

The Pearson coefficient, the daily ratio of electricity to gas price, and the Clean Spark Spread, equations (4.7)-(4.9), describe the relationship between electricity and gas:

$$\rho_{ElGas} = \frac{\sigma_{El_d C_{gas_d}}}{\sigma_{El_d}\sigma_{C_{gas_d}}} \quad [-] \quad (4.7)$$

$$r_d = \frac{El_d}{C_{gas_d}} \quad [-] \quad (4.8)$$

$$CSS_d = El_d - C_{gas_d} - e \cdot C_{CO_2} \quad [€/MWh] \quad (4.9)$$

Besides, the yearly and daily standard deviation, the peak, and off-peak durations, and the daily spread deal with the electricity price trend itself. Overlines indicate averaged variables.

$$\sigma_{El_y} = \sqrt{\frac{\sum_{j=1}^{365}\left(El_{d_j} - \overline{El_d}\right)^2}{365}} \quad [€/MWh] \quad (4.10)$$

$$\sigma_{El_d} = \sqrt{\frac{\sum_{j=1}^{24}\left(El_{h_j} - \overline{El_h}\right)^2}{24}} \quad [€/MWh] \quad (4.11)$$

$$\Delta El_d = max(El_h) - min\,(El_h) \quad [€/MWh] \quad (4.12)$$

$$\widehat{\Delta El_d} = \frac{\Delta El_d}{\overline{El_d}} \quad [-] \quad (4.13)$$

$$Pk1_d = count\begin{pmatrix} El_h > 0.9 \cdot max(El_h)\ and \\ El_h > 1.1 \cdot \overline{El_h} \end{pmatrix} \quad [h] \quad (4.14)$$

$$Pk2_d = count\begin{pmatrix} El_h > max(El_h) - 0.15 \cdot \Delta El_d\ and \\ El_h > 1.1 \cdot \overline{El_h} \end{pmatrix} \quad [h] \quad (4.15)$$

$$OffPk1_d = count\begin{pmatrix} El_h < 1.1 \cdot min(El_h)\ and \\ El_h < 0.9 \cdot \overline{El_h} \end{pmatrix} \quad [h] \quad (4.16)$$

$$OffPk2_d = count\begin{pmatrix} El_h < min(El_h) + 0.15 \cdot \Delta El_d\ and \\ El_h < 0.9 \cdot \overline{El_h} \end{pmatrix} \quad [h] \quad (4.17)$$

Moreover, the Pearson coefficient and the peaks' locations shift analyze the relationship between the electricity price and the ambient temperature, equations (4.18) and (4.19). The HDD, the CDD, equations (4.20)-(4.21), besides the raw hourly temperature concern the local climate.

$$\rho_{ElT} = \frac{\sigma_{El_h T_h}}{\sigma_{El_h}\sigma_{T_h}} \quad [€/MWh] \quad (4.18)$$

$$\Delta Pk_d = h_{max(El_h)} - h_{max(T_h)} \quad [€/MWh] \quad (4.19)$$

$$HDD_y = \sum_{i=1}^{8760}\left(19 - T_{h_i}\right) \text{ for } T_{h_i} < 19 \quad [€/MWh] \quad (4.20)$$

$$CDD_y = \sum_{i=1}^{8760}\left(T_{h_i} - 24\right) \text{ for } T_{h_i} > 24 \quad [h] \quad (4.21)$$

The parameters which rely on an hourly daily or yearly discretization, identified by the relative subscript, were considered for their arithmetical averages. Additionally, to fully describe the scenarios and consider the variability the 1st and the 3rd quartiles were also assumed for 6 parameters[30] so that each location was characterized by 28 values. Figure 4.2 reports the correlation heatmap which shows the 2D correlation matrix between the defined market parameters. For visualization purposes, the heatmap is limited to the average value excluding the quartiles. Figure 4.2 allows drawing some considerations: cold climates seem to imply a stronger electricity-gas market interdependency and lower CSS; a warm climate is generally followed by higher daily fluctuations in electricity prices, but with a limited duration of the peak period.

[30] The parameters considered for their quartiles values in addition to the average are those defined by equations (4.8, 4.9, 4.12, 4.13, 4.19) plus the hourly temperature.

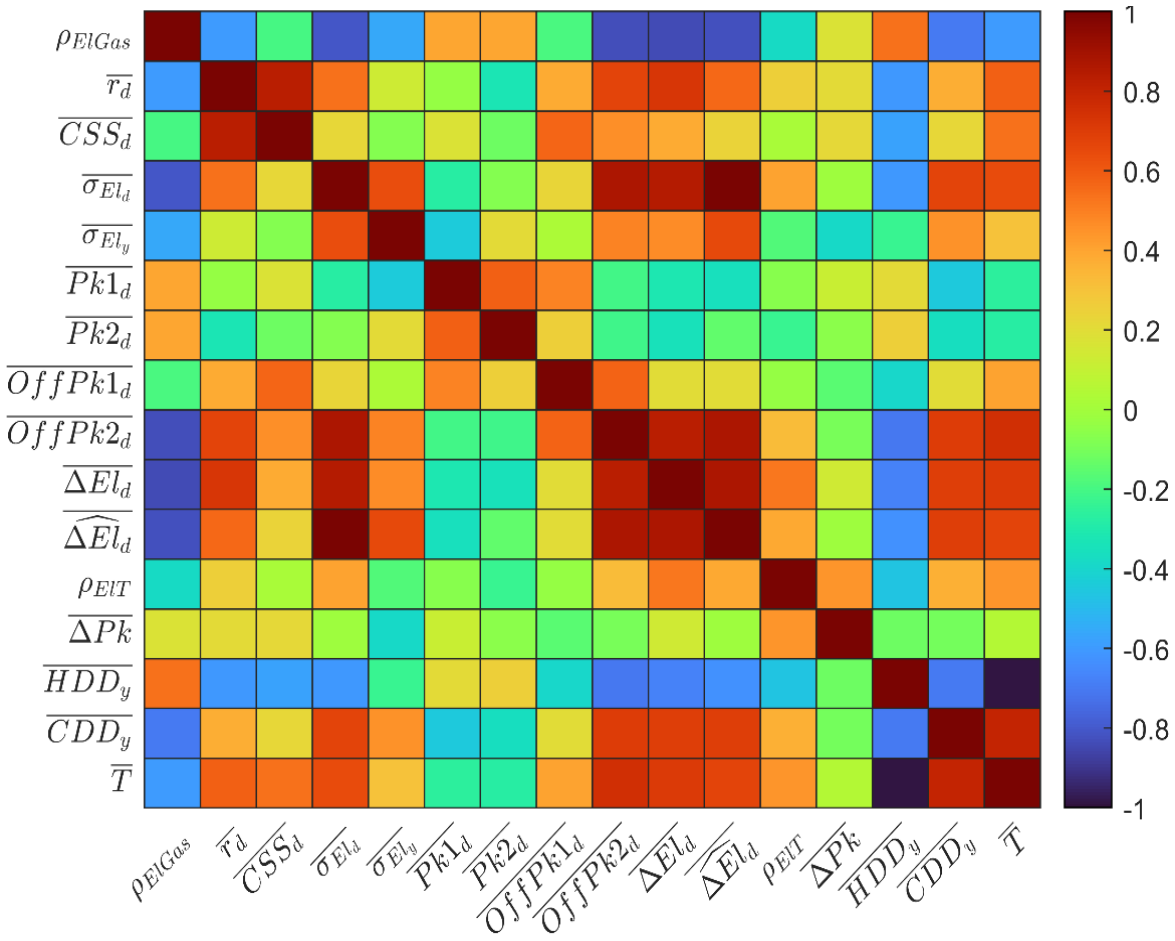

Figure 4.2: Correlation heatmap.

Then, in order to define a relevant statistical sample, a clustering procedure based on a k-Nearest Neighbor (kNN) algorithm was performed. A principal components analysis preceded to exclude redundant information from the dataset. The first six components, retaining over 90% of the initial database variability, were selected and KNN clustering was performed on these. The predetermined number of clusters has been set to 9 as it represents the best compromise between the over-segmentation of considered markets and too-large clusters with excessive internal variability.

The clustering can be visualized by means of the maps reported in Figure 4.3 and summarized as follows: California (green), Texas (light green), Southern Midcontinent (blue), New York (yellow), New England & France (turquoise), Mittel-Baltic Europe & Northern Midcontinent (orange), Scandinavia (purple), Peripheral Europe (red) and Sicily (cyan). For each cluster, the closest observation to the cluster's centroid was selected as the most representative. The reference locations of the most representative zones are pointed on the map with star markers, while the other locations, also reported in Table 4.3, are identified with a red dot. In Figure 4.4 and Figure 4.5 the reference location is indicated by the filled markers.

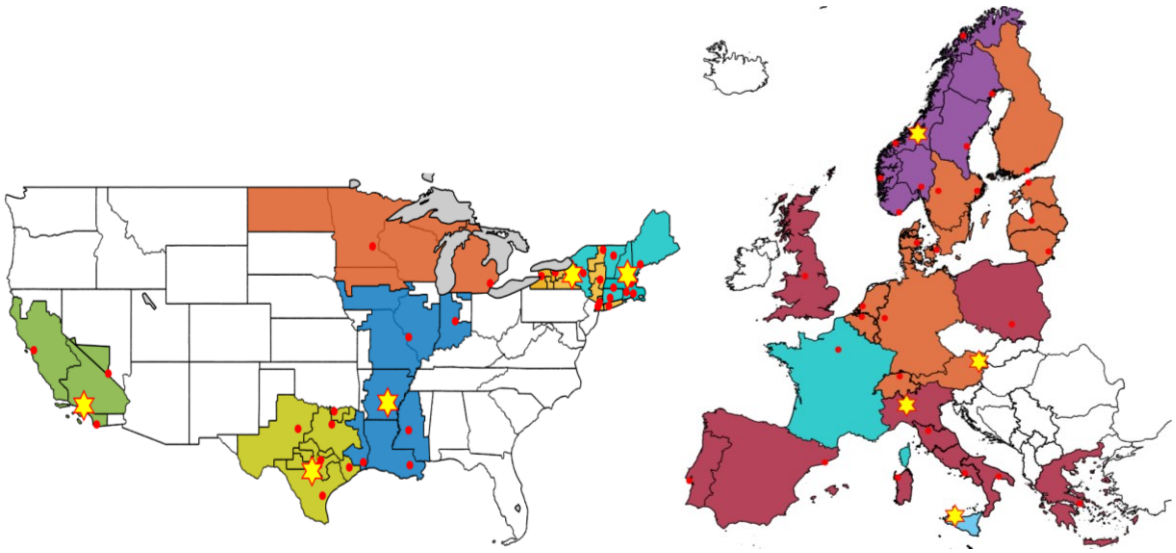

Figure 4.3: Clustering Mapping.

Figure 4.4 shows how the clustering procedure is also appreciable on the $\overline{\Delta El_d}$ vs $\overline{CSS_d}$ plane. The relationship between these two variables can be deduced also from Figure 4.2, but here is pointed out how the correlation is stronger among European countries, and that positive, or slightly negative, average CSS is generally followed by significant daily electricity price fluctuations. These two market indicators help in distinguishing stable low-price regions (like Scandinavia (purple), New York (yellow), and Mittel-Baltic Europe & Northern Midcontinent (orange)). Then all the other regions, with a CSS between -5 to +5 €/MWh, are characterized by an increasing degree of volatility from the stable US Southern Midcontinent to Texas with a daily spread in electricity cost of about 70 €/MWh. In such a scenario, the ICU integration may improve the power plant performance using the TES to exploit the variability of the markets, these conditions usually occur in warm or hot climates. However, the clustering is not so self-evident in Figure 4.5, which analogously to Figure 4.4 reports the average ambient temperature and the daily electricity price off-peak period focusing on the climate electricity market interdependency. Higher ambient temperatures increase the possibility of boosting the power output through inlet cooling, longer electricity price off-peak periods could be an opportunity to charge the TES. This variable appears to be correlated with the daily price spread, (e.g., Texas presents the highest off-peak duration (9h)), so all the conditions favorable to the PUMPHEAT layout appear to be positively correlated. The clustering in Figure 4.5, is less clear since among the clustering parameters the climate indicators are underrepresented if compared to the market ones.

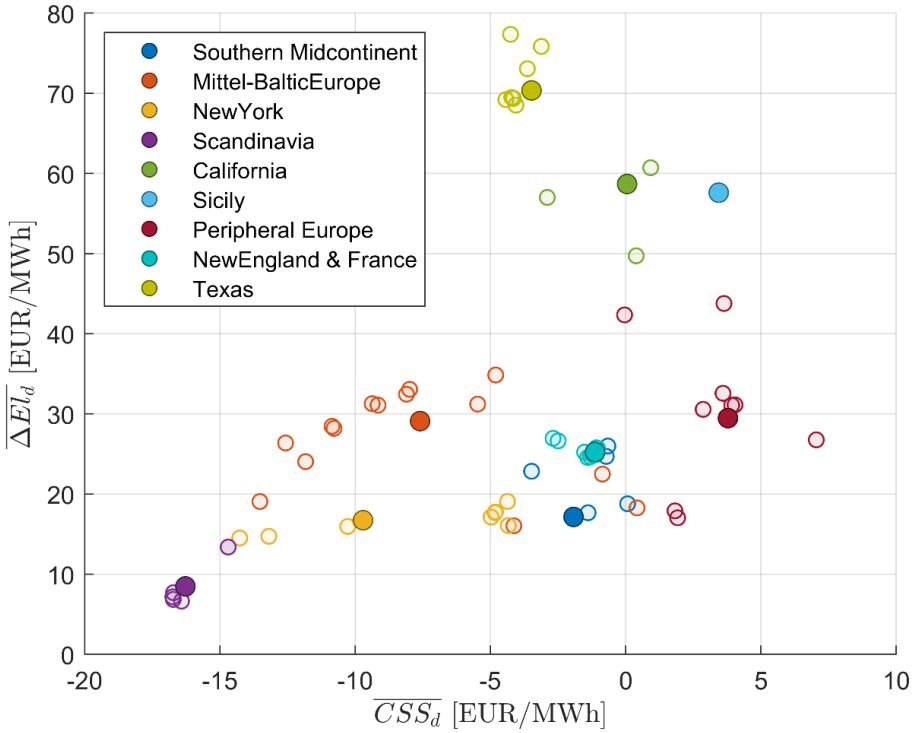

Figure 4.4: Clusters on the daily spread axis vs clean spark spread axis.

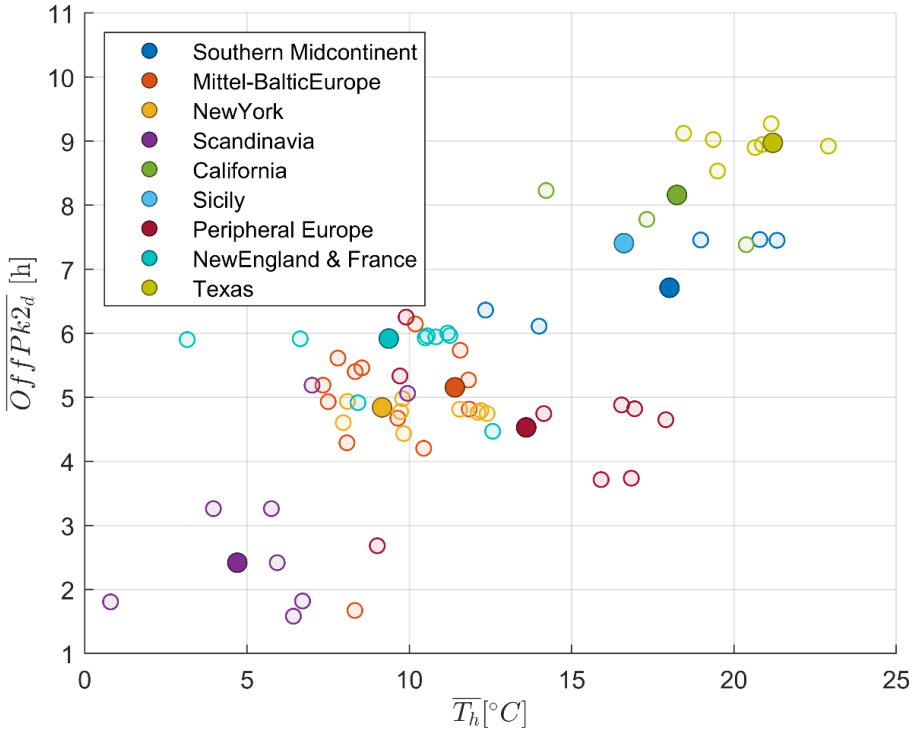

Figure 4.5: Clusters on Off-Peak duration vs the average ambient temperature axis.

4.1.1.3. Market and Climate's Impact Assessment

Since a one-year simulation of both the ICU and BAU scenarios, in order to assess the ICU integration benefits, is time expensive (4 to 7 hours per year by location), the investigation is carried out on the most representative sample identified in the previous section. Input data were selected to be from 2019, the last year not affected by the market distortions due to the pandemic prevention measures. HP and TES were sized to 3.5 MW and 10 MWh respectively following the suggestion in [197].

Table 4.4 reports the techno-economic and environmental KPIs, the best performances are achieved in those locations characterized by hot climates and high and variable electricity prices, such as Texas or Sicily where the NPV is expected to be above 60 M€ and the PBP less than 2 years. On the other hand, less profitable locations are characterized by low and stable electricity prices, often in cold climates. However all the investigated locations reported a positive NPV; it is interesting to look at the Trondheim (NO) case, the total profits are negative since the revenues are not enough to pay the fixed O&M cost back, nevertheless, the ICU integration allows to save 350 k€/yr and increases the operating hours by 7%. It is possible to generalize this outcome by stating that where there are no conditions to operate profitably a CCGT power plant, the ICU may not have such a strong impact as to make the CCGT profitable, but it may reduce the cost to operate a plant that may be essential to the grid or that cannot be taken out of service for any other reason.

Trondheim reports also the highest increase in generated electricity but the Δel_{gen_abs} is very close to the Δel_{gen} since this market, characterized by flat prices, does not require a highly flexible operation. On the contrary, location such as Syracuse (NY) uses the ICU to gain flexibility lowering the electricity production for many hours. However, the overall difference in dispatched electricity is positive for all the considered locations, moreover, the carbon footprint is almost constant, and even if slightly, the mean efficiency increase is reflected in a specific emission decrease. Thus, the ICU integration enhances the economic indicators without any environmental cost, from the system operator's point of view an ICU installation spread would allow dispatching flexible resources, pursuing a higher level of system security, and keeping constant the system's environmental impact.

Table 4.4: Key Performance Indicators values.

Location	**Trondheim**	**Vienna**	**Milano**	**Palermo**	**Los Angeles**	**San Antonio**	**Manchester**	**Pine Bluff**	**Syracuse**
State/Country	**Norway**	**Austria**	**Italy**	**Italy**	**California**	**Texas**	**New Hampshire**	**Arkansas**	**New York**
Bidding Zone	**NO3**	**AT**	**NORD**	**SICI**	**SCE**	**LZ_CPS**	**NEWHAMPSHIRE**	**ARKANSASHUB**	**CENTRL**
OP^{ICU} [M€/yr]	-0.51	8.24	38.88	83.49	36.55	58.98	20.71	7.29	0.68
ΔOP [M€/yr]	0.35	0.58	1.17	3.5	1.55	3.77	0.78	0.48	0.34
ΔRevenue [%]	9.91	2.2	2.71	3.94	3.75	4.82	2.07	2.46	2.05
NPV [M€]	0.48	4.88	16.13	60.43	23.37	65.67	8.52	2.96	0.25
PBP [yr]	17.73	10.75	5.35	1.8	4.05	1.67	8.1	12.98	18.37
el_{gen} [TWh/yr]	1.2	2.01	3.24	3.17	2.83	2.93	2.68	3.11	1.37
Δel_{gen} [%]	9.08	1.9	2.85	4.05	3.68	2.62	1.48	2.05	0.85
Δel_{gen_abs} [%]	9.21	3.28	4.37	4.43	4.52	4.61	2.48	4.02	3.99
ΔCO_{2_spec} [%]	-0.01	-0.03	-0.01	-0.02	-0.04	-0.06	-0.01	-0.04	-0.03
$\Delta\bar{\eta}$ [p.p.]	0.01	0.02	0.01	0.01	0.02	0.03	0	0.02	0.02
OH^{ICU} [h/yr]	2929	5135	7966	7801	7222	8043	6757	8072	3676
ΔOH [%]	7.13	0.2	-0.13	0.15	0.1	0.07	0.24	-0.28	-0.08
TES UF [%]	8.15	40.16	24.63	19.47	62.72	77.56	37.26	66.55	26.47
HP UF [-]	0.31	0.36	0.35	0.43	0.44	0.44	0.33	0.4	0.4

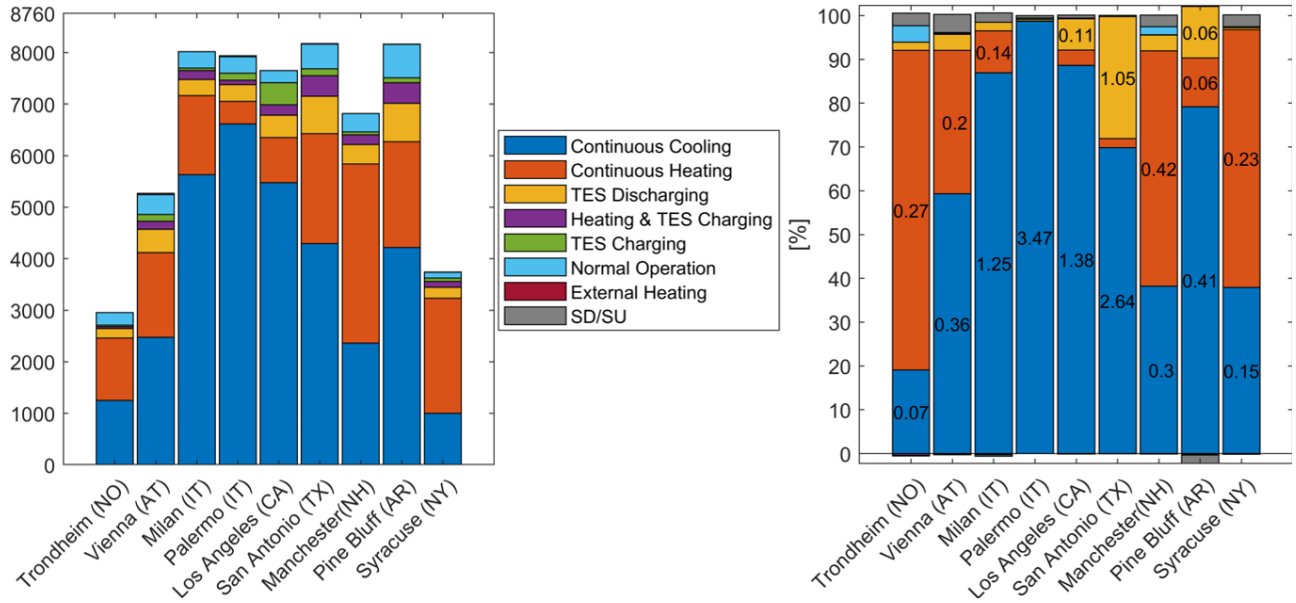

(a) *(b)*

Figure 4.6: ICU operational mode: (a) hour of use, (b) percentage operational profits increase (absolute value [M€/yr] in the figure).

Figure 4.6 well describes in detail the operation of the integrated ICU in each location, Figure 4.6(a) reports the operating hours for each operational mode, while Figure 4.6(b) quantifies the contribution to the ΔOP of each operation mode, labels report the absolute contribution [M€/yr], if relevant, of continuous cooling, continuous heating and TES discharging modes.

The impact of different operation modes is strongly related to the local conditions; however, most of the profits are generated with the continuous cooling mode, except for those locations characterized by severe cold climates: Trondheim (NO), Manchester (NH), and Syracuse (NY), here the continuous heating is the main source of profits (73%, 54%, and 59% respectively); however, the absolute values are limited. It is worth noting that also more profitable sites but characterized by highly fluctuating prices, such as San Antonio (TX) reporting $(\Delta El)^{-}_{d}$=70 €/MWh, exploit the continuous heating mode for a remarkable amount of time, up to 2100 h. Although the contribution to overall profits from this mode is neglectable here (≈2%) it is crucial in reducing the cost of keeping the power plant operating during off-peak periods, ready to exploit the continuous cooling opportunities during peak hours typically in the late afternoon or evening. The TES is mainly exploited by the locations with a considerable electricity price variability: San Antonio (TX), 725 discharge hours and 1.05 M€/yr in profits, or Los Angeles (CA), 433 discharge hours and 110 k€/yr. despite low price variability, Pine Bluff (AR) also reports a significant TES impact (744 discharging hours and 11.7% ΔOP), the reason is the large number of off-peak price hours during which it is advantageous to charge the TES.

Finally, the model does not forecast a significant impact of the ICU on the cost due to the number of SU/SD cycles, almost unaltered everywhere, the gray segments in Figure 4.6(b) are below the 0 line if the number of SU/SD cycles increases as the ICU is integrated.

The discussed results are related to the most representative locations of the clusters identified in the previous section, to verify the assumption that the KPIs variability is limited within the cluster, one whole cluster was simulated. The Peripheral Europe cluster was selected for this purpose because of its potential heterogeneity, it includes different climates, such as the UK, Poland, and the southern European countries, and different electricity generation mixes (which are diriment in determining the electricity market behavior), coal-based (Poland), gas and RES based (Italy and UK), nuclear and RES (Spain) and others.

Figure 4.7 shows how all the locations of the Peripheral Europe cluster operate similarly, strongly relying on the continuous cooling mode and performing a difference in operational profits between 0.75 and 2.56 M€, excluding Greece and UK as outliers the variability is limited to 33%. Milano (Italy, NORD zone) was selected as the most representative location of the cluster since it is the closest to its centroid, looking at the economic results and the distribution of the operational modes, is possible to note how this location represents its cluster, achieving a net difference in profits of 1.39 M€/year with a moderate contribution of the inlet heating mode and almost null TES usage. This confirms that the parameters listed in the previous subsection 2 are appropriate in describing the ICU integration potentialities.

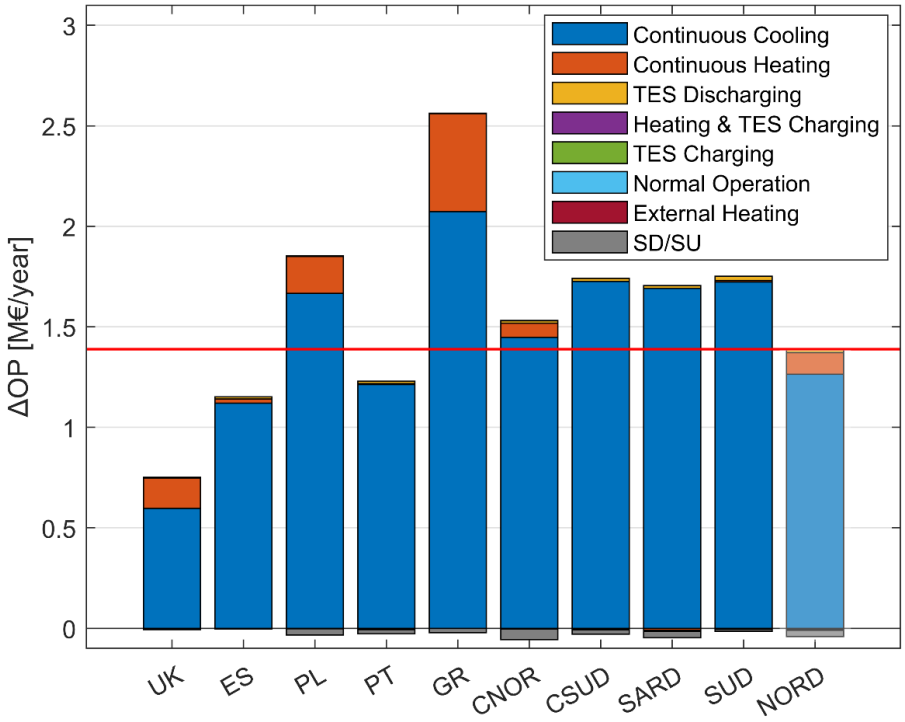

Figure 4.7 Peripherical Europe variability ΔOP and composition.

A further analysis was performed to identify among these parameters those that best predict the techno-economic performance of the ICU integration. A new methodology, based on linear regression modeling, is proposed for this purpose. All the possible models considering a number of regressors equal to k, among the parameters selection shown in Figure 4.2, are trained to fit the NPV and ΔOP results reported in

. The number of predictor k varies between 1 and 7 for linear terms models and from 1 to 3 for pure quadratic terms models. The model with the highest adjusted R^2 is selected and a score equal to $AdjR^2/k$ is assigned to the relative regressors. The scores are summed together for all the considered values of k, equation (4.22). The overall score S_i describes the ability of the i^{th} regressor in predicting the NPV and ΔOP since it includes the information about how often it is selected as the best regressor and about the goodness of fitting when it is selected. The scores are normalized on 4, the maximum value theoretically achievable, so that S=1 corresponds to an ideal regressor that is always selected and whose relative model reports $AdjR^2=1$.

Note that the ordinary R^2 value was used to select the best model among those that had been trained with the same number of predictors k, while the adjusted value of R^2 was used to compute the score, in order to properly account for the contributions of models trained on a different number of predictors.

$$S_i = \frac{\sum_{j=1}^{7}\left(\frac{AdjR_{i,j}^2}{k_j}\cdot\left(R_{i,j}^2 == max\left(R_j^2\right)\right)\right)}{4} \quad [-] \qquad (4.22)$$

Figure 4.8 shows that electricity price daily variability turns out to be the variable more related to economic KPIs, confirming that the ICU is designed to address the need for the

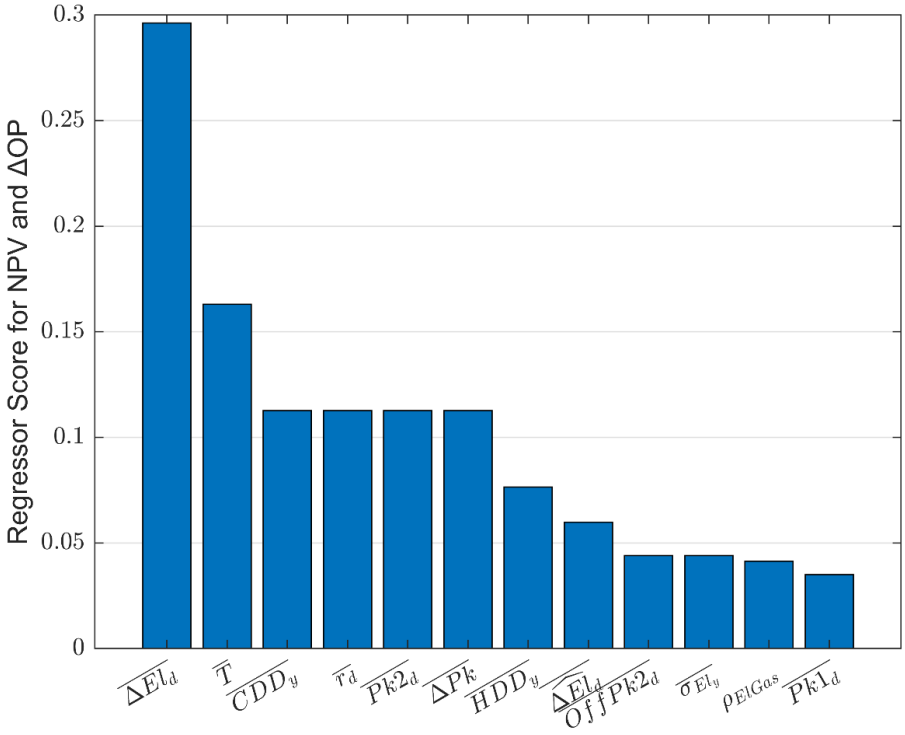

Figure 4.8: Predictors' score as a linear regressor.

flexibility required by modern electricity markets. Then climatic parameters follow, and the CDD are directly related to the location's inlet cooling potential which is demonstrated to be the most profitable way to operate the ICU and these results justify the better performance observed within warm and hot climates.

In order to provide an effective tool to roughly assess the potentialities of a new site for CCGT and ICU integration, the NPV values reported in Table 4.4 and the clusters identified by Section 4.1.1.2 are plotted in Figure 4.9 against two of the main indicators found in the analysis above.

For this purpose, the daily price variability is selected since it reports the highest score and the CSS, even if this indicator is not among those in Figure 9 it is strongly correlated to $\overline{r_d}$ the third most important indicator, tied with others. Indeed, CSS represents a standard for CCGTs' profitability assessment, and including it in Figure 10 makes the tool more accessible to the potential user.

In Figure 4.9, the authors identified 3 main zones. (I) characterized by low and flat electricity prices, in which the ICU benefits are limited to continuous heating in cold locations. (II) characterized by daily variability greater than 20 €/MWh or positive CSS, where an NPV comparable to the CAPEX is almost certain. (III) where the NPV is up to 10 times the CAPEX benefiting from the extreme price variability or the significant profit margin on the energy market (CSS up to 5-10 €/MWh).

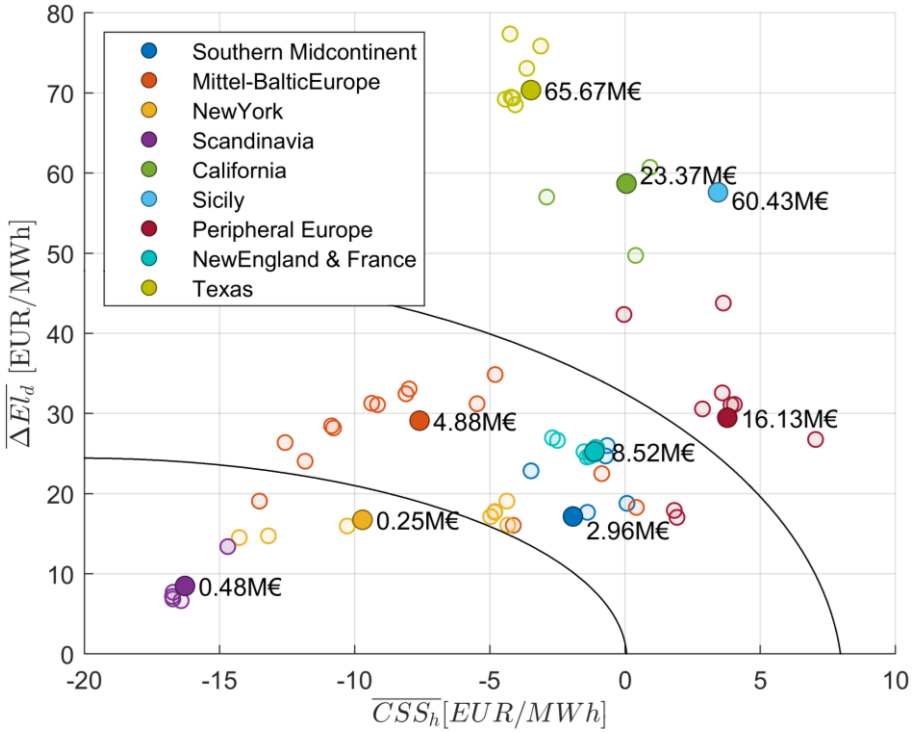

Figure 4.9: ICU integration profitability assessment.

4.1.2. Power oriented applications concluding remarks

To select the most representative locations a statistical analysis, including a k-Nearest Neighbor clustering, was performed based on electricity (only the Day-Ahead market is included) and gas price, carbon pricing policy, and ambient temperature. This analysis also allows outlining some interesting considerations about how the climatic and the energy market features are correlated to each other. It is shown how, especially in Europe, a positive average Clean Sparks Spread often implies fluctuating electricity prices; moreover, cold climates are generally associated with a flat electricity price daily curve. The variability of the observed KPIs within a cluster is reduced, so the validity of the proposed methodology is confirmed and the outcomes relative to a specific location can be generalized to its own cluster.

Continuous inlet cooling, utilizing the heat pump without the TES, boosts the power output and is demonstrated to be the operational mode able to guarantee the highest profits increase with respect to the Business as Usual scenario (standard CCGT). Thus, hot climates with high peaks in electricity price can fully exploit this potential. Among them, Sicily and Texas report the best economic KPIs, demonstrating to pay the Inlet Conditioning Unit (ICU) back in less than 2 years.

Furthermore, within colder climates the ICU is exploited to improve the partial load efficiency heating the GT intake, this strategy can lead to an increase of up to 7% in annual operative hours and 9% in the electricity generation. This possibility is particularly attractive for those power plants that are no longer able to operate viably because of the changes in the electricity market demanding more flexibility, but whose mothballing would jeopardize the stability of the grid.

Texas and California, presenting highly fluctuating electricity prices, with an average daily spread of 70 and 60 €/MWh respectively, are also able to exploit the TES. In San Antonio (TX) an integrated CCGT-ICU system can guarantee up to 1 M€ of profits, 28% of the overall income while discharging the TES to cool down the GT intake.

Figure 4.10 qualitatively illustrates the outcome listed above. Three different hypothetic scenarios are highlighted by the chart under which the ICU integration has a positive impact operating in different ways. Under high and stable electricity prices (i.e positive Clean Spark Spread), the system can be used as an inlet cooling device, just to take full advantage of the full capacity of the installed CCGT. When the electricity prices and the chances of revenues are variable on a daily basis, the complete PUMPHEAT layout, equipped with the TES can be beneficial, with higher benefits under higher average ambient temperature. Lastly, when average temperatures are lower than 15°C, the impact of the cooling is reduced and the benefit is limited to only increasing off-design efficiency through inlet heating. This solution can be easily adopted, with a reduced installation cost, and in general, can be seen as an extended anti-ice system. The solution applies to off-design operating conditions.

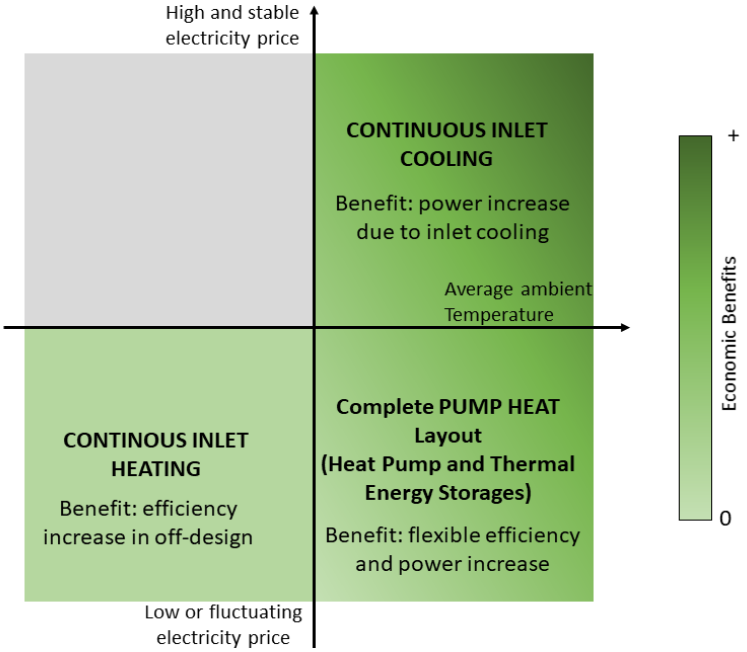

Figure 4.10: Qualitative intake conditioning economic benefits under different market and climate conditions.

Concerning the ICU sizing, the study has highlighted how for locations characterized by variable electricity prices the TES is a key component and 10 MWh can be considered a proper size for a 400 MW CCGT. In Texas, characterized by extreme electricity price variability, the TES discharging mode realizes 28% of the profits difference. However, the TES utilization factor results to be 78%, which indicates that a further increase in size could not be completely exploited. On the contrary, TES turns out to be almost unuseful in electricity markets, such as the Scandinavian, where the electricity price is very stable because of the preponderant hydro generation. Then a 3.5 MW heat pump results to be oversized for all the considered locations, in which it works on average below 50% load. The HP is the most expensive component in the ICU, so proper sizing is pivotal. To perform the sizing optimization local inputs and the targeted objective function should be provided to the optimizer.

Finally, the study focused on determining the best predictor among the considered parameters in a linear regression model of the simulation's outcomes. A novel methodology was proposed to assign to each parameter a score quantifying its ability to fit the results. The daily electricity price spread turns out the best predictor, followed by the average ambient temperature, confirming that is essential to consider both the climate and the market factors to properly assess the local potentialities of retrofitting a CCGT with an inlet conditioning unit.

Many of the parameters considered are dependent on policy or macroeconomic factors, however, they have demonstrated their effectiveness as predictors regardless of the cause and can be used as a first step in assessing the rough profitability of such a system in the future and other locations. By means of Figure 4.9, presenting the distribution of the bidding zones in relation to the main predictors (i.e., daily electricity price variability and Clean Spark Spread), it is easy to determine which cluster is closest to the given conditions, and consequently which results can be taken as a reference.

4.2. CHP applications

The previous chapters has been deepen how heat pumps and CCGT-CHP can contribute to the energy transition by reducing the carbon emissions due to the heat supply and promoting the coupling of the heating to the electricity sectors. However, these technologies have been considered separately while the coupling between them can provide further benefits which this section aims to discuss.

Some previous works discussed the optimal operation distribution between thermal power production, co-production of heat, and heat pump. Lowe [204] showed that the steam cycle of a combined heat and power generator is thermodynamically equivalent to a conventional steam cycle generator plus an additional virtual steam cycle heat pump and assesses the heat production capabilities at varying condensing temperatures of the CHP plant. Malinowska and Malinowski [205] presented a parametric study of exergetic efficiency performed on a serially coupled HP and small-scale CHP plant. The integration of CHP with HP was proposed by Dagilis [206] and applied to a specific CCGT case study, selecting as the HP's low-temperature heat source the bottoming cycle steam condenser. Blarke et al. [207,208] discussed the integration of an efficient high-temperature compression heat pump that uses only sensible heat recovered from flue gases (FG) as the low-temperature heat source, and an intermediate cold thermal storage. Using flue gas as low-temperature source for large-size HPs is particularly interesting when also the latent heat exploitation through condensation is considered, allowing to increase significantly the heat recovered and consequently the global efficiency of the plant, reducing also its carbon footprint. This solution was explored by previous studies applied to biomass boilers adopting a direct heat exchange with a water quench cooled by an HP [209] or to a coal-fired power plant via a direct contact mode, which exploits the flue gas desulfurization scrubber [210]. Finally, while none of these studies discussed more than one or two configurations, or mentioned the possibility of other plausible configurations, Ommen et al. [211] presented a comprehensive investigation of different configurations of heat pumps in combined heat and power plants even without taking into account flue gas condensation.

The operational range of CHP plants is well described by its own Iron diagram, which has been presented in Section 2.2 (Figure 2.5, Figure 2.6, and Figure 2.7), and the Z factor. The Iron diagram reports the electrical output vs the thermal output. While the Z factor quantifies the cost of heat supply in terms of electric power (equation (2.2)). As pointed out

the Z factor is analogous to the HPs' COP, indeed within a coupled system, the thermal demand can be coped by both the CCGT (e.g., bleeding low-pressure steam from the bottoming cycle as described in Section 2.2) and the HP according to which, between the Z factor and the COP is higher. Moreover, the coupling usually allows extending the operative range since the power output has a limit below which cannot be lower to increase the thermal generation (e.g., a minimum steam amount of steam is required to flow through the turbine), however, the CCGT electricity can be used to drive the HP lowering the electrical and increasing the thermal outputs further. Additionally coupling an HP to a CCGT-CHP will allow the first to exploit a privileged heat source increasing both the COP, since the HP is exploiting a good (warm, stable, and reliable) heat source, and the plant's overall efficiency, since some wasted heat is recovered.

This section focuses on two possible coupled layouts exploiting two different heat sources, moreover for each configuration is carried out an analysis to determine if the HP should be coupled in series or in parallel to the CCGT's DHN-HX. The flue gas condensing layout (ref. Section 4.2.2) is the most promising since the flue gases' latent heat is exploited, making over 100% efficiency values achievable. However, it implies relevant investments which may jeopardize the economic viability. Then, on this layout, a techno-economic assessment is carried out, also keeping into consideration the uncertainties of the markets.

4.2.1. Bottoming Cycle Condensate as Heat Pump's Heat Source

An opportunity for CCGT-HP coupling is represented by the exploitation of the low-temperature condensate as a heat source. According to this concept, the bottoming cycle condensed steam is cooled further, feeding the HP's evaporator. The HP rises the temperature up to the supply level required by the DHN, or other users. The overcooled condensate is then redirected to the HRGS.

Actually, there is a minimum temperature requirement for entering the Feed Water Heater (FWH), i.e. the first heat exchanging section of the HRSG. Since temperature below the Flue Gasses (FG) dew point would imply the formation of acid condensate on the heat exchanger's surface. An acid environment would imply corrosion issues so suitable materials are required, determining increased investment costs. The exact dew point temperature depends on the flue gas composition and pressure, so on the GT load and the HRSG design. Subsection 4.2.2 investigates this determining value of about 50°C. However, to keep a safety margin independent of the operating condition a minimum requirement of 55°C is a standard for entering the HRSG. To accomplish this requirement, a loop is implemented even in standard CCGTs, to recirculate a fraction of the warm water mass flow from the FWH outlet to the FWH inlet. The recirculated flow is that guarantees 55°C at the FWH inlet.

So this subsection proposes to investigate the possibility of heat extraction, by means of a heat pump, from a CCGT's bottoming cycle condensate. The concept does not any major intervention in the plant, since the already implemented loop to control the FWH inlet temperature is used to maintain the HRSG operating condition unchanged. The only component affected by the HP coupling is the FWH since the more frequent and intense use of the temperature control loop would lead this component to elaborate a higher mass flow rate, the consequence is an increase in the amount of heat that needs to be exchanged to maintain the design condition at the FWH outlet. In other words, the HP extracts heat from

the condensate, cooling it below the design point so that to achieve the design point at the FWH outlet the FG has to be cooled further.

The heat potential within the flue gases at the stack is a thermal loss since it represents an unexploited fraction of the fuel energetic potential which is dumped into the environment. Then a stack temperature reduction is beneficial in terms of fuel exploitation rate (i.e., global efficiency). Nevertheless, there is a minimum temperature required in order to guarantee flue gas buoyancy and pollutant dispersion, avoiding excessive concentration within the area surrounding the power plant. Moreover, even if it has no environmental consequences, plants operator generally prefer to avoid visible plume formation at the stack because the perception of people who associate with a visible plume increased pollutant emissions.

The following subsections investigate how this concept can be implemented with respect to the minimum temperature requirement at the stack. Two options are considered as the best point of coupling (i.e., where the HP's evaporator extracts heat from the bottoming cycle). Two configurations, series and parallel, are also assessed to determine how the HP should be connected to the DHN-HX.

4.2.1.1. Case of Study: Moncalieri Power Plant

The plant under investigation is the 2nd GT of the Moncalieri[31] cogeneration plant. Moncalieri, together with the North Turin plant, feeds the city's DHN. The Moncalieri plant consists of two CCGT-CHP plants, which provide a total electrical power of 800 MW_{el} and thermal power in cogeneration mode of 520 MW_{th}, supported by an integration and reserve plant of 141 MW_{th}. Turn's DHN can be classified as a 2nd generation DHN (ref. Subsection 1.2.3) whose return and supply temperatures are 70°C and 120°C respectively.

The 2nd GT plant has an electrical power capacity of 395 MW_{el}, such electric power is provided in full condensing mode while the full cogenerative mode can guarantee 260 MW_{th} of thermal power. The CCGT is driven by an F-class GT, characterized by an annular combustion chamber, powered by natural gas, without the possibility of using other fuels. The HRSG consists of three-pressure levels with reheat, as the standard described by Subsection 2.2. The steam is then condensed exploiting the draught of the cooling water from the Po river. Finally, the entire condensing and district heating system is supported by the presence of several auxiliaries including some pumps. Figure 4.11 and Figure 4.12 illustrate the operating range on the Iron Diagram and the overall plant layout.

It is worth noting that, as shown in Figure 4.12, this layout includes the possibility of redirecting an amount of water from the FWH outlet to the DHN-HX rather than to the bottoming cycle.

[31] Province of Turin, Italy. NORD electricity market zone.

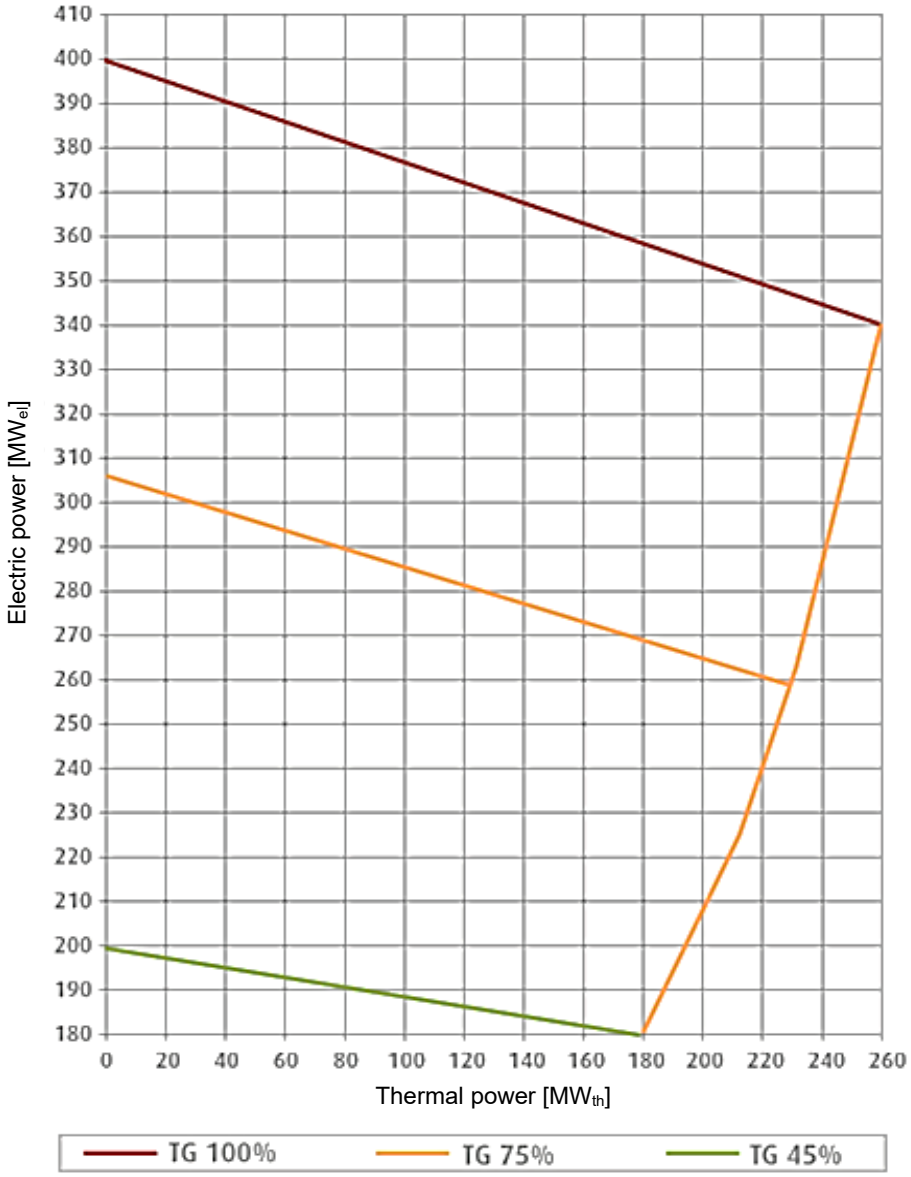

Figure 4.11: Moncalieri 2nd GT Iron Diagram.

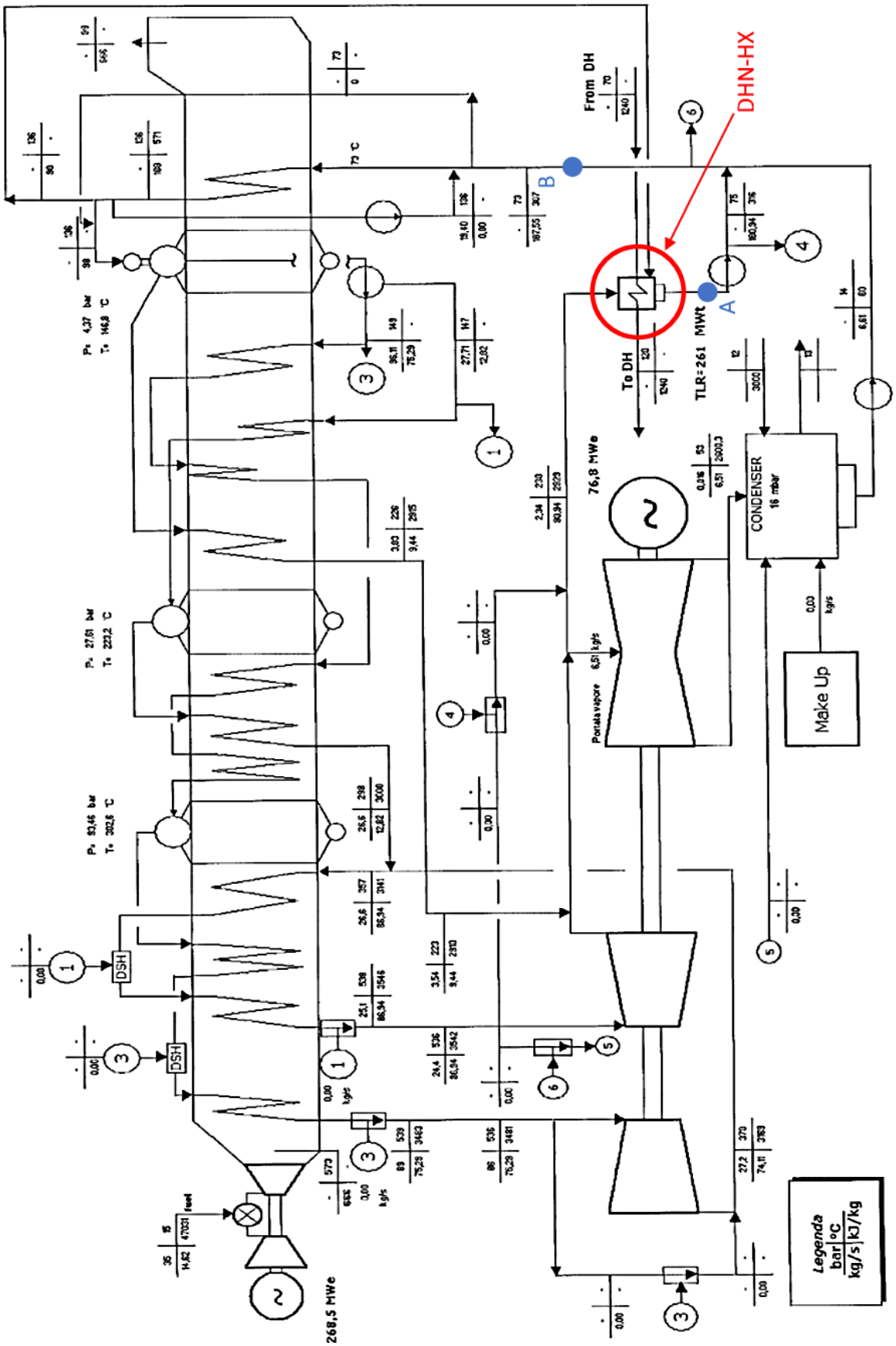

Figure 4.12: Moncalieri 2nd GT Plant Layout.

4.2.1.2. Proposed layout for HP coupling

Two different options were considered, both for the connection of the HP's evaporator and condenser. In Figure 4.12 two possible locations for heat extraction are marked by the blue circles. Letter "A" denotes the first option in which the HP's evaporator is placed after the DHN-HX cooling down the same steam bleeding which condensed in the DHN-HX. This condensate is hereinafter defined as "hot condensate" since because of the relative high DHN return temperature (70°C) the condensate temperature is higher if compared to the bottoming cycle condensate which is cooled down by the Po river's water (in this study assumed 15°C) and thus defined as "cold condensate". The second option of extraction is marked by the letter "B" in Figure 4.12, according to this layout, the HP's evaporator exchanges heat with the bottoming cycle's condensate once the cold and the hot condensate have been mixed.

Then the HP's condenser can be connected both in series and parallel to the DHN-HX, which is highlighted in Figure 4.12. On the other hand, Figure 4.13 reports the options for the connection of the HP's condenser to the DHN with respect to the DHN-HX. The Parallel coupling implies that only a fraction of the DHN water is heated up to 120°C by the HP. While the Series coupling requires the HP to elaborate the whole DHN water mass flow, preheating it at an intermediate temperature, the DHN-HX will heat up the water up to 120° as required by the network. Moreover, a hybrid approach is also considered, it consists of parallel heating up to an intermediate temperature, and a high-temperature section of the DHN-HX operating in series with the low-temperature section and the HP. As intermediate temperature different values have been considered (from 90°C up to 110°C).

All the configurations will determine an increase of the water which is heated up from 70°C to 120°, so an increase of the overall thermal production, they differ for the amount of water heated by the HP and the HP's supply temperature. Table 4.5 summarizes the investigated options. Moreover, two different approaches were studied, first the use of the HP as an alternative to the cogenerative thermal production, so even the CCGT-CHP full thermal capacity was not reached. Then, the exploitation of the HP to extend the operative range when the CCGT-CHP is working in full cogenerative mode.

Table 4.5: Investigated layouts summary.

	Heat Source	
Coupling Type	A-sourced Series HP	B-sourced Series HP
	A-sourced Parallel HP	B-sourced Parallel HP
	A-sourced Hybrid HP	B-sourced Hybrid HP

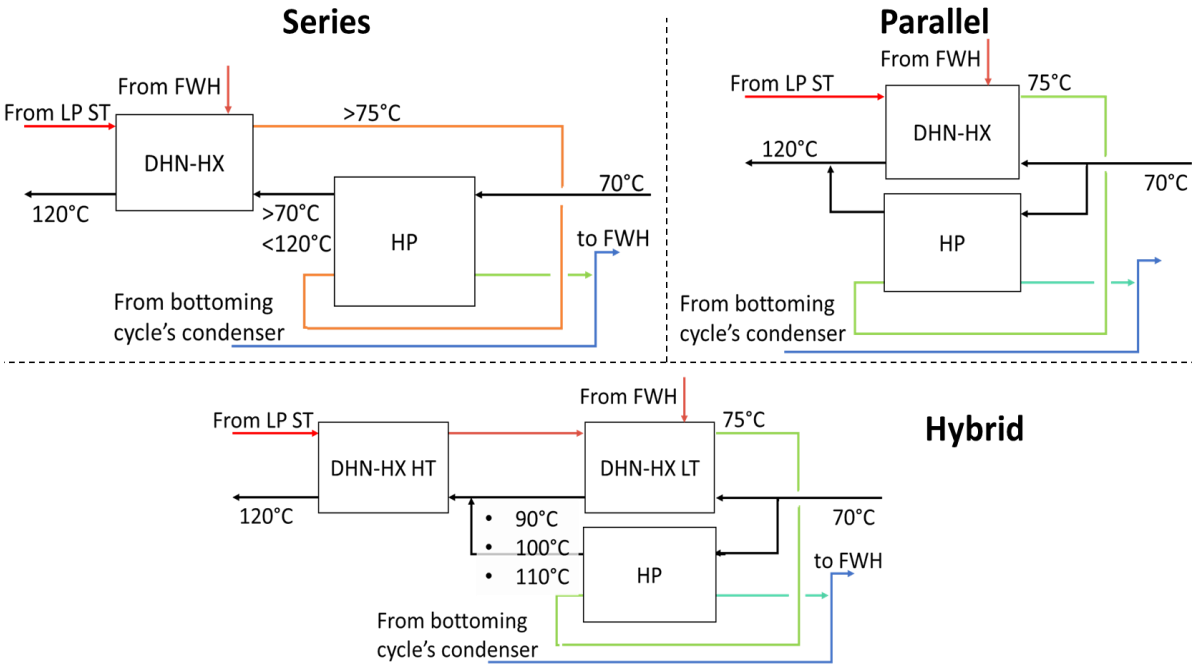

Figure 4.13: Option for HP and DHN-HX coupling, the heat source is here sketched according to option "B". Black lines indicate the DHN water, while colored lines refer to different condensate temperatures.

4.2.1.3. Modeling Assumptions

The HP capacity was studied from 0 up to 30 MW_{th}, with a step of 5 MW_{th}. Boundary conditions to the problem, i.e., the temperature and mass flow values have been imposed according to complete modeling of the CCGT [128] and reported in Table 4.6.

The HP COP was assumed according to the data provided by the PUMPHEAT project's HP manufacturer, COP=3.64 corresponding to a ΔT_{lift}=55 K, COP= to 4.16 if ΔT_{lift}=45 K, by linear interpolation the HP's coefficient of performance was determined for the desired thermal level application.

Since the first investigation was clear that within the CCGT-CHP operational range, the COP was always lower than the Z factor. Thus there is no advantage in operating the HP to cope with thermal demands, lower than the CCGT-CHP thermal capacity. However, the HP can be used to extend the operational range once the CCGT is operating in full cogenerative mode. This is the reason why Table 4.6 reports the input values to the problem only related to the full cogenerative mode.

The model is based on simple equations, balances of mass and energy on the different components (DHN-HX, FWH, and the LP ST), the overall electrical and thermal power outputs, and FG temperature at the stack are the model outputs.

Table 4.6: Modeling assumptions values, from CCGT-CHP model full cogenerative mode.

	GT load 100%	**GT load 45%**
$\dot{m}_{DHN}$	1240 kg/s	790 kg/s
$T_{DHN_{return}}$	70°C	70°C
$T_{DHN_{supply}}$	120°C	120°C
$\dot{m}_{FWH \rightarrow DHN-HX}$	90 kg/s	90 kg/s
$h_{w_{FWH_{out}}}$	571 kJ/kg	521 kJ/kg
$T_{w_{FWH_{out}}}$	136°C	124°C
$\dot{m}_{bleeding}$	90.94 kg/s	54.45 kg/s
$h_{bleeding} = h_{DHN-HX_{in}}$	2929 kJ/kg	3012 kJ/kg
$T_{bleeding} = T_{DHN-HX_{in}}$	230°C	271°C
$\dot{m}_{LP\ ST}$	6.51 kg/s	7.67 kg/s
$h_{LP\ ST_{in}}$	2929 kJ/kg	3012 kJ/kg
$T_{LP\ ST_{in}}$	230°C	271°C
$h_{LP\ ST_{out}} = h_{COND_{in}}$	2600 kJ/kg	2621 kJ/kg
$T_{LP\ ST_{out}} = T_{COND_{in}}$	53°C	84°C
$h_{COND_{out}}$	60 kJ/kg	61 kJ/kg
$T_{COND_{out}}$	14°C	14°C
$\dot{m}_{FG}$	666 kg/s	444 kg/s
$T_{FG_{FWH_{in}}}$	163°C	156°C
$c_{p_{FG}}$	1.008 kJ/kg·K	

4.2.1.4. Best practices for exploiting the CC's bottoming cycle as HP's heat source

Firstly, the target is to determine which of the two considered sources performs better. The most important feature is the minimum temperature at which the source is cooled down. This temperature will determine the HP's low-pressure level and the ΔT_{lift} with a direct consequence on the COP. So A-coupled HP is compared against a B-coupled HP, for this purpose the series case is selected, but it has no impact since to a fair comparison it is sufficient to guarantee the same power at the HP evaporator and assess the $T_{source\ out}$.

The analysis results are plotted in Figure 4.14 where the sensitivity of $T_{source\ out}$ to the HP power and GT load can be visualized, the markers highlight where the calculation is actually performed but a linear dependency is demonstrated. To a null HP's power, the $T_{source\ out}$ corresponds to the T_{source} availability temperature. It is equal to $T_{DHN\ return}$ + 5K of DHN-HX's pinch point difference (75°C) for the A-coupled heat pump, while the source temperature is lower for B-coupled HP since the hot condensate from the DHN-HX outlet is mixed to the cold condensate from the bottoming cycle's condenser (c.a. 16°C). However since the CCGT-CHP full cogenerative mode is selected the cold condensate mass flow is the minimum required to flow through the LP ST, thus the temperature drop after the mixing process is not so high, it would be more relevant if the considered CCGT power output was higher.

Increasing the HP power, i.e., moving towards the right side of Figure 4.14, the $T_{source\ out}$ progressively decreases, since more and more heat is extracted from the source. It is possible to appreciate how the decrease is faster from the A-coupled HP because the source mass flow rate is lower. On the other hand the B-coupled HP, despite the lower initial temperature decreases more slowly, because of the mixing the source mass flow is higher. The described trends are independent of the GT load, of course, the lower the GT load the lower is source's mass flow for both the coupling and the decrement is stronger for the same amount of extracted power.

It is reasonable to expect that for a certain amount of power the two lines cross each other and the $T_{source\ out}$ results higher for the B-coupled HP. However, it does not happen for the investigated power, corresponding to reasonable HP sizes. Then the A is selected as the best possible point to exploit the bottoming cycle as a heat source for the following investigation of the Series vs Parallel installation.

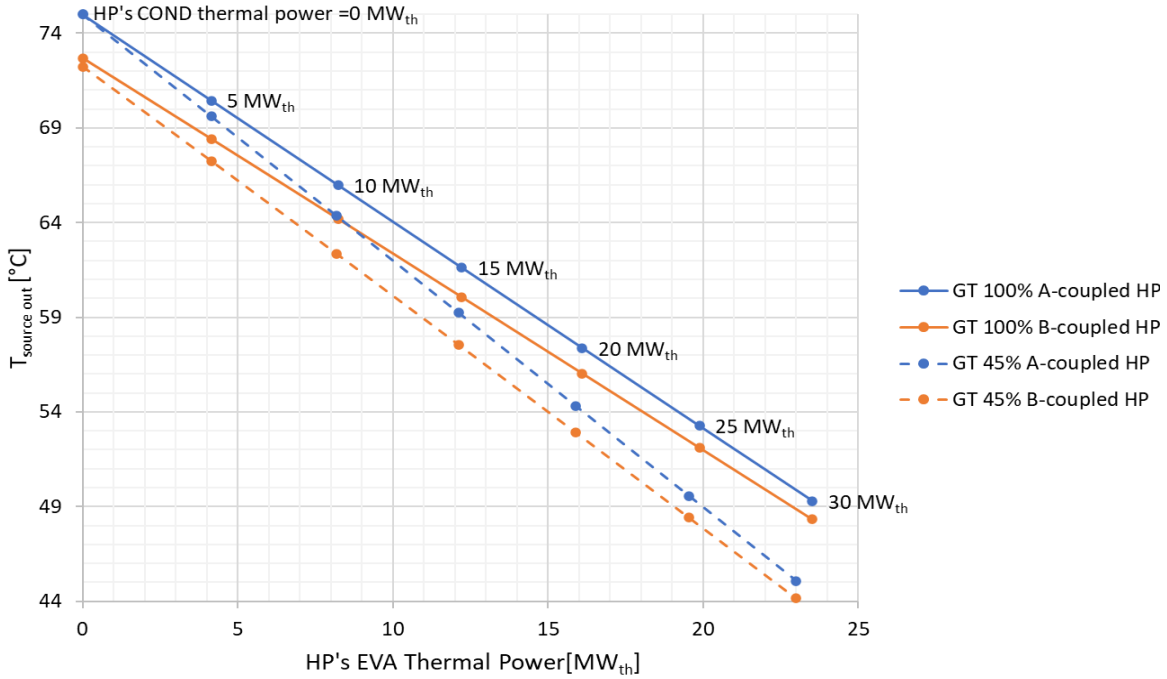

Figure 4.14: Best possible coupling for bottoming cycle exploitation as HP's heat source, $T_{source\ out}$ sensitivity to the coupling type, and GT load.

The main factor determining the HP's COP is the temperature lift ΔT_{lift}, provided by the HP to increase the heat thermal level from the low-temperature source to the sink. So, for the same heat source, it is possible to state that the COP mainly depends on the supply temperature. The higher the supply temperature the higher the lift and, consequently, the lower the COP. Looking at the case study, it follows that the best would be achieved, by progressively increasing the temperature.

Figure 4.15 reports the described trends. The Series HP always reports a higher COP if compared against the Parallel case for the same HP thermal power. The hybrid approach HPs have an intermediate COP depending on the HP's supply temperature. The COP is decreasing with the HP power since the more heat is extracted from the sources the lower is the $T_{source\ out}$ which is reflected in an increased ΔT_{lift} for the same supply temperature. Analogous trends can be drawn for other GT loads.

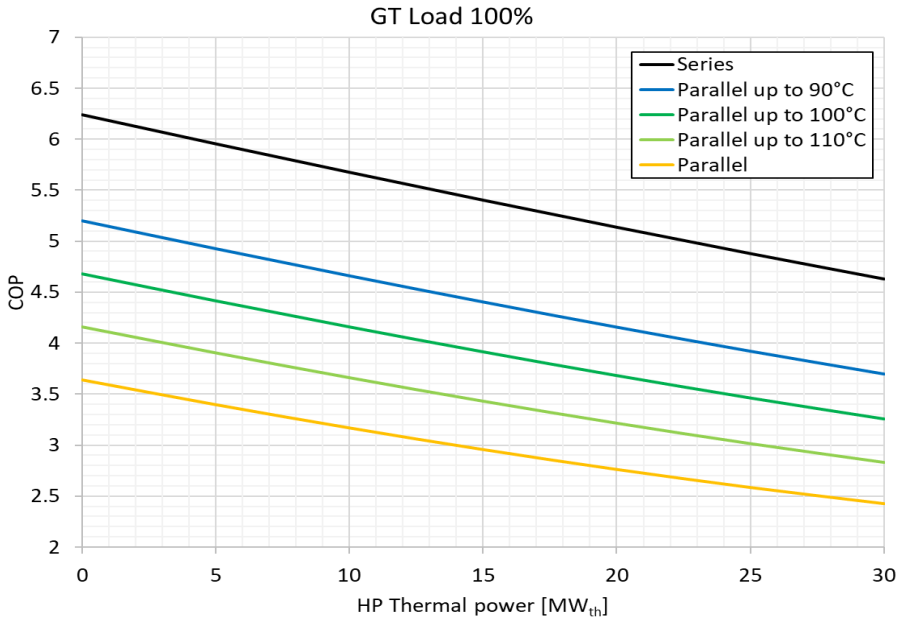

Figure 4.15: COP trends vs HP thermal power for full load GT. The A-coupling is selected.

However, as stated within the first part of Subsection 4.2.1 there is a temperature constraint at the stack, hereby this constraint is assumed 60°C. It is impossible to assume a lower temperature because a minimum FWH pinch point temperature difference of 5K must be guaranteed. Higher temperature requirements are common however it is easy to generalize the outcome here reported to draw the best practices with higher temperature requirements at the stack.

The higher is the COP the less electric power should be provided to the HP. Thus, comparing two HPs with different COP but the same thermal output at the condenser, it turns out that the HP with the higher COP extracts more thermal power from the heat source through the evaporator. In other words, a higher COP is reflected in a higher fraction of the supplied heat coming from the source rather than from the compressor power. Consequently, looking at the hybrid and the Parallel HPs, the higher is the COP more power comes from the bottoming cycle's condensate. Then if the condensate temperature approaching the FWH is lower an increased amount of heat will be required from the flue gas to maintain constant the temperature of water feeding the HRSG. In conclusion, HPs with higher COP, such as the Parallel up to 90°C, imply a lower condensate temperature approaching the FWH which is reflected in a temperature decrease at the stack.

Concerning the Series HP, it should also be considered that by increasing the HP power the exploitability of the heat from the FWH to the DHN is reduced since the cold side's inlet of the DHN-HX is preheated by the HP. In fact, an increase in HP power is not linearly reflected in an increase in the thermal output of the coupled system CCGT-HP. This also explains the different trends of the Series HP line in Figure 4.16.

Since the maximum cogenerative capacity of the CCGT-CHP is reached, and the flow through the LP ST is the minimum required, the heat dissipated into the environment by the condenser bottoming cycle is constant. Then the temperature decrease of the flue gas at the stack is a symptom of a higher global efficiency since the heat dumped into the environment

is reduced. If the GT is operating full load the flue gas mass flow is higher so that the decrement of temperature in the FWH is slower and the temperature requirement at the stack is respected up to considerable HP's power. However, if the GT is operating at partial load, dealing with the 60°C limit is more challenging, Figure 4.16(b) shows that all the investigated configurations do not respect the limits for thermal power output beyond 10-15 MW_{th}.

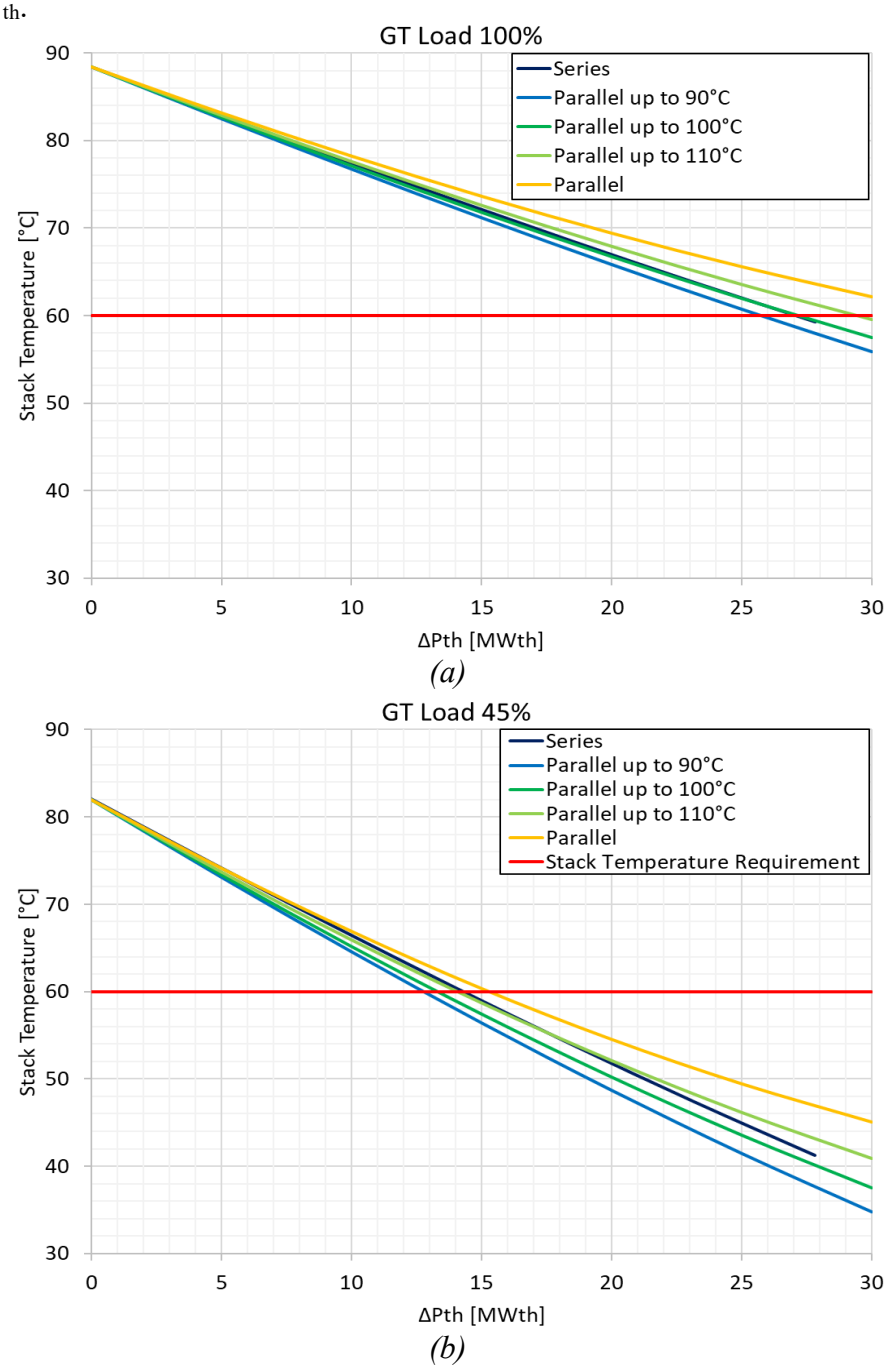

Figure 4.16: Flue gasses stack temperature vs heat pump thermal output.

Figure 4.17 reports the global efficiency increase, i.e., the difference in percentage global efficiency between the cogenerative CCGT coupled with the HP (CCGT-HP) and the standard investigated CCGT-CHP. The global efficiency increase is plotted against the increase in thermal capacity. These are the most interesting indicators since the targets of the

coupling are the increase of fuel's energetic potential and the ability in providing an extended thermal output. Figure 4.17(a) shows that the Series HP allows achieving higher global efficiency values, for the same potential recovered by the flue gas this configuration operates the HP more efficiently requiring less electric power to be driven. However, Figure 4.17(b) demonstrates as, especially at lower GT loads, the maximum achievable global efficiency increase is limited by the temperature constraint at the stack. The dotted lines in Figure 4.17 indicate the theoretical global efficiency increase if the flue gasses were cooled down below the 60°C limit.

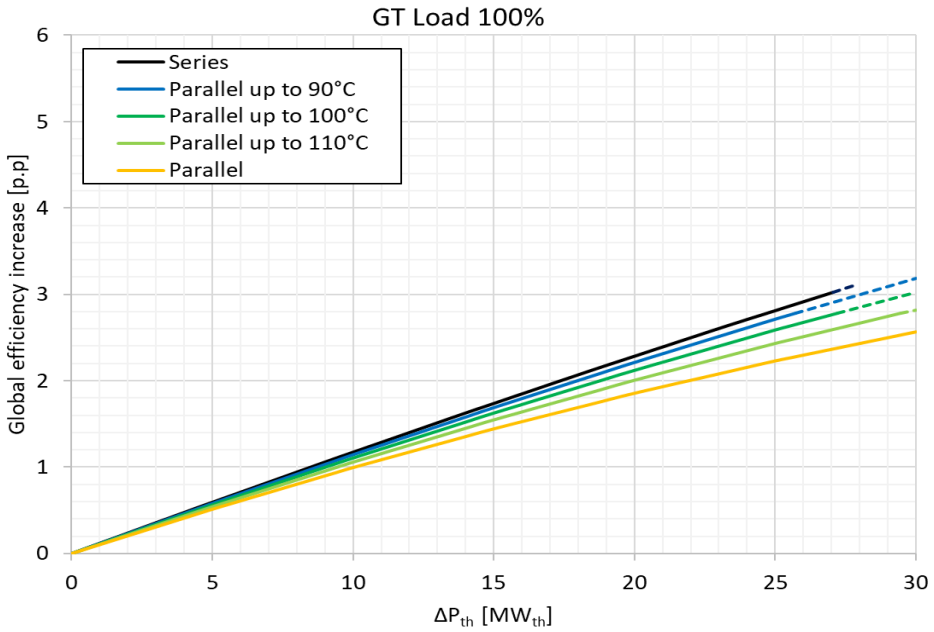

(a)

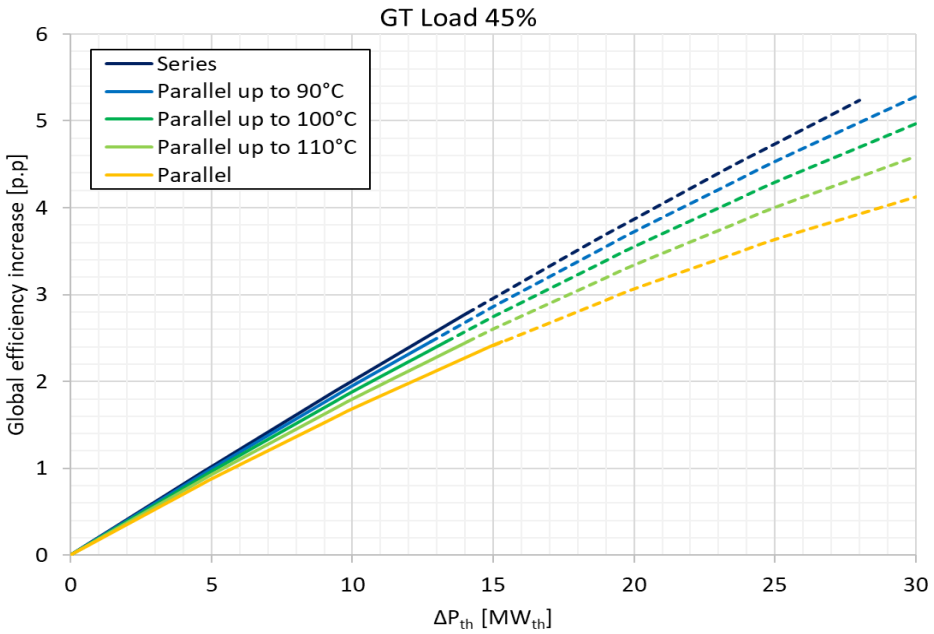

(b)

Figure 4.17: Coupled CCGT-HP global efficiency increase vs heat pump thermal output.

It might be observed that the Parallel HP allows increasing further the thermal power output, but this increase is only due to the higher electric power required by the HP. It is possible to conclude that the Series HP is the most efficient solution. However, it could perform so well from a techno-economic perspective. If the Parallel and the Hybrid solutions determine an increase of the overall thermal capacity equal to the HP size, this is not true for the Series HP, since it was highlighted as the preheating of the DHN-HX cold side causes a decrease of the exploitable heat from the LP ST and the FWH. For instance, a 30 MW Series HP corresponds to an overall thermal capacity increase of 27.8 and 28.0 MW, at 100% and 45% GT load respectively. This implies that a Series HP needs to be sized 7-8% bigger than another configuration to provide the same operative range increase.

From this perspective, Hybrid solutions are an interesting option up to a low intermediate temperature since they allow an adequate HP efficiency, thanks to the reduced temperature lift, and avoid the HP oversizing keeping a 1:1 ratio between the HP size and the increased thermal output. On the other hand, hybrid solutions require a more complex retrofitting since they require splitting the DHN-HX into low-temperature and high-temperature sections.

4.2.2. Flue Gas Condensation as Heat Pump's Heat Source

The aim of this subsection is to study the integration of flue gas condensing heat pumps with a CCGT power plant. The layout of CCGTs is well defined by the market and, usually, no room is left for a scrubber or similar equipment between the Heat Recovery Steam Generator (HRSG) and the stack. This paper introduces the condensing section within the Heat Recovery Steam Generator's tail, maintaining the overall shape and configuration of a standard CCGT, adopting an indirect not regenerative heat exchanger. Two strategies of integration of the heat pump with the existing DHN Heat Exchanger (DHN-HX) are presented and compared: a series and a parallel layout. Finally, a parametric cost analysis is performed in order to evaluate the viability of the investment compared to a traditional solution coupling the CHP plant to a Heat Only Boiler, HOB, taking into account the effect of electricity market price, the cost of CO_2, and the installation cost of an HP

4.2.2.1. Reference system description

The proposed flue gas condensing heat pump was designed to be coupled with a three-pressure level reheat CCGT power plant driven by a series F-class turbine, schematized in Figure 4.18. The sequence of heat exchangers within the Heat Recovery Steam Generators and their connection with the steam turbine are presented in [140]. HRSG includes high pressure, reheater, intermediate pressure, and low-pressure sections as in a state-of-the-art combined cycle. The last heat exchange section, the Feed Water Heater (FWH) in which the mass flow rate of all the three-pressure levels is preheated is highlighted in the figure between the A-A, and B-B red dashed lines since will be subject to the modification proposed. The standard plant, here presented, operates in CHP mode feeding a second-generation DHN with a forward temperature of 120°C and a return temperature of 70°C. The heat generation is guaranteed by the steam, extracted upstream from the low-pressure turbine, which is redirected to the District Heating Network heat exchanger (DHN-HX) delivering the heat to the thermal users. The combined cycle was previously modeled using Gate Cycle and presented alongside the results in [128]. The model requires ambient conditions, GT load and the DHN required thermal output as inputs to return all the thermodynamic properties at each component's control volume boundaries.

The CCGT standard layout was modeled within Gate Cycle as a state-of-the-art three-pressure level reheat Combined Cycle adopting the F-Class gas turbine model and a water-cooled condenser, as reported in Figure 4.18(a). The CCGT has a capacity of 400 MW. The Gas Turbine, Steam turbine, and the 14 heat exchangers of the Heat Recovery Steam Generator (HRSG) were modeled using inbuilt Gate Cycle components and introducing operative constraints. Water sprays between high pressure and reheat superheaters were used in the hotter part of the HRSG to not exceed the pipes' maximum temperature constraints, 540°C, maintaining appropriate live steam temperatures at GT part load.

The cogenerative function is performed by extracting the steam before the low-pressure turbine at a pressure of 3.75 bar in max cogeneration condition, blue line, in Figure 4.18(b). This condition is limited by the steam turbine ventilation losses, so a minimum mass flow rate of ca 6.5 kg/s must be expanded through the rotating machine. The extracted steam condenses within the DHN Heat Exchanger (DHN-HX) heating up from 70°C to 120°C the DHN mass flow rate, which is controlled in order to meet the thermal demand. The liquid from the DHN-HX is then mixed with the condensate from the steam turbine condenser, feeding the HRSG. the steam turbine condenser cooling water is fed at 12°C.

The GT load is varied between 45% and 100% and the thermal output was progressively increased from the full condensing mode to the full cogenerative mode (i.e., shifting from left to right in Figure 4.18(b). The 45% load condition represents the Minimum Environmental Load, MEL, which is constrained in reality by CO-specific emission (and then air to fuel ratio upper threshold). In this condition, with fully close IGV a further decrease in fuel will have a negative impact on the CO emissions. The 100% GT load, with fully open IGV, represents the condition at maximum power, which is limited by the maximum acceptable TIT.

Figure 4.18(b) summarizes the behavior of the reference power plant reporting the trends of both electrical and global efficiency, characterized by 42 complete calculations. The simulations cover the operating range of the thermal load up to the maximum steam extraction level at different relative Gas Turbine percentage loads (100%, 75%, 60%, 45%) at ambient ISO conditions (15°C, 101325 Pa, 60% Relative Humidity).

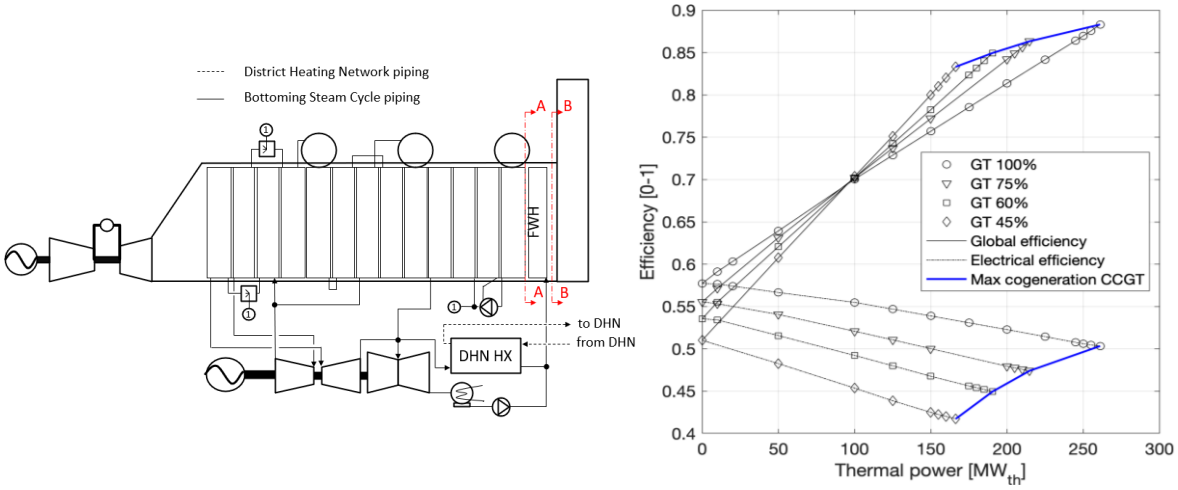

(a) *(b)*

Figure 4.18: Combined Heat and Power three pressure level Combined Cycle: (a) Reference power plant scheme, (b) Performance: global and electrical efficiency trends vs generated thermal power [128].

The standard CHP 400 MW CCGT performance is depicted in Figure 4.18(b) as a function of the thermal power provided to the DHN. The electrical and global efficiency is calculated as in Equations (4.23) and (4.24):

$$\eta_{el} = \frac{P_{el}}{L\dot{H}V} \tag{4.23}$$

$$\eta_{gl} = \frac{P_{el} + P_{th}}{L\dot{H}V} \tag{4.24}$$

Where P_{th} and P_{el} are the electrical and the thermal net power output of the plant, $L\dot{H}V$ is the primary energy consumption, evaluated over the lower heating value of natural gas.

The CCGT global efficiency (solid line in Figure 4.18) grows with the increase of heat production up to a maximum of 88.3% at 261 MW_{th} for the 100% GT load (flue gas temperature 86.4°C), while the electrical efficiency

4.2.2.2. Integration of the flue gas condensing heat pump

4.2.2.2.1. Integrated system layout description

To integrate the heat pump and enhance the plant performance the last part of the Heat Recovery Steam Generator between the Feed Water Heater and the stack, was re-designed, as shown in Figure 4.19. The Feed Water Heater (FWH) highlighted in the standard CCGT layout of Figure 4.18(a) by the red lines (A-A, B-B), is here divided into a high temperature (HT) and a low-temperature section, LT. As in a standard layout, the two sections of the FWH warm up the condensate entering the bottoming cycle (ca 98 kg/s at full load), while the FHW-HT is also directly fed by the DHN water, the purpose of the low-temperature section is to heat the condensate to the temperature of the DHN water entering high-temperature section, to operate here in parallel but on comparable thermal levels.

The new design must comply with the constraint of maintaining a stack temperature that guarantees pollutant dispersion. At the same time to recover the latent heat, the flue gases must be cooled below the dew point (50-55°C depending on the chemical composition). The heat pump evaporator, the flue gas condenser in Figure 4.19, is located then on the FG path to recover sensible and latent heat. The henceforth defined HP is s set of 5 Heat Pumps working in parallel (equally sharing the load between the activated machines) to mitigate the off-design effects. The HP can be coupled in series or parallel (scheme in Figure 4.19(a) and Figure 4.19(b) respectively) to the District Heating Network Heat Exchanger (DHN-HX) and the Feed Water Heater (FWH). Both configurations were studied, and the results are presented in the following section. On the environmental side, to guarantee flue gas buoyancy, and so pollutant dispersion, a minimum temperature of 60°C is required at the stack, thus flue gas needs to be reheated after the latent heat exploitation. To avoid a huge gas-gas regenerative heat exchanger surface, implying high costs and a change in the HRSG layout, the final reheat is performed with an indirect heat exchange by the water returning the DHN at 70°C. The behavior of this flue gas Reheater is driven by the flue gas (FG) temperature: if the FG temperature at the flue gas reheater inlet is below 60 °C, reheat is performed in order to satisfy the temperature requirement at the stack. Otherwise, if the FG temperature is higher than 75 °C the heat exchange takes place reversely (from the flue gas to the DHN water), in order to exploit the residual heat potential, finally, if the temperature value is between 60 °C and 75°C, no heat exchange happens and the DHN water bypasses the flue gas reheater.

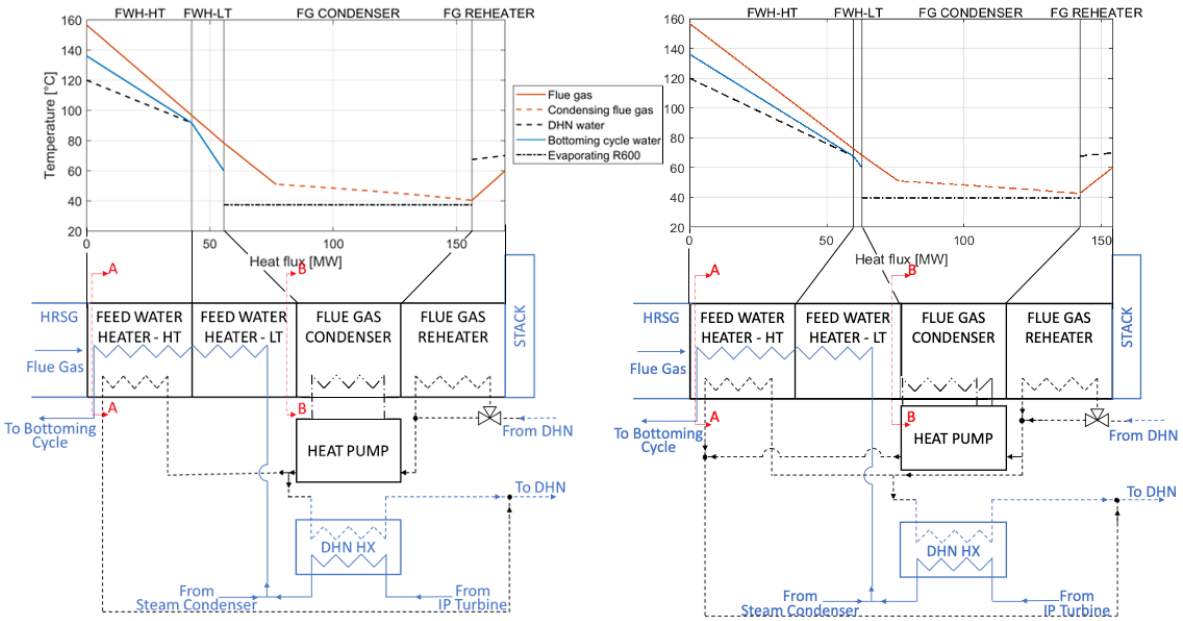

Figure 4.19: Proposed layouts integrating the CCGT and the heat pump: Temperature-heat load diagram and layouts a) series layout and b) parallel layout. In blue are reported the piping and the components existing in the reference power plant, while in black are the ones added by the relative proposed solution. The bottoming cycle piping is reported with continuous lines, while District Heating Network water piping with dashed lines.

4.2.2.2.2. Flue gas condensation corrosion avoidance

Even though condensation of flue gas from natural gas combustion doesn't imply as severe corrosion issues as for coal or heavy fuel oil, due to the significantly less sulfur dioxide content in the chemical composition of flue gas [210], it Is not possible to ignore its corrosive potential. The flue gas condenser heat exchanger has to be built with corrosion-resistant materials: austenitic steel with high Cr, Mo, and N contents [212], coating the outer surface with special materials such as polypropylene [213], polyurethane, or other organic coatings [214]. Otherwise, also titanium is used for flue gas condensers operating in a very corrosive environment [215]. A different design strategy is instead adopted for the heat exchanger in which the DHN water is introduced within the HRSG, dashed lines in Figure 4.19: using standard boiler steel and avoiding condensation. The corrosion, caused by water vapor and sulfuric acid in the exhaust gas, occurs whenever the flue gas is cooled below the acid dew point of these vapors. Since the surface temperature of the tubes is approximately the same as the water within them, the minimum water temperature within the HRSG plays a major role in condensation phenomena. The water dew point in a no-sulfur fuel is generally between 40°C and 45°C [216], so 55°C is adopted as a water temperature threshold to avoid condensation. As a comparison, based on the flue gas composition calculated through Gate Cycle, condensation of water occurs at 51.01°C at full GT load and 48.82°C running at the minimum load confirming the general assumption.

Thus, the temperature of the DHN water within the HRSG must be high enough (i.e., >55 °C) to avoid condensation in this component and related corrosion issues, allowing the use of ordinary heat exchanger materials and limiting capital expenditure. While the flue gas condensation is concentrated just on the HP heat exchanger, adopting corrosion-resistant materials [17].

4.2.2.2.3. Mathematical model

A mathematical model was developed in MATLAB in order to assess the performance of the two proposed layouts under different operating conditions. The psychometrics of flue gas and the condensation process are modeled based on equations reported in the ASHRAE handbook [217] and computing the value of dry gasses' specific heat from their chemical composition. Although the flue gas condenser model is a 0D model, Figure 4.19 reports the actual temperature-load curve highlighting the division between a sensible heat exploitation stage and a condensing stage (with a slighter slope) where sensible and latent heat are exploited simultaneously.

The modelized heat pump, which architecture is such as modelized in Chapter 3, Subsection 3.2, is a standard vapor compression heat pump with regeneration between the subcooler and evaporator outlets, to cope with the requested high temperature the selected working fluid is butane (R600), the pressure levels at the evaporator and condenser is set to maximize the COP while respecting the constrains resumed in Table 4.7. The Thermodynamics properties of butane were modelized according to the CoolProp database [175]. While the butane mass flow rate comes from the required HP capacity and the enthalpy differences. The HP model was validated against data provided by the HP manufacturer within the European project PUMPHEAT [9]. Figure 4.20 reports the temperature-load diagram, for the considered case study, within each heat pump component. It can be appreciated how the temperature lift in the heat pump is significantly lower when it is coupled in series with positive effects on the performance.

Table 4.7: Heat pump model assumption.

Property	**Symbol**	**Value**
Refrigerant Fluid	Butane	R600
Compressor Efficiency	η_{comp}	0.64
Super Heat Temp. Increase	ΔT_{SH}	25 K
Evaporator pinch point temp. difference	ΔT_{EVA}	3 K
Condenser pinch point temp. difference	ΔT_{COND}	4 K
Regenerator pinch point temp. difference	ΔT_{REG}	3 K

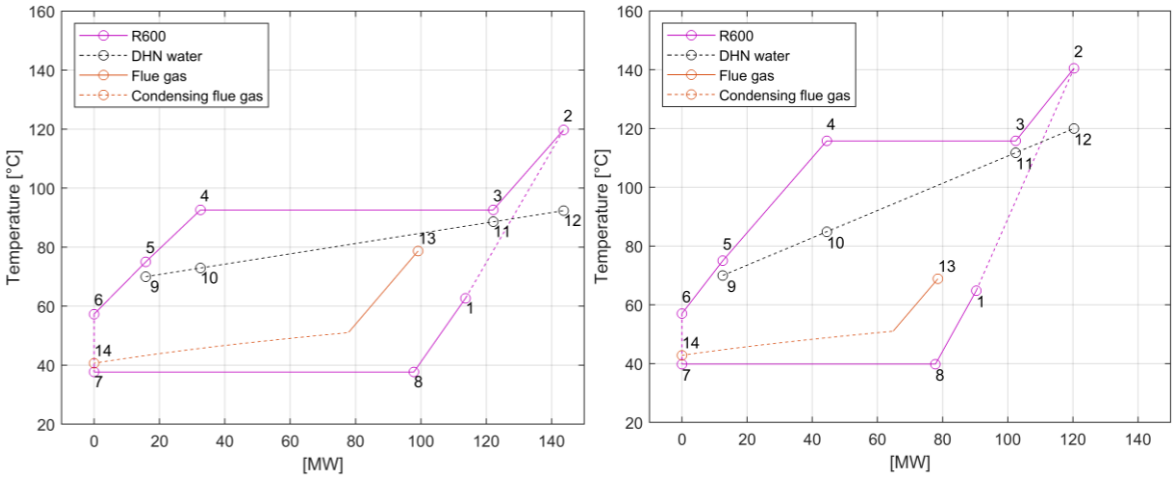

Figure 4.20: Temperature-load diagram for the heat pump working in series-coupled (a) and parallel-coupled (b) to the combined cycle. The R600 line is dotted when it describes a non-reversible process.

The results from the Gate Cycle model were used as boundary conditions for the new layout models. The energy and mass balances of each component were solved by a nested iterative logic. Pressure drops in the heat exchangers have been neglected.

For the Series case, the inner cycle iterates firstly on the temperature of water at the heat pump outlet that enters the Feed Water Heating High Temperature (FWH-HT) and the DHN-HX. This value is used to calculate the heat pump's COP and so the heat transferred from the condensing flue gas to the water exiting the flue gas reheater. A second level of iteration is performed on the total DHN mass flow, thus on the overall thermal production. The new value for this iteration is computed by summing the amount of mass flow which can be heated up to 120°C from the FWH-HT and the DHN-HX respectively. Finally, the last iteration level is on the temperature entering the Feed Water Heating low temperature (FWH-LT) as a result of the mixing process of steam coming from the DHN-HX and the main condenser of the CCGT bottoming cycle.

In the Parallel case, one less level of iteration is required. Because the HP hot side, the DHN-HX, and the FWH-HT are all fed by the flue gas reheater and have the outlet temperature fixed at 120°C. Thus, from the imposed HP capacity the temperatures at the flue gas reheater's inlet and outlet follow. The temperature of water at the flue gas condenser outlet determines the amount of water that can be heated up by each heat exchanger. But this value also affects directly the HP temperature lift, so the COP. A change in the COP implies different boundary conditions on the flue gas reheater, a first iteration step is then performed until the overall DHN water mass flow reaches convergence. Secondary, as well as in the Series case, the last iteration is on the FWH-LT inlet temperature. More detail about the heat pump model can be found in Subsection 3.2.

4.2.2.3. Thermodynamic performance of the integrated system

The Iron diagram (i.e., the CHP operating range represented on an electrical power vs thermal power graph) can be used also to represent the heat pump behavior: Figure 4.21 presents the result for the series HP activated once the CCGT maximum steam extraction limit is reached. Extracting steam upstream from the low-pressure turbine causes similar effects to switch on the heat pump: a thermal output increment is pursued by decreasing the electrical output. The inherent efficiency of the heat production at the expense of electricity production is the derivative of the ISO GT load lines presented in Figure 4.21. In general, it is possible to observe that achieving the same thermal output by extracting steam, rather than by means of the heat pump, allows maintaining a higher electrical production, thus higher global efficiency. Within the CCGT operating range, the heat pump performs better than the simple CHP just for high GT load and for relevant thermal demand (higher than 120 MW_{th}), not highlighted in the graph. The maximum advantage of 0.12 percentage points in global efficiency occurs (just for a serially coupled heat pump) for 2 MW_{el} of heat pump power, 245 MW_{th} thermal load, and 100% GT load. However, this benefit is too small to justify such a complication in the integrated operational strategy. The main potential of coupling the HP is due to the extension of the operative range to higher thermal power, increasing the flexibility of the plant. Practically, the best way to operate the plant is to run the HP only when the maximum flow of steam is extracted, increasing progressively the electric power to the HP compressor to deal with the thermal demand. Figure 4.21 reports the Iron diagram for the serially CCGT-HP coupled plant operating according to the logic described above; the difference to the parallel case is too small to be appreciated in this figure and will be highlighted in the next subsection.

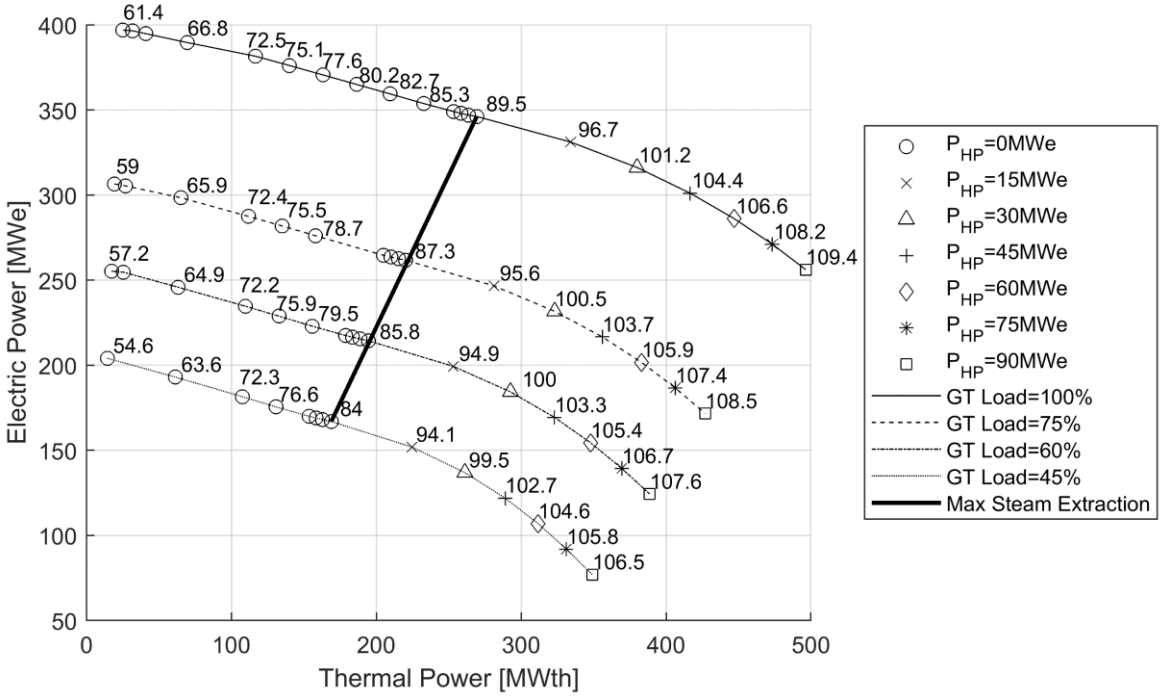

Figure 4.21: Series CCGT-HP Iron Diagram. Global efficiency is reported in labels.

4.2.2.3.1. Series and Parallel comparison

In order to assess the opportunity to couple the heat pump in series, rather than in parallel, a further analysis was performed. Firstly, it was evaluated how much of the exploitable latent heat in the flue gasses are used in each layout as a function of the HP electrical consumption, Figure 4.22(a). In general, higher COP is obtained with the HP-Series layout due to the lower temperature lift between the evaporator and condenser. So, by supplying the same electrical power to the HP compressor, the HP-Series configuration can transfer more energy from the flue gas side to the DHN. Due to that, at HP-Evaporator the temperature is lower than in the HP Parallel configuration. Consequently, the flue gasses are cooled to a lower temperature, and more latent heat is exploited. This can be appreciated by looking at Figure 4.22(a) in which both the fraction of sensible heat on the overall recovered heat and the condensed H_2O fraction are reported. As a matter of example, a 100 MW_{el} HP could exploit up to 87% of the latent heat with the series layout and 83% with the parallel layout. In this situation the latent heat recovered contributes to about 25% of the overall thermal energy provided to the DHN. Furthermore, the trends of CCGT global efficiency and the heat pump COP were investigated in both the two layout options considered. Increasing the HP electric power, by steps of 5 MW_{el}, the overall thermal production grows, as reported on the x-axis of Figure 4.22(b). In the HP-Series configuration the global efficiency increases and remains higher than the layout HP-Parallel due to the higher COP. (whose values are reported in labels in Figure 4.22(b)). The reduction of COP with the HP power is faster for the series layout configuration with respect to the parallel one since the increase in the generated thermal load is reflected in both an increase of the condenser temperature and a decrease of evaporator temperature and thus a higher increase of the overall temperature lift through the HP with respect to the parallel configuration where the 120 °C output temperature is maintained constant.

Thus, looking both at COP and at global efficiency, the series configuration performs better up to very high heat pump power (80 MW_{el} at 100% GT load). However, the break-even point in global efficiency presented in Figure 4.22(b) is not justified just by the change of COP value, which remains always higher for the series configuration, but is related also to the heat recovered by the DHN-HX.

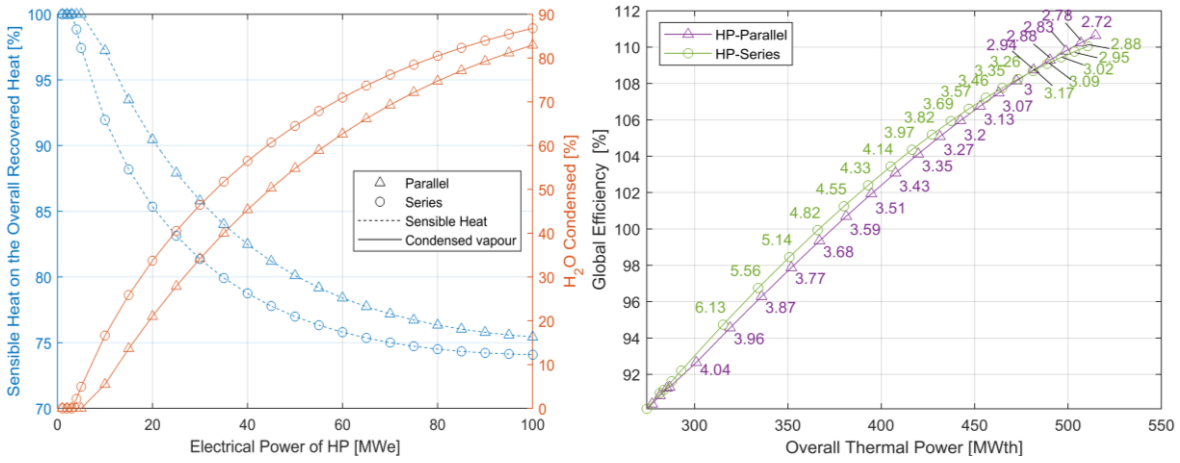

(a) *(b)*

Figure 4.22: Series and Parallel configuration comparison on the latent heat recovering process (a) and the CCGT global efficiency and HP COP (b). Data in the charts are related to the maximum steam extraction condition at full GT load.

For large HP sizes, due to the amount of heat delivered by the heat pump, the temperature at the HP-series outlet, which corresponds to the HT-FWH and DHN-HX inlets, is too high to allow complete exploitation of the heat coming from the steam extraction. Figure 4.23 shows how the DHN-HX performances are affected by the layout and the heat pump power at different GT loads. The fraction reported on the y-axis is the ratio of the heat exchanged in this component to the heat theoretically exchangeable if the DHN-HX cold inlet was maintained at the DHN return temperature of 70°C. When the HP is turned off there is no difference between the HP-Series and the HP-Parallel layout, the fraction of exploited heat is slightly lower than 1 due to heat recovery in the Flue Gas Reheater, as the DHN water enters the DHN-HX with a temperature higher than 70 °C.

In the Parallel configuration the fraction of exploitable heat is mainly affected by the flue gas reheater behavior, the more the heat pump works the more heat is needed by flue gasses to comply with the minimum temperature requirement at the stack and the cold side DHN-HX inlet temperature decreases, causing a fraction slightly higher than 1, as reported in the Figure 4.23. Nevertheless, the major impact on the trends in global efficiency shown in Figure 4.22(b) is the decrement of exploitable heat in the DHN-HX coupled in series to the heat pump: the more the heat pump pre-heats the water, the more the DHN-HX cold side inlet temperature increases, causing a decrement of the exploitable heat up to 4.5% for a 100 MW_{el} HP. This leads the HP-Parallel configuration to be more efficient at a very high heat pump power level despite the lower COP.

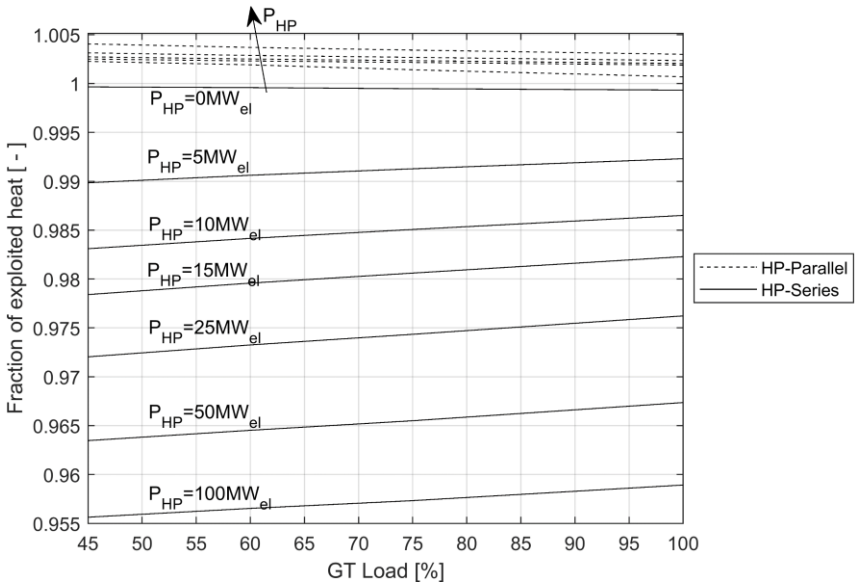

Figure 4.23 Exploitable heat in the DHN-HX.

4.2.2.3.2. Benchmarking of the Heat Pump against Heat Only Boiler integration

The HP Series layout, schematized as in Figure 4.18(a), was then selected for the economic analysis developed in the following sections. To fulfill the thermal demand, presented in the next subsection, the heat pump was sized to 30 MW_{el}, to which an increment of 110 MW_{th} in the CHP plant maximum thermal power follows. Since the heat exchanged in the reheater by the DHN return water is restored by the HP, the thermal power capacity of the HP is equal to 137 MW_{th}, with a COP of 4.55 at 100% GT load. The selected integrated solution (CCGT-HP) is compared with a conventional integration of the same CCGT power

plant with a Heat Only Boiler (CCGT-HOB), a gas-fired device coupled with the CHP plant to cover the heat peaks that exceed the CCGT maximum thermal output. The boiler was sized to provide the same thermal output increase as the heat pump, 110 MW_{th}, its energy efficiency was assumed to vary with the load, according to the Satyavada and Baldi model [186], therefore linearly decreasing from 0.875 at 5% load, the minimum value of thermal production, to 0.86 at the design point. These efficiency values consider that, since the DHN return temperature is 70°C, the condensation of the flue gas cannot be exploited in the HOB. The possible operative range of the two compared solutions is schematized by the respective Iron diagrams reported in Figure 4.24. It is important to highlight that, while in the layout with the HP (Figure 4.24(a)) the iso-GT load conditions are also iso-fuel, this is not true once the HOB is activated (Figure 4.24(b)), since additional fuel is burnt to cover the heat demand. However, activating the HOB the global efficiency of the integrated CHP plant slightly increases at low GT load, since the boiler efficiency is always higher than the efficiency of the reference CHP in full extraction conditions, and slightly decreases at high GT load, for the opposite reason. The CCGT-HOB solution increases the thermal production without a further reduction of the electrical output so is favored in a high-priced electrical market. On the other side, the CCGT-HP allows to provide the same additional heat without increasing the fuel consumption, thus is expected to save primary energy, reduce the emissions, and be beneficial in a market condition with high natural gas costs with respect to the electrical cost, as it would occur in case of high renewable or nuclear share.

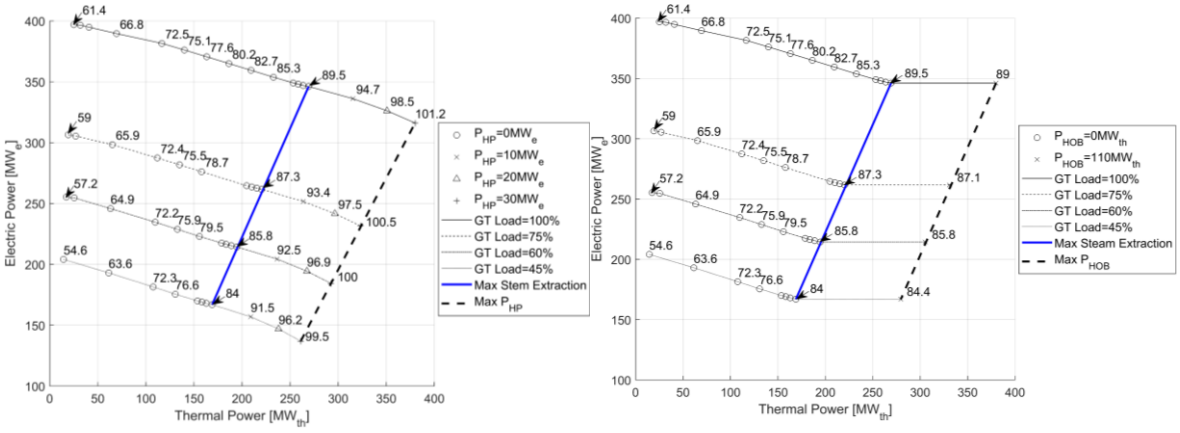

(a) *(b)*

Figure 4.24: Iron diagram of (a) CCGT-HP, (b) CCGT-HOB., the global efficiency is shown in labels.

Table 4.8 shows the extreme point of operation for CCGT, CCGT-HP, and CCGT-HOB, reporting the values of the fuel energetic potential, the thermal and electrical output, the afore defined global and electric efficiency, and the exegetic efficiency defined by equation (4.25) that weights the heat produced for its ability to produce work through a reversible thermodynamic Carnot cycle.

$$\eta_{ex} = \frac{P_{el} + P_{th}\left(1 - \frac{288.15}{120 + 273.15}\right)}{\dot{LHV}} \tag{4.25}$$

Looking at Figure 4.24(a) it could be appreciated that the maximum HP consumption and maximum steam extraction lines are slightly diverging. The additional thermal power provided by the HOB is independent of the CCGT operational parameter. On the other hand,

being the HP thermal source internal to the CCGT a GT off-design influences also the HP operations. At full GT load, the FG mass flow is 666 kg/s, and running the HP at 30 MW_{el}, the temperature at the FG condenser exit is 40.0 °C; at 45% GT load the FG mass flow is 444 kg/s and, keeping constant the HP power, FGs are cooled further, until 32.0 °C. This temperature change at the evaporator is reflected in a COP variation from 4.55, at 100% GT load, to 3.79 at 45% GT load with a decrement in the additional thermal power at the extreme operational point.

Table 4.8: Extreme points of operation for CCGT, CCGT-HP, and CCGT-HOB.

GT load		CCGT	CCGT-HP	CCGT-HOB
100%	**LḢV**	687.63 MW	687.63 MW	816.31 MW
	P_{th}	269.33 MW_{th}	380.00 MW_{th}	380.00 MW_{th}
	P_{el}	346.16 MW_{el}	316.16 MW_{el}	346.16 MW_{el}
	η_{gl}	89.51%	101.24%	88.96%
	η_{el}	50.34%	45.98%	42.41%
	η_{ex}	60.08%	60.73%	54.83%
45%	**LḢV**	400.02 MW	400.02 MW	528.70 MW
	P_{th}	168.96 MW_{th}	261.09 MW_{th}	279.63 MW_{th}
	P_{el}	166.94 MW_{el}	136.94 MW_{el}	166.94 MW_{el}
	η_{gl}	83.97%	99.50%	84.47%
	η_{el}	41.73%	34.23%	31.58%
	η_{ex}	53.01%	51.66%	45.70%

4.2.2.4. Economic Model

In this subsection, the boundary conditions of the economic analysis problem are presented, and each subsection exposes the assumptions made related to the capital expenditure (CAPEX) and Operating and Maintenance (O&M) costs, the electricity price model, and the thermal demand model.

4.2.2.4.1. Capital Expenditures and Operating and Maintenance costs

The data reported by the *Technology Data Catalogue* of the Danish Energy Agency were used as a reference to assess the economic investment and operating costs [183]. For the CAPEX prediction, the projected value for 2020 was used. Then, considering a plant lifetime of twenty years, the expected average O&M costs were guessed according to the projections for 2030, as reported in Table 4.9.

Table 4.9: Resume of technology costs [183].

	CCGT	HP	HOB
CAPEX	0.88 M€/MW_{el}	0.66 M€/MW_{th}	0.06 M€/MW_{th}
O&M fixed	27800 €/MW_{el}/yr	2000 €/MW_{th}/yr	1900 €/MW_{th}/yr
O&M variable	4.2 €/MWh_{el}	1.7 €/MWh_{th}	1.0 €/MWh_{th}
Size	400 MW_{el}	137 MW_{th}	110 MW_{th}

With respect to standard CCGT, the new layout CAPEX evaluation must take into account the introduction of two additional heat exchangers, where DHN water exchanges heat directly with the HRSG flue gases, Black dashed lines in Figure 4.19, while the HP evaporator costs are included in the HP CAPEX cost. Those heat exchangers can be made with standard steel for boilers for temperatures below 200°C, usually the SA210 A1. On the other side, since the water temperature within the heat exchanger is always higher than 55°C, dew point condition on the pipe surface is avoided and corrosion issues can be neglected. The increase in CAPEX due to the additional exchange surface was evaluated taking into account the impact of HRSG cost over the breakdown of the capital requirement for CCGT equal to 10% [216] and the relative exchange surface increase with the thermal power exchanged as in the subsequent formula:

$$CAPEX'_{CCGT} = CAPEX_{CCGT}[(1 - CAPEX\%_{HRSG}) + CAPEX\%_{HRSG} * Q'_{HRSG}/Q_{HRSG}] \quad (4.26)$$

Where $CAPEX\%_{HRSG}$, is the percentage impact of the HRSG cost over the CCGT, and Q_{HRSG} represent the absolute value of the maximum heat transferred through the HRSG bundles. 34.96 MW in the standard CCGT and 398.04 MW in the proposed layout, excluding the HP condenser.

With respect to the reference HP CAPEX, based on a 4 MW_{th} /1 MW_{el} heat pump, for a large-scale heat pump system of 30 MW_{el} and 137 MW_{th} as the one considered for this study, it is reasonable to expect a reduction of the capital expenditure due to scale effect. Considering the cost function provided by [218] and satisfying the required capacity with a set of six 27.4 MW_{th}/5MW_{el} HPs, an average reduction of 10% of the expected specific capital expenditure was introduced in the HP CAPEX calculation. This parameter was later considered a variable in the sensitivity analysis. The resulting costs for the proposed CCGT-HP solution are 438.08 M€ of CAPEX, 11.39 M€ per year of fixed O&M, and 4.2 €/MWh_{el} for the CCGT plus 1.7 €/ MWh_{th} for the heat pump of variable O&M. While for the CCGT-HOB the CAPEX is of 358.64 M€, 11.33 M€ per year of fixed O&M and 4.2 €/MWh_{el} for the CCGT plus 1.0 €/MWh_{th} for the HOB of variable O&M.

4.2.2.4.2. Electricity price model

The CHP power plant operates to satisfy firstly the thermal demand, then to optimize the electrical output to maximize the profits by varying the GT load and HP power. In high electricity price conditions, it results to be convenient to run the power plant at full load as the income generated by the sale of electricity would compensate for the expenditures caused by the higher fuel consumption. Instead, in low-price conditions, the best strategy is to minimize the load in order to save fuel and money. For these reasons, an accurate electricity price model is the key feature of this investigation. An electrical price data-driven model was set on the winter price during plant operating, focusing on the average daily price profile. The model was trained and tested against the Italian single electricity price (PUN) data [219]. The last three winter seasons (from the 15th of October until the 14 of April), corresponding to 4368 hours, were considered, distinguishing between weekdays and holidays. For each hour the ratio between the average hourly price and the overall average price is computed. To introduce future market scenarios, those scaling factors are multiplied by the guessed average PUN to rebuild the daily profiles. The model was cross-validated: each season was alternatively used to train or test the reconstruction algorithm, the average PUN of the testing season multiplied by the dimensionless profile learned by the two training seasons and then compared to the actual profile (Figure 4.25(a), (b) and (c)). The results of the validation

process are shown in Figure 4.25, the three first charts report the comparison between the predicted prices and the actual prices for the 2016/2017, 2017/2018, and 2018/2019 winter seasons respectively. Figure 4.25(d) quantifies the percentage errors in testing, always lower than 7.3%, demonstrating the goodness of the model for the aim of the analysis.

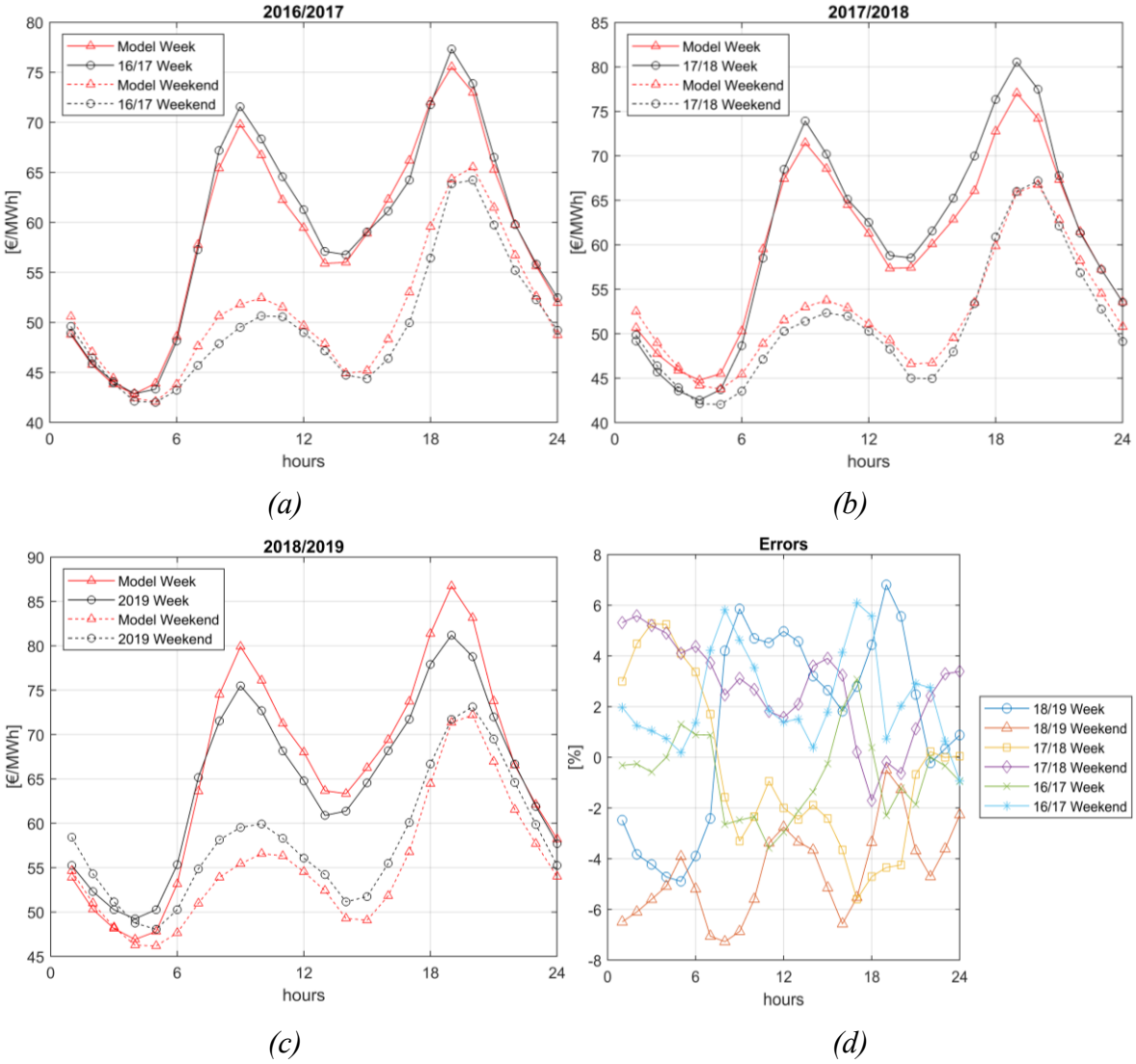

Figure 4.25: Electricity price model validation.

4.2.2.4.3. Thermal Demand Modelling

Looking at the Turin DHN statistical data, the annual thermal demand of the selected DHN was scaled to 744 GWh, consumed between the 15th of October and the 14th of April, as for the Italian decree D.P.R. n. 412 of 26/08/1993 for an E class city as Turin. Looking at the Turin daily consumption profile, it can be stated that the daily thermal demand profile is characterized by three main zones: an off-peak period between 10 p.m. and 6 a.m., a peak period between 6 a.m. and 9 a.m., and a medium load period between 9 a.m. and 10 p.m. During these hours the heat demand has a ratio of 0.33, 1.85, and 1.22 times the average demand of the day respectively. Then, according to the historical data, to model the whole season, the considered 182 days were ideally divided into warm, standard, and cold days. The number of both warm and cold days is assumed to be 30 per season. A comprehensive visualization of the modeled heat demand is provided in Table 4.10 and Figure 4.26.

Table 4.10: Thermal demand.

	6 a.m. – 9 a.m.	9 a.m. – 10 p.m.	10 p.m. – 6 a.m.
Warm Days	252.1 MW_{th}	165.7 MW_{th}	45.0MW_{th}
Standard Days	315.1 MW_{th}	207.2 MW_{th}	56.2 MW_{th}
Cold Days	378.1 MW_{th}	248.6 KW_{h}	67.5 MW_{th}

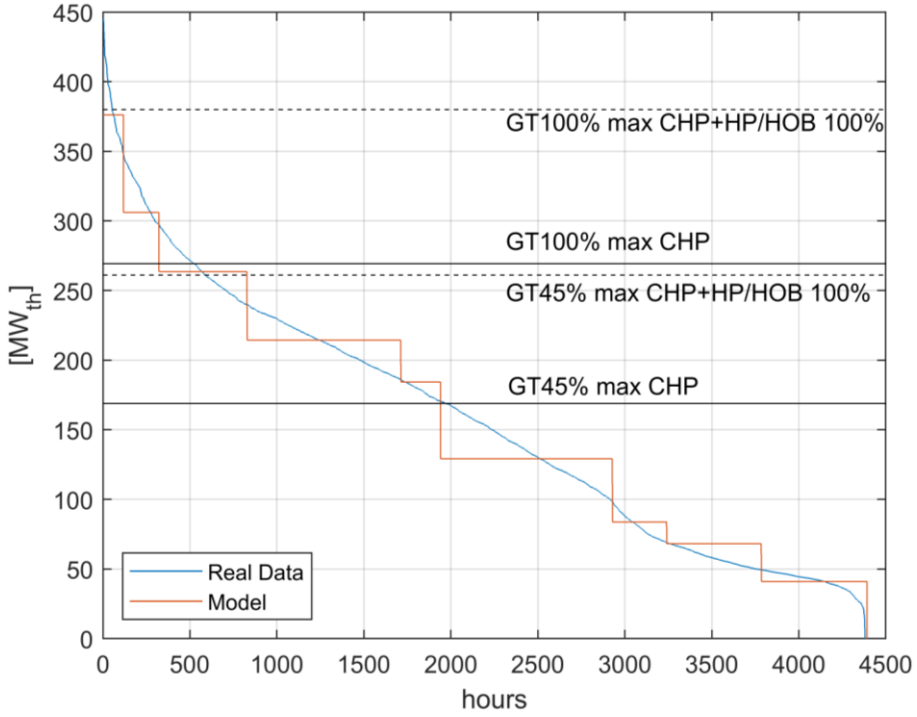

Figure 4.26: Heat demand duration curve, real and modeled.

4.2.2.4.4. Thermal Demand Modelling

To complete the analysis also some assumptions are needed on important variables related to the macroeconomic scenario that can have a strong influence on the viability of the investment. Firstly, the cost of natural gas and its relationship with the heat price. The cost of gas is one of the main components of the levelized cost of heating, together with the O&M costs and the cost of investment [220]. Assuming these two last components and the profit margin are independent of the cost of gas, is possible to state that the price of heat increase linearly according to the following equation:

$$p_{heat} = p_{heat\_ref} + \left(C_{gas} - C_{gas-2018}\right) \quad (4.27)$$

Where p_{heat} is the price at which the heat is sold, C_{gas} is the cost of natural gas, $C_{gas-2018}$ is the reference value of natural gas cost, set to 22.83 €/MWh according to the 2018 cost in Italy [221], and p_{heat_ref} is the reference value of the heat price. Since in countries where the CCGTs are a widespread technology, such as Italy and United Kingdom, the cost of distributing heat by means of DHNs is about 80-90 €/MWh [222], assuming a reasonable profit margin, the reference price of heat was set to 100 €/MWh.

Nowadays economic considerations about the viability of investment in a fossil fuel-based power plant should consider the European Emission Trading System (EU-ETS) price. The cost for each emitted ton of carbon dioxide is projected to increase almost linearly with

a rate of 1.6 €/ton per year until 2040 [223]. Thus, starting from the current value of 25 €/ton[32] [2] an average value of 40 €/ton during the plant's lifetime can be considered. The emission factor, i.e., the ratio between the amount of emitted carbon dioxide and consumed primary energy, is then selected according to Italian government data [225] and set to 55.954 ton/TJ for the natural gas.

Table 4.11: Resume of the most important economic and technical assumptions.

	Symbol	**Value**
C_{gas} reference value	$C_{gas\text{-}2018}$	22.83 €/MWh
P_{heat} reference value	P_{heat_ref}	100 €/MWh
Cost of emitted CO_2	C_{CO_2}	40 €/ton
Emission factor	e	55.934 ton/TJ
Annual heat demand		744 GWh

4.2.2.4.5. Economic analysis methodology

The combination of three climatic periods, the weekdays and holidays, and the hourly profile of the price of electricity, results in 144 standardized hours. Each of these is characterized by a thermal demand, an electricity price, and a frequency of occurrence, r, defined as the number of hours during a season on which the condition occurs. Then, according to the assumptions described in the previous section, it is possible to simulate an average season of the operating power plant. The model selects the most profitable operating condition, maximizing the incoming while varying the GT load and the HP or HOB power, calculated as in the following equation:

$$I = P_{th}p_{heat} + P_{el} \cdot PUN - \dot{LHV}\left(C_{gas} + eC_{CO_2}\right) - \left(O\&M_{CCGT\_var} \cdot P_{el_{CCGT}} + O\&M_{HP/HOB\_var} \cdot P_{th_{HP/HOB}}\right) \quad (4.28)$$

Where I is the incoming excluding the fixed O&M costs, P_{th} is the thermal output of the CHP power plant, coincident with the thermal demand, P_{el} is the electrical output, $\dot{LHV}$ is the primary energy consumption rate, e is the emission factor and C_{CO_2} is the cost of the emitted carbon dioxide. CCGT, HP, and HOB as subscripts refer respectively to the Combined Cycle Gas Turbine, the Heat Pump, and the Heat Only Boiler.

The economic analysis was performed by simulating the whole season and estimating the annual cash flow as the sum of the incomings (defined by equation (4.28)) on all the possible standardized hours and subtracting the fixed O&M costs (equations (4.29) and (4.30)).

$$CashFlow_{HP} = \sum_{i=1}^{n} I_i r_i - O\&M_{CCGT-HP_{fix}} \quad (4.29)$$

$$CashFlow_{HOB} = \sum_{i=1}^{n} I_i r_i - O\&M_{CCGT-HOB_{fix}} \quad (4.30)$$

[32] Since this study was performed, 2019 S2, the carbon price increased drastically from the 2020 S2. However both the sensitivity analysis and the uncertainty quantification reported in the following pages allow to estimate the impact of an increased carbon price.

Where n =144 is the number of standardized hours, I is the hourly incoming as shown by Equation (5), r the occurrence, and i the index of summation. The simple Pay Back Period is then calculated taking into account CAPEX and the annual cash flow:

$$PBP = \frac{CAPEX}{CashFlow} \tag{4.31}$$

Finally, the Net Present Value, NPV, was computed according to the following equation, which can give a better overview of the investment profitability over the 20 years lifetime, where the discount rate, i, was introduced and t is the year index:

$$NPV = -CAPEX + \sum_{t=1}^{20} \frac{CashFlow_t}{(1+i)^t} \tag{4.32}$$

4.2.2.5. Optimized operating conditions and economic assessment

Figure 4.27 shows how the optimal operating conditions vary with the PUN average price. Four average PUN conditions are reported both for CCGT-HP and CCGT-HOB.

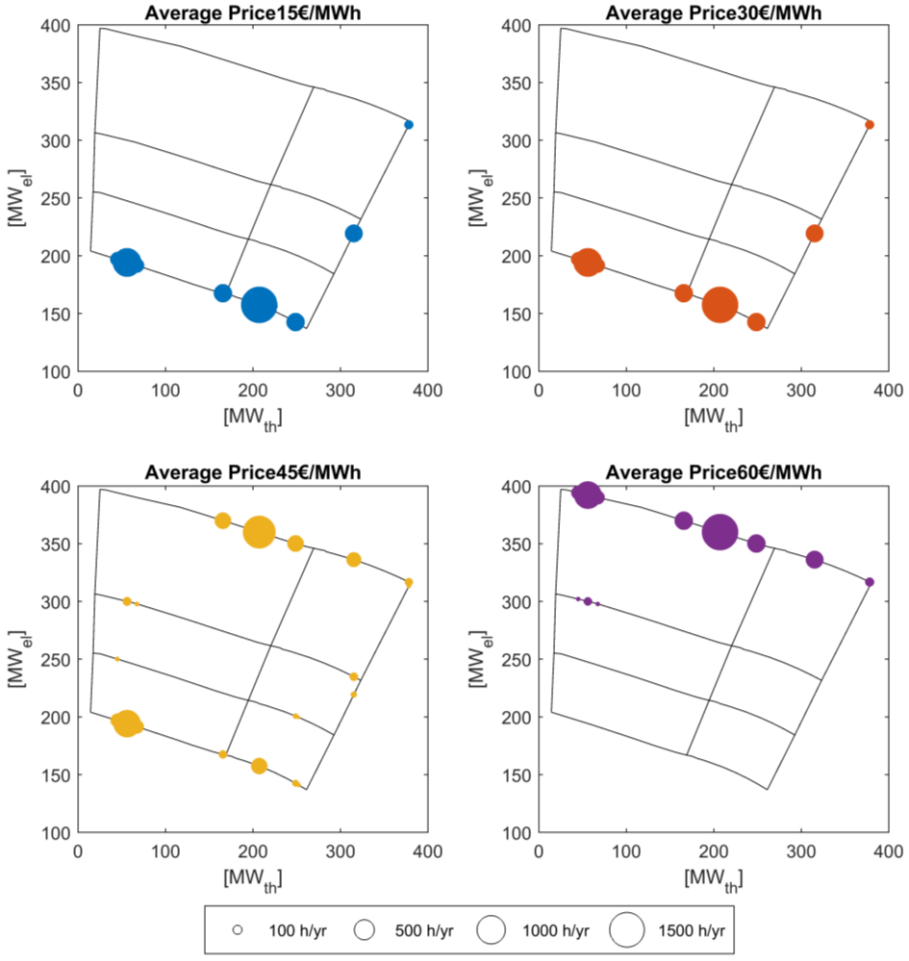

(a)

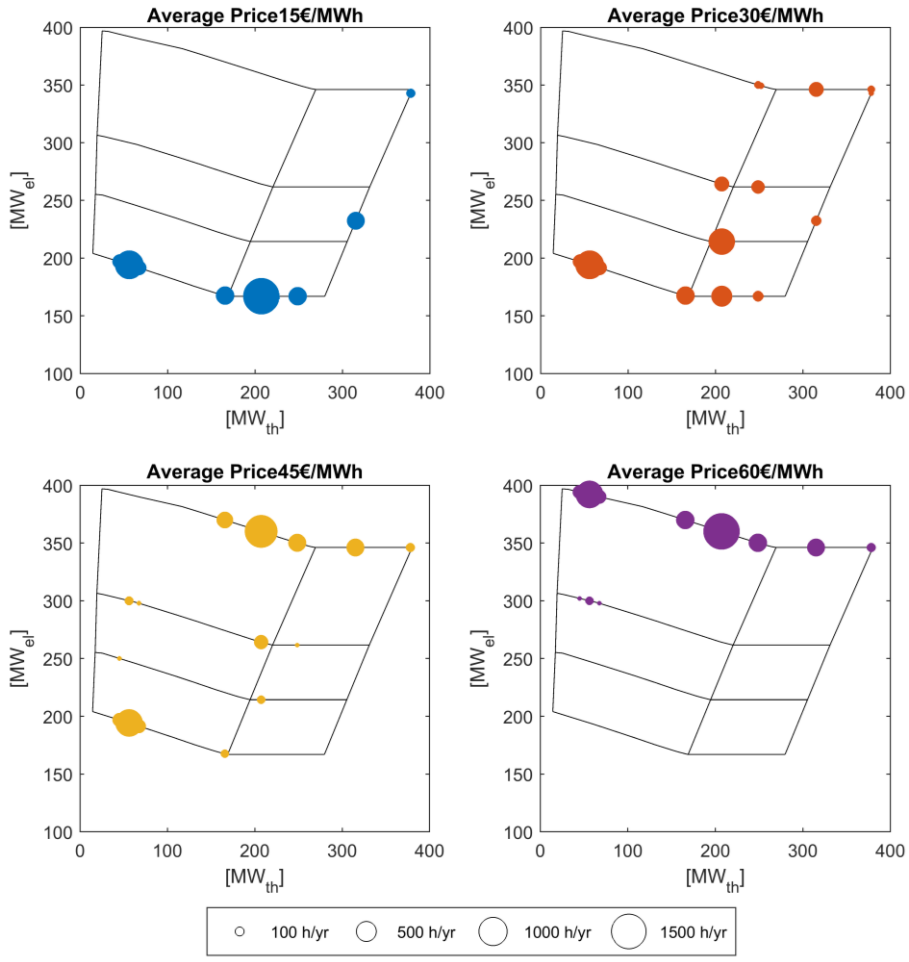

(b)

Figure 4.27: Optimal operating conditions distribution under four different PUN scenarios for CCGT-HP (a) and CCGT-HOB (b).

If the average PUN is really low the best way to operate the power plant is to minimize fuel consumption and save money by decreasing GT load. With a PUN lower than 15 €/MWh the lowest electrical production is always selected, while increasing the electrical market profitability, it is more often convenient to increase the electrical output since the well-paid sold electricity compensates for the cost of additional fuel. When the average PUN is 60 €/MWh or higher, maximizing the electrical output results to be always advantageous. Comparing the CCGT-HP and the CCGT-HOB behavior, it can be highlighted a main difference: in average PUN conditions (ca 30 €/MWh) the intermediate thermal loads between 160 MW_{th} and 250 MW_{th} are covered using the HP with the CCGT at minimum load due to the highest global efficiency, while in the CCGT-HOB the CCGT load is increased operating at partial load, and the HOB is used just to cover the peak demand.

Assuming the dependence of operating conditions on the average PUN, it is possible to analyze the effect over some thermodynamic, environmental, and economic key performance indicators. Figure 4.28 presents the average annual global efficiency (according to equation (4.33)) and the emitted carbon dioxide as a function of the average electricity price.

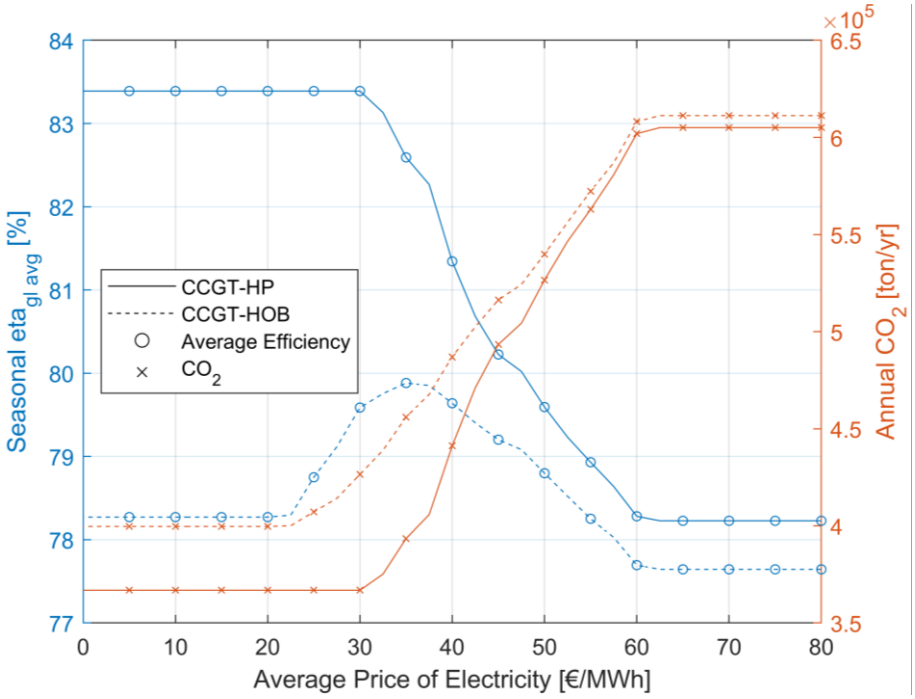

Figure 4.28: Seasonal average global efficiency and carbon dioxide emissions trends against the average price of electricity.

$$\eta_{gl\_avg} = \frac{\sum_{i=1}^{n} P_{el_i} r_i + \sum_{i=1}^{n} P_{th_i} r_i}{\sum_{i=1}^{n} L\dot{H}V_i \, r_i} \tag{4.33}$$

Adopting the CCGT-HP solution, the average global efficiency decreases when the price of electricity increases. In fact, these market conditions lead the GT to run at full load and most of the thermal demand is satisfied without integrating the flue gas condensing HP, consequently, the latent heat from flue gas is not exploited and the efficiency drops.

On the other hand, with the increase in the price of electricity in the CCGT-HOB, the average global efficiency first increases. This can be observed in Figure 4.27 when increasing the average PUN from 15 €/MWh to 30 €/MWh, changes occur in the high thermal demand conditions which are satisfied by running the gas turbine at a higher load and progressively turning the HOB off. In this case, the system operates in the region of the higher HOB efficiency, along the full extraction line. Increasing further the price of electricity up to 60 €/MWh, also the low thermal demands are satisfied at full GT load and both the corresponding electrical production and global efficiency increase (from ca 63% to ca 66%, with reference to Figure 4.24). Due to the increment in the corresponding electrical output and primary energy consumption, the annual average global efficiency is more affected by those operating conditions, and since the global efficiency is lower than the seasonal average, this parameter decreases, as shown in Figure 4.28. Over 60 €/MWh, the GT load is always at 100%, the two systems integrate just the peak energy and the difference is related only to the different global efficiency in such conditions.

Figure 4.28 also reports the annual carbon dioxide emissions: this value reflects both the variations in average global efficiency and electrical production. Increasing the PUN beyond 30 €/MWh for CCGT-HP and 20 €/MWh for CCGT-HOB, the electrical production progressively increases, as well as the carbon dioxide emissions. The CCGT-HOB emits

more carbon dioxide than the CCGT-HP since it presents always a higher electrical production and a lower global efficiency. In high electricity price scenarios, the CHP power plant can satisfy most of the thermal demand without any integration, thus the difference in emissions, as well as other parameters, between CCGT-HP and CCGT-HOB decreases significantly.

Figure 4.29 shows how the annual cash flow and the Pay Back Period vary under different average PUN scenarios. The annual cash flow is always higher in the CCGT-HP case, even if the difference between the two systems decreases for high average electricity prices. On the other hand, the PBP is strongly affected by the capital expenditures illustrated in Section 4.2.2.4.1, it decreases for both CCGT-HP and CCGT-HOB increasing the average PUN. Low PUN scenarios are favorable to the CCGT-HP, while with high electricity prices the CCGT-HOB presents a lower PBP. Anyway, the CCGT-HP manages to pay the investment cost back in a shorter period than the CCGT-HOB only with a PUN lower than 24.78 €/MWh which corresponds to a PBP higher than 19.89 years. Considering that the lifetime of a such power plant is expected to be 20 years, the CCGT-HP solution cannot be considered economically viable under these conditions.

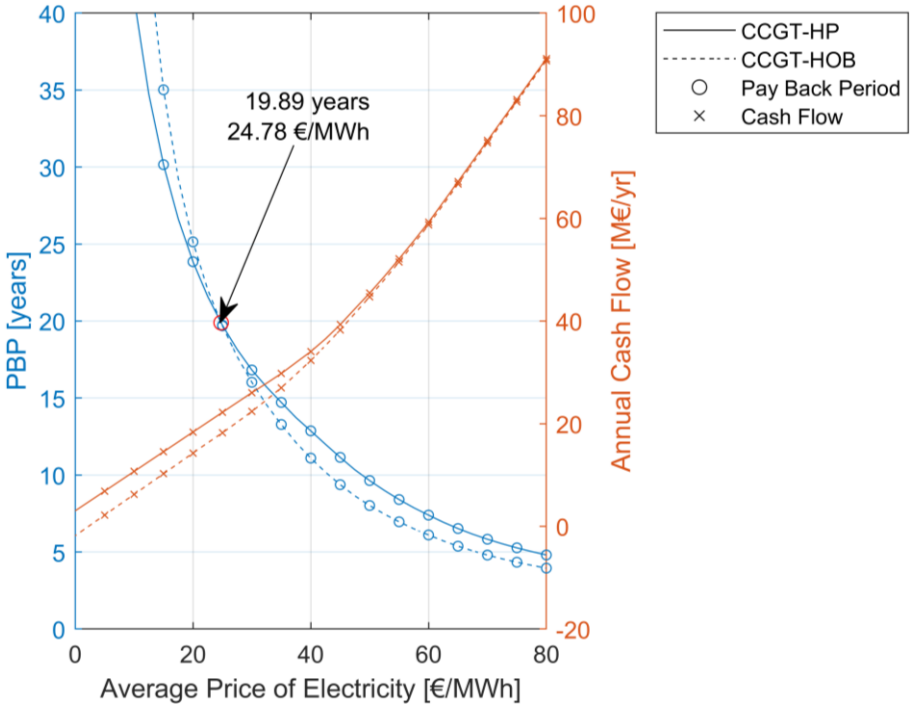

Figure 4.29: Pay Back Period and annual Cash Flow trends against the average price of electricity, is highlighted the point for which the CCGT-HP and CCGT-HOB payback periods are equal.

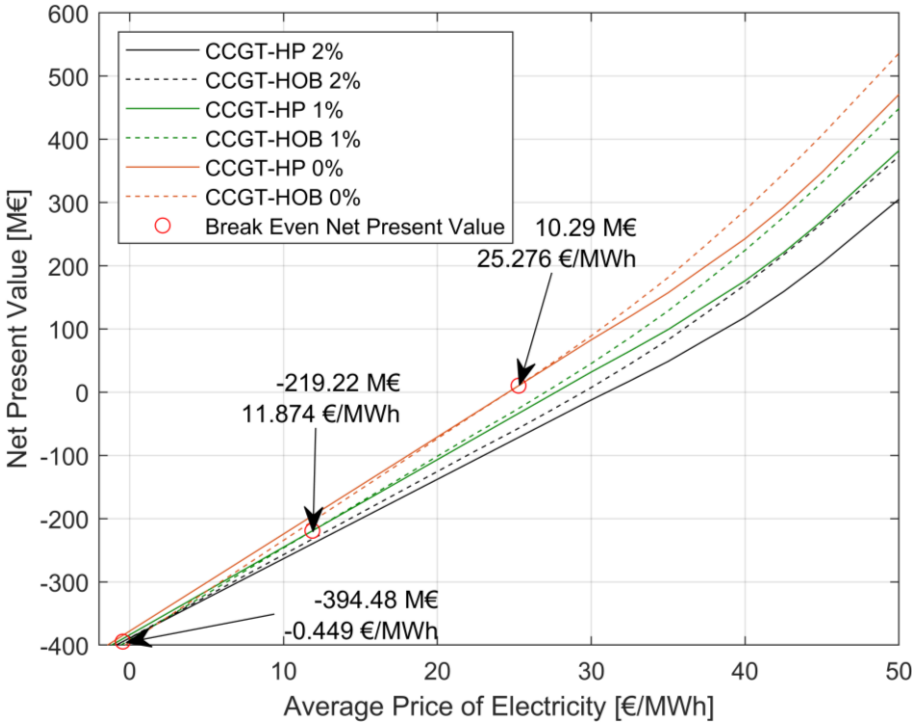

Figure 4.30: Net Present Value trends against the average price of electricity for different discount rates. Within the figure are highlighted the values of the Break Even Net Present Value [M€] and Break-Even PUN [€/MWh].

As emphasized before, in low-price conditions the CCGT-HP minimizes the electrical power production covering the thermal peak without increasing the fuel consumption. On the other hand, when both the PUN and the thermal demand are high, the lower electrical output, due to the HP consumption, reduces the related revenues when compared to the CCGT-HOB solution. Due to this reason, Figure 4.30 shows that CCGT-HP presents a higher Net Present Value (NPV) in low-PUN scenarios, while CCGT-HOB is more profitable in favorable market conditions. The red circle highlights the maximum average price of electricity for which the CCGT-HP presents a higher NPV than CCGT-HOB, determining the so-called Break-Even Net Present Value (BENPV). The BENPV point is associated with an average price of electricity, the BEPUN, On the left side of this point the NPV of CCGT-HP is higher than the CCGT-HOB, so this investment is preferred. Figure 4.30 also reports how the NPV and the BENPV are affected by the discount rate. If getting the funds for the initial investment is more expensive, it would be reasonable to assume a higher discount rate. In such conditions, the profitability decreases for both CCGT-HP and CCGT-HOB, and the BENPV shifts left, leading to a negative NPV. This means that the financial conditions can represent a no-go condition for such capital-intensive investments. Those financial effects were neglected in the subsequent parametric analysis but must be kept in consideration while planning an investment or while designing the incentives to support CAPEX-intensive low carbon footprint technologies. The main drawback of the CCGT-HP solution is the high Capital Investment cost of the HP compared to the HOB (about an order of magnitude) which highly reduces the Net Present Value. CAPEX is expected to reduce with the increase in the size of the components, so also this parameter was considered in the following analysis with CO_2 allowance cost and fuel cost.

4.2.2.6. Parametric Analysis

Following the same method presented in the previous section, a parametric analysis is carried out to assess the economic viability of the proposed solution under different economic conditions. As stated in the last subsection, the Net Present Value is evaluated for a null discount rate.

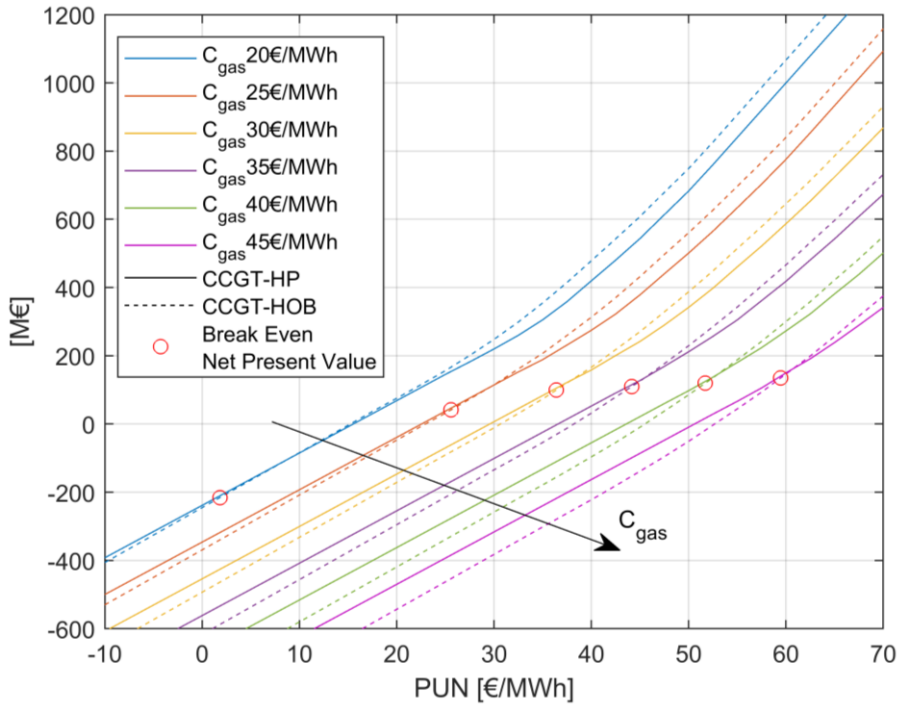

Figure 4.31: Net Present Value trends against the average price of electricity for different costs of gas. CAPEX factor 0.9.

First, Figure 4.31 reports how the NPV trend is affected by the gas cost. A higher cost of fuel brings a decrement in profitability, quantified by NPV, for both solutions (under the same electrical market condition). Nevertheless, requiring more primary energy, the CCGT-HOB is more affected, than the CCGT-HP, by the fuel cost increase; this is well-shown by the trends of Break-Even Net Present Value (BENPV) which shifts upward, and by the corresponding average price of electricity (BEPUN) increasing too. Moreover, it is possible to appreciate how in higher gas cost scenarios the CCGT-HOB NPV is more sensitive to PUN variation, so on the left side of the BENPV the two lines diverge faster. This means that in high gas cost and low electricity price scenarios the advantages of CCGT-HP could be significant.

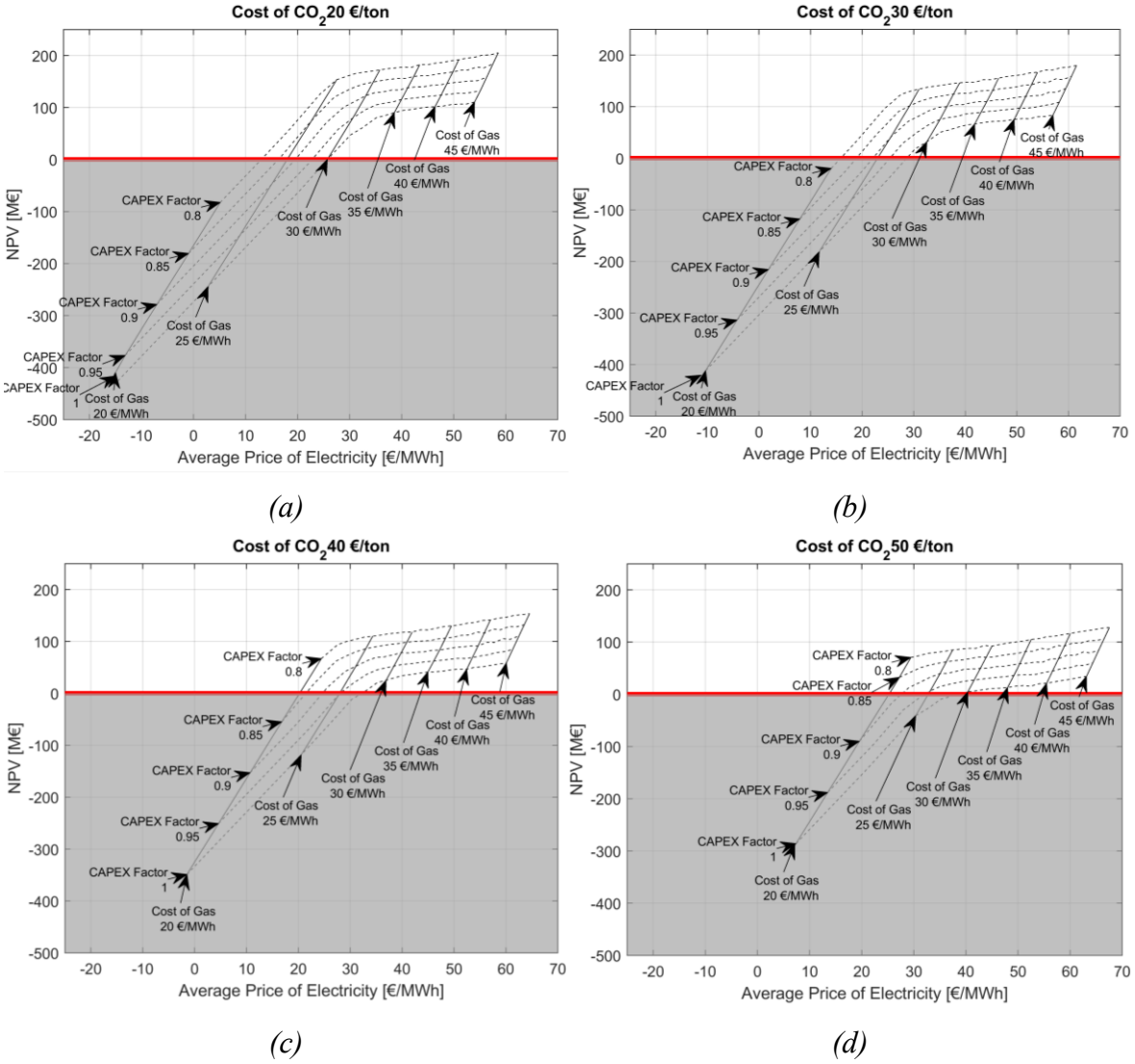

Figure 4.32: Parametric analysis of CCGT-HP and CCGT-HOB Break-Even Net Present Value as a function of the CO_2 EU-ETS price, the cost of gas, and the heat pump's Capital Expenditure.

Figure 4.32 describes how BENPV (i.e., the Net Present Value achieved when CCGT-HP and CCGT-HOB are equally profitable) as a function of the average price of electricity is affected by HP's CAPEX reduction and the variation of the cost of gas variation and of the emitted CO_2. Thus, selecting a value for three of the variables presented, the point uniquely determined on the chart, indicates the maximum average price for which the CCGT HP is favorable with respect to the CCGT-HOB, the BEPUN, and the corresponding NPV, the previously presented BENPV. Negative NPV, shaded in grey, is an index of a non-profitable investment.

Analyzing Figure 4.32, it can be observed that the cost of emitted CO_2 and the cost of fuel affect the economic outcomes in the same way, as stated by equation (4.32), directly impacting the overall cost of primary energy consumption. An increment of 10 €/ton of carbon dioxide corresponds to an increment of 2.01 €/MWh for the fuel cost. The main difference is that an increase in gas cost is reflected in the thermal customer, while an increase in CO_2 cost is paid internally by the CHP's annual income, reducing the profit

margin. An increase in the CO_2 cost reduces the NPV of both systems but increases the profitability of CCGT-HP over the CCGT-HOB so the BENPUN increases, while the corresponding NPV decreases, reducing the attractiveness of the investment.

The behavior of the presented break-even points is strongly nonlinearly dependent on the cost of fuel, as shown in Figure 4.31: on the thermal side, the increase of the gas cost is covered by the increase of the thermal consumer tariff, with no variation in the revenues on this market. On the electrical side, the gas cost directly affects the electricity production cost, and so the electrical market condition for which it is convenient to maximize the electrical output. The less the primary energy costs, the lower the cost of electricity production, which implies that the electric power generation is maximized for lower PUN conditions. Since the CCGT-HOB consumes more primary energy, it is more sensible to the variation of this parameter, so high fuel costs benefit the CCGT-HP system. Looking at the third parameter, a reduction of the HP capital expenditure only increases the NPV of the CCGT-HP solution (as for equation (4.28)). The dotted lines of Figure 4.32 are shifted upwards, increasing the corresponding NPV.

Concluding, it can be stated that the CCGT-HP solution could be economically viable in the high cost of primary energy and quite low electricity prices condition. It was observed that there is a ratio between the cost of fuel and the average PUN above which the market condition can be considered favorable to the CCGT-HP solution. Decreasing the CAPEX factor from 1 to 0.8 this ratio decreases approximately from 0.8 to 0.7. Currently, this scenario is improbable since the price of electricity is correlated to the cost of fossil fuel and in particular to natural gas. In fact, among the EU countries, the ratio between the cost of gas and the average electricity price presents typical values of 0.4±0.1 [1]. An uncorrelation between the cost of gas and electricity price could happen in an electricity system with a strong presence of renewable energy sources, where the electricity generation is mostly performed by fossil fuel free technologies. Looking at historical data, just in France, in past years a ratio of 0.6 was registered, due to the high nuclear generation in the country's production mix.

4.2.2.7. Uncertainties quantification

The uncertainties quantification about the techno-economic indicators of a CCGT coupled with a large-size condensing HP was performed in this subsection considering as benchmark a CCGT coupled with a HOB, as well for the deterministic assessment, the parametric and the sensitivity analysis carried out within the previous subsections.

To evaluate the economic viability of the system within a 20-year span (2020-2040), the variability of the forecast of the future price should be considered, as there is no certainty about the values that they will take on in the coming years. A case study based on the Italian market is proposed but the method presented has a general application.

The expected distribution of the single national price of electricity (PUN) was modeled with probability density functions trained on historical data, building an hourly profile of the PUN which would take into consideration the uncertainties derived from market variability. A similar process was done for the gas cost, building however a single probability density function with a standard deviation that could take into account the uncertainties about the forecasted values.

4.2.2.7.1. Methodology for uncertainty quantification

To account for the uncertainties, a Monte Carlo simulation was performed, adopting a number of samples that could minimize the mean square pure error (MSPE) [227], on a deterministic model built to simulate the behavior of the CCGT-HP and CCGT-HOB systems, subject to a deterministic daily thermal demand. The economic and environmental KPIs can be assessed on a yearly basis, not just as deterministic values but including the effect of input uncertainties and thus the risk of a wrong forecast.

In Figure 4.33, a simplified scheme of the method described above is presented to clarify the process. The blue frame refers to the model presented in the previous subsection whose outputs are KPIs characterized by unique deterministic values. What this analysis wants to quantify is the KPIs' uncertainty due to the uncertainty of inputs, i.e., the electricity price and the gas price. The figure highlights how the operating condition optimization is carried out for 144 standardized hours each of them characterized by a frequency of occurrence, as pointed out by subsection 4.2.2.4.5.

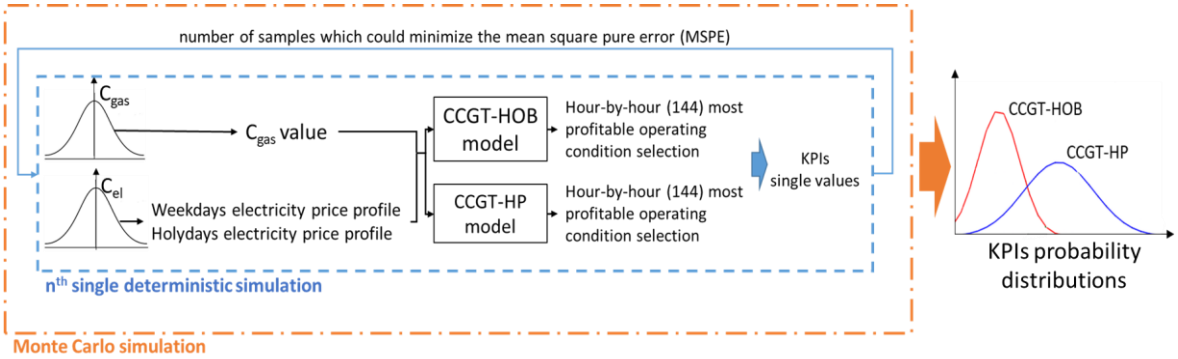

Figure 4.33: Uncertainties quantification methodology by means of Monte Carlo simulation.

Of course, the cost of gas and the electricity prices are not the only inputs to the CCGT-HP and the CCGT-HOB model but they are reported in the figure since the method hereby presented requires a different modeling approach with respect to that which was reported for the deterministic analysis.

4.2.2.7.2. Electricity and gas price and variability

As concerns the gas cost, an average forecasted trend was considered, based on the EU Reference Scenario [223]. From Figure 4.34 it can be observed that to take into account the variability of the gas cost in the future, a confidence interval was considered (blue area) around the average projection (line with markers), the uncertainty increases the more the projection is a long-term forecast. The cost of gas was considered normally distributed, averaged on the intermediate projected price and within a probability of 95.5% of being in the confidence interval, as can be observed from the Gaussian distribution plotted in red in Figure 6 over the auxiliary axes. The related Gaussian probability density function has a mean of 30 €/MWh and a standard deviation equal to 5 €/MWh.

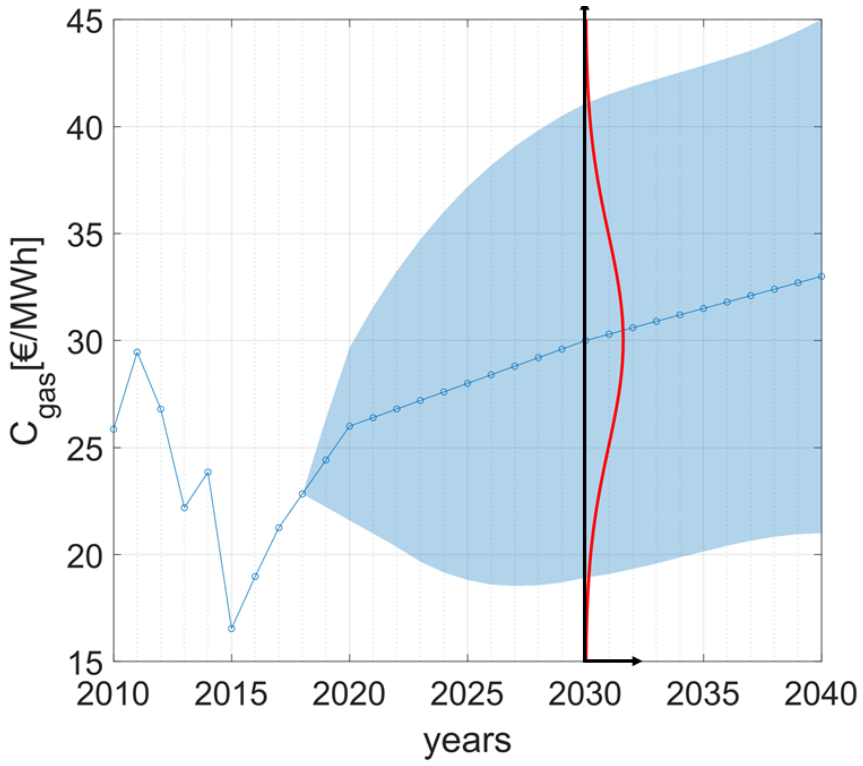

Figure 4.34: Historical and projected cost of gas [223].

The profitability of a power system throughout its life is highly dependent on the distribution of electricity prices over the years. The focus of the proposed model is the long-term modeling of electricity price distributions approximating the hourly distribution during the two winter seasons of the years between 2016 and 2018 [219] with a specific probability density function. In this study, the single national price (PUN) of electricity in Italy was considered, as this country was chosen as representative of the case study. To create the model the following steps were taken:

- The PUN was divided according to the "day-type": between weekdays and holidays, as it usually presents a different behavior in relation to that;
- The weekday and holiday PUNs were divided hour by hour, and the data corresponding to the same hour and day-type were then gathered;
- The gathered data were then analyzed and a MATLAB function was created to evaluate the probability density function (PDF) which would best fit the data, according to the log-likelihood criteria [228].

In Table 4.12 the PDF obtained and their characteristic parameters are listed, divided hour by hour. In Figure 4.35 the visual representation of the PDFs along the day, both for weekdays and holidays, is shown and the trend of the PDFs' peak is highlighted (red line). The symbols used to represent the PDF parameters are listed in the following with their corresponding PDF [229]:

- Normal: mean μ and standard deviation σ
- Gamma: shape parameter k and scale parameter θ
- Inverse Gaussian: mean μ and shape parameter λ
- Logistic: mean μ and scale parameter δ
- Weibull: shape parameter *b*, scale parameter *a*

Table 4.12: Hourly PDFs of the Single National Prices

Hour	Weekdays PDFs	Weekdays main PDF parameters	Holidays PDFs	Holidays main PDF parameters
1	Normal	$\mu = 47.43$, $\sigma = 12.26$	Gamma	$\theta = 20.83$, $k = 2.34$
2	Normal	$\mu = 44.22$, $\sigma = 12.00$	Normal	$\mu = 45.09$, $\sigma = 10.18$
3	Normal	$\mu = 42.33$, $\sigma = 11.86$	Normal	$\mu = 42.54$, $\sigma = 9.85$
4	Normal	$\mu = 41.32$, $\sigma = 11.63$	Normal	$\mu = 40.63$, $\sigma = 9.87$
5	Normal	$\mu = 42.06$, $\sigma = 11.22$	Logistic	$\mu = 40.54$, $\delta = 5.55$
6	Gamma	$\theta = 15.93$, $k = 2.95$	Logistic	$\mu = 42.03$, $\delta = 5.71$
7	Inverse Gaussian	$\mu = 55.83$, $\lambda = 931.92$	Logistic	$\mu = 45.16$, $\delta = 5.85$
8	Inverse Gaussian	$\mu = 64.38$, $\lambda = 878.16$	Logistic	$\mu = 47.92$, $\delta = 6.04$
9	Inverse Gaussian	$\mu = 68.62$, $\lambda = 787.85$	Normal	$\mu = 49.71$, $\sigma = 10.75$
10	Inverse Gaussian	$\mu = 65.77$, $\lambda = 714.97$	Logistic	$\mu = 50.40$, $\delta = 6.32$
11	Inverse Gaussian	$\mu = 61.77$, $\lambda = 676.06$	Normal	$\mu = 50.34$, $\sigma = 11.25$
12	Gamma	$\theta = 11.16$, $k = 5.29$	Normal	$\mu = 48.55$, $\sigma = 12.09$
13	Gamma	$\theta = 10.95$, $k = 5.05$	Normal	$\mu = 46.45$, $\sigma = 12.98$
14	Gamma	$\theta = 11.06$, $k = 4.99$	Weibull	$b = 4.08$, $a = 48.10$
15	Gamma	$\theta = 11.28$, $k = 5.12$	Weibull	$b = 4.28$, $a = 48.13$
16	Inverse Gaussian	$\mu = 60.73$, $\lambda = 644.20$	Weibull	$b = 4.88$, $a = 51.03$
17	Inverse Gaussian	$\mu = 64.25$, $\lambda = 678.49$	Normal	$\mu = 51.09$, $\sigma = 10.48$
18	Inverse Gaussian	$\mu = 70.68$, $\lambda = 686.42$	Normal	$\mu = 57.62$, $\sigma = 11.77$
19	Inverse Gaussian	$\mu = 74.60$, $\lambda = 830.07$	Normal	$\mu = 62.93$, $\sigma = 12.06$
20	Inverse Gaussian	$\mu = 71.60$, $\lambda = 1130.85$	Normal	$\mu = 64.09$, $\sigma = 11.37$
21	Gamma	$\theta = 18.41$, $k = 3.47]$	Normal	$\mu = 59.47$, $\sigma = 10.70$
22	Gamma	$\theta = 19.55$, $k = 2.98$	Normal	$\mu = 54.77$, $\sigma = 9.80$
23	Gamma	$\theta = 18.86$, $k = 2.89]$	Normal	$\mu = 51.21$, $\sigma = 9.75$
24	Gamma	$\theta = 17.85$, $k = 2.86$	Normal	$\mu = 47.81$, $\sigma = 9.49$

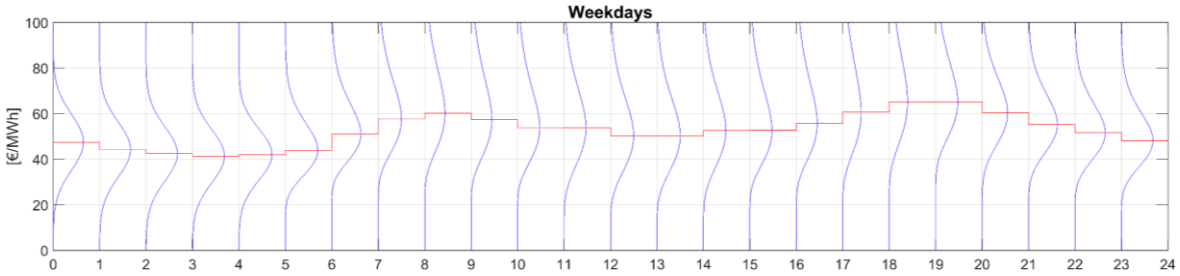

(a)

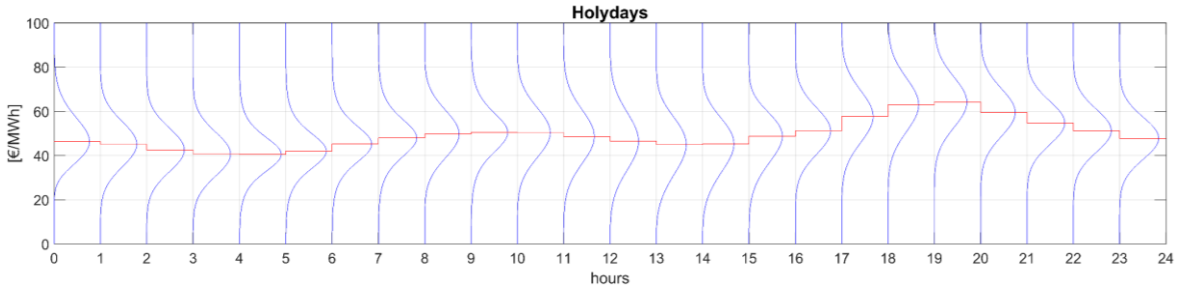

(b)

Figure 4.35: Electricity price probability density functions for weekdays and holidays.

It is interesting to notice that for weekdays, the Normal distribution is the best fit for the first hours of the day, while it is highly representative of the PUN behavior during holidays for most of the hours, so this PDF appears to be representative of low price periods. As concerns weekdays, Inverse Gaussian is representative of the morning hours and again the late afternoon-evening hours, where the peak prices are usually located (as can also be observed in Figure 4.35(a)). The Gamma distribution seems to have the effect of leading the transition between those different periods of the day, covering the "middle price period". During holidays instead, the Logistic PDF is selected to represent the morning hours, meaning that the related prices present heavier tails than the Normal distribution.

The PDFs were then expressed as a function of their mean, so that they could then be used to represent a different PUN behavior, assuming however that the shape expressed by the PDF and by the standard deviation would remain unchanged over the years.

The selection of the best fitting PDFs and the estimation of their parameters was made considering three winter seasons, through a cross-validation procedure. The average error in the test phase is 4.85% (2.90 €/MWh) on weekdays and 7.4% (3.78 €/MWh) on holidays, making the model suitable for the proposed analysis.

As stated before, the plant was assumed to operate for a 20-year life span, between 2020 and 2040. Three different PUN scenarios were considered [230]: a constant trend, an increasing, and a decreasing trend. While an increase in the PUN is expected due to the forecasted increase in the gas cost, the constant and the decreasing PUN price scenarios are representatives of an electricity market with a high share of RES production, leading to a decoupling of the electrical price variation with respect to the gas price. As for gas, since linear trends were adopted, the average values are equal to the average of the distribution in 2030 for the three scenarios.

In the average PUN scenario, the average of the distributions remains the same over the years as the mean corresponding to the winter season 2018/2019 (i.e., 60.77 €/MWh for

weekdays and 55.18 €/MWh for holidays). In the High PUN scenario an increase of the average price of electricity by 2.5%/year, compared to the current value, is forecasted, resulting in an average of 75.96 €/MWh for weekdays and 68.97 €/MWh for the others. In the low PUN scenario, a decrease in the average price of electricity of 2.5%/year, compared to the current value, is considered with an average of 45.58 €/MWh for weekdays and 41.38 €/MWh during weekends and holidays. These values were used as the mean to build the PDF listed in Table 4.12.

4.2.2.7.3. KPIs uncertainties

This subsection reports the results of the analysis performed, according to the methodology described in 4.2.2.7.1. The number of samples for which the Monte Carlo simulation gave an acceptable MSPE value turned out to be 15000. Firstly, the average HOB and HPs' load distribution is presented to validate the off-design assumptions and guarantee the reliability of the results. Then, the results related to the economic viability and profitability of the proposed solutions are reported, while the second compares the CCGT-HP and CCGT-HOB under the carbon emission reduction perspective. The last one presents a sensitivity analysis with respect to carbon emission cost.

Figure 4.36 shows how the HPs and the HOB mean value loads are distributed in the Average PUN scenario. It is possible to appreciate how the average load of each single HP is never lower than 60%, and the same minimum value is observed in the two other PUN scenarios, thus the assumption related to the off-design operations made in Section 4.2.2.2.1 results to be validated. Also, the minimum HOB load is never lower than 10% in any scenario, justifying the application of the Satyavada et al. model [186].

Table 4.13 integrates the information of Figure 4.36, providing a comprehensive report of the yearly operating hours for the HPs and HOB in every considered PUN scenario. In the high PUN scenario, the CCGT works at a higher load, in most cases without requiring any integration to satisfy the thermal demand. To quantify this data, it is important to remark that the seasonal overall number of hours is 4368.

Decreasing the price of electricity, it results to be preferable, especially for the CCGT-HP solution, to lower the GT load by integrating the HPs or the HOB to provide the required thermal power. This is directly reflected in an increase in the yearly operating hours of these components.

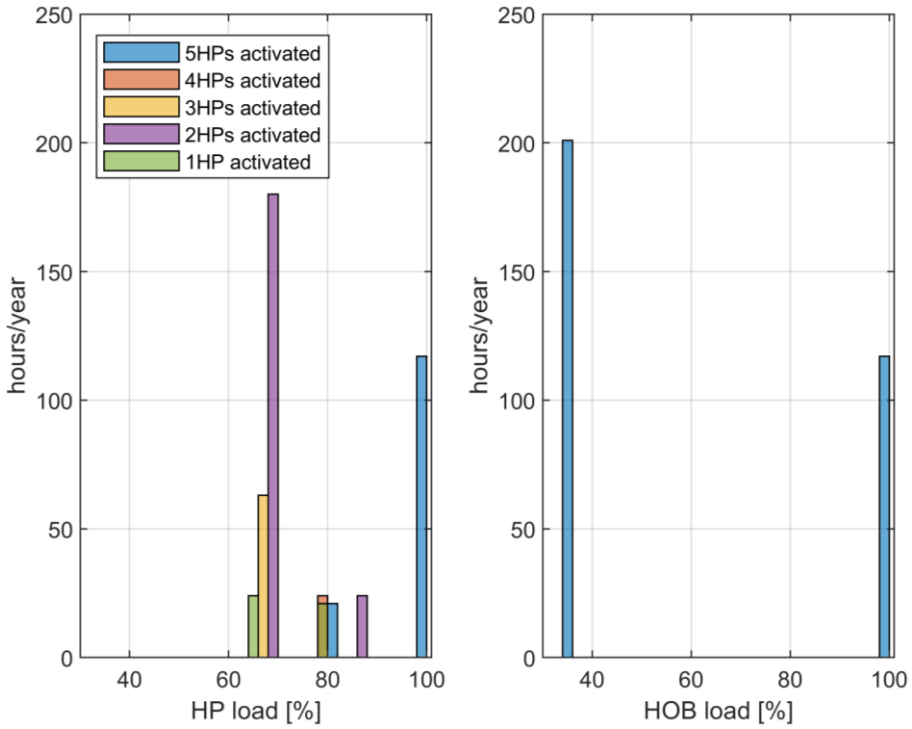

Figure 4.36: HPs and HOB yearly off-design operating hours (average PUN scenario).

Table 4.13: HPs and HOB yearly operating hours (average PUN scenario).

	HPs	**HOB**
Low PUN	1587	486
Average PUN	474	318
High PUN	318	318

Looking at the three scenarios in which the analysis was carried out, it is important to observe how the annual cash flow (as shown in Figure 4.37) always has a median value, red line, higher for the CCGT-HP than the CCGT-HOB. It is also important to point out that the integrated heat pump system seems to be less affected by market uncertainties, as shown by the distance between the 1st and the 3rd quartile, blue box, and the 95th and 5th percentile (exact values are reported in the table immediately below the figure). This is strictly connected to the fact that, in order to achieve higher thermal power levels, electrical power is employed instead of primary energy and so, in case of low electricity prices, the gas consumption can be reduced by consuming a cheaper source. Thus, the CCGT-HP solution is less sensitive to the market uncertainties considered.

This trend becomes more evident when the price of electricity decreases, which would represent the most critical condition from the sustainability point of view, due to lower annual cash flow. In fact, while in the High PUN scenario the expected cash flow value for the CCGT-HP is 1.3% higher than CCGT-HOB, this advantage increases up to 13.2% in the low PUN scenario. This shows the potentialities of the CCGT-HP in critical scenarios: while the variability (expressed as the difference between the 75th and 25th percentiles) in the High PUN scenario is 3.18% lower than the CCGT-HOB solution, for the low PUN scenario the cash flow variability reduction becomes equal to 15.25%.

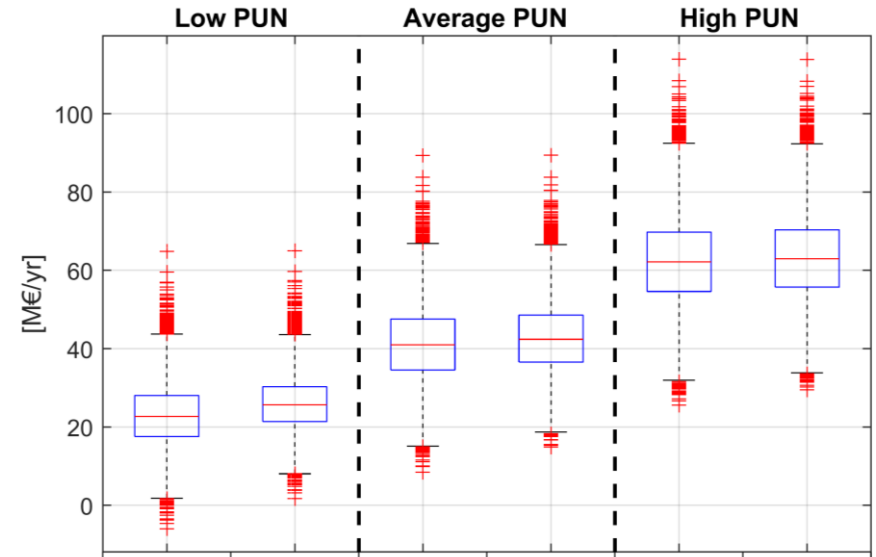

	CCGT-HOB	CCGT-HP	CCGT-HOB	CCGT-HP	CCGT-HOB	CCGT-HP
Median	22.6653	25.6654	40.954	42.3909	62.1438	62.9575
75^{th}-25^{th}	10.4861	8.8865	13.0059	12.018	15.133	14.6513
95^{th}-5^{th}	25.7499	21.9028	31.5634	29.1072	36.4951	35.2244

Figure 4.37: Annual Cashflow distribution.

Nevertheless, as reported in subsection 4.2.2.4.1, the capital expenditures are considerably higher for the solution integrating the heat pump, consequently, despite the higher annual cash flow, the CCGT-HP presents a lower expected Net Present Value (NPV). In particular, the NPV presented in Figure 4.38 is calculated as in equation (4.32).

From Figure 4.38 it can be observed that the High PUN scenario would be particularly beneficial in terms of NPV for both solutions (CCGT-HP and CCGT-HOB), presenting an expected NPV higher than 700 M€ thanks to the higher revenues of the electrical production. This high electricity price gives benefits, particularly to the CCGT-HOB system, in which all electrical production can be sold at market price. On the other hand, in a low PUN scenario, the CCGT-HP presents just a slightly lower average NPV, but with lower variability. Nevertheless, in such a critical situation, both systems present negative values for the first NPV quartile, with a risk of not even covering the investment costs (i.e., 358.64 M€ for CCGT-HOB and 433.12 M€ for CCGT-HP). This risk is quantified in 35.9% of probability for the CCGT-HOB and 39.8% for CCGT-HP.

The economic conditions foreseen in this analysis indicate that the HOB solution tends to be more profitable in high electrical price scenarios. On the other hand, in the event of decreasing electrical prices, as in the case of a high share of renewables, the economic performance would be comparable, but with a lower variability associated with the CCGT-HP solution. The NPV increases in case of higher cash flows: this can be obtained in sites where a larger annual thermal demand exists (e.g., in countries colder than northern Italy) or by increasing the heating price paid by the consumers. Moreover, it is also important to remark that with the advent of the most recent generations of DHN, and the following decrease in temperature levels, the heat pumps will be able to work with a higher COP with a benefit to the thermodynamic efficiency and the economic profitability.

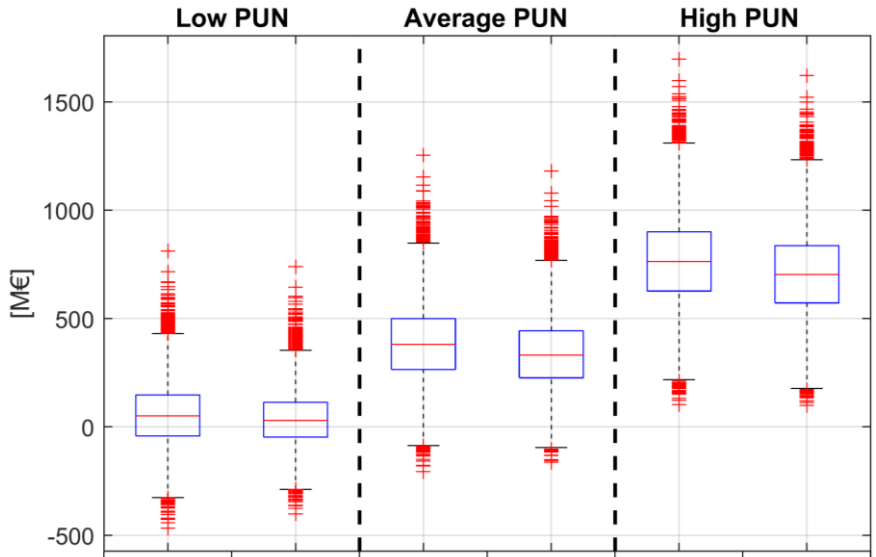

	CCGT-HOB	CCGT-HP	CCGT-HOB	CCGT-HP	CCGT-HOB	CCGT-HP
Median	50.3678	30.0315	380.3975	331.8517	762.7793	702.9882
75^{th}-25^{th}	189.2279	160.3617	234.6992	216.8721	273.0838	264.3901
95^{th}-5^{th}	464.672	395.2474	569.5788	525.2551	658.574	635.6446

Figure 4.38: Net Present Value distributions.

Under the GHG emission perspective, Figure 4.39 shows that the CCGT-HP presents a reduced amount of emitted carbon dioxide. The reason is twofold: on one hand, the CCGT-HP system works with higher global efficiency, as highlighted by Figure 4.40, on the other hand, the electricity production is also lower since lower electricity prices lead the system to run closer to the minimum load that enables the fulfillment of the thermal demand.

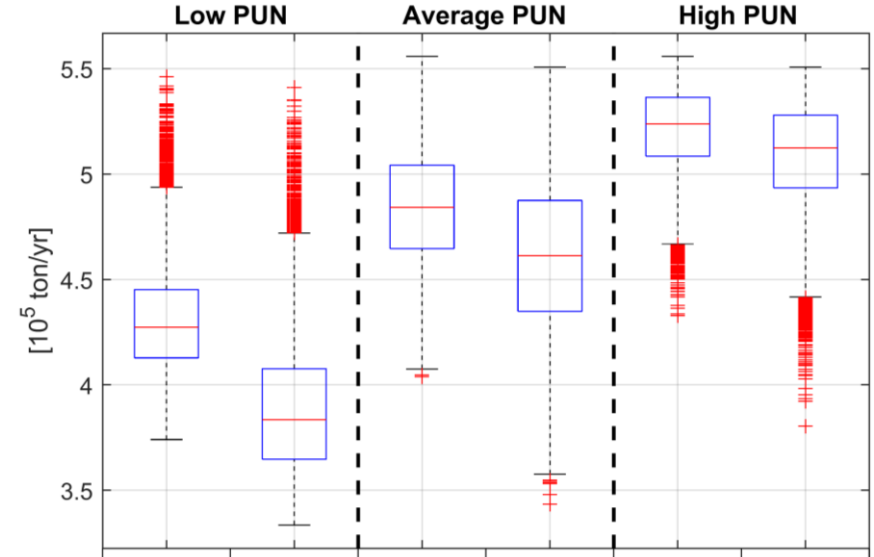

	CCGT-HOB	CCGT-HP	CCGT-HOB	CCGT-HP	CCGT-HOB	CCGT-HP
Median	4.2738	3.8353	4.8417	4.6123	5.2375	5.1241
75^{th}-25^{th}	0.32366	0.42942	0.3957	0.52642	0.27881	0.3453
95^{th}-5^{th}	0.81593	1.0609	0.89933	1.1965	0.64325	0.8031

Figure 4.39: Carbon dioxide emission distributions.

Increasing the price of electricity, the emitted carbon dioxide distribution (Figure 13) moves towards higher values (increments of $0.96 \cdot 10^5$ and $1.29 \cdot 10^5$ ton/year for CCGT-HOB and CCGT-HP respectively) and shows a lower standard deviation for both proposed solutions. This is due to the fact that the power plant increases the number of hours at which it operates in full load conditions, where it can provide a higher thermal power without any integration, consequently increasing the number of hours in which there is no difference between the CCGT-HOB and the CCGT-HP environmental behavior.

It is also interesting to observe how the carbon dioxide emission distributions, Figure 4.39, as well as the average global efficiency, Figure 4.40, in the Low and High PUN scenario present opposite skewness. This is due to the electricity price which leads the power plant always to operate at the minimum or at full load. Thus, decreasing or increasing further the PUN does not affect the power plant's emissions.

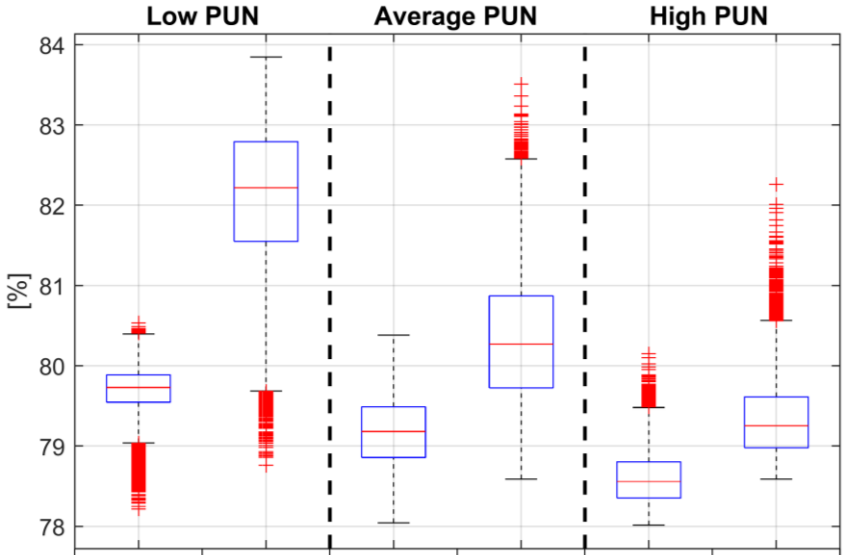

	CCGT-HOB	CCGT-HP	CCGT-HOB	CCGT-HP	CCGT-HOB	CCGT-HP
Median	79.7291	82.2169	79.1804	80.2693	78.5542	79.2526
75^{th}-25^{th}	0.34002	1.2427	0.63052	1.1444	0.45182	0.63449
95^{th}-5^{th}	0.90286	2.9215	1.3898	2.6345	1.0535	1.527

Figure 4.40: Global efficiency distributions.

The larger variabilities registered in yearly average global efficiency and CO_2 emissions for CCGT-HP are due to the larger enhancement in global efficiency that can be reached operating the HP with respect to the HOB. This reflects also on the CO_2 emissions.

Finally, a sensitivity analysis was performed with respect to the emitted carbon dioxide cost. The effect of the cost of emitted CO_2 is similar to the cost of fuel in calculating the overall cost of primary energy consumption: an increment of 10 €/ton of carbon dioxide corresponds to an increment of 2.01 €/MWh for the fuel cost. The main difference is that CO_2 cost change, in the proposed model, is not reflected on the thermal customers but is repaid by the CHP annual income affecting the profit margin. Table 4.14 presents the yearly emission value: from the policy/environmental point of view, an increase in the cost of the emitted CO_2 is appreciable, since it leads to a decrease in the environmental impact, keeping fixed the satisfied heat demand. In fact, a higher carbon cost leads the plant to operate at partial load saving primary energy. Nevertheless, as shown in Figure 4.41, this implies an

increase in the risk of not paying the investment cost back, and it is discouraging for a real plant owner to keep the plant operating in such market conditions.

Table 4.14: CO_2 [ton] emitted for different carbon cost scenarios (Average PUN scenario).

	30 €/ton		40 €/ton		50 €/ton	
	CCGT-HOB	**CCGT-HP**	**CCGT-HOB**	**CCGT-HP**	**CCGT-HOB**	**CCGT-HP**
Median	$4.94 \cdot 10^5$	$4.75 \cdot 10^5$	$4.84 \cdot 10^5$	$4.61 \cdot 10^5$	$4.74 \cdot 10^5$	$4.47 \cdot 10^5$
75^{th}-25^{th}	$0.402 \cdot 10^5$	$0.525 \cdot 10^5$	$0.396 \cdot 10^5$	$0.526 \cdot 10^5$	$0.385 \cdot 10^5$	$0.523 \cdot 10^5$

Indeed, an increase in CO_2 cost is reflected in a decrement in final profitability without significant differences between the CCGT-HP and CCGT-HOB. Averagely for an increase of 10 €/ton an 18.2% decrement in NPV occurs, while for the CCGT-HOB this decrement is 19.4%.

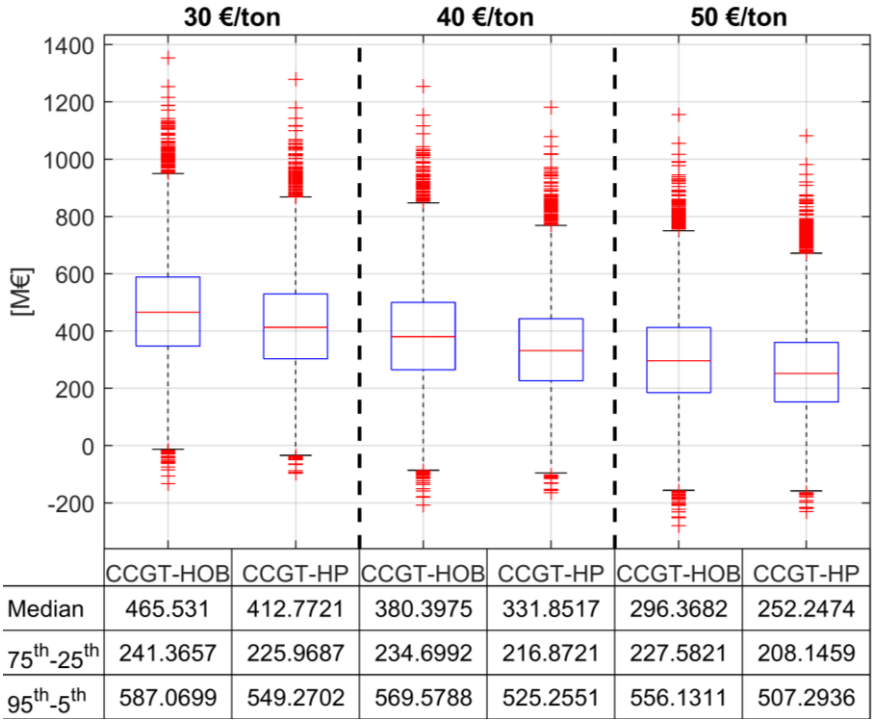

	CCGT-HOB	CCGT-HP	CCGT-HOB	CCGT-HP	CCGT-HOB	CCGT-HP
Median	465.531	412.7721	380.3975	331.8517	296.3682	252.2474
75^{th}-25^{th}	241.3657	225.9687	234.6992	216.8721	227.5821	208.1459
95^{th}-5^{th}	587.0699	549.2702	569.5788	525.2551	556.1311	507.2936

Figure 4.41: NPV's distribution sensitivity to the carbon price (Average PUN scenario).

4.2.2.8. Concluding remarks

Subsection 4.2.2 explored a new solution for CHP generation, integrating a Combined Cycle Gas Turbine, CCGT, with a flue gas condensing heat pump. Two different configurations (series and parallel) were investigated. Coupling the heat pump, HP, in series to the District Heating Network Heat Exchanger, preheating the DHN water, demonstrated to be preferable thanks to the lower HP's temperature lift, which implies a higher COP and then a greater global efficiency. This is valid up to a share of thermal energy generated between the heat pump and CCGT of ca 1:1.3. Increasing the HP size over this value, it is worth considering the parallel configuration. For a reasonable heat pump size, the series configuration is, thus, preferable. This configuration was then benchmarked against the integration of the same cogenerative CCGT plant with a Heat Only Boiler, HOB, sized to provide the same peak thermal output of the system integrating the flue gas condensing heat pump, CCGT-HP. CCGT-HP solution allows to extend the maximum thermal capacity,

satisfying the peak demand, without consuming further primary energy but lowering the electrical output, thus it allows to maximize the profits, or minimize the losses, with respect to the CCGT-HOB, under not favorable market conditions (high primary energy cost coupled with relatively low electricity price conditions). CCGT-HOB allows satisfying the thermal demand peaks without reducing the electrical production and this result to be particularly advantageous in scenarios with a high average electrical price.

The proposed system allows increasing the average annual efficiency by up to 5 percentage points, especially in low electrical prices conditions, and reducing the annual CO_2 emission, with a maximum of -13.9% (when the average electricity price is 30 €/MWh). At high electricity prices, the advantage reduces to 0.6 percentage points of higher global efficiency and just -1% of CO_2 reduction.

From the economic perspective, the CCGT-HP demonstrated to be advantageous in only low electricity price conditions, the maximum electrical price for which it is more profitable than the CCGT-HOB was defined as Break Even PUN to which corresponds a Break-Even Net Present Value (BENPV). A parametric analysis was carried out to investigate the sensitivity of the investment profitability with respect to the cost of gas, the cost of emitted CO_2, and the heat pump capital expenditure. A CAPEX reduction slightly affects the BEPUN increasing significantly the corresponding NPV, while a cost of gas variation has a stronger influence on the BEPUN increasing the electrical market condition in which CCGT-HP is preferable to CCGT-HOB. On the other hand, an increase in the carbon emissions allowances prices will lead to a slight advantage to the lower carbon footprint of the CCGT-HP, but reducing the corresponding NPV decreases the attractiveness of the investment.

Besides, a Monte-Carlo simulation was performed on the two systems in other to quantify the uncertainties about the outcomes:

- Despite a higher annual cash flow for the CCGT-HP solution, the higher investment costs of this solution ended up in a lower NPV when compared to the CCGT-HOB solution. However, lower variability of the CCGT-HP solution was also highlighted, ending in a more robust solution, especially in the more critical situation, the one with decreasing electrical prices.
- From the environmental point of view, CO_2 emission was analyzed. As concerns this variable, the CCGT-HP presents lower emissions than the CCGT-HOB, because the thermal capacity of the CHP power plant is extended by exploiting the flue gas latent heat by the heat pump, thus increasing global efficiency, rather than burning additional fuel as in the HOB.

The proposed integration of HP and CCGT appears to be interesting under a generation mix with a strong presence of renewable generators which brings to an electrical price uncorrelated to the gas cost[33] (Low PUN scenario): in this case, the revenues related to the electricity market are no more covering the production cost and the system profitability is just related to the thermal demand and the depreciated electricity can be used to generate heat through the HP. Under this condition, the CCGT-HP could be of interest to municipalities interested in fulfilling the local thermal demand guaranteeing lower emissions and reducing the risk over the years of deviating from the expected plan.

[33] The minimum ratio between the cost of natural gas and the average cost of electricity that make the solution viable was found to be between 0.7 and 0.8, against a current value of this ratio around 0.4±0.1 among the EU energy markets.

Finally, it is interesting to highlight that economic performances and environmental/thermodynamic performances have an inverse correlation with the electrical prices: the NPV grows with the electrical market price for both systems while efficiency reduces, and the CO_2 emissions increase due to the higher use of the CCGT at full load. The cost of emitted CO_2 has a similar impact: an increase of this parameter, if repaid internally by the CHP, will bring a decrease in carbon emission but also a reduction in system profitability.

Generalizing the results: the NPV could increase, for both systems, in case of higher cash flows: this can be obtained in sites where a larger annual thermal demand exists (e.g. in countries colder than northern Italy) or by increasing the heating price paid by the consumers. Moreover, it is also important to remark that with the advent of the most recent generations of DHN, and the following decrease in temperature levels, the heat pumps will be able to work with a higher COP with a benefit to the thermodynamic efficiency and the economic profitability. Finally, since a lower average electricity price is beneficial to the proposed CCGT-HP, a market with an excess of production from renewable generators could be interested for such applications.

4.2.3. Combined heat and power applications concluding remarks

Concerning the combined generation of power and heat, the HP and CCGT coupling aims to extend the operational range and increase the global efficiency of a CCGT-CHP. Section 4.2.1 investigates the optimal heat source exploitable by an HP as retrofitting option of a CCGT-CHP. Moreover, series and parallels HP and DHN heat exchanger arrangements are evaluated. The best heat source is represented by the hot condensate extracted from the low-pressure steam turbine for the cogenerative purpose. Even if the mass flow is limited, within a reasonable HP size range, it allows the HP to work with a reduced temperature lift, thus a higher COP. The minimum temperature requirement at the stack, to which CCGTs are usually subjected, poses a limit on the maximum HP power, especially at reduced GT load operations. Concerning the optimal coupling arrangement, a hybrid series-parallel solution is proposed, this combines the advantage of a higher COP proper of the series HP with the full exploitation of the condensate enthalpic potential in the DHN-HX guaranteed by the parallel coupling.

However, the most advanced coupled layout addressing both the power and the heat generation is proposed in section 4.2.2. The described flue gas condensing HP allows increasing drastically the global efficiency, by recovering the flue gas latent heat potential which is characterized by too low temperature to be exploited otherwise. The proposed solution is benchmarked against a traditional coupling to a heat-only-boiler. The lower CAPEX characterizing the boiler is an advantage however the growing RES penetration is expected to cause an increase in the gas to electricity price ratio under which the flue gas condensing HP is competitive, this scenario would allow a significant cut in emission (up to 14%) for the combined heat and power supply. Additionally, the uncertainty quantification presented in this section shows how the CCGT-HP coupling outcomes are more robust than the CCGT-HOB with respect to the variability of the macroeconomic parameters such as the price of essential commodities such as natural gas and electricity.

5. Electricity market in depth

The previous chapters explored different solutions to provide flexible and sustainable heat and power, as required by the macroclimate and economic scenario described in Chapter 1. The proposed solutions allow good exploitation of the primary fuel energetic potential and favor an efficient dispatch of the RES generators through the electricity grid. However, they are often characterized by relevant CAPEX that may limit the economic viability of these technology jeopardizing the potential contribution in terms of emissions reduction.

For these reasons this thesis besides a thermodynamic and energy analysis carries out some economic assessment, because in a marked-based energy system if the solution is not profitable there is no possibility of an application on the large scale, despite the benefits it can bring.

A proper understanding and modeling of the market are crucial to performing a reliable assessment and reducing errors and uncertainties in the outcomes. Particularly challenging is to evaluate the economic value of flexibility. As mentioned, flexible solutions have a cost in terms of investment, however, flexibility can be reflected in higher economic income and paying back the initial investment. Nevertheless, the value of flexibility is not recognized by the traditional energy-only markets and is awarded in other markets such as the services market or the balancing market, thus and a traditional approach to techno-economic analysis, focused on the day-ahead market, may fail.

The first section of this chapter explores the limitation of the main energy-only market, i.e., the day-ahead market. The second Section presents a statistical analysis that describes how flexibility's economic value is recognized in the Italian electricity market, quantifying the economic income from services provision against power generation. Finally, the third section introduces a novel mixed integer linear programming approach to the energy systems' optimal dispatch problems considering the uncertain opportunities in the services markets, where the flexibility is valued.

5.1. Day Ahead Market's limitations

Since the regulatory framework has moved toward a market-based approach, aiming at minimizing overall generation costs, power generators exploit the electricity market to recover the operating costs, the fixed costs, and to realize profits. Within Chapter 1 the marginal price system, which characterized most of the electricity market has been illustrated.

Then, assuming a perfect competition scenario on the market, a power generator should offer the minimum price which allows it to recover the costs of operating. According to this strategy, it will avoid operating losing money and extra revenues will be realized when the market-clearing price results to be higher than the marginal cost. To be the generator economically viable the extra revenues should be enough to recover all the fixed costs and the initial investment. In other words, the generator is a pure price taker, it cannot influence the price so it operates only if the System Marginal Price (SMP) is higher than its operating costs.

This is not generally a problem for those generators, such as RES generators, with low or null marginal cost, since they have no marginal cost when operating all the revenues, paid back the fixed cost, are profits. On the other hand generators with high marginal cost operates a few hours per year, when the demand for electricity is very high and/or when there is a scarcity of power from cheaper generators. Within this little amount of hours, these generators should be able to pay back the operating variable costs plus the fixed cost for the whole year. As a consequence, the less they operate during the year the higher the price they need to offer on the DAM to guarantee their viability, this could be reflected in increased price volatility.

Figure 5.1 reports an exemplary day ahead auction in Spain, relative to the 5th of December 2021, the day is characterized by a high wind generation so the electricity price, i.e., the black dashed line, is very low during the off-peak demand period such as the early morning. When the demand increases the cheapest generators (nuclear, hydro, and wind) are no longer sufficient to cope with it, and turning on some natural gas-fired capacity is needed. As a result, the System Marginal Price (SMP) starts increasing. However a couple of hours later, the PV generation increment is enough to cover the demand without the gas-fired generators, and the electric price falls down again until the evening when solar sourced generators are no longer available and the demand peaks, so the gas fleet has to restart and the price rises up to 250 €/MWh.

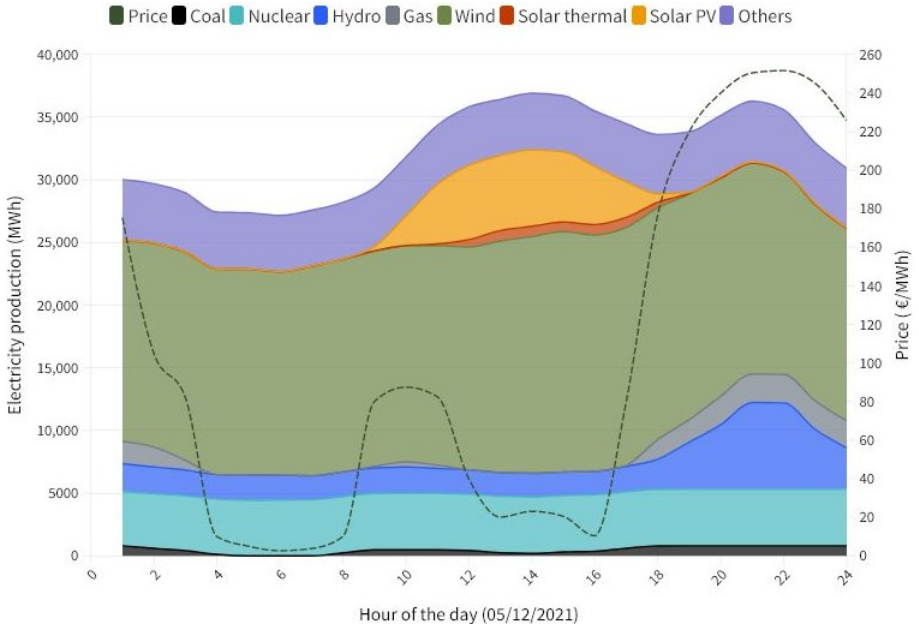

Figure 5.1: Exemplary electricity price volatility in a highly RES penetrated DAM.

The operating cost for CCGTs generators (for whose this thesis explored innovative solutions to provide flexible dispatchable power with a reduced environmental impact) are mostly related to the natural gas cost. From the fourth quarter of 2021, and while this thesis is being essayed the gas price increased up to the maximum historical level [63]. What is shown in Figure 5.1 is much more stressed within a high price scenario. Figure 5.2 well illustrates how the price offered on the DAM by the CCGTs power plants linearly depends on the price of fuel.

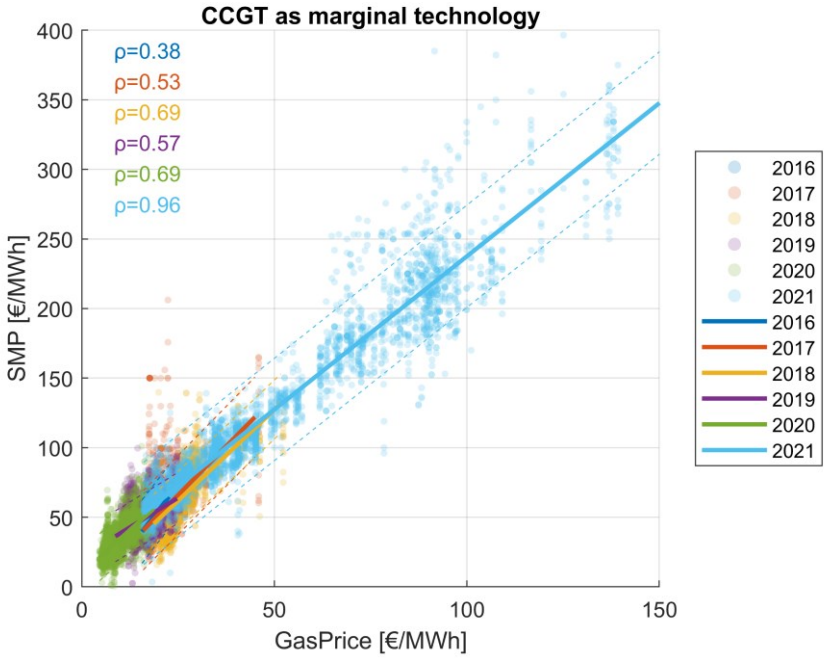

Figure 5.2: Italian system marginal price when CCGT results to be the marginal technology. Pearson coefficient values are indicated in the figure.

As visualized in Figure 5.3 the electricity price is highly correlated to the gas price. This is due to the role that GTs still play in the electricity system, the more often this is the marginal technology the more the system marginal price is the GTs marginal cost, thus dependent on the gas market value.

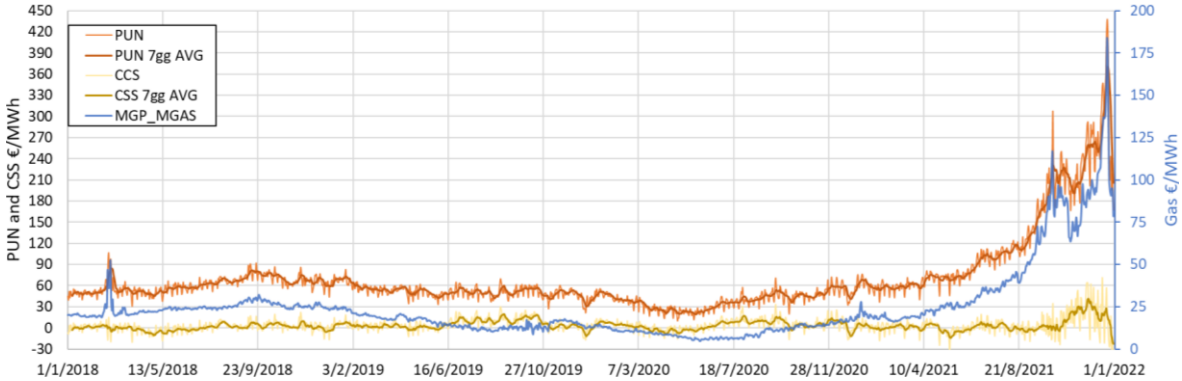

Figure 5.3: Italian national single price (PUN), CSS, and Italian spot gas price (righty-axis).

However, the dependency of the electricity price on gas is today more than due. It is not possible to observe a significant dependency of the dimensionless price profile[34] (i.e., the average daily average curve normalized by the mean), and the off-peak price value seems to be highly dependent on the gas price too. What is illustrated in Figure 5.1, is an example that well suits the theory but it is not a standard nowadays. Many generators do not offer their marginal price on the market, this is denoted by Figure 5.4 reporting the SMP when

[34] The invariability of the dimensionless price profile was a fundamental assumption of the economic model proposed by the section 4.2.2.4.2 which was validated with good results

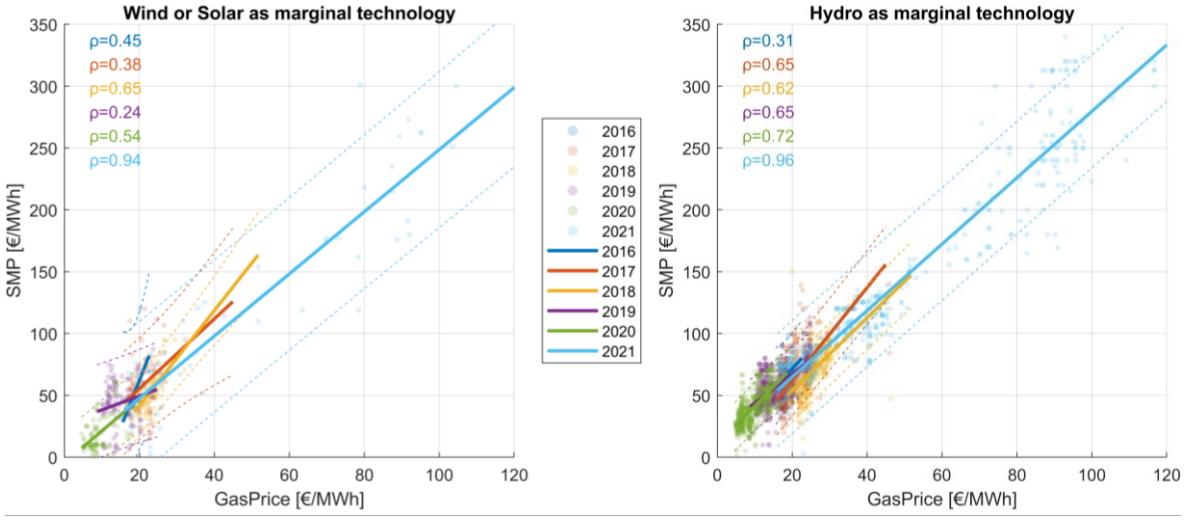

(a) *(b)*

Figure 5.4: Italian system marginal price when Wind or Solar (a) or Hydro(b) results to be the marginal technology. Pearson coefficient values are shown in the figure.

the marginal technology is a non-gas-fired generator, it is expected to report almost flat trends, while a dependency is clear. Under imperfect competition generators act as price makers rather than pure price takers, it represents a market failure that should be seriously considered by the market operator since it is increasing further the overall price of electricity.

It is worth noticing how this problem was extremized within the last month of 2021, presenting fast increasing gas and electricity price, under these condition offer from RES generators up to 200 €/MWh have been common on the DAM. On the other hand despite the increasing cost of fuel during this period the CSS (yellow line in Figure 5.3) was one of the highest recorded in recent years. However, this parameter was highly variable and the value reported should be intended as an average national value.

It is also interesting to look at the CSS in the long term, Figure 5.5 shows how the duration curve changed across the years, the curves are reported for the last four years (continuous lines) and three years of the previous decade (black lines), immediately before the massively subsidizing of solar photovoltaic in Italy [231].

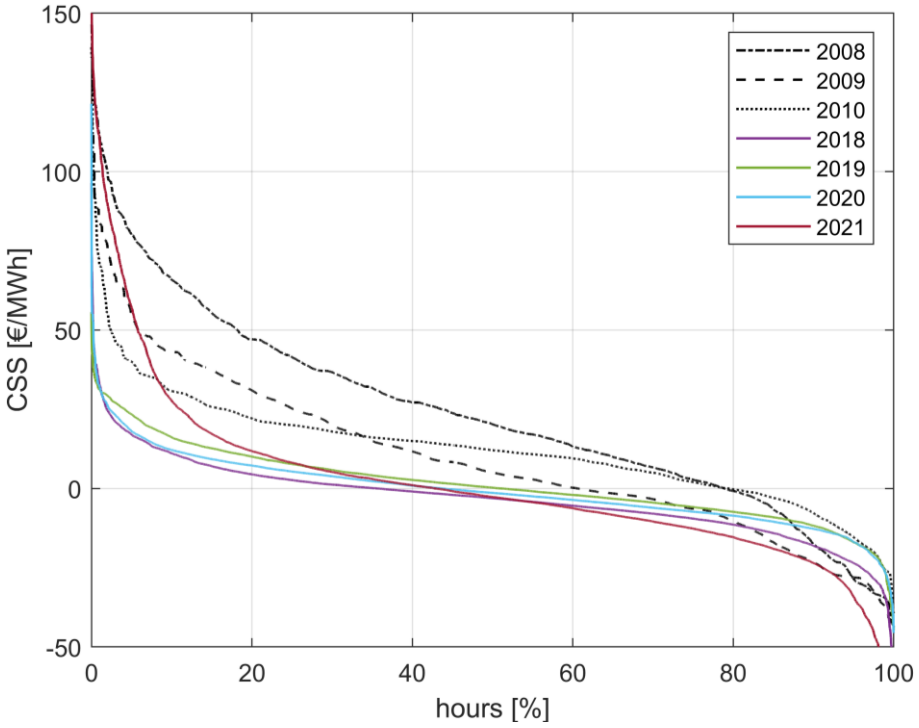

Figure 5.5: Italian Clean Spark Spread duration curve.

The CCS has been calculated according to the following formula:

$$CSS = pr_{el} - COE = pr_{el} - \left(\frac{pr_{gas} + e \cdot pr_{CO_2}}{\eta_{CCGT}} + O\&M_{var}\right) \quad (5.1)$$

Where it is assumed that the natural gas emission factor e is equal to 55.91 ton/TJ according to the Italian government directives [232], and the variable operating and maintenance costs ($O\&M_{var}$) equal to 3.15 €/MWh referring to the report issued by the Italian Electric System Research institute [200]. The electricity prices, as well as the daily spot gas market price from 2011 onward, are available on the GME's website [144], while the gas price of 2008, 2009, and 2010 Eurostat [233] is the source. Table 5.1 reports the yearly average CCGTs efficiency, and the CO_2 emission cost.

Two considerations can be drawn from this comparison: the number of hours with a positive spread significantly decreases during the years, in 2018 only roughly 30% of hours of the year would be profitable for a CCGT. Moreover, the CSS is lower during all the hours of the year: the area between the curve and the zero is drastically reduced and this is directly correlated to the annual income of the power plant on the DAM. Additionally, it has to be considered that today the positive spread hours are very sparse during the day, typically some hours in the early evening, forcing the plants to sudden expensive startups, even daily, or to operate at the minimum load during the negative spread hours waiting for more profitable times [140].

Table 5.1: Annual variability of CSS components.

	η_{CCGT} [%]	p_{CO2} [€/ton]
Reference	Terna [219]	Ember [147]
2008	52.95	24.9
2009	51.92	13.78
2010	51.30	14.41
2018	52.21	15.96
2019	52.33	24.85
2020	52.08	24.78
2021	-[35]	51.99

Even if 2020 can be considered an outlier because of the strong effect of the COVID-19 pandemic on the demand, it may be also representative of the ratio between the electricity demand and RES installed capacity. Anyway, also looking at the pre-pandemic years (2018 and 2019) the trend that occurred during the 2010s decade is clear, in 2021 the profits opportunities seem to have been increased but under so fast-changing price the methodology here adopted could lead to some errors since the spot price for gas and CO_2 allowances is not exactly what the generator pays.

5.2. Ancillary Services market potentialities

For all the reasons listed in the previous subsection, the DAM profits maybe not be sufficient to fully recover the operating cost and the capital expenditure and operators must exploit other markets to achieve economic viability. Besides the capacity market, which has started in Italy in November 2019 [90,91] and is intended to repay directly the capital expenditure through long-term procurement contracts awarded through competitive auctions, resulting out of the scope of this paper, Intraday Market (IDM), Ancillary Services Market (ASM) and Balancing Market (BM) are today a relevant source of revenues, even when compared to DAM. The nomenclature and the market mechanism have been introduced in subsection 1.1.1.1.

In order to carry out a complete analysis of different spot markets' profitability, all offers/bids presented by CCGTs on these markets have been considered [144]. The power plant database is the same used in subsection 2.3.2.1, so the focus is on the 45 power-oriented CCGTs (i.e., only devoted to power generation) that were considered since CHP power plants operations on the electricity markets are strongly dependent on the local thermal demand. Table 5.1 reports, for each zone, the number of active units and overall zonal installed capacity included in the analysis.

[35] Not available, the mean of 2018 and 2019 was assumed.

Table 5.2: Power-oriented CCGT zonal distribution.

	CCGT n	Overall zonal capacity
NORD	22	10,394 MW
CNORD	2	756 MW
CSUD	10	4,077 MW
SUD	4	2,713 MW
SICI	1	780 MW
SARD	0	0 MW
ROSN	6	3,275 MW

Revenues are a common parameter used to quantify the profits opportunities in the markets. For each offer, revenues are calculated as the product of the awarded quantity by the price, then the value has been normalized on the amount of the capacity installed within the zone. So, the normalized annual revenues indicate the market value generated by 1 MW of installed capacity for each zone.

Nevertheless, revenues do not consider the costs of generating electricity, moreover, it is not possible to include the contribution from bidding the electricity, already sold in previous markets, at a lower price into the revenues. Thus, revenues are useful in order to evaluate the relevance of each market at glance but could provide a distorted perception of the impact on CCGT profitability. Therefore, to fully assess the viability of a power plant it is needed to focus on the net income rather than on the revenues. For each accepted offer the resulting net income is:

$$NetIncome_{OFF} = (p_{aw} - COE_2) \cdot Q_{aw} + (COE_1 - COE_2) \cdot Q_1 \qquad (5.2)$$

Where subscript 1 refers to the operating condition before the offer was accepted, 2 to the operating condition after the offer was accepted. pr_{aw} is the price and Q_{aw} is the quantity awarded by GME or the TSO. The first term of equation (2) comes directly from the additional quantity sold on the market, and the second term deals with the fact that the offer acceptance imposes a different operating condition and so a different cost of generating the already sold electricity. Since an offer revises the load upward, the plant efficiency increases and this term is expected to be positive. While for each accepted bid the resulting net income is:

$$NetIncome_{BID} = (COE_1 - p_{aw}) \cdot Q_{aw} + (COE_1 - COE_2) \cdot (Q_1 - Q_{aw}) \qquad (5.3)$$

With the same nomenclature as in equation (5.3). It must be noticed that for a power plant is worthwhile to bid electricity only at prices lower than its operating costs, even null prices are common among the bids, while negatives are not allowed. The first term of this equation is expected to be positive on ASM and BM, where the bid is valued at the offered price, on the IDM it depends on the zonal clearing price, so it can be also negative. The second term concerns the operating costs' variation. Since a bid revises the plant's load downward, it implies a decrement in efficiency, thus this term is expected to be negative. The cost of electricity is computed as in equation (5.1), and the price of gas is assumed according to the daily value on the Gas Day Ahead Market, whose historical data are available on the GME website [144]. To take into account the distribution tariffs and the excise duties 1,7 €/MWh is added according to what the Italian regulation authority averagely reports for 2018 and 2019 [146]. The cost of emitting CO_2 is considered on an annual basis [147]. While properly

estimating the efficiency before and after the offer/bid acceptance results to be pivotal in assessing the income on the markets.

The design efficiency, η_{ref}, is assumed equal to 58% in ISO conditions (15ºC ambient temperature, 1,013 bar, 60% relative humidity), but the actual value is strongly affected by partial load operating. Combined Cycles including 2 gas turbines and 1 steam turbine ("2+1" configuration) are today a widespread technology able to increase partial load efficiency with respect to the most traditional "1+1" configuration. Within the set of power plants included in the analysis 16 are "2+1" and 29 are "1+1". Performing second-degree polynomial fittings of a fully detailed Gate Cycle model of a standard CCGT power plant [128], the dimensionless efficiency is expressed as a function of the ratio between the current and maximum possible power output. Equations (5.4) and (5.5) report the adopted dimensionless efficiency formulas for "1+1" and "2+1" configuration respectively and Figure 5.6 graphically represents the trends, for P/P_{max} values higher than 50% equation (5.4) is used on "2+1" plants as well since the load is assumed to be equally distributed on the two gas turbines. The minimum GT load is assumed to be 30%, consequently, the CCGT load is limited to 18,7% and 37,4% for "2+1" and "1+1" configurations respectively.

$$\eta/\eta_{ref} = -0.315\left(\frac{P}{P_{max}}\right)^2 + 0.732\left(\frac{P}{P_{max}}\right) + 0.583 \tag{5.4}$$

$$\eta/\eta_{ref} = -0.207\left(\frac{P}{P_{max}}\right)^2 + 0.570\left(\frac{P}{P_{max}}\right) + 0.640 \tag{5.5}$$

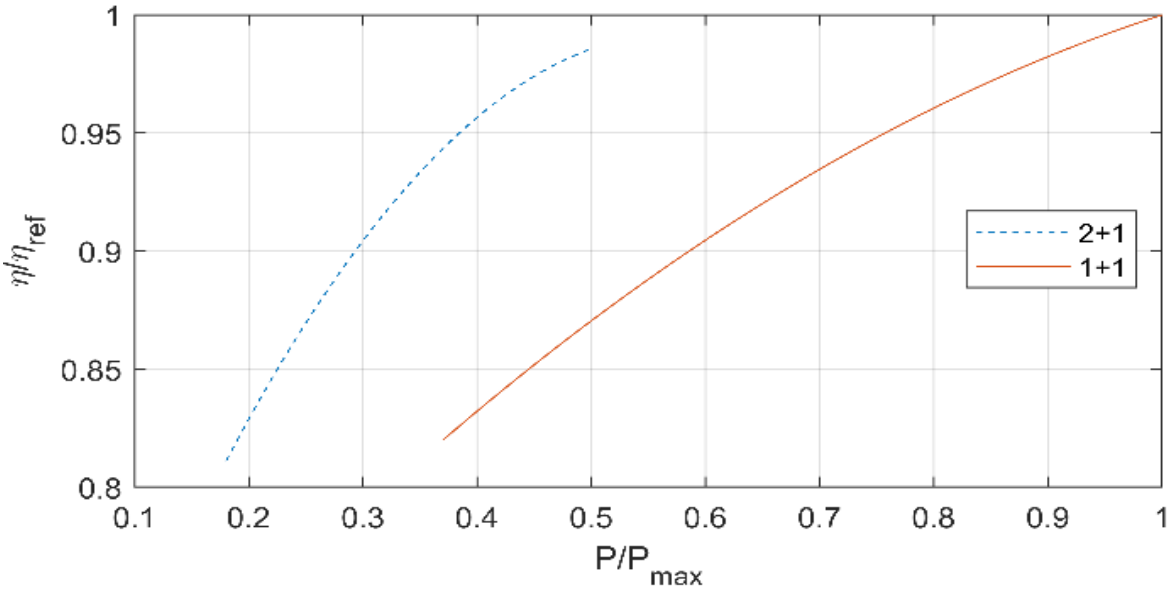

Figure 5.6: Off-design efficiency model.

On the other hand, since also ambient conditions have a relevant effect on CCGT profitability, this parameter was taken into account. The design efficiency η_{ref} is affected, even slightly, by the ambient temperature. Moreover, the temperature influences the maximum net power output P_{max}, then the off-design percentage. For this reason, the geographical coordinates of each power plant have been included in the collected information. The ambient temperature at the power plant location, for any time at which an

offer/bid was presented, is estimated by means of hourly geospatial data of the temperature at 2 m of height from the soil available on the ERA5 dataset [148] with a resolution of 9 km. The influence of the inlet temperature was the object of a previous study [128] and the adopted formulas for η_{ref} and P_{max} dependency are reported by equations (5.6) and (5.7).

$$\eta_{ref}/\eta_{ref_{ISO}} = -2.4 \cdot 10^{-5} \cdot T^2 + 8.94 \cdot 10^{-4} \cdot T + 0.993 \quad (5.6)$$

$$P_{max}/P_{max_{ISO}} = -6.5 \cdot 10^{-5} \cdot T^2 - 1.70 \cdot 10^{-5} \cdot T + 1.04 \quad (5.7)$$

Finally, the power output P is assessed by looking in the database for all the offers/bids awarded, presented by the same power plant for the same time interval, within all the market sessions whose outcomes are already published at the time the offer/bid is presented (Figure 1.7: Italian spot electricity market timing reports the spot market timing during the day).

Figure 5.7 shows the revenue distribution among the zones and the spot market sections, while Figure 5.8 reports the amount of net income for all the zones and the four spot markets, for both offers and bids. Averagely the expected income on DAM is between 40 k€/MW·yr (CNOR and CSUD zones) and 27 k€/MW·yr (SUD zone), except for Sicily, where this figure drops below 10 k€/MW·yr. The IDM demonstrates to be negligible for all the zones except for the CNOR zone, where it is a considerable source of losses. The Balancing Market, on which the prices are usually higher than on the DAM, is a source of income that covers 12.7% of the total. Most of the income on BM is realized by offers; only in the Rossano constrained zone, bids significantly contribute to the overall income. Is worth noticing how, despite the high revenues obtained in this zone, especially on DAM, net income reveals that these offers are made close to production price, just to be able to operate in the other markets. ASM is the main source of income for CSUD, SICI, and SUD zones, where on average it accounts for 2, 12, and 2 times the contribution of the DAM to the total income, providing between 62.2% and 81.0% of the profit. Thanks to the ASM contribution, CSUD results to be the most profitable zone. Here a capacity investment paid back 110 k€/MW·yr in 2018 and 159 k€/MW·yr in 2019. For CNOR and NORD zones, even if the DAM remains the most profitable market, ASM accounts 25.1% and 19.2% of the total income respectively. It is remarkable how the contribution of ASM bids is almost null when compared to the offers on the same market: only within the NORD and ROSN zone those values are comparable.

Comparing Figure 5.7 and Figure 5.8, it is possible to state that when the ratio between the revenues and the net income is low if compared to the average (e.g., SICI Day Ahead Market), generally offers are valued at high prices. On the other hand, higher ratios (e.g., ROSN Day Ahead Market) imply that offers are awarded at prices only slightly higher than the COE.

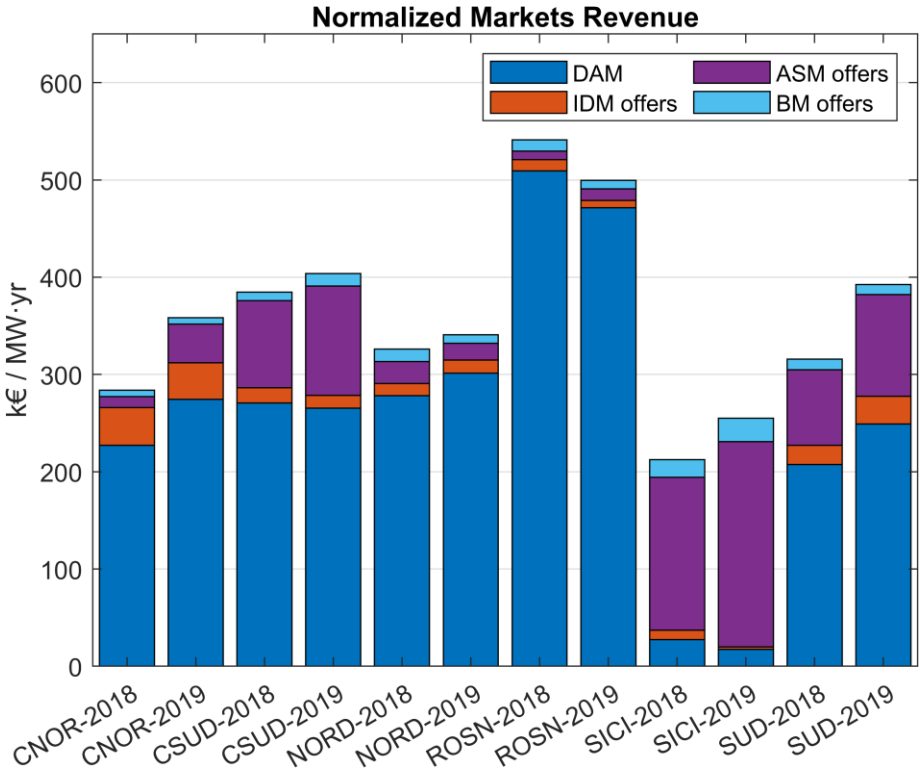

Figure 5.7: Annual revenues normalized by installed capacity.

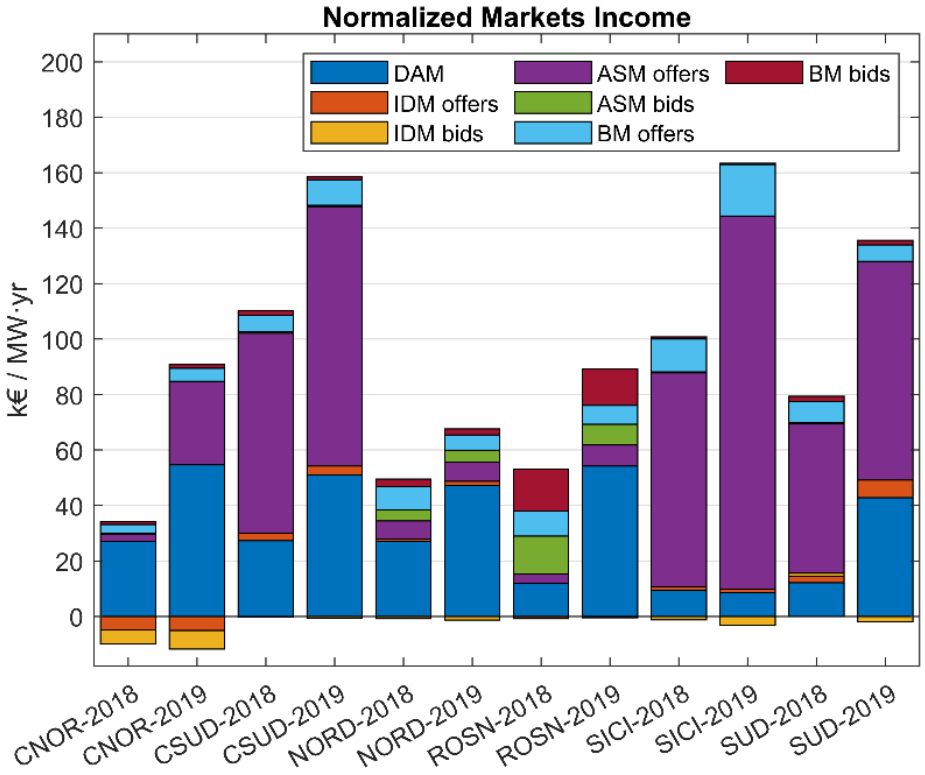

Figure 5.8: Annual net income normalized by installed capacity.

The illustrated methodology is here used to deepen the analysis, considering how the hour of the day or the month could affect the profitability of the markets. The two zones with the largest amount of installed CCGT capacity were considered: NORD and CSUD. The zone selection allows to study two different market shares: in the NORD zone the DAM is the most profitable market and offers and bids provide a similar amount of income on the ASM, while the CSUD strongly relies on the offers on the ASM and BM. The following paragraphs do not focus on the annual variability, showing for each month or hour the average between 2018 and 2019.

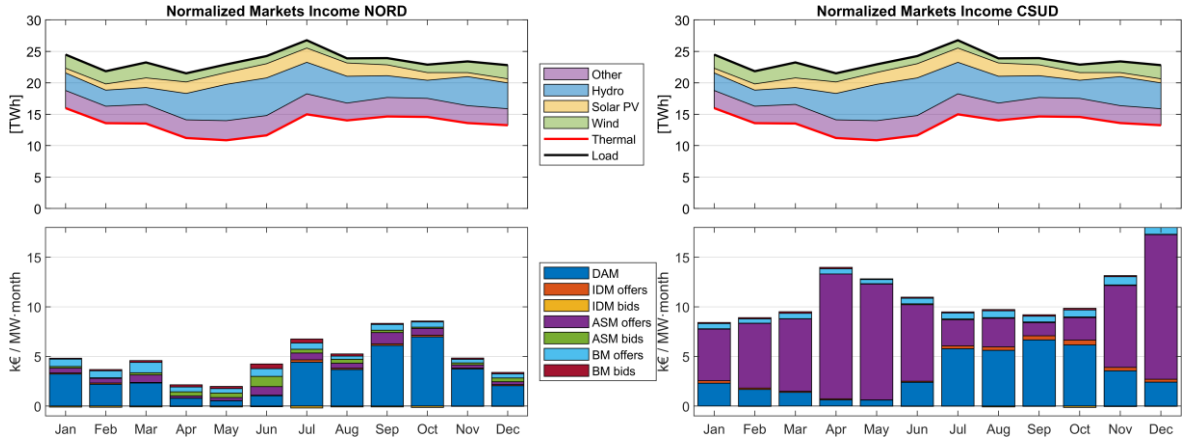

(a) *(b)*

Figure 5.9: 2018-2019 monthly net income normalized by installed capacity.

Figure 5.9 reports the month-based distribution of the normalized net income, this leads to the following considerations. Spring is the less profitable period of the year on the DAM for CCGTs in both the considered zones. Then, looking at the above chart, where the monthly average national electrical load is reported, black line, it is possible to note that during these months both hydro and solar photovoltaic increase their production [219], leaving the thermal power plants the minimum residual load, red continuous line. This affects the price in the DAM and the related opportunity of income for CCGTs, which reduces the operating hours: the residual load reaches the minimum in May (10.8 TWh/month). What differentiates the two zones are the opportunities on the ASM, since one of the main issues of this market is to provide services to the TSO to solve the intra-zonal congestions, the opportunities are dependent on the local grid characteristics. The hydroelectric energy penetration is higher within northern Italy, and these power plants are strong competitors, able to provide services at cheap prices. Indeed, during winter and late summer, when the hydro reservoirs reach the yearly minimum, CCGTs in the NORD zone (Figure 5.9 (a)) generally perform better both on DAM and ASM. On the other hand, in CSUD (Figure 5.9 (b)), CCGTs are more essential in providing services to the grid and this market position is reflected in an income increment.

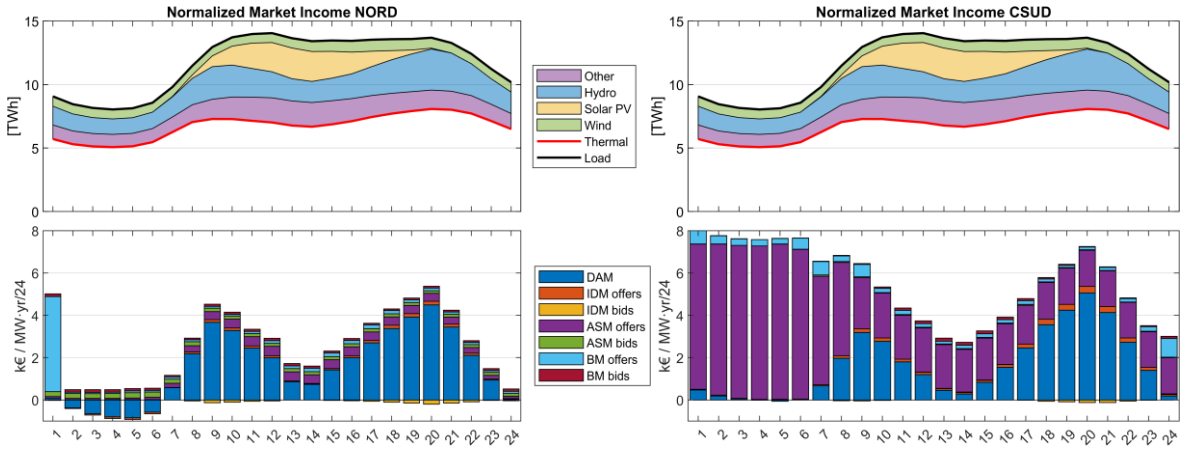

(c) *(d)*

Figure 5.10: 2018-2019 hourly net income normalized by installed capacity.

Figure 5.10 reports the hour-based distribution. In both zones, the DAM income demonstrates to be strongly dependent on the hourly market clearing price, typically peaking in the morning and the early evening and directly correlated to the residual load curve, the red line on the above chart. Nevertheless CCGT power plants follow a different offer strategy in the two zones. In the NORD (Figure 5.10 (a)) the DAM income is negative during the night, this means that operators prefer to keep the plant running despite the low electricity price, even if losing money, to avoid an expensive daily start-up. On the other hand, in the CSUD zone, due to the little hydro capacity installed, CCTGs are more essential for grid stability, providing services all day long. In particular, during low load or DAM price periods, operating in ASM results to be more profitable, and operators prefer this market rather than DAM because of the higher prices. The contribution from the IDM and BM is lower than other markets, nevertheless, it is always proportionate to the DAM income for the same hour. Only during the first hour of the day, in the NORD zone the BM overcontributes to the overall profits, this strange behavior, present in both years, is related to market resolution at D-1 and probably represents a market distortion effect. The ratio between the profitability of offers and bids on the ASM shows no variability with the hour of the day and it seems to be more related to grid characteristics within the zone.

5.3. Ancillary Services market modeling

In previous chapters of this thesis, many times the need to flexibilize the energy system, power plants, and storage technologies has been emphasized. The previous section of this chapter has highlighted how the economic value of flexibility is awarded in the services markets. Classic techno-economic modeling, considering only the energy markets, can lead to relevant errors in assessing the viability of new, or existing, technologies providing services to the electrical grid. These errors have been quantified in Section 5.2. These are the motivations that have led to the development of a reliable tool able to solve dispatch optimization taking into account the opportunities both in the Day-Ahead Market and Ancillary Services Market considering the uncertainty of offer acceptance in the latter.

Subsection 5.3.1 describes a Mixed Integer Linear Programming (MILP) approach to the problem, the mathematical formulation includes the probability of acceptance of each offer presented by the power plant. Subsection 5.3.2 faces the problem of probability quantification by a machine learning approach applied to the Italian market as a case study. The last subsection reports some application examples of the developed tools.

5.3.1. MILP problem formulation

The model introduced in this section presents a novel approach that implements a simultaneous optimization of both the market strategies (on the day ahead and ancillary services market), taking a relevant step further from the methodology presented in [234], where the DAM dispatch is optimized first and the following ASM optimization is limited by the plant capacity and minimum load and DAM schedule. A simultaneous optimization could lead to a non-optimal solution on the single market but the expected optimum is reached summing of the two markets together.

The MILP approach address the dispatch optimization of a general power generation in which power output has been discretized into nLoad operational modes including 0 MW (0%) and the maximum capacity. A storage technology can be modeled analogously, during the discharging it can be assimilated to a power generator (100% at full discharging load), during the charging it is equivalent to a generator with negative power output (-100% at full charging load). The discretization does not require to be evenly spaced so that if a specific technology requires to operate at the least at a minimum load it will be sufficient to discretize its power output including a null output, the minimum load, the maximum capacity, and a variable number of mode at intermediate loads. It should be considered that the power output resolution has a great impact on the time required to solve the problem.

The problem consists in determining the best load (among those considered by the discretization) and the best offer or bid to present on the ASM for each time step t. Basically, the generator will be allowed to operate according to nMod operational modes. With nMod=nLoad^2, in fact for each load scheduled after the DAM closure there the generator can present an offer to increase its power output to any higher load, can present a bid to lower the output according to the discretization, eventually, it can maintain its schedule without any offer or bid on the ASM.

The best operational mode (i.e., a combination of DAM load and offer/bid on the ASM) is that which maximizes the overall expected profits considering both markets. Equation 5.8 defines the objective function.

$$ExpProf = \sum_{t=1}^{n\ hours} Profits^{DAM}{}_t + ExpProfits^{ASM}{}_t - ExpC_{SU}{}_t \quad (5.8)$$

The total expected profits must be maximized and are the sum of three main components:

- Profits on the DAM, as defined by Equation 5.9, are the difference between the electricity price and the cost of generating the electricity [€/MWh] times the quantity sold on this market [MWh]. The electricity price on the DAM is assumed to be known in advance so that there is no uncertainty about this profit

$$Profits^{DAM}{}_t = \left(pr_{el}^{DAM}{}_t - COE^{DAM}{}_t\right) \cdot Q^{DAM}{}_t \quad (5.9)$$

- Expected Profits on the ASM, equations 5.2 and 5.3 define the profits associated with each offer and bid on the ASM, the expected profits takes also into account the probability of offer/bid acceptance

$$ExpProfits^{ASM}{}_t = Profits^{ASM}{}_t \cdot ACC_{prob}{}_t \quad (5.10)$$

- The expected start-up cost. The start-up in many cases has a relevant cost, in terms of fuel and components life consumption due to thermal and mechanical stresses

in this transient. However, even if the cost of start-up at the time t is known, there is no certainty about the offers/bids acceptance which can modify the generator status (on/off) at the time t and at the time t-1. Because of that, it must be defined the expected SU costs in equation 5.8. Equations 5.12 and 5.13 define the SU probability, where the $Load^{DAM}$ is the load after the DAM closure and $Load^{ASM}$ is the load that the power plant should adopt if the presented offer/bid is accepted.

$$ExpC_{SU_t} = C_{SU_t} \cdot SU_{prob_t} \tag{5.11}$$

$$SU_{prob_t} = On_{prob_t} \cdot Off_{prob_{t-1}} = On_{prob_t} \cdot \left(1 - On_{prob_{t-1}}\right) \tag{5.12}$$

$$On_{prob_t} = \begin{cases} 1, & Load^{DAM} > 0 \; and \; Load^{ASM} > 0 \\ ACC_{prob_t}, & Load^{DAM} = 0 \; and \; Load^{ASM} > 0 \\ 1 - ACC_{prob_t}, & Load^{DAM} > 0 \; and \; Load^{ASM} = 0 \\ 0, & Load^{DAM} = 0 \; and \; Load^{ASM} = 0 \end{cases} \tag{5.13}$$

Equation 5.12 states clearly that the profits at the time t depend on the operational mode (i.e., the combination of DAM schedule and offer/bid presented on the ASM) at the time t-1. To deal with this, the number of the operational mode that can be selected is increased to $nMod^* = nMod^2$. Each mode* defines an operational mode at the time t and at the time t-1.

Equation 5.14 defines the MILP problem:

$$\max_x f^T \cdot x, \qquad subject\ to \begin{cases} x(1{:}\, nMod^*)\ are\ integers \\ 0 \le x \le 1 \\ A \cdot \mathrm{x} \le \mathrm{b} \end{cases} \tag{5.14}$$

Even if most linear programming solvers require f and x to be 1-D vectors, is possible to implement the problem by initializing f as a 5-D array reshaping it before calling the solver, and reshaping x back to 5 dimensions once the solution has been found. The 5 dimensions are relative to:

- $Load^{DAM}$ at time t
- $Load^{ASM}$ at time t
- $Load^{DAM}$ at time t-1
- $Load^{ASM}$ at time t-1
- Time interval

So that:

$$f^*_{i,j,k,z,t} = \left(pr_{el}^{DAM}{}_t - COE^{DAM}{}_{i,t}\right) \cdot Q^{DAM}{}_{i,t} + Profits^{ASM}{}_{i,j,t} \cdot ACC_{prob}{}_{i,j,t} \tag{5.15}$$

After f^* has been implemented and reshaped to the column vector f^{**} further elements (as many as the considered time intervals nInterval) must be added to obtain the vector f of equation 5.14.

$$f = \begin{bmatrix} f^{**} \\ -C_{SU} \end{bmatrix} \tag{5.16}$$

According to the aforereported equations, the solution x will be a vector of N elements, with $N = nLoad^4 \cdot nInterval + nInterval$. The first $nLoad^4 \cdot nInterval$ elements are constrain to

be 0 or 1, $x^*(i,j,k,z,t)=1$ if and only if the relative mode is selected[36]. The last nInterval elements of x represent auxiliaries variables to take into account the expected start-up cost as defined by equation 5.11.

MILP formulation, equation 5.14, reports also the constraint to which the problem is subject to. In addition to integer constraints and upper and lower bounds, which need no further explanation, the problem is subject to linear inequality constraints defined by matrix A and column vector b. A is sized N-by-M, b has a length equal to M, where M is the number of constraints, $M=3\cdot nInterval + nInterval \cdot nLoad^2$.

- nInterval constraints impose that the start-up auxiliary variable at the time t is equal to, or greater than, the start-up probability at the time t. Of course, the optimal value of the auxiliary variables is the minimum allowed, since it multiplies $C_{SU\ t}$. However, imposing an equality constraint is much more expensive in terms of computational time. So the constraint is expressed by the inequality of equation 5.16 and the solver will select the minimum allowed value

$$x_{\mathrm{nInterval}\cdot nLoad^4+t} \geq SU_{prob_{i,j,k,z,t}} \tag{5.17}$$

- $2\cdot nInterval$ constraints impose that at the least one, and no more than one, operating mode is selected for the time t

$$\exists!\, x^*_{i,j,k,z,t} = 1, \qquad \forall 1 \leq t \leq nInterval \text{ and } \forall 1 \leq, i,j,k,z \leq nLoad \tag{5.18}$$

- $nInterval \cdot nLoad^2$ constraints impose the consistency between the time t and t-1. For the first time interval (t=1) the consistency is imposed with respect to the status t-1=0 which is imposed as a boundary condition.

$$x^*_{i,j,a,b,t} = x^*_{a,b,k,z,t-1}, \qquad \forall 2 \leq t \leq nInterval \text{ and } \forall 1 \leq a,b,i,j,k,z \leq nLoad \tag{5.19}$$

$$x^*_{i,j,a,b,1} = x^*_{t=0}, \qquad \forall 1 \leq i,j \leq nLoad \tag{5.20}$$

Defined the problem and all the constraints the problem can be solved, the Subsection 5.3.3 shows some outputs of the problem solved in MATLAB by the intlinprog function [235].

Time discretization in many markets is on an hourly basis, but the resolution adopted can be reduced (some service markets work with 15-min time intervals) without any change in the mathematical formulation given in this subsection.

However, it should be considered that the assumption of a known price on the DAM is no longer reliable as nInterval increases covering a period of many days. To simulate longer periods they are divided into subperiods, covering a time horizon on which is reasonable to assume the DAM price as known, typically 1 or 2 days. Defined this period then the simulation time window is progressively shifted. This approach is a well-known practice for MILP problems, successfully applied by [236]. Figure 5.11 shows a sliding window application for a period of n days, the window size is selected to be 2 days but only the first day is kept, the second day will be overwritten by the first day of the second simulation, and so on. The solution relative to the last time interval considered (e.g., the 24th according to the example in Figure 5.11) is imposed to the following simulation as the $x^*_{t=0}$ constraint.

[36] x^* is the reshaped 5-D solution excluding the auxiliary variables.

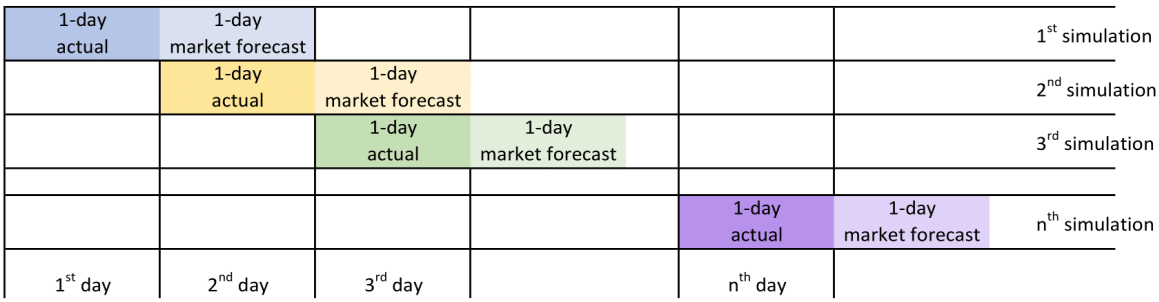

Figure 5.11: Visualization of the sliding windows approach for MILP.

5.3.2. Machine Learning approach for the prediction of offers and bids acceptance

The previous subsection described the MILP approach including the objective function and the constraints. It is clarified how the uncertainty of success in the service market plays a crucial role (equations 5.12, 5.13, 5.15, and 5.16). This subsection is focused on how to assess the $ACC_{prob\ i,j,t}$ (i.e., for each DAM schedule, each possible offer/bid, and each time interval t). The described MILP methodology is general and can be applied to different contexts, however, to predict the ASM offer/bid probability is needed to select a specific case study since the local market designs and the available data impose to differentiate the approach. For this purpose the Italian ASM (*Mercato dei Servizi di Dispacciamento*) is selected.

5.3.2.1. Italian case study: raw data and pre-processing

Subsection 1.1.1.1 addresses the Italian market design, describing how each unit (e.g., power generator, storage facility, or virtual aggregator) can present offers and bids showing its availability to revise the schedule, defined after the DAM and the IDM closure, upward or downward.

On the *Gestori dei Mercati Energetici* (GME) website [144], a public domain of the presented offers and bids is available. Data are available as a zipped file for every single day, containing a .xml file for each market. Figure 5.12 and Figure 5.13 provide the file, relative to 31/12/2021, imported in Microsoft Access in Datasheet and Design view respectively. The Appendix's Table A.1 reports the list of all the power plants active in the ancillary services markets from 2018 to 2021 which was possible to identify and to which the analysis is therefore limited.

OfferteOperatori

PURPOSE_CD	TYPE_CD	STATUS_CD	MARKET_CD	UNIT_REFERENCE_NO	INTERVAL_NO	BID_OFFER_DATE_DT	TRANSACTION_REFERENCE_NO	QUANTITY_NO	AWARDED_QUANTITY_NO
BID	STND	REJ	MSD	UP_ACTV_1	1	20211231	3349476483	31	0
BID	STND	REJ	MSD	UP_ACTV_1	1	20211231	3349476483	0	0
OFF	STND	REJ	MSD	UP_ACTV_1	1	20211231	3349476483	5.2	0
OFF	STND	REJ	MSD	UP_ACTV_1	1	20211231	3349476483	5	0
OFF	STND	REJ	MSD	UP_ACTV_1	1	20211231	3349476483	0	0
OFF	STND	REJ	MSD	UP_ACTV_1	1	20211231	3349476483	0	0
OFF	STND	SUB	MSD	UP_ACTV_1	1	20211231	3349476483	26	0
BID	STND	REJ	MSD	UP_ACTV_1	2	20211231	3349478835	31	0
BID	STND	REJ	MSD	UP_ACTV_1	2	20211231	3349478835	0	0
OFF	STND	REJ	MSD	UP_ACTV_1	2	20211231	3349478835	5.1	0
OFF	STND	REJ	MSD	UP_ACTV_1	2	20211231	3349478835	5	0
OFF	STND	REJ	MSD	UP_ACTV_1	2	20211231	3349478835	0	0
OFF	STND	REJ	MSD	UP_ACTV_1	2	20211231	3349478835	0	0
OFF	STND	SUB	MSD	UP_ACTV_1	2	20211231	3349478835	26	0
BID	STND	REJ	MSD	UP_ACTV_1	3	20211231	3349481187	31	0
BID	STND	REJ	MSD	UP_ACTV_1	3	20211231	3349481187	0	0
OFF	STND	REJ	MSD	UP_ACTV_1	3	20211231	3349481187	5.1	0
OFF	STND	REJ	MSD	UP_ACTV_1	3	20211231	3349481187	5	0
OFF	STND	REJ	MSD	UP_ACTV_1	3	20211231	3349481187	0	0
OFF	STND	REJ	MSD	UP_ACTV_1	3	20211231	3349481187	0	0
OFF	STND	SUB	MSD	UP_ACTV_1	3	20211231	3349481187	26	0
BID	STND	REJ	MSD	UP_ACTV_1	4	20211231	3349483539	31	0
BID	STND	REJ	MSD	UP_ACTV_1	4	20211231	3349483539	0	0
OFF	STND	REJ	MSD	UP_ACTV_1	4	20211231	3349483539	5.1	0
OFF	STND	REJ	MSD	UP_ACTV_1	4	20211231	3349483539	5	0
OFF	STND	REJ	MSD	UP_ACTV_1	4	20211231	3349483539	0	0
OFF	STND	REJ	MSD	UP_ACTV_1	4	20211231	3349483539	0	0
OFF	STND	SUB	MSD	UP_ACTV_1	4	20211231	3349483539	26	0
BID	STND	REJ	MSD	UP_ACTV_1	5	20211231	3349485891	31	0
BID	STND	REJ	MSD	UP_ACTV_1	5	20211231	3349485891	0	0
OFF	STND	REJ	MSD	UP_ACTV_1	5	20211231	3349485891	0	0
OFF	STND	REJ	MSD	UP_ACTV_1	5	20211231	3349485891	5.1	0
OFF	STND	REJ	MSD	UP_ACTV_1	5	20211231	3349485891	5	0
OFF	STND	REJ	MSD	UP_ACTV_1	5	20211231	3349485891	0	0
OFF	STND	SUB	MSD	UP_ACTV_1	5	20211231	3349485891	26	0
BID	STND	REJ	MSD	UP_ACTV_1	6	20211231	3349488243	0	0
BID	STND	REJ	MSD	UP_ACTV_1	6	20211231	3349488243	31	0
OFF	STND	REJ	MSD	UP_ACTV_1	6	20211231	3349488243	5.2	0
OFF	STND	REJ	MSD	UP_ACTV_1	6	20211231	3349488243	5	0
OFF	STND	REJ	MSD	UP_ACTV_1	6	20211231	3349488243	0	0
OFF	STND	REJ	MSD	UP_ACTV_1	6	20211231	3349488243	0	0
OFF	STND	SUB	MSD	UP_ACTV_1	6	20211231	3349488243	26	0
BID	STND	REJ	MSD	UP_ACTV_1	7	20211231	3349490595	0	0
BID	STND	REJ	MSD	UP_ACTV_1	7	20211231	3349490595	31	0
OFF	STND	REJ	MSD	UP_ACTV_1	7	20211231	3349490595	5.2	0
OFF	STND	REJ	MSD	UP_ACTV_1	7	20211231	3349490595	5	0

ENERGY_PRICE_NO	PARTIAL_QT	ADJ_QUANTITY_NO	ADJ_ENERGY_PRICE_NO	GRID_SUPPL	ZONE_CD	AWARDED_PRICE_NO	OPERATORE	SUBMITTED_DT	SCOPE
89	N	0		89 PSR_193	NORD		89 ALPIQ ENERGIA ITALIA S.p.A.	20211230170503403	AS
89	N	0		89 PSR_193	NORD		89 ALPIQ ENERGIA ITALIA S.p.A.	20211230170503403	GR1
453	N	4.9		453 PSR_193	NORD		453 ALPIQ ENERGIA ITALIA S.p.A.	20211230170503403	GR3
453	N	5		453 PSR_193	NORD		453 ALPIQ ENERGIA ITALIA S.p.A.	20211230170503403	GR2
453	N	0		453 PSR_193	NORD		453 ALPIQ ENERGIA ITALIA S.p.A.	20211230170503403	GR1
453	N	31		453 PSR_193	NORD		453 ALPIQ ENERGIA ITALIA S.p.A.	20211230170503403	AS
97	N	26		97 PSR_193	NORD		0 ALPIQ ENERGIA ITALIA S.p.A.	20211230170503403	ACC
89	N	0		89 PSR_193	NORD		89 ALPIQ ENERGIA ITALIA S.p.A.	20211230170504357	AS
89	N	0		89 PSR_193	NORD		89 ALPIQ ENERGIA ITALIA S.p.A.	20211230170504357	GR1
453	N	4.9		453 PSR_193	NORD		453 ALPIQ ENERGIA ITALIA S.p.A.	20211230170504357	GR3
453	N	5		453 PSR_193	NORD		453 ALPIQ ENERGIA ITALIA S.p.A.	20211230170504357	GR2
453	N	0		453 PSR_193	NORD		453 ALPIQ ENERGIA ITALIA S.p.A.	20211230170504357	GR1
453	N	31		453 PSR_193	NORD		453 ALPIQ ENERGIA ITALIA S.p.A.	20211230170504357	AS
97	N	26		97 PSR_193	NORD		0 ALPIQ ENERGIA ITALIA S.p.A.	20211230170504357	ACC
89	N	0		89 PSR_193	NORD		89 ALPIQ ENERGIA ITALIA S.p.A.	20211230170505123	AS
89	N	0		89 PSR_193	NORD		89 ALPIQ ENERGIA ITALIA S.p.A.	20211230170505123	GR1
453	N	4.9		453 PSR_193	NORD		453 ALPIQ ENERGIA ITALIA S.p.A.	20211230170505123	GR3
453	N	5		453 PSR_193	NORD		453 ALPIQ ENERGIA ITALIA S.p.A.	20211230170505123	GR2
453	N	0		453 PSR_193	NORD		453 ALPIQ ENERGIA ITALIA S.p.A.	20211230170505123	GR1
453	N	31		453 PSR_193	NORD		453 ALPIQ ENERGIA ITALIA S.p.A.	20211230170505123	AS
97	N	26		97 PSR_193	NORD		0 ALPIQ ENERGIA ITALIA S.p.A.	20211230170505123	ACC
89	N	0		89 PSR_193	NORD		89 ALPIQ ENERGIA ITALIA S.p.A.	20211230170505950	AS
89	N	0		89 PSR_193	NORD		89 ALPIQ ENERGIA ITALIA S.p.A.	20211230170505950	GR1
453	N	4.9		453 PSR_193	NORD		453 ALPIQ ENERGIA ITALIA S.p.A.	20211230170505950	GR3
453	N	5		453 PSR_193	NORD		453 ALPIQ ENERGIA ITALIA S.p.A.	20211230170505950	GR2
453	N	0		453 PSR_193	NORD		453 ALPIQ ENERGIA ITALIA S.p.A.	20211230170505950	GR1
453	N	31		453 PSR_193	NORD		453 ALPIQ ENERGIA ITALIA S.p.A.	20211230170505950	AS
97	N	26		97 PSR_193	NORD		0 ALPIQ ENERGIA ITALIA S.p.A.	20211230170505950	ACC
89	N	0		89 PSR_193	NORD		89 ALPIQ ENERGIA ITALIA S.p.A.	20211230170506687	AS
89	N	0		89 PSR_193	NORD		89 ALPIQ ENERGIA ITALIA S.p.A.	20211230170506687	GR1
453	N	31		453 PSR_193	NORD		453 ALPIQ ENERGIA ITALIA S.p.A.	20211230170506687	AS
453	N	4.9		453 PSR_193	NORD		453 ALPIQ ENERGIA ITALIA S.p.A.	20211230170506687	GR3
453	N	5		453 PSR_193	NORD		453 ALPIQ ENERGIA ITALIA S.p.A.	20211230170506687	GR2
453	N	0		453 PSR_193	NORD		453 ALPIQ ENERGIA ITALIA S.p.A.	20211230170506687	GR1
97	N	26		97 PSR_193	NORD		0 ALPIQ ENERGIA ITALIA S.p.A.	20211230170506687	ACC
89	N	0		89 PSR_193	NORD		89 ALPIQ ENERGIA ITALIA S.p.A.	20211230170507420	GR1
89	N	0		89 PSR_193	NORD		89 ALPIQ ENERGIA ITALIA S.p.A.	20211230170507420	AS
453	N	4.9		453 PSR_193	NORD		453 ALPIQ ENERGIA ITALIA S.p.A.	20211230170507420	GR3
453	N	5		453 PSR_193	NORD		453 ALPIQ ENERGIA ITALIA S.p.A.	20211230170507420	GR2
453	N	0		453 PSR_193	NORD		453 ALPIQ ENERGIA ITALIA S.p.A.	20211230170507420	GR1
453	N	31		453 PSR_193	NORD		453 ALPIQ ENERGIA ITALIA S.p.A.	20211230170507420	AS
97	N	26		97 PSR_193	NORD		0 ALPIQ ENERGIA ITALIA S.p.A.	20211230170507420	ACC
89	N	0		89 PSR_193	NORD		89 ALPIQ ENERGIA ITALIA S.p.A.	20211230170508187	GR1
89	N	0		89 PSR_193	NORD		89 ALPIQ ENERGIA ITALIA S.p.A.	20211230170508187	AS
453	N	4.9		453 PSR_193	NORD		453 ALPIQ ENERGIA ITALIA S.p.A.	20211230170508187	GR3
453	N	5		453 PSR_193	NORD		453 ALPIQ ENERGIA ITALIA S.p.A.	20211230170508187	GR2

Figure 5.12: Microsoft Access Datasheet view of the file 20211231MSDOffertePubbliche.xml relative to MSD offers and bids presented on 31/12/2021.

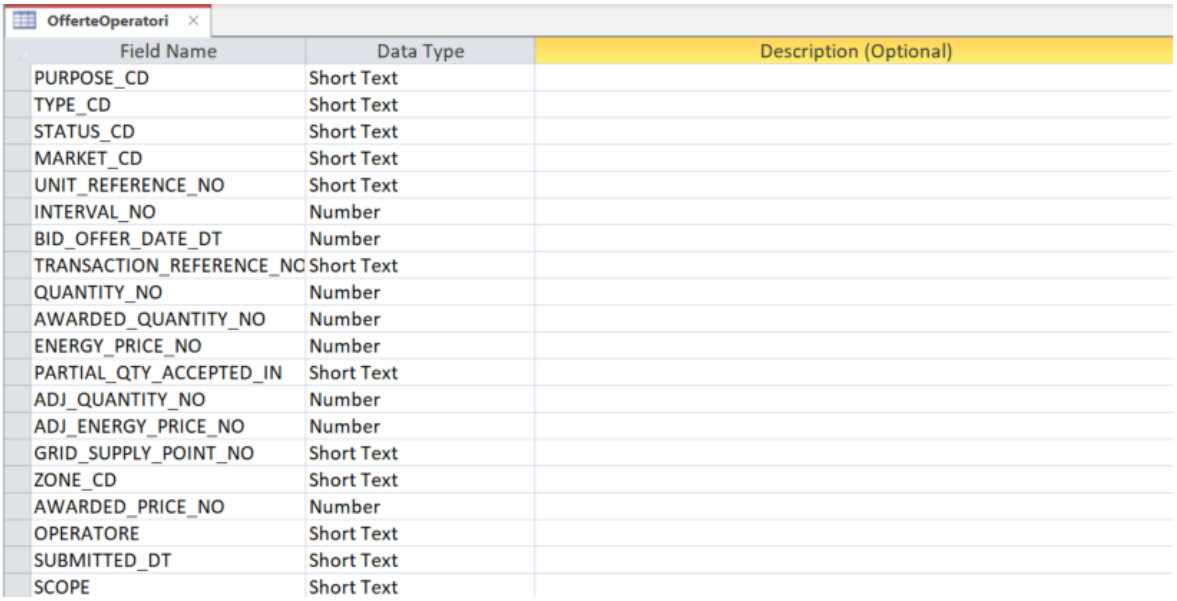

OfferteOperatori

Field Name	Data Type	Description (Optional)
PURPOSE_CD	Short Text	
TYPE_CD	Short Text	
STATUS_CD	Short Text	
MARKET_CD	Short Text	
UNIT_REFERENCE_NO	Short Text	
INTERVAL_NO	Number	
BID_OFFER_DATE_DT	Number	
TRANSACTION_REFERENCE_NO	Short Text	
QUANTITY_NO	Number	
AWARDED_QUANTITY_NO	Number	
ENERGY_PRICE_NO	Number	
PARTIAL_QTY_ACCEPTED_IN	Short Text	
ADJ_QUANTITY_NO	Number	
ADJ_ENERGY_PRICE_NO	Number	
GRID_SUPPLY_POINT_NO	Short Text	
ZONE_CD	Short Text	
AWARDED_PRICE_NO	Number	
OPERATORE	Short Text	
SUBMITTED_DT	Short Text	
SCOPE	Short Text	

Figure 5.13: Microsoft Access Design view of the file 20211231MSDOffertePubbliche.xml relative to MSD offers and bids presented on 31/12/2021.

Each .xml file has the following fields:

- PURPOSE_CD: can be OFF or BID, indicate if the purpose is to increase or decrease the injection to the grid
- TYPE_CD: indicates whether the offer/bid is predefined (STND) or current (REG)
- STATUS_CD: Status of offer/bid after the market execution, accepted (ACC), rejected (REJ), inadequate (INC), replaced (REP), revoked (REV), submitted (SUB)
- MARKET_CD: identify the market, MSD for the ancillary services market.
- UNIT_REFERENCE_CD: Identification code of the market unit
- INTERVAL_NO: Is an integer number identifying the hourly time interval, from 1 to 24 (25 in the day of daylight saving time to standard time switch)
- BID_OFFER_DATE_DT: Date on which the bid/offer refers in the YYYYMMDD format
- TRANSACTION_REFERENCE_NO: Offer identifier
- QUANTITY_NO: Volume [MWh] offered/bid
- AWARDED_QUANTITY_NO: Volume awarded on the market
- ENERGY_PRICE_NO: Price [€/MWh] offered/bid
- PARTIAL_QTY_ACCEPTED_IN: Binary variable indicating if the offer/bid has been partially accepted, N if the AWARDED_QUANTITY_NO is equal to 0 or to ADJ_QUANTITY_NO, Y otherwise.
- ADJ_QUANTITY_NO: Adjusted offer/bid volume to fulfill the constraints imposed by the grid code
- ADJ_ENERGY_PRICE_NO: Adjusted offer/bid price to fulfill the constraints imposed by the grid code

- GRID_SUPPLY_POINT_NO: Grid supply point to which the unit is associated
- ZONE_CD: Bidding zone to which the unit belongs
- AWARDED_PRICE_NO: Awarded price on the market, in Italy the ASM is a pay-as-bid market, so the awarded price is equal to the adjusted price
- OPERATORE: Market operator, typically the
- SUBMITTED_DT: Date on which the offer/bid has been submitted YYYYMMMDDhhmmssfff
- SCOPE: type of service offered

The described raw data are processed and selected to create the dataset on which the machine learning algorithms are trained and tested. The period covers the last complete four years (from 2018 to 2021) the number of offers/bids is in the order of 10^7. Only predefined offers/bids and only accepted or rejected, have been considered. The analysis is also limited to the 216 units which were possible to identify (99 gas-fired generators, 19 coal-fired, 5 oil-fired, and 93 hydro). And, to train proper models the predictors are selected or derived from the raw data and gathered as follows:

- Offer/bid specificity predictors: PURPOSE_CD, SCOPE
- Offer/bid time predictors: INTERVAL_NO, MONTH (month on which the offer is submitted), DAY_TYPE (H for holydays, B for weekdays)
- Offer/bid strategy predictors: ADJ_QUANTITY_NO and ADJ_ENERGY_PRICE, so that the fulfillment of the grid code is assumed
- Market indicator predictors: MGAS_MGP (the spot gas market price on the day the bid/offer is presented), PUN (Single National electricity price on the DAM on the hour on which the offer/bid is presented), Zonal_price (zonal electricity price on the DAM on the hour the offer/bid is presented)
- Units predictors: Voltage (the voltage level of the grid to which the unit is connected [kV]), Lat, and Long (latitude and longitude degrees of the capital of the administrative province in which the unit is located)[37]

[37] Include geographical information can have a twofold effect. On one side the geospatial dependency of the ASM opportunities is widely acknowledged, so including this information to the Machine Learning algorithms would allow to keep it into consideration. On the other hand it could lead to overfitted models, especially for Tree and Ensemble model the risk is to train specific sub models for each latitude and longitude couple (i.e., each unit). So the geographical information is provided to the algorithm as the coordinates of the province capital. So that the information is general enough to mitigate the overfitting risk, province can however describes the opportunities, as assumed by [240], since often the boundaries coincides with orographic barriers which have constrained the grid development in the past.

Different models are trained including or not including the Lat and Long, which will be referred to as GEO and NOGEO respectively. Different degree of model optimization is also tested differentiating between Corse and Fine models:

- Coarse: 5 cross-validation folders, maximum 30 function evaluations during optimization, MATLAB automatic selection of optimized hyperparameters
- Fine: 15 cross-validation folders, maximum 50 function evaluations during optimization, all hyperparameters are optimized

Concerning the training and test split, in order to test the ability of the model to predict the probability of acceptance in different years, data from one year forms the test dataset, and data from the other years are used for training. To include in the training set offers/bids from both exceptionally high and low gas price market scenarios, 2019 is selected to be the test dataset, 2018, 2020, and 2021 the training. In fact, market prices in 2020 were very low, because of the COVID-19 pandemic measures, while in 2021 (especially during Q4) prices were extremely high because of the beginning of the current energy crisis. To reduce computational time training is carried out on stratified partitions equal to 1%, 5%, and 10% of the whole dataset. Figure 5.14 provides a visualization of the preprocessed data in MATLAB.

6214458x13 table

	1 PURPOSE_CD	2 STATUS_CD	3 INTERVAL_NO	4 ADJ_QUANTITY_NO	5 ADJ_ENERGY_PRICE_NO	6 ZONE_CD	7 SCOPE	8 MONTH	9 DAY_TYPE	10 MGAS_MGP	11 Voltage	12 PUN	13 Zonal_price
1	OFF	REJ	1	31	130	NORD	AS	1	H	27.2877	132	51	51
2	OFF	REJ	1	5	130	NORD	GR2	1	H	27.2877	132	51	51
3	OFF	REJ	1	5.2000	130	NORD	GR3	1	H	27.2877	132	51	51
4	OFF	REJ	1	31	130	NORD	AS	2	B	27.2877	132	51	51
5	OFF	REJ	1	5	130	NORD	GR2	2	B	27.2877	132	51	51
6	OFF	REJ	1	5.3000	130	NORD	GR3	2	B	27.2877	132	51	51
7	OFF	REJ	1	31	130	NORD	AS	3	B	27.2877	132	51	51
8	OFF	REJ	1	5	130	NORD	GR2	3	B	27.2877	132	51	51
9	OFF	REJ	1	5	130	NORD	GR3	3	B	27.2877	132	51	51
10	OFF	REJ	1	31	100	NORD	AS	4	B	27.2877	132	51	51
11	OFF	REJ	1	5	100	NORD	GR2	4	B	27.2877	132	51	51
12	OFF	REJ	1	4.3000	100	NORD	GR3	4	B	27.2877	132	51	51
13	OFF	REJ	1	31	100	NORD	AS	5	H	27.2877	132	51	51
14	OFF	REJ	1	5	100	NORD	GR2	5	H	27.2877	132	51	51
15	OFF	REJ	1	3.8000	100	NORD	GR3	5	H	27.2877	132	51	51
16	OFF	REJ	1	29.6000	100	NORD	AS	6	H	27.2877	132	51	51
17	OFF	REJ	1	5	100	NORD	GR2	6	H	27.2877	132	51	51
18	OFF	REJ	1	3.4000	100	NORD	GR3	6	H	27.2877	132	51	51
19	OFF	REJ	1	25.6000	75	NORD	AS	7	B	27.2877	132	51	51
20	OFF	REJ	1	4	75	NORD	GR2	7	B	27.2877	132	51	51
21	OFF	REJ	1	3.1000	75	NORD	GR3	7	B	27.2877	132	51	51
22	OFF	REJ	1	26.3000	75	NORD	AS	8	B	27.2877	132	51	51
23	OFF	REJ	1	4	75	NORD	GR2	8	B	27.2877	132	51	51
24	OFF	REJ	1	3.4000	75	NORD	GR3	8	B	27.2877	132	51	51
25	OFF	REJ	1	27.4000	79	NORD	AS	9	H	27.2877	132	51	51
26	OFF	REJ	1	4	79	NORD	GR2	9	H	27.2877	132	51	51
27	OFF	REJ	1	3.6000	79	NORD	GR3	9	H	27.2877	132	51	51
28	OFF	REJ	1	29.2000	79	NORD	AS	10	B	27.2877	132	51	51
29	OFF	REJ	1	4	79	NORD	GR2	10	B	27.2877	132	51	51
30	OFF	REJ	1	4.1000	79	NORD	GR3	10	B	27.2877	132	51	51
31	OFF	REJ	1	31	79	NORD	AS	11	H	27.2877	132	51	51
32	OFF	REJ	1	4	79	NORD	GR2	11	H	27.2877	132	51	51
33	OFF	REJ	1	4.6000	79	NORD	GR3	11	H	27.2877	132	51	51
34	OFF	REJ	1	21	101	NORD	AS	12	H	27.2877	132	51	51
35	OFF	REJ	1	5	101	NORD	GR2	12	H	27.2877	132	51	51

Figure 5.14: MATLAB visualization of the training table, input of algorithms training the classifiers, STATUS_CD is the target variables, the others column the predictors, Lat and Long are excluded (NOGEO model).

5.3.2.2. Models assessment and selection

Different models have been trained with the purpose of comparing each other. In addition to the already mentioned features (GEO/NOGEO, fine/coarse), models are distinguished for the algorithm, and the following options have been tested[38]:

- Classification tree (fitctree)
- Ensemble classifier (fitcensemble)
- Discriminant Analysis classifier
- Naive Bayes (NB) classifier (fitcnb)
- k-Nearest Neighbors (kNN) classifier (fitcknn)

The hyperparameter options are optimized in order to minimize the cross-validation classification errors. Once the model training has been optimized the test dataset is used to assess the model goodness for each observation in the test dataset the prediction of the target class and the posterior probability of being classified as ACC is assessed. If the posterior probability is higher than the threshold value[39] an ACC label is assigned, otherwise REJ label. Figure 5.15 reports the posterior ACC probability of prediction on the test dataset for the Ensemble NOGEO coarse model, trained on 5% partition of the whole training dataset, assumed as an example for the following paragraphs. The red distribution is relative to the offers/bids which actually have been rejected, the clue distribution is relative to the offers/bids that have been accepted. The distribution is normalized on the overall number of observations reporting the same actual label. E.g., 77% percent of the offers/bids which have been actually rejected are predicted to have an acceptance probability between 0% and 2% (first red bar on the left). Generally can be appreciated how the actual rejected offers/bids are predicted to have a lower probability of acceptance (almost all the actually rejected offers/bids reports an ACC posterior probability lower than 10%-20%). Conversely, actually accepted observations are foreseen to have a higher probability to be accepted, even if probabilities >50% are very rare and 17% of them are foreseen to have an almost null probability.

[38] In the brackets the name of MATLAB function for training.

[39] During the training the threshold value is set to 0.5.

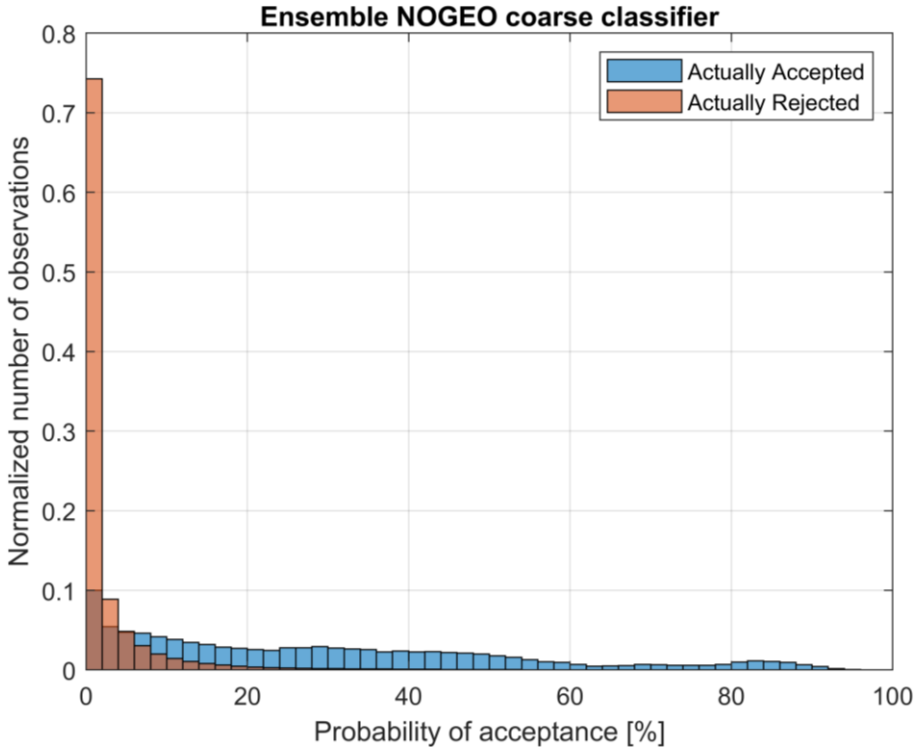

Figure 5.15: Posterior ACC probability distributions for Ensemble NOGEO coarse classifier.

Looking at Figure 5.15 is clear how a further step in optimizing the model can be taken by selecting the best threshold value T. If T=0, all the offers will be classified as ACC, which means that the True ACC rate (TACCR) is equal to 1, but also the False ACC rate (FACCR) is equal to 1. It follows that the profits realized on the market are overestimated. Otherwise if T=1 all the observations are classified as rejected, implying a null TrueACC rate and False ACC rate, and an underestimation of profits. The best classifier for the purpose described in this section is the classifier that minimizes FACCR and the error in estimating revenues, and profits maximizing the TACCR.

$$TACCR = \frac{TACC}{TACC + FREJ} \tag{5.21}$$

$$FREJR = \frac{FACC}{TREJ + FACC} \tag{5.22}$$

Where TACC, FACC, FREJ, and TREJ are respectively the observations correctly classified as accepted, misclassified as accepted, correctly classified as rejected and misclassified as rejected. The Receiver Operating Characteristic (ROC) curve is a common method to visualize the goodness of the classifier varying the threshold value. Figure 5.16 reports the ROC curve for the same model as the previous figure. T=0 corresponds to the point in the up right corner, increasing T to 0.02 the TACCR decrease to 77%, and the FACCR to 17%. With reference to Figure 5.15, this case corresponds to a threshold value between the first and the second bar.

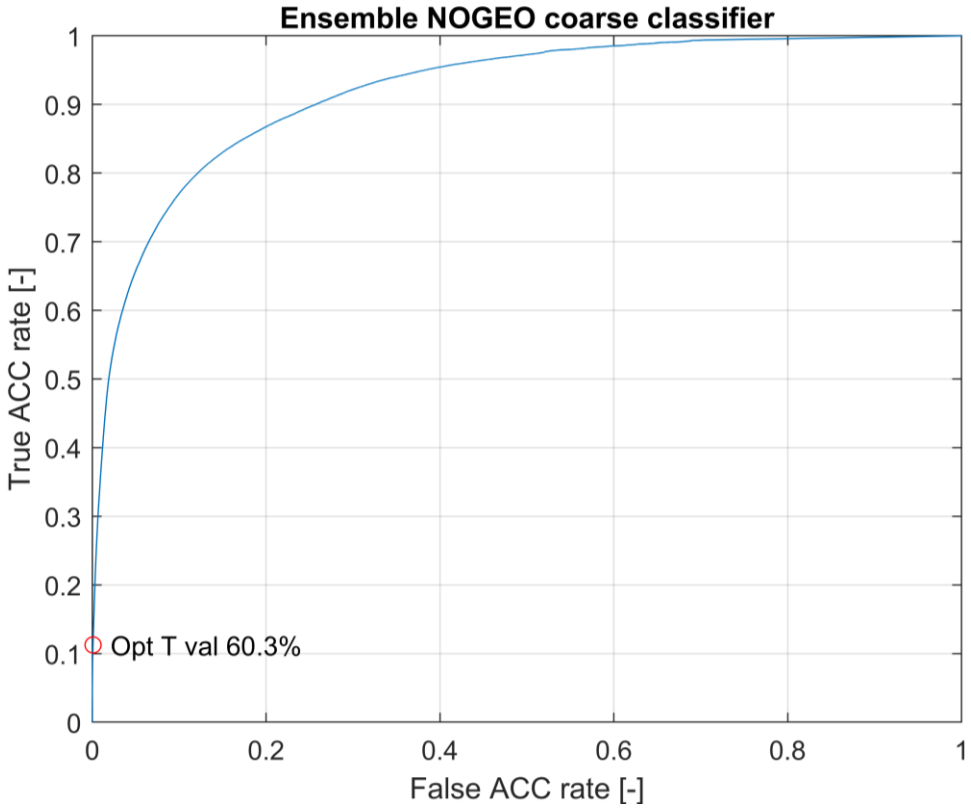

Figure 5.16: Receiver Operating Characteristic curve for Ensemble NOGEO coarse classifier.

Basically, the reader can figure out T as a vertical threshold line moving from left to right in Figure 5.15. The red bars on the left of the threshold value are correctly classified as rejected (TREJ), and the red bars on the right are misclassified as accepted (FACC). Analogously, the blue bars on the line are misclassified as rejected (FREJ) while the blue bars on the right are correctly classified as accepted (TACC). Figuring out to move the threshold line from the left to the right we move from the up right corner to the bottom left corner along the ROC curve in Figure 5.16. It is common to refer as a perfect classifier to a model which is able to separate the acceptance probability distributions of Figure 5.15, so that exists at least one T to which corresponds FACCR=1 and TACCR=1. In this case, the area under the curve (AUC in Figure 5.16) will be 1. AUC is assumed as a parameter to assess the model.

It was pointed out how the aim of this model is to correctly assess the unit's profits and that for T=0 the profits will be overestimated and for T=1 underestimated. For every model exist an optimal T for which the expected profits are equal to the actual profits on the test dataset. Therefore is relevant to assess how the model performs for $T=T_{opt}$.

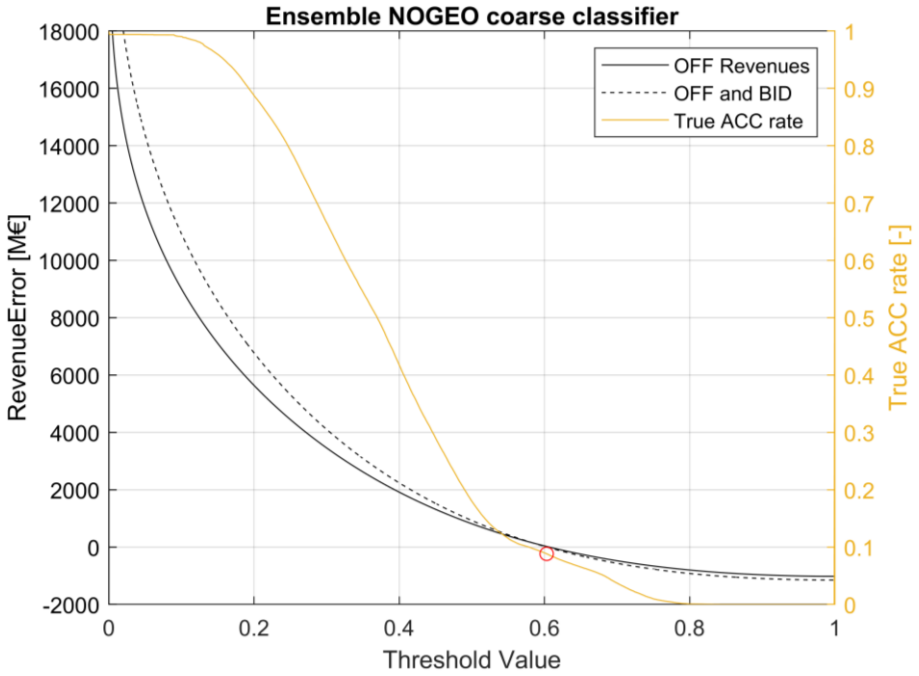

Figure 5.17: Revenue error and True Accepted Rate vs Threshold value.

Assessing the profits error is not trivial, since profits require taking into account the cost of electricity which is dependent on the single generator, the load, the spot fuel price, and many other variables. Two formulas are here proposed, corresponding to the continuous and dashed line of the figure above respectively. The first, equation 5.23, takes into account only the offers' revenues. The second, equation 5.24, includes a simplified calculation of the bid profits in which the cost of electricity is assumed to be the DAM clearing price. Both values are the difference between the expected values of the model and the actual value from historical data. To compute the expected data it is needed to assess the ACC_{prob} which differs from the posterior probability pp based on T. Equations 5.25 and 5.26 impose that $ACC_{prob}=0$ for pp=0, $ACC_{prob}=1$ for pp=1, and $ACC_{prob}=0.5$ for pp=T.

$$Err_{RevOFF} = \left(pr_{aw} \cdot \mathrm{Q}_{aw} \cdot ACC_{prob}\right)_{OFF\ all} - \left(pr_{aw} \cdot \mathrm{Q}_{aw}\right)_{OFF\ actually\ ACC} \tag{5.23}$$

$$\begin{aligned} Err_{RevOFFProfBID} &= Err_{RevOFF} + \left(\mathrm{Q}_{aw} \cdot (pr_{DAM} - pr_{aw}) \cdot ACC_{prob}\right)_{BID\ all} \\ &- \left(\mathrm{Q}_{aw} \cdot (pr_{DAM} - pr_{aw})\right)_{BID\ actually\ accepted} \end{aligned} \tag{5.24}$$

$$ACC_{prob} = pp^{a} \tag{5.25}$$

$$a = \frac{\log(0.5)}{\log(T)} \tag{5.26}$$

Since most of the offers/bids are commonly rejected, the dataset is highly unevenly distributed among ACC and REJ, then TACCR can be very low turning out to be the most critical parameter among the mentioned. As appreciated in Figure 5.17, the TACCR trend is decreasing against T, a perfect classifier would show a step trend and TACCR=1 for $T=T_{opt}$, which means that all the offer/bids are correctly classified leading to a zero error in revenue estimation.

Assuming the AUC, the classification error, and the TACCR, for zero revenue error, as the main model goodness indicators the following figures outline the comparison between the trained models. Besides the goodness of prediction the prediction time is extremely important since, as described in Section 5.1, the probability of offer/bid acceptance is optimized and assessed several times scheduling the optimal dispatch. Then to keep the scheduling process in a reasonable amount of time, models with low prediction time must be prioritized.

kNN and Naive Bayes models are not shown in the figures since the firsts were impossible to train on such a large data set, and an *out of memory* error causes MATLAB to stop, while the Naive Bayes ones take a too long time to predict. For both the training and the testing the duration limit is 24h, afterwards the process is forced to stop. Classification error is around 1.5% for almost all the models since the majority of offers/bids are rejected is not possible to appreciate many a real difference in this parameter. AUC values in the order of 0.9 are reached by Tree classifiers and some Ensemble classifiers. Ensemble classifiers are expected to perform better than Trees since they combine many Tree classifiers, however, some of them report low values in AUC or classification errors higher than the average. This is due to the fact that Ensembles' hyperparameters optimization requires more time than the Trees, so the final Tree classifier is close to the best that is possible to train on that data, while the Ensembles may be far away from the optimum hyperparameters array. The TACCR is up to 0.45 for the Ensemble GEO fine model trained on the 10% partition of the whole training dataset, however, the same model reports the highest classification error.

Table 5.2 reports all the mentioned parameters for each training partition best model. Model Ensemble Coarse GEO was selected, and used in the following section, because of its huge advantage in prediction time.

Table 5.3: Best models goodness parameters.

Partition	**Model**	**AUC**	**Classification Error**	**TACCR**	**Prediction time**
1%	Ensemble Fine GEO	0.934	1.30%	0.094	776s
5%	Ensemble Coarse GEO	0.907	1.33%	0.100	15 s
5%	Tree Coarse GEO	0.919	1.48%	0.213	476 s
10%	Ensemble Fine GEO	0.929	2.59%	0.457	433 s
10%	Tree Fine GEO	0.929	1.69%	0.247	4918s

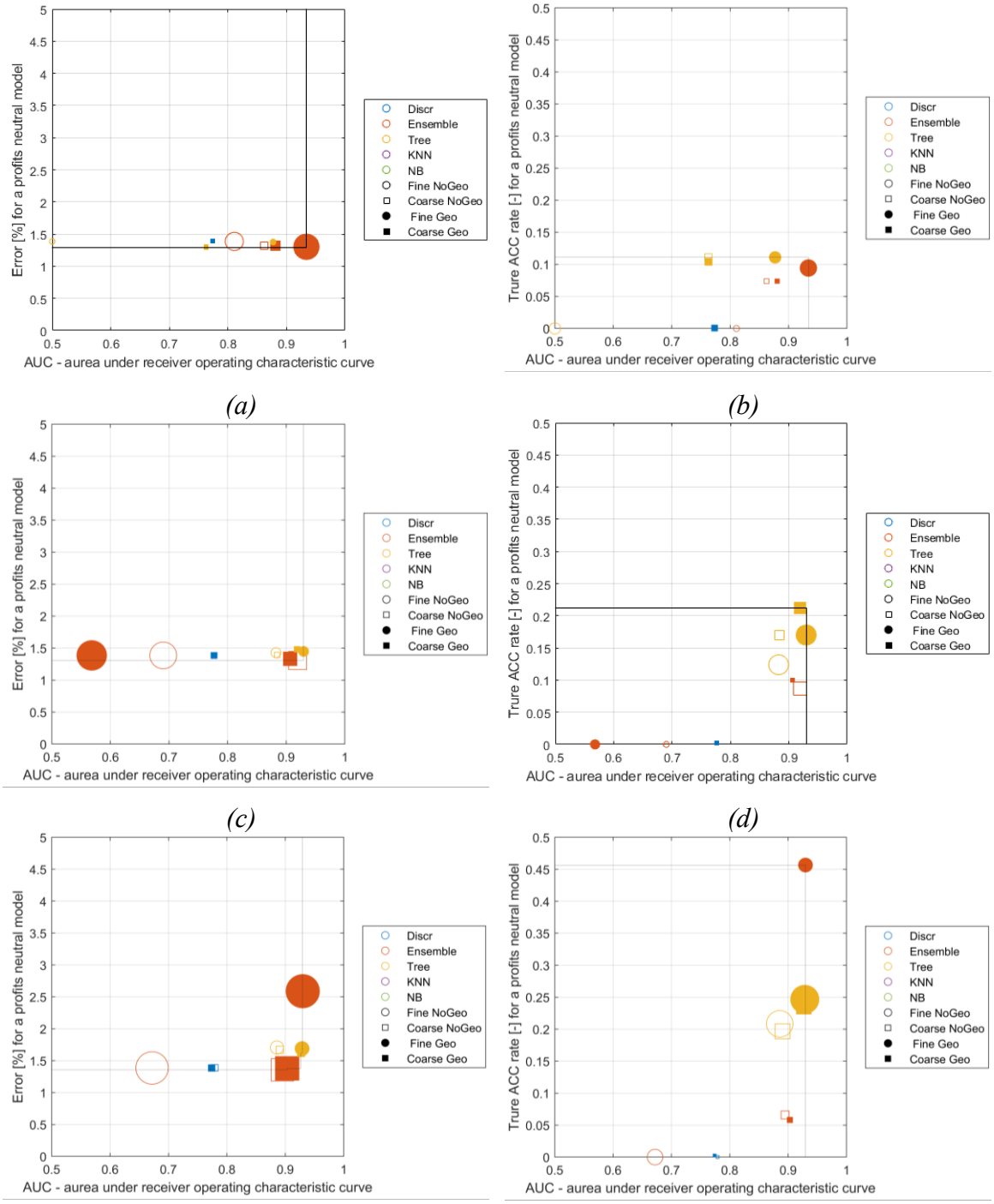

Figure 5.18: Models goodness indicator parameters. Models trained on 1% ((a) and (b)), 5% ((c) and (d)) and 10% ((e) and (f)) stratified partition of the whole training dataset. The figures on the left report the classification error vs AUC, and the size of the markers is proportional to the training time. The figures on the right report the true accepted rate vs AUC, while the markers' size indicates the prediction time.

5.3.2.3. Model of acceptance prediction application within the dispatch optimizer

The acceptance prediction by algorithms described and compared in Sections 5.3.2.1 and 5.3.2.2 are then used in the dispatch optimization described in Section 5.3.1 as a fundamental term of equations (5.10 and 5.13). To predict the probability of acceptance of a new observation ($ACC_{prob_{i,j,t}}$) the algorithms need all the predictors, with reference to the previously reported subdivision:

- Offer/bid specificity predictors: PURPOSE_CD is OFF if $Load^{DAM}_{i,t} < Load^{ASM}_{j,t}$. BID otherwise. SCOPE is selected according to the case study, in the following paragraph is imposed GR1
- Offer/bid time predictors: INTERVAL_NO, MONTH (month on which the offer is submitted), DAY_TYPE (H for holydays, B for weekdays) are imposed by the time t
- Market indicator predictors: MGAS_MGP (the spot gas market price on the day the bid/offer is presented), PUN (Single National electricity price on the DAM on the hour on which the offer/bid is presented), Zonal_price (zonal electricity price on the DAM on the hour the offer/bid is presented), are input to the dispatch optimization, so they depend on the time t and the case study location
- Units predictors: Voltage (the voltage level of the grid to which the unit is connected [kV]), Lat, and Long (latitude and longitude degrees of the capital of the administrative province in which the unit is located), are depending on the case study location.
- Offer/bid strategy predictors: ADJ_QUANTITY_NO is imposed by the $Load^{DAM}_{i,t}$ and $Load^{ASM}_{j,t}$. ADJ_ENERGY_PRICE must be optimized to satisfy the expected profits in the ancillary services market

The only free predictor is the offer/bid price that, since the considered ASM is a pay-as-bid market, influences not only the probability of acceptance but also directly the ASM profits and so the objective function, equation (5.15).

The following three figures describe the price optimization on an example relative to an offer up to a residual capacity of 200 MWh/h. The first figure shows the contour of accepted ASM with respect to the quantity and the price, of course, the higher the quantity and the price the higher are profits. Figure 5.20 concerns the acceptance probability as output from the algorithm. Finally, Figure 5.21 is the product of the two previous, i.e., the expected profits. The optimization is carried out on the expected profits and constrained to be on the lines, yellow dashed lines in the figures, defined by the quantity, thus the difference between $Load^{DAM}_{i,t}$ and $Load^{ASM}_{j,t}$. Red dot markers indicate the maximum, and it is possible to appreciate that it corresponds neither to the profits nor to the acceptance probability maximum.

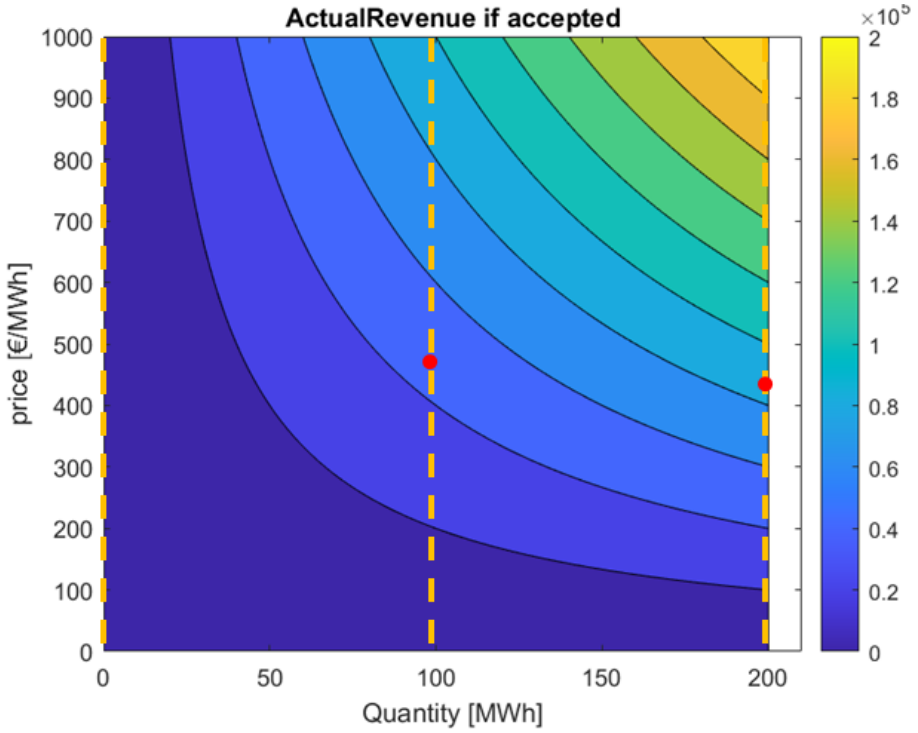

Figure 5.19: ASM profits [EUR] contour vs the offered quantity and price. Yellow dashed lines represent the constraint imposed by i and j indices.

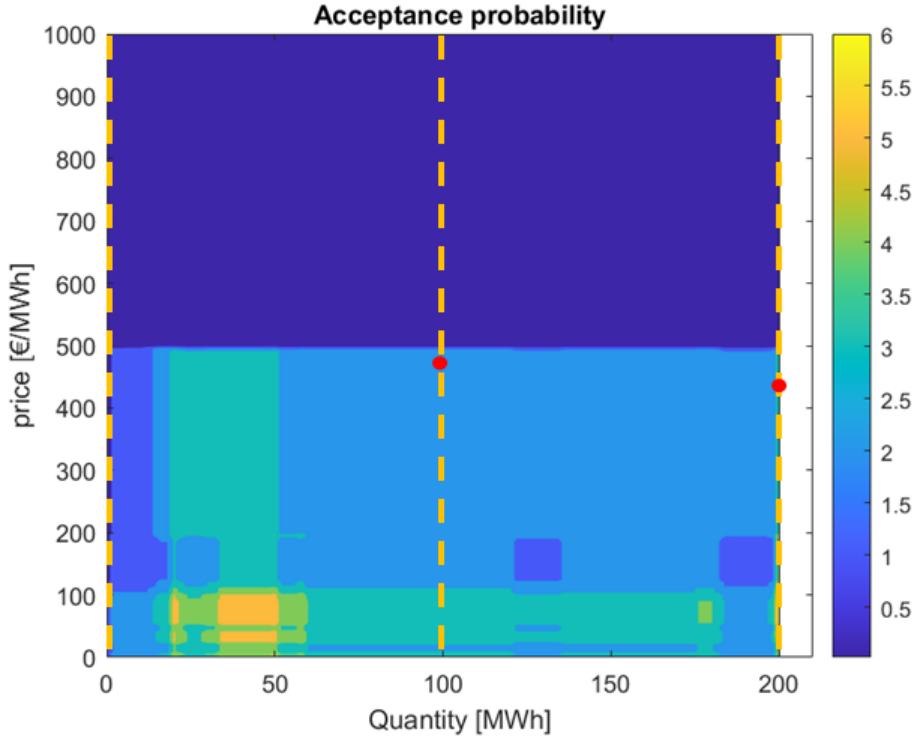

Figure 5.20: ASM offer acceptance probability [%] contour vs the offered quantity and price. Yellow dashed lines represent the constraint imposed by i and j indices.

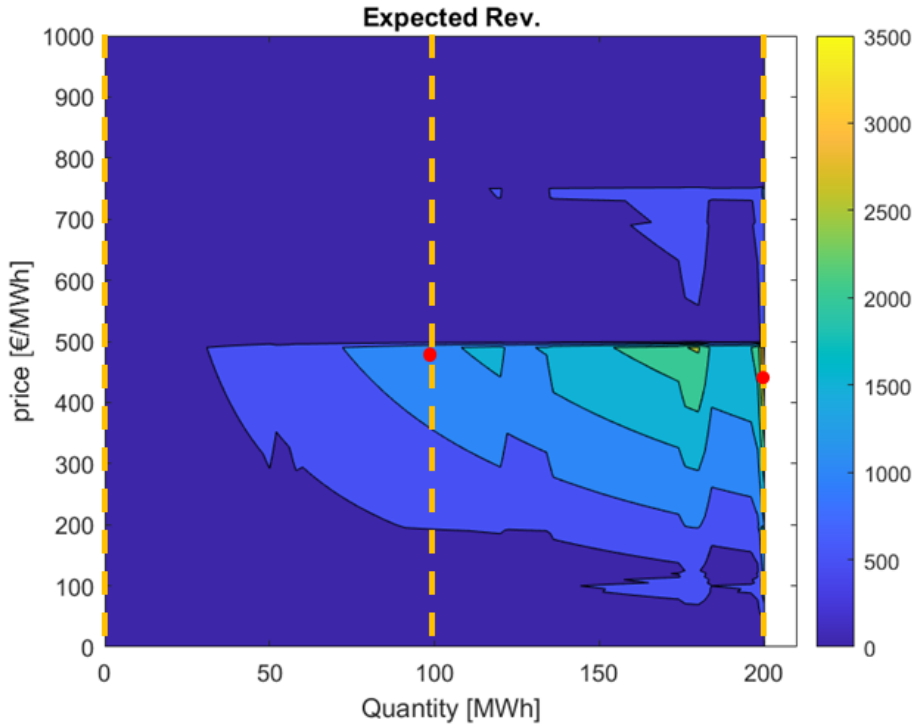

Figure 5.21: Expected ASM profits [EUR] contour vs the offered quantity and price. Yellow dashed lines represent the constraint imposed by i and j indices.

5.3.3. Applied examples

The model of optimal dispatch, described in Section 5.1, using the algorithm, selected in Section 5.2, for the probability prediction of ASM offers/bids is here applied to a specific case study to show how it works and its potentialities.

The case study assumes a 400 MW CCGT, the GT load is discretized to 0%, 45%, 60%, 75% and 100%. The CCGT off-design and nominal efficiency are modeled as in Chapter 4. The CCGT is assumed to be in Turbigo (province of Milan, Italy) 43.52°N, 8.74°E, where a real power plant owned by IREN Energia is located[40]. The location belongs to the NORD electricity market bidding zone and is connected to the 380 kV electricity grid. Input data (electricity price, natural gas price, CO_2 allowance cost, and ambient temperature are the real data from the year 2018). The scheduling process takes approximately 24-30h for one month[41].

This section focuses on a comparison between a DAM-only scheduler and the proposed ASM and DAM integrated scheduler on week 15, 2018.

---

[40] In Turbigo is actually located a 2+1 CCGT with an installed capacity of 800 MW, however to reduce the complexity of the problem and facilitate the comparison between the model proposed in this chapter and the other dispatch optimization presented in this thesis the case study in Section 5.3.3 is imposed to be a 1+1 configuration of 400 MW.

[41] MATLAB 2019b was used on a computer reporting the following features. Processor Intel(R) Xeon(R) E-2176G CPU @ 3.70GHz, Memory 16 GB, OS Microsoft Windows 10 64bit.

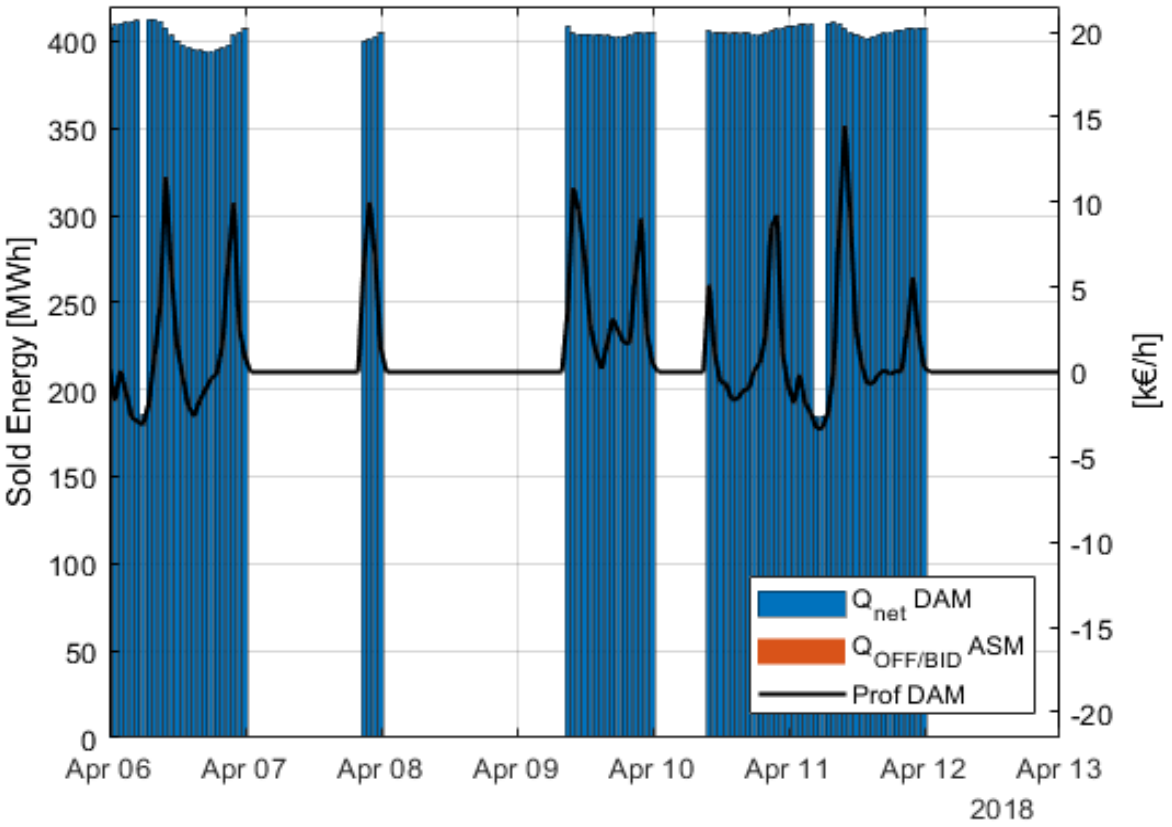

Figure 5.22: DAM-only scheduler, between April 6 and April 13, 2018.

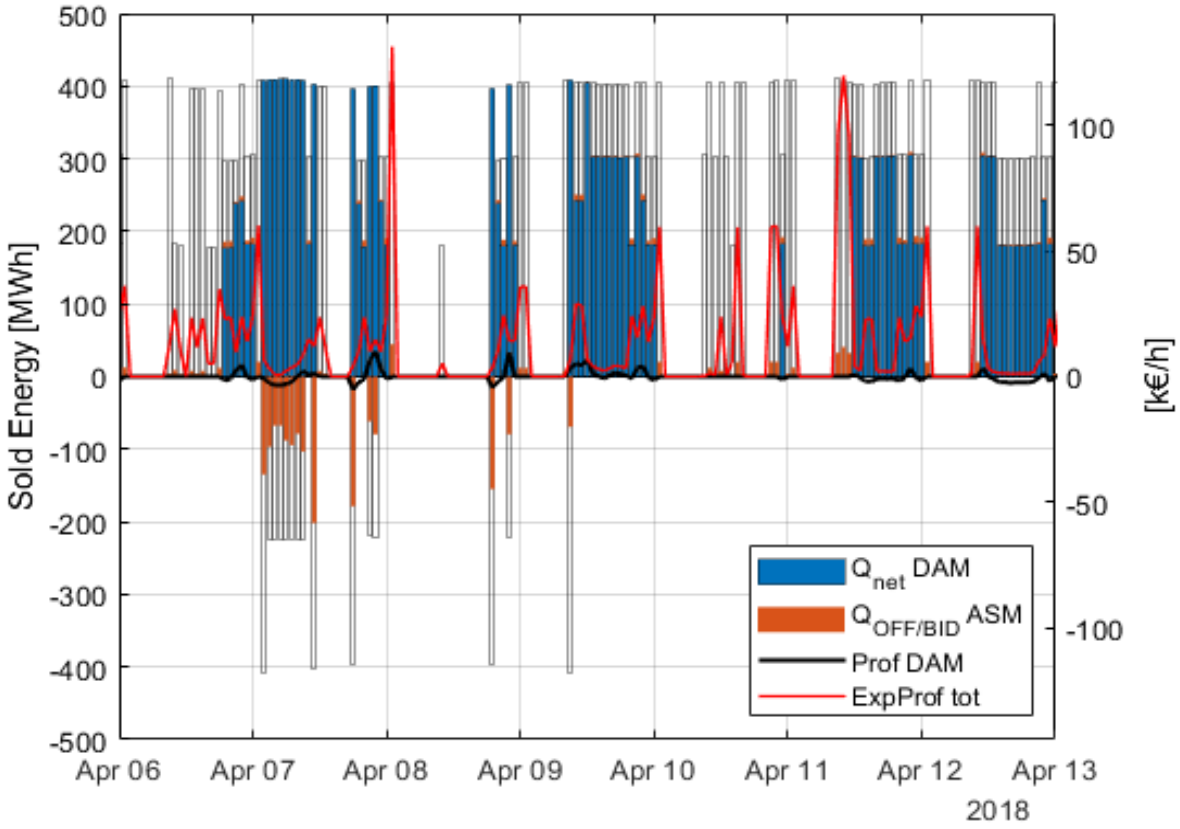

Figure 5.23: DAM and ASM integrated scheduler, between April 6 and April 13, 2018.

The DAM model of optimal dispatch schedules the CCGT start-up when the number of profits from the following operating hours can pay the cost of the start-up back. Then the power plant is run full load if the COE is lower than the price of electricity, in such situation the more power il sold the higher are the revenues and the profits. If the COE is slightly higher than the electricity price and the power plant is on, full load is still the best option to limit the losses, since lowering the load implies an absolute saving in fuel but a lower efficiency so higher COE and specific losses. The minimum load is adopted only if the difference between COE and electricity price is relevant, is worth keeping the powerplant operating even if the COE is higher than the electricity price only if the overall amount of losses in such an unprofitable period is lower than the start-up cost that should be paid later to exploit new favorable market hours. The power output is not constant neither at full nor at minimum load since it depends on the ambient temperature.

Figure 5.23 reports the scheduling optimized in order to maximize the sum of DAM profits (black line in the figure) and the expected ASM profit, the red line in the figure shows the sum. The blue bars indicate the quantity sold in the DAM, while the white and red bars are the quantity offered or bid in the ASM. The ASM bar filling is proportional to the probability of acceptance of the relative offer/bids, e.g., a full red bar indicates that such quantity has a 100% probability to be accepted in the ASM, otherwise an almost empty bar On April 6, the two scheduling differs because of the previous days' operations, according to the optimal DAM-only scheduling the CCGT is on at April 6 00:00, so it is managed to minimize the losses during low price hours and maximizing the profits during profitable hours, according to the strategy described in the previous paragraph. Considering also the ASM the best option is to present any offers in the DAM until the last high price hours, in facts is more profitable to offer energy on the ASM, if the offer will be accepted the profits will be higher if it will be rejected the plants will remain off and the start-up cost is avoided.

April 7 is characterized by unprofitable prices in the DAM, however, the model predicts a good probability (40-50%) of bid acceptance in the ASM, so the strategy is to sell in DAM and then bid to buy the energy at a lower price on the services market.

Another interesting scheduling is the one for the second half of April 9. These hours are characterized by good prices in the DAM, so the DAM-optimizer schedule to run the power plant full load, nevertheless prices on the ASM can be much higher so the integrated optimizer imposes to sell an intermediate load in the DAM and offer what remains in the ASM. Even if the probability of acceptance is not high, ASM prices are higher so it is worth risking losing extra profits from the DAM and betting for offer acceptance on the ASM. If the acceptance probability reaches zero then is better to sell the whole available capacity in the DAM, as it happens for two hours in the morning.

On April 11 and 12 the strategy is similar but in many hours is better to offer only a fraction of the residual available capacity, since offering the whole amount would imply a lower probability in this case. On April 11 is interesting to look at how the start-up time is delayed, the DAM-only optimizer switches it on earlier to exploit a high-price hour at the end of the morning and this justifies the slight losses in the central day hours. But considering also the ASM the best option is to address the ASM, where the prices are higher and probability acceptance is moderately high, before the profitability on the DAM is stable to sell in this market the baseload.

Finally, on April 10 the power plant is off but some energy is offered in the ASM, and the expected profits are considerable, up to 50 k€/h. Thus, the viability of this strategy

depends on the ASM potential price, sometimes, e.g., on April 8 except for one hour, the best option is to not offer any quantity, since even in case of acceptance the profits would be lower than the start-up cost.

5.3.4. Final Considerations

Finally, Chapter 5 investigates how flexibility is valued in the markets. The presented statistical analysis highlights the market failures because of which the market marginal price is not correlated to the cost of the marginal technology, increasing the cost for the final users. Moreover, the profit margin for CCGTs, i.e., the Clean Spark Spread is lower and lower, while the relevance the growing relevance of ancillary services markets is growing, from which more than half of profits can come. Consequently, is essential to develop a methodology able to quantify the real economic value of flexibility. The previous chapters underlined how flexibility is today an indispensable feature of programmable power plants, however, the viability of many solutions, including some of the ones presented in this thesis, oriented to a flexibility enhancement is not certain because of the high investments they often imply. However, the profit opportunities are not limited to the traditional energy-only markets.

The methodology proposed in Section 5.3 presents an application of linear programming optimization to define the best dispatch of energy systems both in the day-ahead and ancillary services markets. The MILP model is described in detail, besides a machine learning approach to estimate the probability of offers/bids acceptance on the ancillary services markets. The developed scheduler is compared to a traditional DAM MILP scheduler highlighting the increased opportunities for profits in the ancillary services market. The results show how considering these markets in scheduling the best power plant dispatch the flexibility value is properly awarded. While, from the grid operator's point of view is clear how the availability of a programmable power plant to fluctuating load gives a relevant contribution to managing the grid, regulating the frequency, and properly meeting the demand.

The model presented in Section 5.3, represents a novel approach to MILP application in the energy technology operation scheduling. The novelty of the presented concept consists of the integrated optimization of two markets. One of them has no certainties about price and offers acceptance.

The core element of the proposed scheduling model is the data-driven algorithm for the prediction of a specific offer/bid probability of acceptance. The algorithm must perform good predictions in order to provide a reliable schedule, at the same time it is used to optimize the offer/bid price (nLoad-1)·nLoad·t times, each optimization call the prediction several times then a fast to predict model is essential to keep the optimization time within an acceptable value.

The development of data-driven algorithms for offer/bid acceptance probability is the issue on which future works can focus more. The predictors' list can be varied looking for the best possible model, the objective function of the training optimization can be improved by setting the goodness indicator defined by this thesis to search for the best hyperparameters of each classifier. Then training optimization should prioritize fast-to-predict models, for this purpose other machine learning algorithms can be tested further than those listed here.

Section 5.3.3 reports an interesting comparison between the DAM-only dispatch optimizer and the proposed integrated approach. The solutions are compared and the optimization logic is explained allowing a full understanding of the problem complexity and the developed tool potentialities.

It is possible to conclude that considering services markets, in scheduling the best power plant dispatch, allows accounting for the proper value of flexibility. While, from the grid operator's point of view is clear how the availability of a programmable power plant to fluctuating load gives a relevant contribution to managing the grid, regulating the frequency, and properly meeting the demand.

Conclusions

The first chapter introduces the current global scenario and the motivation which have led to this thesis. The data here presented highlights how the global energy demand is foreseen to increase in the following years with the economic and demographic growth of many developing countries. At the same time, the climate change mitigation targets claims for carbon dioxide emissions cut. As a consequences word wide policies focus on increasing RES penetration, within the last decades the electricity sector was the one mainly addressed by these.

As a result, some sectors, such as heating and transport are still characterized by a strong carbon footprint, but many steps are still to take in the electricity sector as well. Nevertheless, the integration between all the energy sectors is more and more promoted, often referred to as "sector coupling". Thus is possible to generalize the conclusions to all the sectors. Solutions to satisfy the need for a reliable, affordable, and sustainable energy supply is today one of the main challenges that the scientific community is called to face.

This thesis investigates the potentialities of two different technologies and proposes different solutions to couple them combining the respective advantages, promoting the integration of the heating and electricity sectors, and providing flexible power generation to the grid. The different chapters address the research questions illustrated in the Introduction, introduce the state of the art, the pertaining literature, and the adopted methodology.

The following table summarizes the answers to the research questions and indicates the relative sections in which the full detailed answers are given.

Table 1: Research Questions and related answers

RQ 1	Is the flexibilization (i.e., increased number of start-ups and reduced operative hours) of Combined Cycle Gas Turbine Power plants reflected in increased pollutant emissions?
Answer	Stat-ups, and shutdowns to a lesser degree, have a relevant impact on pollutant emissions. Especially concerning carbon monoxide (CO). While the amount of NO_x is not so relevant if compared to the amount emitted during normal operating hours. Each start-up and shutdown cycle is equivalent to 546 fired hours in terms of CO and 3 h in terms of NO_x. As a consequence increased flexibility is probably reflected in increased carbon monoxide emissions but not in nitrogen oxides emissions. Moreover, a CO-catalyzer demonstrates to cut the emission even within the start-up transient limiting them to 44 equivalent fired hours. With an installed CO-catalyzer the CO emissions remain more-less constant as the operational flexibility increases. It should be remarked that the institutional Environmental Impact Assessment (*Valutazione di Impatto Ambientale*), neglecting the transients emissions and considering 8760h per year, always overestimate the real emissions.
Section	2.3

Paper	Vannoni, A., Belotti, D., Sorce, A., & Massardo, A. (2021). *Analysis of the impact of Combined Cycle in the energy transition*. E3S Web of Conferences, 312, 1001. https://doi.org/10.1051/e3sconf/202131201001	[10]
RQ 2	Could the inlet air heating of a gas turbine improve its off-design efficiency, and is this reflected in relevant fuel-saving or emission reduction?	
Answer	Due to the independence of efficiency from inlet temperature, and the relevant impact of this on output power, inlet air heating, can be used for the purpose of improved off-design performance. Benefits depend on the operational profiles, i.e., the number of hours operated in off-design conditions, and the average ambient temperature of the power plant location. However are expected to be in the 0.5-0.8% range of economic savings, directly reflected in an emissions cut.	
Section	2.4	
Paper	Vannoni A., Sorce a., Guedez R., Barberis, B., & Traverso A. (2021). *Combined Cycle Performance Gain Through Intake Conditioning*. Proceeding of Gas turbines in a carbon-neutral society 10th International Gas Turbine Conference 11-15 October 2021.	[11]
RQ 3	Are High-Temperature Heat Pumps a viable solution to provide low-carbon heating and couple the electric and heating sectors?	
Answer	Heat pumps designed for high-temperature applications demonstrated to be more expensive and less efficient than others in supplying heat at a lower temperature. The increased temperature lift limits the COP and the high temperature required at the compressor discharge makes many fluids unsuitable for such a purpose, R600, more expensive than other fluids at lower temperatures, is the only one (among the investigated fluid) able to guarantee 120°C of supply temperature. Despite the considerable cost of investment, the sensitivity analysis of economic viability to the cost of energy and the potential time usage scenario demonstrated that such machines are for sure viable within favorable markets, such as the Scandinavia and Baltic countries, but it can be considered also in many other zones of Europe. Especially as a centralized heat generator operating many hours a year.	
Section	3.3	
Paper	Vannoni, A., Sorce, A., Traverso, A., & Aristide, F. M. (2021). *Techno-Economic Analysis of Power-to-Heat Systems*. EDP Sciences. https://doi.org/10.1051/e3sconf/202123803003	[12]
RQ 4	How do market and climate parameters affect opportunities for Heat Pumps coupled with Combined Cycle Gas Turbines that aim to condition inlet air for power modulation purposes?	
Answer	An Inlet Conditioning Unit, consisting of a Heat Pump and a Thermal Energy Storage, demonstrated to be a viable solution able to modulate the power output and increase the off-design efficiency in different markets, Within cold locations characterized by low and stable electricity prices the prevalent operating mode is the Continuous Heating (i.e., the use of the HP to	

	heat the inlet air), in this case, the expected net present value is of the same order of the initial investment. Hot climates are generally also characterized by high electricity prices, in this case, the Inlet Cooling mode (i.e., the use of the HP to cool the inlet air) gives the major contribution. Finally, if the electricity price daily variability is 20 €/MWh or higher the complete layout, integrating the HP and TES is fully exploited. The NPV in the best circumstances is up 10 times the initial investment's cost.	
Section	4.1	
Paper	Vannoni, A, Garcia, Guedez, R, & Sorce, A. (2022) Combined Cycle, Heat Pump, And Thermal Storage Integration: Techno-Economic Sensitivity To Market And Climatic Conditions Based On A European And United States Assessment. Proceedings of the ASME Turbo Expo 2022: Turbomachinery Technical Conference and Exposition. Rotterdam, The Netherlands. June 13–17, 2022.	[13]
RQ 5	How Heat Pumps could be coupled to Combined Cycle Power Plants, devoted to the simultaneous generation of heat and power, in order to maximize the market viability and reduce the uncertainty of techno-economic performances?	
Answer	The best possible heat source for an HP coupled to an existing CCGT-CHP, with the aim of extending the operative range and increasing the global efficiency, is the hot condensate after it has exchanged heat through the devoted heat exchanger. Moreover, a hybrid series and parallel arrangement turns out to be the best solution combining the benefits of the two layouts. For new CCGT a new layout is proposed using the heat pump to exploit the fluid latent heat potential, this layout is characterized by high global efficiency and high costs. Its viability was explored with respect to different parameters.	
Section	4.2	
Papers	Vannoni, A., Giugno, A., & Sorce, A. (2021). *Integration Of A Flue Gas Condensing Heat Pump Within A Combined Cycle: Thermodynamic, Environmental And Market Assessment*. Applied Thermal Engineering, 184, 116276. https://doi.org/10.1016/j.applthermaleng.2020.116276.	[14]
	Vannoni, A., Giugno, A., & Sorce, A. (2021). Thermo-Economic Assessment Under Electrical Market Uncertainties of a Combined Cycle Gas Turbine Integrated With a Flue Gas-Condensing Heat Pump. ASME. J. Eng. Gas Turbines Power. April 2021; 143(4): 041003. https://doi.org/10.1115/1.4049769	[15]
RQ 6	How the economic value of flexibility is awarded in the markets and how it can be assessed by a techno-economic analysis?	
Answer	Traditional energy-only markets do not award the value of flexibility, however, Italian CCGTs perform, on average, between 62% and 81% of profits in the ancillary services markets. In these markets, flexible power generators, located in strategic locations are awarded for their operational flexibility as a contribution to the grid management. The proposed methodology is based on a data-driven MILP scheduling of optimal dispatch simultaneously accounting	

	for the DAM and ASM is an effective method to quantify the economic benefits of flexible retrofitting concepts or a new design's value.	
Sections	5.2 and 5.3	
Paper	Vannoni, A, Garcia, JA, Mantilla, W, Guedez, R, & Sorce, A. (2021) *Ancillary Services Potential for Flexible Combined Cycles*. Proceedings of the ASME Turbo Expo 2021: Turbomachinery Technical Conference and Exposition. Volume 4: Controls, Diagnostics, and Instrumentation; Cycle Innovations; Cycle Innovations: Energy Storage; Education; Electric Power. Virtual, Online. June 7–11, 2021. https://doi.org/10.1115/GT2021-59587	[13]

Glossary

Acronyms and abbreviations

ACC	Accepted
AHP	Adsorption Heat Pump
AmbHX	Ambient Heat Exchanger
ASHP	Air Sourced Heat Pump
ASM	Ancillary Services Market
BAU	Business as Usual
BENPV	Break-Even Net Present Value
BEPUN	Break-Even Average single national price of electricity
BM	Balancing Market
CAPEX	Capital Expenditure
CC	Combined Cycle
CCGT	Combined Cycle Gas Turbine
CFC	Chlorofluorocarbon
CFR	Capital Recovery Factor
CHP	Combined Heat and Power
COE	Cost of Electricity
COMP	Compressor
COND	Condenser
COP	Coefficient of Performance
COP	Conference of Parties
CS	Climate Spread
CSP	Concentrating Solar Power
CSS	Clean Spark Spread
DAM	Day Ahead Market
DHN	District Heating Network
DHN-HX	District Heating Network Heat Exchanger
ECO	Economizer
EENS	Excepted Energy Not Served
EIA	Environmental Impact Assessment

ETS	Emission Trading System
EU	European Union
EVA	Evaporator
FACC	False Accepted
FEM	Forward Electricity Market
FG	Flue Gas
FH	Fired Hours
FREJ	False Rejected
FWH	Feed Water Heating
GDP	Gross Domestic Power
GHG	Greenhouse gas
GSHP	Ground Sourced Heat Pump
GT	Gas Turbine
GTHX	Gas Turbine Heat Exchanger
GWP	Global Warming Potential
HCFC	Hydrochlorofluorocarbon
HDI	Human Development Index
HFC	Hydrofluorocarbon
HFO	Hydrofluoroolefin
HHV	Higher Heating Value
HOB	Heat Only Boiler
HP	High Pressure
HP	Heat Pump
HRSG	Heat Recovery Steam Generator
HT	High Temperature
HTF	Heat Transfer Fluid
HTHP	High Temperature Heat Pump
HX	Heat Exchanger
IBR	Inverter Based Resources
ICE	Internal Combustion Engine
ICU	Inlet Conditioning Unit
IDM	Intraday Market
IP	Intermediate Pressure

IQR	Interquartile Range
ISO	International Organization for Standardization
KNN	K-nearest neighbors
KPI	Key Performance Indicator
LCOE	Levelized Cost of Electricity
LCOH	Levelized Cost of Heating
LHV	Lower Heating Value
LOLE	Loss of Load Expectation
LOLP	Loss of Load Probability
LP	Low Pressure
LT	Low Temperature
MEL	Minimum Environmental Load
MGP	*Mercato del giorno prima* (Day-ahead market)
MILP	Mixed Integer Linear Programming
MSPE	Mean Square Pure Error
NB	Naive Bayes
NECP	National and Climate Plan
NPV	Net Present Value
NZE	Net Zero Emissions
O&M	Operation and Management
O&M	Operation and Maintenance
OCGT	Open Cycle Gas Turbine
ODFH	Off-design Fired Hours
ODP	Ozone Depletion Potential
OEM	Original Equipment Manufacturer
OPEX	Operating Expenditure
ORC	Organic Rankine Cycle
PBP	Pay Back Period
PCM	Phase Change Material
PDF	Probability Density Function
PM	Particulate Matter
prc	Percentage
PUN	*Prezzo Unico Nazionale* (National Single Price)

PV	Photovoltaic
REJ	Rejected
RES	Renewable Energy Source
RH	Reheater
ROC	Receiver Operating Curve
RQ	Research Question
SAHP	Solar Assisted Heat Pump
SCR	Selective Catalytic Reduction
SD	Shutdown
SH	Superheater
SMP	System Marginal Price
SS	Spark Spread
SS	Stand Still
ST	Steam Turbine
SU	Start Up
TACC	True Accepted
TCI	Total Cost of Investment
TES	Thermal Energy Storage
TIT	Turbine Inlet Temperature
TREJ	True Rejected
TOT	Turbine Outlet Temperature
TSO	Transmission System Operator
UF	Utilization Factor
UN	United Nation
UNFCCC	United Nation Framework convention on climate Change
UP	Production Unit
US	United States
VC	Variable Cost
VCHP	Vapor Compression Heat Pump
VIA	*Valutazione di Impatto Ambientale*
VLE	*Valore Limite di Emissione*
WSHP	Water Sourced Heat Pump

Parameters and variables

A	Area	[m^2]
ACC_{prob}	Acceptance probability	[%]
AUC	Area Under the (ROC) Curve	[-]
ΔT	Temperature difference	[K]
a	Scale parameter (Weibull PDF)	[-]
b	Shape parameter (Weibull PDF)	
C	Cost	[€]
CAPEX	Capital Expenditure	[€]
CCD	Cooling Degree Days	[CDD]
cp	Specific heat at constant pressure	[J/kgK]
CSS	Clean Spark Spread	[€/MWh]
d	Discount rate	[-]
e	Emission factor	[ton/MWh]
El	Electricity price	[€/MWh]
el	Generated electricity	[MWh]
Err	Classification error	[%]
f	MILP objective	
FREJR	False rejected rate	[-]
g	Gravity acceleration	[m/s^2]
h	Convection coefficient	[W/m^2K]
h	Specific enthalpy	[J/kg]
HDD	Heating Degree Days	[HDD]
I	Inertia	[kgm^2]
i	Interest rate	[-]
i_{eff}	Effective interest rate	[-]
i_L	Inflation rate	[-]
I	Income	[€]
K	Thermal resistance	[W/K]
k	Conductivity	[W/m K]
k	Heat capacity ratio	[-]

k	Shape parameter (Gamma PDF)	[-]
LMTD	Logarithmic Mean Temperature Difference	[K]
$\dot{m}$	Mass flow	[kg/s]
n	Lifespan	[years]
O&M	Operating and Maintenance Costs	[€], [€/MW], or [€/MWh]
OffPk	Off-Peak duration	[hour]
OH	Operating hours	[hour]
OP	Operational profits	[€]
Nu	Nusselt number	[-]
P	Power	[W]
p	Pressure	[Pa] or [bar]
Pr	Prandtl number	[-]
pr	Price	[€]
Pk	Peak duration	[hour]
Q	Heat	[J], or [MWh]
Q	Quantity	
$\dot{Q}$	Heat Flow	[W]
r	Occurrence	[#]
Re	Reynolds number	[-]
Rev	Revenues	[€]
s	Specific entropy	[J/kg K]
t	Time	[s], or [hour]
T	Temperature	[°C] or [K]
T	ACC probability threshold value	[%]
TACCR	True accepted rate	[-]
U	Overall Heat Transfer Coefficient	[W/m^2K]
UF	Utilization Factor	[%], or [-]
V	Binary Start-up Variable	
v	Specific volume	[m^3/kg]
W	Work	[J], or [MWh]
x	MILP solution	
Z	Zeta Factor	[-]
β	Compression ratio	[-]

Δ	Difference, Spread	
δ	Scale parameter (Logistic PDF)	
ΔPk	Peak time shift	[hour]
η	Efficiency	[%] or [-]
θ	Scale parameter (Gamma PDF)	
λ	Shape parameter (Inverse Gaussian PDF)	[-]
μ	Mean, Volumetric compressor clearance ratio	
ρ	Pearson Coefficient	[-]
σ_X	Standard deviation of X	
σ_{XY}	Covariance of X and Y	
φ	Area enlargement factor	[-]
χ	Fraction of non-regenerative superheating	[%]
ω	Frequency	[rad/s]
$\dot{\omega}$	Angular Acceleration	[rad/s^2]

Subscripts

avg	Average
aw	Awarded
C	Cost
COMP	HP compressor
critic	Critical
d	Daily
el	Electricity, Electrical
ex	exergetic
fg	flue gas
fix	Fixed
gen	Generated
gl	Global
h	Hourly, Hot
hs	Hot start-up
i	i-th hour standard
liq	Liquid
LM	Logarithmic Mean
max	Maximum

ns	Non-synchronous
opt	Optimal
Pp	Pinch point
prod	Produced
ref	Reference
REG	HP regenerator
S	Isentropic
s	Synchronous
SH	Superheating
SH	Superheater
spec	Specific
th	Thermal
v	Vapor
var	Variable
vol	Volumetric
w	Water
wf	Working Fluid
ws	Warm start-up
y	Yearly

List of tables

List of figures

Bibliography

[1] BP, 2021, *Statistical Review of World Energy Globally Consistent Data on World Energy Markets. and Authoritative Publications in the Field of Energy*.

[2] The World Bank, "World Development Indicators" [Online]. Available: https://datacatalog.worldbank.org/search/dataset/0037712. [Accessed: 03-Jan-2021].

[3] Fragaszy, R. J., Santamarina, J. C., Amekudzi, A., Assimaki, D., Bachus, R., Burns, S. E., Cha, M., Cho, G. C., Cortes, D. D., Dai, S., Espinoza, D. N., Garrow, L., Huang, H., Jang, J., Jung, J. W., Kim, S., Kurtis, K., Lee, C., Pasten, C., Phadnis, H., Rix, G., Shin, H. S., Torres, M. C., and Tsouris, C., 2011, "Sustainable Development and Energy Geotechnology - Potential Roles for Geotechnical Engineering," KSCE J. Civ. Eng., **15**(4), pp. 611–621.

[4] United Nations, 2015, "Transforming Our World: The 2030 Agenda for Sustainable Development."

[5] Osservatorio Italiano sulla Povertà Energetica, 2019, *Rapporto Sullo Stato Della Povertà Energetica in Italia*.

[6] Bouzarovski, S., Thomson, H., and Cornelis, M., 2021, "Confronting Energy Poverty in Europe: A Research and Policy Agenda," Energies, **14**(4), pp. 1–19.

[7] Global Energy Institute, 2018, "International Index of Energy Security Risk."

[8] World Energy Council, 2020, *World Energy Trilemma Index 2020*, London.

[9] "Https://Www.Pumpheat.Eu."

[10] Vannoni, A., Belotti, D., Sorce, A., and Massardo, A. F., 2021, "Analysis of the Impact of Combined Cycle in the Energy Transition," *E3S Web of Conferences*, p. 1001.

[11] Vannoni, A., Sorce, A., Guedez, R., Barberis, S., and Traverso, A., 2021, "Combined Cycle Performance Gain Through Intake Conditioning," *Gas Turbines in a Carbon-Neutral Society 10th International Gas Turbine Conference*.

[12] Vannoni, A., Sorce, A., Traverso, A., and Massardo, A. F., 2021, "Techno-Economic Analysis of Power-to-Heat Systems," **03003**, pp. 1–8.

[13] Vannoni, A., García, J., Guedez, R., and Sorce, A., 2021, "Ancillary Services Potential for Flexible Combined Cycles," *ASME Turbo Expo 2021: Turbomachinery Technical Conference and Exposition, June 7-11 2021*, Virtual.

[14] Vannoni, A., Giugno, A., and Sorce, A., 2021, "Integration of a Flue Gas Condensing Heat Pump within a Combined Cycle: Thermodynamic, Environmental and Market Assessment," Appl. Therm. Eng.

[15] Vannoni, A., Giugno, A., and Sorce, A., 2021, "Thermo-Economic Assessment Under Electrical Market Uncertainties of a Combined Cycle Gas Turbine Integrated With a Flue Gas-Condensing Heat Pump," J. Eng. Gas Turbines Power, **143**(4).

[16] United Nations Framework Convention on Climate Change Secretariat (UNFCCC), 2012, *Doha Amendment to the Kyoto Protocol*, Doha, Qatar.

[17] UNFCCC, 2015, *Adoption of the Paris Agreement. Report No. FCCC/CP/2015/L.9/Rev.1,*.

[18] Global Carbon Project, 2021, "Supplemental Data of Global Carbon Budget 2021 (Version 1.0) [Data Set]."

[19] Hove, A., 2020, "Current Direction for Renewable Energy in China," Oxford Energy Comment, (June).

[20] The People's Republic of China, 2021, *China's Achievements, New Goals and New Measures for Nationally Determined Contributions*.

[21] The United States of America, 2021, *The United States of America Nationally Determined Contribution. Reducing Greenhouse Gases in the United States: A 2030 Emissions Target*.

[22] European Parliament, 2018, "Directive (EU) 2018/2001 of the European Parliament and of the Council on the Promotion of the Use of Energy from Renewable Sources," Off. J. Eur. Union, **2018**(L 328), pp. 82–209.

[23] Bayer, P., and Genovese, F., 2021, "The Political Battle over the EU's New Climate Plan Is Just Beginning," London Sch. Econ. [Online]. Available: https://blogs.lse.ac.uk/europpblog/2021/08/11/the-political-battle-over-the-eus-new-climate-plan-is-just-beginning/.

[24] Germany, and European Commission, 2020, *Update of the Nationally Determined Contribution of the European Union and Its Member States*, Berlin.

[25] European Commission, 2021, *Communication from the Commission to the European Parliament, the Council, The European Economic, and the Social Committee and the Committee of Regions "Fit for 55": Delivering the EU's 2030 Climate Target on the Way to Climate Neutrality Delivering the E*, Brussels.

[26] Lombardini, M., 2021, "'Fit for 55', Il Nuovo Pacchetto Climatico Dell'UE e Le Sfide per l'Italia," ISPI Ist. per gli Stud. di Polit. Internazionale [Online]. Available: https://www.ispionline.it/it/pubblicazione/fit-55-il-nuovo-pacchetto-climatico-dellue-e-le-sfide-litalia-31197.

[27] European Commission, 2019, "Clean Energy for All Europeans," Euroheat Power (English Ed.

[28] The Republic of India, 2016, *India's Intended Nationally Determined Contribution: Working towards Climate Justice*.

[29] IEA, 2021, "COP26 Climate Pledges Could Help Limit Global Warming to 1.8 °C, but Implementing Them Will Be the Key."

[30] IEA, 2021, "The IEA at COP26."

[31] IEA, 2021, *India Energy Outlook 2021*, Paris.

[32] Russian Federation, 2020, *Nationally Determined Contribution of the Russian Federation*.

[33] Japan, 2021, *Japan's Nationally Determined Contribution, Updated Submission*.

[34] IEA, 2018, "Global CO2 Emissions by Sector" [Online]. Available: www.iea.org/data-and-statistics/charts/global-co2-emissions-by-sector-2018.

[35] Hernandez, Aguiar-Curry, and Wood, 2018, *Senate Bill No. 100*.

[36] France, 2020, *Plan National Intégré Énergie-Climat de La France*.

[37] Ministero dello Sviluppo Economico, Ministero dell'Ambiente e della Tutela del Territorio e del Mare, and Ministero delle Infrastrutture e dei Trasporti, 2019, *Piano Nazionanale Integrato per l'energia e Il Clima*.

[38] Germany, 2020, *Integrierter Nationaler Energie- Und Klimaplan*.

[39] Taylor, B. Y. M., 2020, *Energy Subsidies: Evolution in the Global Energy Transformation to 2050*.

[40] *State and Trends of Carbon Pricing 2017-2020*, Washington DC.

[41] European Commission, 2011, "Energy Roadmap 2050."

[42] Tanaka, K., Cavalett, O., Collins, W. J., and Cherubini, F., 2019, "Asserting the Climate Benefits of the Coal-to-Gas Shift across Temporal and Spatial Scales," Nat. Clim. Chang., **9**(5), pp. 389–396.

[43] Taylor, M., 2020, *Energy Subsidies: Evolution in the Global Energy Transformation to 2050*, Abu Dhabi.

[44] IRENA, 2018, *Renewable Energy Statistics 2018*, Abu Dhabi.

[45] ARERA, 2021, "Costo Degli Strumenti Di Incentivazione Dell'energia Elettrica Prodotta Da Fonti Rinnovabili."

[46] Terna, 2021, *Annuario Statistico 2020: Introduzione*.

[47] The World Bank, 2021, *State and Trends of Carbon Pricing 2021*.

[48] Hsu, M., 1998, "Spark Spread Options Are Hot!," Electr. J., **11**(2), pp. 28–39.

[49] Elias, R. S., Wahab, M. I. M., and Fang, L., 2016, "The Spark Spread and Clean Spark Spread Option Based Valuation of a Power Plant with Multiple Turbines," Energy Econ., **59**, pp. 314–327.

[50] Bodell, T., 2014, "Natural Gas & Electricity Pricing: Outlook-Spark Spreads, Dark Spreads, and Bed Spreads Showing Cutthroat Competition," Nat. Gas Electr., **30**(7), pp. 24–27.

[51] Alberola, E., Chevallier, J., and Chèze, B., 2011, "European Carbon Prices Fundamentals in 2005-2007: The Effects of Energy Markets, Temperatures and Sectorial Production," SSRN Electron. J., (0).

[52] Sijm, J., Neuhoff, K., and Chen, Y., 2006, "CO2 Cost Pass-through and Windfall Profits in the Power Sector," Clim. Policy, **6**(1), pp. 49–72.

[53] Hayhoe, K., Kheshgi, H. S., Jain, A. K., and Wuebbles, D. J., 2002, "Substitution of Natural Gas for Coal: Climatic Effects of Utility Sector Emissions," Clim. Change, **54**(1–2), pp. 107–139.

[54] Arora, V., Cai, Y., and Jones, A., 2016, "The National and International Impacts of Coal-to-Gas Switching in the Chinese Power Sector," Energy Econ., **60**, pp. 416–426.

[55] Kim, M.-K., and Kim, T., 2016, “Estimating Impact of Regional Greenhouse Gas Initiative on Coal to Gas Switching Using Synthetic Control Methods,” Energy Econ., **59**, pp. 328–335.

[56] Wilson, I. A. G., and Staffell, I., 2018, “Rapid Fuel Switching from Coal to Natural Gas through Effective Carbon Pricing,” Nat. Energy, **3**(5), pp. 365–372.

[57] Knittel, C., Metaxoglou, K., and Trindade, A., 2016, “Are We Fracked? The Impact of Falling Gas Prices and the Implications for Coal-to-Gas Switching and Carbon Emissions,” Oxford Rev. Econ. Policy, **32**(2), pp. 241–259.

[58] European Parliament, and European Council, 1996, *Directive 96/92/EC of the European Parliament and of the Council of 19 December 1996 Concerning Common Rules for the Internal Market in Electricity*.

[59] Pollitt, M. G., 2019, “The European Single Market in Electricity: An Economic Assessment,” Rev. Ind. Organ., **55**(1), pp. 63–87.

[60] GME, “Glossary” [Online]. Available: www.mercatoelettrico.org/En/Tools/Glossario.aspx. [Accessed: 25-Nov-2020].

[61] GME, 2020, *Relazione Annuale 201 9*.

[62] ARERA, 2017, *Prima Apertura Del Mercato per Il Servizio Di Dispacciamento (MSD) Alla Domanda Elettrica e Alle Unità Di Produzione Anche Da Fonti Rinnovabili Non Già Abilitate Nonché Ai Sistemi Di Accumulo.*

[63] Fulwood, M., and Sharples, J., 2021, “Why Are Gas Prices So High?,” Oxford Energy Comment, (September).

[64] Californian Independent System Operator, 2020, *Preliminary Root Cause Analysis - Mid-August 2020 Heat Storm*.

[65] Littlechild, S., and Kiesling, L., 2021, “Hayek and the Texas Blackout,” Electr. J., **34**(6), p. 106969.

[66] Busby, J. W., Baker, K., Bazilian, M. D., Gilbert, A. Q., Grubert, E., Rai, V., Rhodes, J. D., Shidore, S., Smith, C. A., and Webber, M. E., 2021, “Cascading Risks: Understanding the 2021 Winter Blackout in Texas,” Energy Res. Soc. Sci., **77**, p. 102106.

[67] U.S. Energy Information Administration (EIA), 2021, “Texas Natural Gas Production Fell by Almost Half during Recent Cold Snap - Today in Energy” [Online]. Available: https://www.eia.gov/todayinenergy/detail.php?id=46896. [Accessed: 11-Jan-2021].

[68] ERCOT, 2021, “ERCOT Calls for Rotating Outages as Extreme Winter Weather Forces Generating Units Offline” [Online]. Available: http://www.ercot.com/news/releases/show/225210. [Accessed: 11-Jan-2022].

[69] C. Traywick, Chediak, M., Malik, N. S., and Saul, J., 2021, “The Two Hours That Nearly Destroyed Texas’s Electric Grid,” Bloomberg.com.

[70] National Grid, 2019, *Technical Report on the Events of 9 August 2019*.

[71] AEMO, 2022, “Power System Operating Incident Reports” [Online]. Available: https://aemo.com.au/en/energy-systems/electricity/national-electricity-market-nem/nem-events-and-reports/power-system-operating-incident-reports. [Accessed: 11-Jan-2022].

[72] Billimoria, F., Mancarella, P., and Poudineh, R., 2020, “Market Design for System Security in Low-Carbon Electricity Grids : From the Physics to the Economics.”

[73] Terna, 2021, *Piano Di Sviluppo*.

[74] Ibrahim, H., Ilinca, A., and Perron, J., 2008, “Energy Storage Systems—Characteristics and Comparisons,” Renew. Sustain. Energy Rev., **12**(5), pp. 1221–1250.

[75] Gyamfi, S., Krumdieck, S., and Urmee, T., 2013, “Residential Peak Electricity Demand Response—Highlights of Some Behavioural Issues,” Renew. Sustain. Energy Rev., **25**, pp. 71–77.

[76] Goo, B., and Hur, J., 2018, “Estimation for Expected Energy Not Served of Power Systems Using the Screening Methodology of Cascading Outages in South Korea,” Energies, **11**(1).

[77] Pillai, V., 2015, “Loss of Load Probability of a Power System Fundam,” J. Fundam. Renew. Energy Appl., **5**(1), pp. 1–9.

[78] Billinton, R., Nerode, R., and Wood, A. J., 1973, *Power-System Reliability Calculations*, The Massachusetts Institute of Technology.

[79] Husain Saleh, M. J. A., Abbas Hasan Abdulla, S. A., Aziz Altaweel, A. M. A., and Qamber, I. S., 2019, “LOLP and LOLE Calculation for Smart Cities Power Plants,” *2019 International Conference on Innovation and Intelligence for Informatics, Computing, and Technologies, 3ICT 2019*, IEEE, pp. 1–6.

[80] ENTSO-E, 2020, *Mid-Term Adequacy Forecast - Executive Summary*.

[81] Winter, W., Elkington, K., Bareux, G., and Kostevc, J., 2015, “Pushing the Limits: Europe’s New Grid: Innovative Tools to Combat Transmission Bottlenecks and Reduced Inertia,” IEEE Power Energy Mag., **13**(1), pp. 60–74.

[82] Debry, M., Denis, G., Prevost, T., and Xavier, F., 2016, “Maximizing the Penetration of Inverter-Based Generation on Large Transmission Systems : The MIGRATE Project,” 6th Sol. Integr. Work., (1).

[83] Tielens, P., and Van Hertem, D., 2016, “The Relevance of Inertia in Power Systems,” Renew. Sustain. Energy Rev., **55**, pp. 999–1009.

[84] Milano, F., Dörfler, F., Hug, G., Hill, D. J., and Verbič, G., 2018, “Foundations and Challenges of Low-Inertia Systems (Invited Paper),” *2018 Power Systems Computation Conference (PSCC)*, pp. 1–25.

[85] Danish Energy Agency, 2018, *Technology Data for Energy Plants for Electricity and District Heating Generation*.

[86] LAZARD, 2021, *Lazard’s Levelized Cost of Energy Analysis V15.0*.

[87] Gardumi, F., 2016, “A Multi-Dimensional Approach to the Modelling of Power Plant Flexibility,” Politecnico di Milano.

[88] Caldecott, B., and McDaniels, J., 2014, “Stranded Generation Assets : Implications for European Capacity Mechanisms, Energy Markets and Climate Policy,” Stranded Assets Program. SSEE, Univ. Oxford, (January), pp. 1–62.

[89] Brouwer, A. S., van den Broek, M., Seebregts, A., and Faaij, A., 2015, “Operational Flexibility and Economics of Power Plants in Future Low-Carbon Power Systems,” Appl. Energy, **156**, pp. 107–128.

[90] Perico, G., Checchi, C., and Canazza, V., 2018, “The Italian Capacity Market: An Attractive Design for Market Players?,” Int. Conf. Eur. Energy Mark. EEM, **2018-June**.

[91] Mastropietro, P., Fontini, F., Rodilla, P., and Batlle, C., 2018, “The Italian Capacity Remuneration Mechanism: Critical Review and Open Questions,” Energy Policy, **123**(October), pp. 659–669.

[92] Zwijnenburg, J., 2017, “The Impact of Interconnection on System Adequacy on the Dutch Electricity Market An Optimization Modelling Approach,” pp. 1–6.

[93] Bhagwat, P., and De Vries, L., 2017, “Capacity Mechanisms in Interconnected Markets,” pp. 1–6.

[94] IEA, 2021, *Heating*, Paris.

[95] Bauermann, K., 2016, “German Energiewende and the Heating Market – Impact and Limits of Policy,” Energy Policy, **94**, pp. 235–246.

[96] Bloess, A., Schill, W.-P., and Zerrahn, A., 2018, “Power-to-Heat for Renewable Energy Integration: A Review of Technologies, Modeling Approaches, and Flexibility Potentials,” Appl. Energy, **212**, pp. 1611–1626.

[97] Kavvadias, K., Jimenez Navarro, J., and Thomassen, G., 2019, *Decarbonising the EU Heating Sector: Integration of the Power and Heating Sector*, Luxembourg.

[98] Gjorgievski, V. Z., Markovska, N., Abazi, A., and Duić, N., 2021, “The Potential of Power-to-Heat Demand Response to Improve the Flexibility of the Energy System: An Empirical Review,” Renew. Sustain. Energy Rev., **138**, p. 110489.

[99] Kohlhepp, P., Harb, H., Wolisz, H., Waczowicz, S., Müller, D., and Hagenmeyer, V., 2019, “Large-Scale Grid Integration of Residential Thermal Energy Storages as Demand-Side Flexibility Resource: A Review of International Field Studies,” Renew. Sustain. Energy Rev., **101**, pp. 527–547.

[100] Wang, J., Zhong, H., Ma, Z., Xia, Q., and Kang, C., 2017, “Review and Prospect of Integrated Demand Response in the Multi-Energy System,” Appl. Energy, **202**, pp. 772–782.

[101] IEA, 2021, *Heat Pumps*, Paris.

[102] Zhang, H., Zhou, L., Huang, X., and Zhang, X., 2019, “Decarbonizing a Large City’s Heating System Using Heat Pumps: A Case Study of Beijing,” Energy, **186**, p. 115820.

[103] Al-Rabghi, O. M., Beirutty, M., Akyurt, M., Najjar, Y., and Alp, T., 1993, “Recovery and Utilization of Waste Heat,” Heat Recover. Syst. CHP, **13**(5), pp. 463–470.

[104] Wahlroos, M., Pärssinen, M., Manner, J., and Syri, S., 2017, "Utilizing Data Center Waste Heat in District Heating – Impacts on Energy Efficiency and Prospects for Low-Temperature District Heating Networks," Energy, **140**, pp. 1228–1238.

[105] Brückner, S., Liu, S., Miró, L., Radspieler, M., Cabeza, L. F., and Lävemann, E., 2015, "Industrial Waste Heat Recovery Technologies: An Economic Analysis of Heat Transformation Technologies," Appl. Energy, **151**, pp. 157–167.

[106] Mahmoudi, A., Fazli, M., and Morad, M. R., 2018, "A Recent Review of Waste Heat Recovery by Organic Rankine Cycle," Appl. Therm. Eng., **143**, pp. 660–675.

[107] Jouhara, H., Khordehgah, N., Almahmoud, S., Delpech, B., Chauhan, A., and Tassou, S. A., 2018, "Waste Heat Recovery Technologies and Applications," Therm. Sci. Eng. Prog., **6**, pp. 268–289.

[108] Forman, C., Muritala, I. K., Pardemann, R., and Meyer, B., 2016, "Estimating the Global Waste Heat Potential," Renew. Sustain. Energy Rev., **57**, pp. 1568–1579.

[109] Connolly, D., Lund, H., Mathiesen, B. V, Werner, S., Möller, B., Persson, U., Boermans, T., Trier, D., Østergaard, P. A., and Nielsen, S., 2014, "Heat Roadmap Europe: Combining District Heating with Heat Savings to Decarbonise the EU Energy System," Energy Policy, **65**, pp. 475–489.

[110] Kavvadias, K. C., and Quoilin, S., 2018, "Exploiting Waste Heat Potential by Long Distance Heat Transmission: Design Considerations and Techno-Economic Assessment," Appl. Energy, **216**, pp. 452–465.

[111] Sipilä, K., 2016, *Advanced District Heating and Cooling (DHC) Systems*.

[112] IEA, 2021, *District Heating*, Paris.

[113] Zhang, L., Li, Y., Zhang, H., Xu, X., Yang, Z., and Xu, W., 2021, "A Review of the Potential of District Heating System in Northern China," Appl. Therm. Eng., **188**, p. 116605.

[114] 2020, "Danish District Heating – The Heat of the Moment," ICIBSE J.

[115] SDH Solar District Heating, 2016, "Silkeborg Gets the World Largest Solar Thermal Plant" [Online]. Available: https://www.solar-district-heating.eu/silkeborg-gets-the-world-largest-solar-thermal-plant/#:~:text=In the Danish city of,front of the city's gate. [Accessed: 16-Jan-2022].

[116] Weiss, W., and Spörk-Dür, M., 2021, *Solar Heat World Wide*.

[117] Lund, H., Werner, S., Wiltshire, R., Svendsen, S., Eric, J., Hvelplund, F., and Vad, B., 2014, "4th Generation District Heating (4GDH) Integrating Smart Thermal Grids into Future Sustainable Energy Systems," Energy, **68**, pp. 1–11.

[118] Lund, H., Østergaard, P. A., Nielsen, T. B., Werner, S., Thorsen, J. E., Gudmundsson, O., Arabkoohsar, A., and Mathiesen, B. V., 2021, "Perspectives on Fourth and Fifth Generation District Heating," Energy, **227**, p. 120520.

[119] David, A., Mathiesen, B. V., Averfalk, H., Werner, S., and Lund, H., 2017, "Heat Roadmap Europe: Large-Scale Electric Heat Pumps in District Heating Systems," Energies, **10**(4), pp. 1–18.

[120] Lozza, G., 2006, *Turbine a Gas e Cicli Combinati*, Società Editrice Eusculapio, Bologna.

[121] Rovira, A., Sánchez, C., Muñoz, M., Valdés, M., and Durán, M. D., 2011, "Thermoeconomic Optimisation of Heat Recovery Steam Generators of Combined Cycle Gas Turbine Power Plants Considering Off-Design Operation," Energy Convers. Manag., **52**(4), pp. 1840–1849.

[122] Lefebvre, A. H., and Ballal, D. R., 2010, *Gas Turbine Combustion Alternative Fuel and Emissions*, CRC Press.

[123] Bhargava, R. K., Bianchi, M., De Pascale, A., di Montenegro, G., and Peretto, A., 2007, "Gas Turbine Based Power Cycles - A State-of-the-Art Review," *Challenges of Power Engineering and Environment*, K. Cen, Y. Chi, and F. Wang, eds., Springer Berlin Heidelberg, Berlin, Heidelberg, pp. 309–319.

[124] Cincotta, G. A., 1991, "The Testing of GE's MS7001F Gas Turbine," Diesel Gas Turbine Worldw., (January-February).

[125] Vandervort, C., 2018, "Advancements in H Class Gas Turbines and Combined Cycle Power Plants."

[126] McCoy, 2014, *Gas Turbines*.

[127] Tiwari, A. K., Hasan, M. M., and Islam, M., 2013, "Effect of Ambient Temperature on the Performance of a Combined CyclePower Plant," Trans. Can. Soc. Mech. Eng., **37**(4).

[128] Sorce, A., Giugno, A., Marino, D., Piola, S., and Guedez, R., 2019, "Analysis of a Combined Cycle Exploiting Inlet Conditioning Technologies for Power Modulation," *Proceedings of ASME Turbo Expo 2019: Turbomachinery Technical Conference and Exposition, June 17-21 2019*, Phoenix, Arizona, USA.

[129] Kelhofer, R. ., 2009, *Combined-Cycle Gas & Steam Turbine Power Plants*, McGraw-Hill.

[130] Kavvadias, K. C., 2016, "Energy Price Spread as a Driving Force for Combined Generation Investments: A View on Europe," Energy, **115**, pp. 1632–1639.

[131] Majanne, Y., and Vázquez Seisdedos, L., 2012, "Sliding Back Pressure Control in Industrial CHP Plants," IFAC Proc. Vol., **45**(21), pp. 639–644.

[132] Lee, J. H., Kim, T. S., and Kim, E., 2017, "Prediction of Power Generation Capacity of a Gas Turbine Combined Cycle Cogeneration Plant," Energy, **124**, pp. 187–197.

[133] Jarre, M., Noussan, M., and Poggio, A., 2016, "Operational Analysis of Natural Gas Combined Cycle CHP Plants: Energy Performance and Pollutant Emissions," Appl. Therm. Eng., **100**, pp. 304–314.

[134] PUMPHEAT consortium, 2017, *D1.1 Report on PHCC Layout Options*.

[135] Graus, W., and Worrell, E., 2011, "Methods for Calculating CO2 Intensity of Power Generation and Consumption: A Global Perspective," Energy Policy, **39**(2), pp. 613–627.

[136] Broos, W., 2014, "Flexibility in European Power Plants," *ETN Congress October 14, 2014*.

[137] Turconi, R., O'Dwyer, C., Flynn, D., and Astrup, T., 2014, "Emissions from Cycling of Thermal Power Plants in Electricity Systems with High Penetration of Wind Power: Life Cycle Assessment for Ireland," Appl. Energy, **131**, pp. 1–8.

[138] Gonzalez-Salazar, M. A., Kirsten, T., and Prchlik, L., 2018, "Review of the Operational Flexibility and Emissions of Gas- and Coal-Fired Power Plants in a Future with Growing Renewables," Renew. Sustain. Energy Rev., **82**(July 2017), pp. 1497–1513.

[139] Blondeau, J., and Mertens, J., 2019, "Impact of Intermittent Renewable Energy Production on Specific CO 2 and NO x Emissions from Large Scale Gas-Fired Combined Cycles," J. Clean. Prod., **221**, pp. 261–270.

[140] Rossi, I., Sorce, A., and Traverso, A., 2017, "Gas Turbine Combined Cycle Start-up and Stress Evaluation: A Simplified Dynamic Approach," Appl. Energy, **190**, pp. 880–890.

[141] Suess, D. T., Suess, E. A., and Gregory, S. R., 2009, "Development of Startup and Shutdown Permit Limits Based upon Historical Data from Combustion Sources Monitored by Continuous Emission Monitoring Systems," *Proceedings of the Air and Waste Management Association's Annual Conference and Exhibition, AWMA*, pp. 3232–3248.

[142] Geng, Z., Member, S., Chen, Q., Member, S., Xia, Q., Member, S., Kirschen, D. S., Kang, C., and Member, S., 2017, "Environmental Generation Scheduling Considering Air Pollution Control Technologies and Weather Effects," IEEE Trans. Power Syst., **32**(1), pp. 127–136.

[143] Bass, R. J., Malalasekera, W., Willmot, P., and Versteeg, H. K., 2011, "The Impact of Variable Demand upon the Performance of a Combined Cycle Gas Turbine (CCGT) Power Plant," Energy, **36**(4), pp. 1956–1965.

[144] "GME Download Page" [Online]. Available: https://www.mercatoelettrico.org/En/Download/DownloadDati.aspx?val=MGP_Prezzi. [Accessed: 25-Nov-2020].

[145] "Valutazioni e Autorizzazioni Ambientali: VAS - VIA - AIA" [Online]. Available: www.va.minambiente.it. [Accessed: 30-Jun-2021].

[146] "ARERA" [Online]. Available: https://www.arera.it/it/inglese/index.htm. [Accessed: 27-Jan-2021].

[147] Ember, "Carbon Price Viewer" [Online]. Available: https://ember-climate.org/data/carbon-price-viewer/. [Accessed: 27-Nov-2010].

[148] Copernicus Climate Change Service (C3S), 2017, "ERA5: Fifth Generation of ECMWF Atmospheric Reanalyses of the Global Climate" [Online]. Available: https://cds.climate.copernicus.eu/cdsapp#!/home. [Accessed: 27-Jan-2021].

[149] Corberan, J. M., 2016, "13 - New Trends and Developments in Ground-Source Heat Pumps," *Advances in Ground-Source Heat Pump Systems*, S.J. Rees, ed., Woodhead Publishing, pp. 359–385.

[150] Pinheiro, J. M., Salústio, S., Rocha, J., Valente, A. A., and Silva, C. M., 2020, "Adsorption Heat Pumps for Heating Applications," Renew. Sustain. Energy Rev., **119**, p. 109528.

[151] Hollingsworth, J., Phillippi, G., Hinchliff, M., Kulhanek, C., Rimpel, A. M., and Maywald, F., 2019, "Chapter 5 - Reciprocating Compressors," *Compression Machinery for Oil and Gas*, K. Brun, and R. Kurz, eds., Gulf Professional Publishing, pp. 167–252.

[152] Winandy, E. L., and Lebrun, J., 2002, "Scroll Compressors Using Gas and Liquid Injection: Experimental Analysis and Modelling," Int. J. Refrig., **25**(8), pp. 1143–1156.

[153] Ferrando, M., Renuke, A., Traverso, A., and Sishtla, V., 2021, "A New Design Method for Two-Phase Nozzles in High Efficiency Heat Pumps," Int. J. Refrig., **127**, pp. 148–156.

[154] Renuke, A., Vannoni, A., Pascenti, M., and Traverso, A., 2019, "Experimental and Numerical Investigation of Small Scale Tesla Turbines."

[155] Mota, F., Carvalho, E., and Ravagnani, M., 2015, "Modeling and Design of Plate Heat Exchanger."

[156] Delafontaine, V. G. A., Kuebler, J., and Oluoch, L., 2018, "HEAT EXCHANGERS."

[157] Hermes, C. J. L., 2019, "Heat Transfer and Pressure Drop Trade-Offs in Liquid-to-Suction Heat Exchangers," Int. J. Refrig., **104**, pp. 496–500.

[158] Reboli, T., Ferrando, M., Mantelli, L., Gini, L., Sorce, A., Garcia, J., and Guedez, R., 2022, "Gas Turbine Combined Cycle Range Enhancer - Part 1 Cyber-Physical Setup," *ASME Turbo Expo 2022: Turbomachinery Technical Conference and Exposition. Rotterdam. June 13–17, 2022.*, pp. 1–14.

[159] Yari, M., and Sirousazar, M., 2007, "Performance Analysis of the Ejector-Vapour Compression Refrigeration Cycle," Proc. Inst. Mech. Eng. Part A J. Power Energy, **221**(8), pp. 1089–1098.

[160] Bertsch, S. S., and Groll, E. A., 2008, "Two-Stage Air-Source Heat Pump for Residential Heating and Cooling Applications in Northern U.S. Climates," Int. J. Refrig., **31**(7), pp. 1282–1292.

[161] Chua, K. J., Chou, S. K., and Yang, W. M., 2010, "Advances in Heat Pump Systems: A Review," Appl. Energy, **87**(12), pp. 3611–3624.

[162] Austin, B. T., and Sumathy, K., 2011, "Transcritical Carbon Dioxide Heat Pump Systems: A Review," Renew. Sustain. Energy Rev., **15**(8), pp. 4013–4029.

[163] Vinnemeier, P., Wirsum, M., Malpiece, D., and Bove, R., 2016, "Integration of Heat Pumps into Thermal Plants for Creation of Large-Scale Electricity Storage Capacities," Appl. Energy, **184**, pp. 506–522.

[164] Wang, Z., Luther, M. B., Amirkhani, M., Liu, C., and Horan, P., 2021, "State of the Art on Heat Pumps for Residential Buildings," Buildings, **11**(8).

[165] United Nations, 1987, *Montreal Protocol on Substances That Deplete the Ozone Layer*, Montreal.

[166] United Nations, 2016, *Amendment to the Montreal Protocol on Substances That Deplete the Ozone Layer*, Kigali.

[167] Ministry of the Environment & Danish Environmental Protection Agency, 2002, *Statutory Order No. 552 of 2 July 2002 Regulating Certain Industrial Greenhouse Gases*, Copenhagen.

[168] Mota-Babiloni, A., Mateu-Royo, C., Navarro-Esbrí, J., and Barragán-Cervera, Á., 2021, "Experimental Comparison of HFO-1234ze(E) and R-515B to Replace HFC-134a in Heat Pump Water Heaters and Moderately High Temperature Heat Pumps," Appl. Therm. Eng., **196**, p. 117256.

[169] McLinden, M. O., Kazakov, A. F., Steven Brown, J., and Domanski, P. A., 2014, "A Thermodynamic Analysis of Refrigerants: Possibilities and Tradeoffs for Low-GWP Refrigerants," Int. J. Refrig., **38**, pp. 80–92.

[170] Ommen, T., Kj, J., Brix, W., Reinholdt, L., and Elmegaard, B., 2015, "Technical and Economic Working Domains of Industrial Heat Pumps : Part 1 e Single Stage Vapour Compression Heat Pumps," Int. J. Refrig., **5**.

[171] Jürgensen, H., 2016, "Propane as R22-Replacement in Commercial Appliances," Danfoss Compressors GmbH.

[172] Bamigbetan, O., Eikevik, T. M., Nekså, P., Bantle, M., and Schlemminger, C., 2019, "Experimental Investigation of a Prototype R-600 Compressor for High Temperature Heat Pump," Energy.

[173] Kozarcanin, S., Hanna, R., Staffell, I., Gross, R., and Andresen, G., 2020, "Impact of Climate Change on the Cost-Optimal Mix of Decentralised Heat Pump and Gas Boiler Technologies in Europe," Energy Policy, **140**, p. 111386.

[174] Bejan, A., Tsatsaronis, G., and Moran, M., 1996, *Thermal Design and Optimization*, John Wiley & Sons, Inc.

[175] Bell, I. H., Wronski, J., Quoilin, S., and Lemort, V., 2014, "Pure and Pseudo-Pure Fluid Thermophysical Property Evaluation and the Open-Source Thermophysical Property Library CoolProp."

[176] Wilfried, R., and Spang, B., 2010, "C3 Typical Values of Overall Heat Transfer Coefficients," *VDI Heat Atlas*, pp. 75–78.

[177] Turton, R., Bailie, R. C., Whiting, W. B., and Shaeiwitz, J. A., 2008, *Analysis, Synthesis and Design of Chemical Processes*, Pearson Education.

[178] Seader, J. D., Seider, W. D., and Lewin, D. R., 2004, *Product and Process Design Principles: Synthesis, Analysis and Evaluation*, Wiley.

[179] Martin, H., 1996, "A Theoretical Approach to Predict the Performance of Chevron-Type Plate Heat Exchangers," Chem. Eng. Process. Process Intensif., **35**(4), pp. 301–310.

[180] Labuntsov, D. A., 1957, "Heat Transfer in Film Condensation of Pure Steam on Vertical Surfaces and Horizontal Tubes," Teploenergetika, **4**(7), pp. 72–79.

[181] Cengel, Y. A., 2008, *Introduction to Thermodynamics and Heat Transfer: Engineering*, McGraw-Hill.

[182] Taal, M., Bulatov, I., Klemeš, J., and Stehlík, P., 2003, "Cost Estimation and Energy Price Forecasts for Economic Evaluation of Retrofit Projects," Appl. Therm. Eng.

[183] Danish Energy Agency, 2016, “Technology Data for Energy Plants for Electricity and District Heating Generation (v.0009 -April 2020).”

[184] Eurostat, 2022, “Energy (T_nrg) Database.”

[185] Istituto Superiore per la Protezione e la Ricerca Ambientale, 2020, “Tabella Dei Parametri Standard Nazionali Applicabili per Il Calcolo Delle Emissioni per Il Periodo 1 Gennaio – 31 Dicembre 2019.”

[186] Satyavada, H., and Baldi, S., 2016, “A Novel Modelling Approach for Condensing Boilers Based on Hybrid Dynamical Systems,” Machines, **4**(2).

[187] Eurostat, 2022, “Climate Change Mitigation (Cli_mit) Database.”

[188] Reboli, T., Ferrando, M., Mantelli, L., Gini, L., Sorce, A., and Traverso, A., 2022, “Gas Turbine Combined Cycle Range Enhancer - Part 2 Performance Demonstration,” *ASME Turbo Expo 2022: Turbomachinery Technical Conference and Exposition. Rotterdam. June 13–17, 2022.*

[189] Abudu, K., Igie, U., Roumeliotis, I., and Hamilton, R., 2021, “Impact of Gas Turbine Flexibility Improvements on Combined Cycle Gas Turbine Performance,” Appl. Therm. Eng., **189**, p. 116703.

[190] Kim, M. J., and Kim, T. S., 2019, “Integration of Compressed Air Energy Storage and Gas Turbine to Improve the Ramp Rate,” Appl. Energy, **247**, pp. 363–373.

[191] Bhargava, R. K., Meher-Homji, C. B., Chaker, M. A., Bianchi, M., Melino, F., Peretto, A., and Ingistov, S., 2006, “Gas Turbine Fogging Technology: A State-of-the-Art Review—Part I: Inlet Evaporative Fogging—Analytical and Experimental Aspects,” J. Eng. Gas Turbines Power, **129**(2), pp. 443–453.

[192] Al-Ibrahim, A. M., and Varnham, A., 2010, “A Review of Inlet Air-Cooling Technologies for Enhancing the Performance of Combustion Turbines in Saudi Arabia,” Appl. Therm. Eng., **30**(14), pp. 1879–1888.

[193] Radchenko, A., Bohdal, L., Zongming, Y., Portnoi, B., and Tkachenko, V., 2020, “Rational Designing of Gas Turbine Inlet Air Cooling System,” *Advanced Manufacturing Processes*, V. Tonkonogyi, V. Ivanov, J. Trojanowska, G. Oborskyi, M. Edl, I. Kuric, I. Pavlenko, and P. Dasic, eds., Springer International Publishing, Cham, pp. 591–599.

[194] Gkoutzamanis, V., Chatziangelidou, A., Efstathiadis, T., Kalfas, A., Traverso, A., and Chiu, J., 2019, “Thermal Energy Storage For Gas Turbine Power Augmentation,” J. Glob. Power Propuls. Soc., **3**, pp. 592–608.

[195] Variny, M., and Mierka, O., 2009, “Improvement of Part Load Efficiency of a Combined Cycle Power Plant Provisioning Ancillary Services,” Appl. Energy, **86**(6), pp. 888–894.

[196] Liu, Z., Ren, X., Yan, Z., Zhu, H., Zhang, T., Zhu, W., and Li, X., 2019, “Effect of Inlet Air Heating on Gas Turbine Efficiency under Partial Load,” Energies, **12**(17).

[197] Mantilla, W., Garcia, J., Guédez, R., and Sorce, A., 2020, "Short-Term Optimization of a Combined Cycle Power Plant Integrated With an Inlet Air Conditioning Unit," *ASME Turbo Expo 2020: Turbomachinery Technical Conference and Exposition, September 21-25 2020: Turbomachinery Technical Conference and Exposition, June 17–21, 2019*.

[198] Guédez, R., García, J., Nuutinen, A., Graziano, G., Chiu, J., Sorce, A., Piantelli, L., Traverso, A., and Laumert, B., 2019, "Techno-Economic Comparative Analysis of Innovative Combined Cycle Power Plant Layouts Integrated With Heat Pumps and Thermal Energy Storage," *ASME Turbo Expo 2019: Turbomachinery Technical Conference and Exposition, June 17–21, 2019*, Phoenix, Arizona, USA, p. 12.

[199] Hermans, M., Bruninx, K., and Delarue, E., 2018, "Impact of CCGT Start-Up Flexibility and Cycling Costs Toward Renewables Integration," IEEE Trans. Sustain. Energy, **9**, pp. 1468–1476.

[200] Ricerca sul Sistema Elettrico - RSE SpA, 2016, *Energia Elettrica, Anatomia Dei Costi*.

[201] Giugno, A., Piantelli, L., and Sorce, A., 2018, "Integration of Heat Pump and Gas Turbine Combined Cycle: Layout and Market Opportunity," *9th International Gas Turbine Conference, 10-11 October 2018*, Brussels.

[202] ENTSO-E, "ENTSO-E Transparency Platform" [Online]. Available: https://transparency.entsoe.eu/transmission-domain/r2/dayAheadPrices/show. [Accessed: 30-Nov-2021].

[203] LCG Consulting, "Energy Online Data" [Online]. Available: http://www.energyonline.com/Data. [Accessed: 30-Nov-2021].

[204] Lowe, R., 2011, "Combined Heat and Power Considered as a Virtual Steam Cycle Heat Pump," Energy Policy, **39**(9), pp. 5528–5534.

[205] Malinowska, W., and Malinowski, L., 2003, "Parametric Study of Exergetic Efficiency of a Small-Scale Cogeneration Plant Incorporating a Heat Pump," Appl. Therm. Eng., **23**(4), pp. 459–472.

[206] Dagilis, V., 2013, "Combined Heat Pump and Power Plant. Part II: Economic Analysis," Mechanika, **19**(2), pp. 172–177.

[207] Blarke, M. B., and Dotzauer, E., 2011, "Intermittency-Friendly and High-Ef Fi Ciency Cogeneration : Operational Optimisation of Cogeneration with Compression Heat Pump, Flue Gas Heat Recovery, and Intermediate Cold Storage," Energy, **36**(12), pp. 6867–6878.

[208] Blarke, M. B., and Lund, H., 2007, "Large-Scale Heat Pumps in Sustainable Energy Systems: System and Project Perspectives," Therm. Sci., **11**(3), pp. 143–152.

[209] Hebenstreit, B., Schnetzinger, R., Ohnmacht, R., and Ho, E., 2014, "Techno-Economic Study of a Heat Pump Enhanced Flue Gas Heat Recovery for Biomass Boilers," **1**.

[210] Li, Y., Yan, M., Zhang, L., Chen, G., Cui, L., Song, Z., Chang, J., and Ma, C., 2016, "Method of Flash Evaporation and Condensation - Heat Pump for Deep Cooling of Coal-Fired Power Plant Flue Gas: Latent Heat and Water Recovery," Appl. Energy, **172**, pp. 107–117.

[211] Ommen, T., Markussen, W. B., and Elmegaard, B., 2014, "Heat Pumps in Combined Heat and Power Systems," Energy, **76**, pp. 989–1000.

[212] Shi, X., Che, D., Agnew, B., and Gao, J., 2011, "An Investigation of the Performance of Compact Heat Exchanger for Latent Heat Recovery from Exhaust Flue Gases," Int. J. Heat Mass Transf., **54**(1–3), pp. 606–615.

[213] Chen, Q., Finney, K., Li, H., Zhang, X., Zhou, J., Sharifi, V., and Swithenbank, J., 2012, "Condensing Boiler Applications in the Process Industry," Appl. Energy, **89**(1), pp. 30–36.

[214] Iliopoulos, I., Karampekios, A., Pandis, P. K., Vourdas, N., Jouhara, H., Tassou, S., and Stathopoulos, V. N., 2018, "Evaluation of Organic Coatings for Corrosion Protection of Condensing Economizers," *Procedia Structural Integrity*, Elsevier B.V., pp. 295–302.

[215] Hwang, K., Song, C. H., Saito, K., and Kawai, S., 2010, "Experimental Study on Titanium Heat Exchanger Used in a Gas Fired Water Heater for Latent Heat Recovery," Appl. Therm. Eng., **30**(17–18), pp. 2730–2737.

[216] Kehlhofer, R., Warner, J., Nielsen, H., and Rolf, B., 1997, *Combined-Cycle Gas & Steam Turbine Power Plants*, PennWell Publidhing Company.

[217] Cycles, R., Comfort, T., Health, I. E., Buildings, A. A., Resources, E., Information, C. D., Estimating, E., Methods, M., and Design, D., "1997 ASHRAE Handbook Preface."

[218] Petters, M. S., Timmerhaus, K. D., and West, E. R., 2002, *Plant Design and Economics for Chemical Engineers*, McGraw-Hill Education.

[219] Terna, 2018, *Dati Statistici Sull'Energia Elettrica in Italia*.

[220] Li, H., Song, J., Sun, Q., Wallin, F., and Zhang, Q., 2019, "A Dynamic Price Model Based on Levelized Cost for District Heating," Energy, Ecol. Environ., **4**(1), pp. 15–25.

[221] Gestore Mercati Energetici, 2018, "Dati Storici Mercati."

[222] Ammermann, H., Hoff, P., Atanasiu, M., Ayllor, J., Kaufmann, M., and Tisler, O., 2015, *Advancing Europe's Energy Systems: Stationary Fuel Cells in Distributed Generation*.

[223] Capros, P., Vita, A. De, Tasios, N., Siskos, P., Kannavou, M., Petropoulos, A., Evangelopoulou, S., Zampara, M., Papadoupoulos, D., Paroussos, L., Fragiadakis, K., and Tsani, S., 2016, "EU Reference Scenario 2016 - A Policy Framework for Climate and Energy in the Period from 2020 to 2030," EU Ref. Scenar. 2016, p. 27.

[224] The European Commission, 2019, "Quarterly Report on European Electricity Markets Second Quarter of 2019," Q. Rep. Eur. Electr. Mark., **12**(2).

[225] Ministero dell'ambiente e della tutela del territorio e del mare, 2019, "Decreto Legislativo n.30 Del 2013, Tabella Allegata Dei Parametri Standard Nazionali per Il Monitoraggio e La Comunicazione Dei Gas Ad Effetto Serra.Pdf."

[226] Eurostat, 2018, *Energy, Transport and Environment Indicators. 2018 Edition*.

[227] Cassettari, L., Mosca, R., and Revetria, R., 2012, “Monte Carlo Simulation Models Evolving in Replicated Runs: A Methodology to Choose the Optimal Experimental Sample Size,” Math. Probl. Eng., **2012**, pp. 73–76.

[228] Fisher, R. A., 1922, “On the Mathematical Foundations of Theoretical Statistics,” Philos. Trans. R. Soc. A Math. Phys. Eng. Sci.

[229] Ghanem, R., Owhadi, H., and Higdon, D., 2017, *Handbook of Uncertainty Quantification*, Berlin, Germany.

[230] European Commission, 2016, *EU Reference Scenario 2016 - Energy, Transport and GHG Emissions - Trends to 2050*.

[231] Stagnaro, B. C., 2012, “How Solar Subsidies Can Distort the Power Market : The Case of Italy.”

[232] “Monitoraggio Delle Emissioni Di Gas Ad Effetto Serra per Gli Impianti Stazionari” [Online]. Available: https://www.minambiente.it/pagina/monitoraggio-delle-emissioni-di-gas-ad-effetto-serra-gli-impianti-stazionari. [Accessed: 27-Nov-2020].

[233] Eurostat, “Gas Prices for Non-Household Consumers - Bi-Annual Data (Nrg_pc_203).”

[234] Vannoni, A., Garcia, J. A., Guedez, R., and Sorce, A., 2021, “Ancillary Service Potential for Flexible Combined Cycles,” *ASME Turbo Expo 2021: Turbomachinery Technical Conference and Exposition. Volume 4: Controls, Diagnostics, and Instrumentation; Cycle Innovations; Cycle Innovations: Energy Storage; Education; Electric Power. Virtual, Online. June 7–11, 2021.*

[235] Mathworks, “Intlinprog, Mixed-Integer Linear Programming (MILP)” [Online]. Available: https://it.mathworks.com/help/optim/ug/intlinprog.html#bts3f9f-f. [Accessed: 12-Apr-2022].

[236] Fang, T., and Lahdelma, R., 2016, “Optimization of Combined Heat and Power Production with Heat Storage Based on Sliding Time Window Method,” Appl. Energy, **162**, pp. 723–732.

[237] Narula, K., De Oliveira Filho, F., Chambers, J., Romano, E., Hollmuller, P., and Patel, M. K., 2020, “Assessment of Techno-Economic Feasibility of Centralised Seasonal Thermal Energy Storage for Decarbonising the Swiss Residential Heating Sector,” Renew. Energy, **161**, pp. 1209–1225.

[238] GE Gas Power, 2018, “Breaking the Power Plant Efficiency Record Again” [Online]. Available: https://www.ge.com/gas-power/resources/articles/2018/nishi-nagoya-efficiency-record. [Accessed: 18-Jan-2022].

[239] Youssef, W., Ge, Y., and Tassou, S. A., 2017, “Indirect Expansion Solar Assisted Heat Pump System for Hot Water Production with Latent Heat Storage and Applicable Control Strategy,” Energy Procedia, **123**, pp. 180–187.

[240] Colbacchini, R., 2014, “Development of a Visualization and Analysis Tool for Public Domain Data of the Italian Electricity Market,” Politecnico di Milano.

Appendix A. Power plants data

This appendix reports the data of Italian power plants utilized within the thesis. Table A.1 includes the production units, which were possible to identify, and active in the Italian ancillary services markets (*Mercato dei Servizi di Dispacciamento*) from 2018 to 2021. Offers and bids from these plants have been used to train and test the machine learning algorithms presented in Section 5.3.2. The capacity column reports the overall capacity installed at the power plant facility, summing together all active production units.

Table A.2 concerns the Italian power-oriented (i.e., devoted exclusively to power generation) Combined Cycle Gas Turbine (CCGT) power plants, including further details with respect to Table A.1. These data have been used in the analyses presented in Chapter 2. Green-highlighted rows indicate those power plants reporting, not only aggregate data but the fully detailed report of emissions during each transient (start-ups, shutdowns, and other generic transients).

Table A.1: Production units active in the Italian ancillary services markets between 2018 and 2021.

UP Name	Code	Power Plant Name	Capacity [MW]	Voltage Level [kV]	Market Zone	Municipality	Prov. Code	Lat.	Long.	Type
UP_AGRI_1	26WIMPI-S17AGRIH	AGRI	39	150	SUD	Gallicchio	PZ	40.27	16.16	Hydro Water Reservoir
UP_ALTOADDA_1	26WIMPITOADDA-1T	VENINA	327	220	NORD	Piateda	SO	46.16	9.92	Hydro Pumped Storage
UP_ALTOMONTE_1	26WIMPI-S18EADS0	ALTOMONTE	808	380	CALA	Cosenza	CS	39.71	16.22	Fossil Gas
UP_ANAPO_C.L_1	26WIMYI-S19ANPAB	ANAPO C.LE	500	220	SICI	Priolo Gargallo	SR	37.11	15.14	Hydro Pumped Storage
UP_ARSIE_1	26WIMPI-S05ARSIQ	ARSIE'	34	132	NORD	Arsiè	BL	45.9	11.94	Hydro Run-of-river and poundage
UP_AZOTATI_5	26WIMPI-S05AZTT6	AZOTATI	236	220	NORD	Venezia	VE	45.46	12.24	Fossil Gas
UP_BARGI_CEN_1	26WIMPI-S08BCRGX	BARGI CENTRALE	281	380	NORD	Camugnano	BO	44.12	11.04	Hydro Pumped Storage
UP_BATTIGGIO_1	26WIMPI-S01BTTG1	BATTIGGIO	20	60	NORD	Bannio Anzino	VB	45.98	8.13	Hydro Run-of-river and poundage
UP_BRNDSSUDCE_1		BRINDISI SUD CE		380	SUD	Brindisi	BR	40.56	18.03	Fossil Hard coal
UP_BRNDSSUDCE_2		BRINDISI SUD CE		380	SUD	Brindisi	BR	40.56	18.03	Fossil Hard coal
UP_BRNDSSUDCE_3		BRINDISI SUD CE		380	SUD	Brindisi	BR	40.56	18.03	Fossil Hard coal
UP_BRNDSSUDCE_4		BRINDISI SUD CE		380	SUD	Brindisi	BR	40.56	18.03	Fossil Hard coal
UP_BRUNICO_M_1	26WIMPI-S04BMRN3	BRUNICO	40	132	NORD	Perca/Percha	BZ	46.76	12.05	Hydro Water Reservoir
UP_BUSSENTO_1	26WIMPI-S15BSSN0	BUSSENTO	60	150	CSUD	Morigerati	SA	40.27	15.68	Hydro Run-of-river and poundage
UP_BUSSI_1	26WIMPI-S13BSSUZ	BUSSI	122	150	CSUD	Bussi sul Tirino	PE	42.2	13.84	Fossil Gas
UP_CANDELA_1	26WIMPI-S16CNDLL	CANDELA	401	380	SUD	Candela	FG	41.2	15.48	Fossil Gas
UP_CARONA_1	26WIMPI-S03CRNAM	CARONA	48	132	NORD	Carona	BG	46.02	9.79	Hydro Water Reservoir
UP_CASSANO_2	26WIMPI-S03ACMNW	CASSANO	748	380	NORD	Cassano d'Adda	MI	45.51	9.51	Fossil Gas
UP_CASTELDEL_1	26WIMPI-S01CSTD6	CASTELDELF	28	132	NORD	Casteldelfino	CN	44.59	7.06	Hydro Water Reservoir
UP_CASTROCUC_1	26WIMPI-S18CSTR3	CASTROCUCCO	83	150	SUD	Trecchina	PZ	39.99	15.8	Hydro Water Reservoir
UP_CCGTPRILIA_1	26WIMPI-0300653B	CCGT APRILIA	787	380	CSUD	Aprilia	LT	41.56	12.63	Fossil Gas
UP_CHIESE_1	26WIMPI-S04CMGI4	CIMEGO	220	220	NORD	Borgo Chiese	TN	45.92	10.63	<undefined>
UP_CHIEVOLIS_2	26WIMPI-S06CHVLZ	CHIEVOLIS	20	132	NORD	Tramonti di Sopra	PN	46.25	12.73	Hydro Water Reservoir
UP_CHIVASSO_1	26WIMPI-S01CHVSE	CHIVASSO	1123	380	NORD	Chivasso	TO	45.19	7.9	Fossil Gas
UP_CHIVASSO_2	26WIMPI-S01CHVSE	CHIVASSO	1123	380	NORD	Chivasso	TO	45.19	7.9	Fossil Gas
UP_CMPLCCIOLI_2	26WIMPI-S01CMPLQ	CAMPLICCIOLI	9	15	NORD	Antrona Schieranco	VB	46.05	8.08	Hydro Water Reservoir
UP_CNTRLDCGNR_46		CENTRALE DI COGENERAZIONE GENOVA SAMPIERDARENA	30	132	NORD	Genova	GE	44.41	8.88	Fossil Gas
UP_CNTRLDSCND_1	26WIMPI-S18SCNDX	CENTRALE DI SCANDALE	821	380	CALA	Scandale	KR	39.1	17.03	Fossil Gas
UP_CNTRLDSCND_2	26WIMPI-S18SCNDX	CENTRALE DI SCANDALE	821	380	CALA	Scandale	KR	39.1	17.03	Fossil Gas

UP Name	Code	Power Plant Name	Capacity [MW]	Voltage Level [kV]	Market Zone	Municipality	Prov. Code	Lat.	Long.	Type
UP_CNTRLDTRNL_1	26WIMPI-S03CDTL1	CENTRALE DI TURANO LODIGIANO - BERTONICO	800	380	NORD	Terranova dei Passerini	LO	45.23	9.64	Fossil Gas
UP_CNTRLDTVRL_1	26WIMPI-S15STTV3	CENTRALE DI TEVEROLA	404	380	CSUD	Teverola	CS	41.01	14.23	Fossil Gas
UP_CNTRLNTRNO_11	26WIMPI-S04NATRE	CENTRALE NATURNO	175	220	NORD	Naturno/Naturns	BZ	46.65	10.99	Hydro Water Reservoir
UP_COTILIA_1	26WIMPI-S12CTLOS	COTILIA	40	150	CNOR	Cittaducale	RI	42.37	12.97	Hydro Water Reservoir
UP_CPODIPONTE_2	26WIMPI-S11CPDPZ	CAPODIPONTE	24	132	CNOR	Ascoli Piceno	AP	42.81	13.5	Hydro Water Reservoir
UP_CSSINOMETA_1	26WIMPI-0817510V	CASSINO-META	41	150	CSUD	Piedimonte San Germano	FR	41.48	13.75	Fossil Gas
UP_CTE_DEL_M_2	26WIMPI-S03ACMSM	CTE DEL MINCIO	381	220	NORD	Ponti sul Mincio	MN	45.4	10.71	Fossil Gas
UP_CTNUCENORD_1	26WIMPI-S19APGPP	CTE NUCE NORD	446	380	SICI	Siracusa	SR	37.18	15.18	<undefined>
UP_CTNUCENORD_2	26WIMPI-S19APGPP	CTE NUCE NORD	446	380	SICI	Siracusa	SR	37.18	15.18	Fossil Gas
UP_CTNUCENORD_3	26WIMPI-S19APGPP	CTE NUCE NORD	446	380	SICI	Siracusa	SR	37.18	15.18	Fossil Gas
UP_CTTAMARETE_1	26WIMPI-S13CTTM2	CTE TAMARETE	115	150	CSUD	Ortona	CH	42.32	14.38	Fossil Gas
UP_CURON_ME_1	26WIMPI-S04CMRNZ	CURON	13	132	NORD	Curon Venosta/Graun im Vinschgau	BZ	46.77	10.53	Hydro Run-of-river and poundage
UP_DOSSI_1	26WIMPI-S03DSSO7	DOSSI	43	132	NORD	Valbondione	BG	47.03	9.98	Hydro Water Reservoir
UP_DUINO_1	26WIMPI-S06SDDT9	DUINO	110	132	NORD	Duino Aurisina-Devin Nabrežina	TS	45.79	13.58	Fossil Gas
UP_EDOLO_1	26WIMPI-S03EDLO9	EDOLO	950	380	NORD	Edolo	BS	46.17	10.34	Hydro Pumped Storage
UP_ETQ_ROVINA_1	26WIMPI-R01ENTRX	ENTRACQUE ROVINA	125	380	NORD	Entracque	CN	44.18	7.35	Hydro Pumped Storage
UP_ETQCHIOTAS_1	26WIMPI-S01ENTRP	ENTRACQUE_CHRO	1064	380	NORD	Entracque	CN	44.17	7.33	Hydro Pumped Storage
UP_FADALTO_1	26WIMPI-S05FDLTJ	FADALTO	220	220	NORD	Vittorio Veneto	TV	46.07	12.33	Hydro Pumped Storage
UP_FIUMESANT_3	26WIMPI-S20FOMSR	FIUMESANTO	534	380	SARD	Sassari	SS	40.85	8.31	Fossil Hard coal
UP_FIUMESANT_4	26WIMPI-S20FOMSR	FIUMESANTO	534	380	SARD	Sassari	SS	40.85	8.31	Fossil Hard coal
UP_FLUMENDOS_4	26WIMPIENDOSA-1A	FLUMENDOSA 2			SARD	Villagrande Strisaili	NU	39.96	9.56	Hydro Run-of-river and poundage
UP_FLUMENDOSA_1	26WIMPIENDOSA-1A	FLUMENDOSA 2			SARD	Villagrande Strisaili	NU	39.96	9.56	Hydro Run-of-river and poundage
UP_FONTANA_B_1	26WIMPI-S04FBNTR	FONTANA BIANCA	10	60	NORD	Ultimo/Ulten	BZ	46.49	10.83	Hydro Water Reservoir
UP_FUSINA_T_1	26WIMPI-S05FTSNK	FUSINA T.	871	380	NORD	Venezia	VE	45.43	12.25	Fossil Hard coal
UP_FUSINA_T_2	26WIMPI-S05FTSNK	FUSINA T.	871	380	NORD	Venezia	VE	45.43	12.25	Fossil Hard coal
UP_FUSINA_T_3	26WIMPI-S05FTSNK	FUSINA T.	871	380	NORD	Venezia	VE	45.43	12.25	Fossil Hard coal
UP_FUSINA_T_4	26WIMPI-S05FTSNK	FUSINA T.	871	380	NORD	Venezia	VE	45.43	12.25	Fossil Hard coal
UP_GARGNANO_1	26WIMPI-S03GRGNY	GARGNANO	137	220	NORD	Gargnano	BS	45.7	10.69	Hydro Pumped Storage
UP_GEROLA_1	26WIMPI-S03GRLE0	GEROLA	13	132	NORD	Gerola Alta	SO	46.03	9.54	Hydro Water Reservoir
UP_GISSI_1	26WIMPI-S13CDGNT	GISSI	840	380	CSUD	Gissi	CH	45.05	14.56	Fossil Gas
UP_GISSI_2	26WIMPI-S13CDGNT	GISSI	840	380	CSUD	Gissi	CH	45.05	14.56	Fossil Gas

UP Name	Code	Power Plant Name	Capacity [MW]	Voltage Level [kV]	Market Zone	Municipality	Prov. Code	Lat.	Long.	Type
UP_GOGLIO_2	26WIMZI-S01GGLO0	GOGLIO	18	132	NORD	Baceno	VB	46.3	8.27	Hydro Water Reservoir
UP_GRAVEDONA_1	26WIMPI-S03GCRV8	GRAVEDONA	14	15	NORD	Gravedona ed Uniti	CO	46.09	9.27	Hydro Run-of-river and poundage
UP_GRESSONEY_1	26WIMPI-S02GRSSV	GRESSONEY	16	132	NORD	Gressoney-La-Trinité	AO	45.83	7.83	Hydro Water Reservoir
UP_GUADALAMI_1	26WIMPI-S19GCDLR	GUADALAMI C.LE	80	150	SICI	Piana degli Albanesi	PA	37.96	13.28	Hydro Pumped Storage
UP_ISABENERGY_2	26WIMPI-S19IESBL	ISAB ENERGY	576	380	SICI	Priolo Gargallo	SR	37.13	15.2	Fossil Coal-derived gas
UP_LA_CASELL_1	26WIMPI-S08LCCS4	LA CASELLA C.LE	1476	380	NORD	Castel San Giovanni	PC	45.09	9.48	Fossil Gas
UP_LA_CASELL_2	26WIMPI-S08LCCS4	LA CASELLA C.LE	1476	380	NORD	Castel San Giovanni	PC	45.09	9.48	Fossil Gas
UP_LA_CASELL_3	26WIMPI-S08LCCS4	LA CASELLA C.LE	1476	380	NORD	Castel San Giovanni	PC	45.09	9.48	Fossil Gas
UP_LA_CASELL_4	26WIMPI-S08LCCS4	LA CASELLA C.LE	1476	380	NORD	Castel San Giovanni	PC	45.09	9.48	Fossil Gas
UP_LANA_1	26WIMPI-S04LNAAQ	LANA	98	220	NORD	Lana/Lana	BZ	46.61	11.15	Hydro Run-of-river and poundage
UP_LAPPAGO_1	26WIMPI-S04LPPGZ	LAPPAGO	26	132	NORD	Selva dei Molini/Mühlwald	BZ	46.89	11.87	Hydro Water Reservoir
UP_LARINO_TG_1	26WIMPI-S14LTRNT	LARINO TG	248	150	SUD	Ururi	CB	41.82	14.97	Fossil Gas
UP_LASA_ME_1	26WIMPI-S04LMSAD	LASA	64	220	NORD	Lasa/Laas	BZ	46.61	10.71	Hydro Water Reservoir
UP_LEINI_1	26WIMPI-S01LNEIG	LEINI	385	380	NORD	Leini	TO	45.16	7.75	Fossil Gas
UP_LEVANTE_3	26WIMPI-S05PMAR7	LEVANTE	516	220	NORD	Venezia	VE	45.45	12.26	Fossil Gas
UP_LEVANTE_4	26WIMPI-S05PMAR7	LEVANTE	516	220	NORD	Venezia	VE	45.45	12.26	Fossil Gas
UP_LIRO_1		MESE	280	132	NORD	Mese	SO	46.3	9.38	Hydro Run-of-river and poundage
UP_M._CIAPEL_1	26WIMPI-S05MCPLT	MALGA CIAPELA	20	132	NORD	Rocca Pietore	BL	46.43	11.9	Hydro Water Reservoir
UP_MAEN_5	26WIMPI-S02MNAEP	MAEN	22	132	NORD	Valtournenche	AO	45.87	7.61	Hydro Water Reservoir
UP_MALPENSA__1	26WIMPI-S03SMLPC	CENTRALE DI MALPENSA	50	132	NORD	Ferno	VA	45.62	8.72	Fossil Gas
UP_MASOCORON_1	26WIMPI-S04MSCRZ	MASOCORONA	40	132	NORD	Ala	TN	45.77	11.01	Hydro Water Reservoir
UP_MATESE_1S_1	26WIMPI-S15M1TS3	MATESE 1S	16	150	CSUD	Piedimonte Matese	CE	41.36	14.37	Hydro Water Reservoir
UP_MONCALIERI_3	26WIMPI-S01MNCLB	MONCALIERI	780	220	NORD	Moncalieri	TO	44.99	7.68	Fossil Gas
UP_MONCALRPW_2	26WIMPI-S01MNCLB	MONCALIERI	780	220	NORD	Moncalieri	TO	44.99	7.68	Fossil Gas
UP_MONFALCO_1	26WIMPI-S06MTNFA	MONFALCONE	315	220	NORD	Monfalcone	GO	45.8	13.55	Fossil Hard coal
UP_MONFALCO_2	26WIMPI-S06MTNFA	MONFALCONE	315	220	NORD	Monfalcone	GO	45.8	13.55	Fossil Hard coal
UP_MONTALTO_1	26WIMPI-S12MCNTU	MONTALTO C.LE	934	380	CSUD	Montalto di Castro	VT	42.36	11.53	Fossil Gas
UP_MONTALTO_2	26WIMPI-S12MCNTU	MONTALTO C.LE	934	380	CSUD	Montalto di Castro	VT	42.36	11.53	Fossil Gas
UP_MONTALTO_3	26WIMPI-S12MCNTU	MONTALTO C.LE	934	380	CSUD	Montalto di Castro	VT	42.36	11.53	Fossil Gas
UP_MONTORIO_1	26WIMPI-S13MNTR3	MONTORIO	110	220	CSUD	Teramo	TE	42.36	11.53	Hydro Run-of-river and poundage
UP_MORASCO_1	26WIMPI-S01MRSC2	MORASCO	41	132	NORD	Formazza	VB	46.42	8.841	Hydro Water Reservoir

UP Name	Code	Power Plant Name	Capacity [MW]	Voltage Level [kV]	Market Zone	Municipality	Prov. Code	Lat.	Long.	Type
UP_MUCONE_1		MUCONE 1S		150	CALA	Acri	CS	39.47	16.41	Hydro Water Reservoir
UP_MUCONE_1S_1	26WIMPIMUCONE-19	MUCONE 1S		150	CALA	Acri	CS	39.47	16.41	Hydro Water Reservoir
UP_NAPOLIL_4	26WIMPI-S15NLPLI	NAPOLI L	400	220	CSUD	Napoli	NA	40.83	14.3	Fossil Gas
UP_NCTLVRNFRR_1	26WIMPI-S01ECLF6	E.ON C.TE LIVORNO FERRARIS	776	380	NORD	Livorno Ferraris	VC	45.24	8.19	Fossil Gas
UP_NERAVELINO_1	26WIMPIVELINO-1Q	GALLETO	295	220	CSUD	Terni	TR	42.55	12.7	Hydro Run-of-river and poundage
UP_NOCE_1		TAIO	161	220	NORD	Predaia	TN	46.33	11.06	Hydro Run-of-river and poundage
UP_NPWRBRNDSI_10	26WIMPI-S16EBNPL	ENIPOWER BRINDISI	1217	380	SUD	Brindisi	BR	40.63	18	Fossil Gas
UP_NPWRBRNDSI_8	26WIMPI-S16EBNPL	ENIPOWER BRINDISI	1217	380	SUD	Brindisi	BR	40.63	18	Fossil Gas
UP_NPWRBRNDSI_9	26WIMPI-S16EBNPL	ENIPOWER BRINDISI	1217	380	SUD	Brindisi	BR	40.63	18	Fossil Gas
UP_NPWRFRRRRB_10	26WIMPI-S03FERRD	ENIPOWER FERRERA ERBOGNONE	1006	380	NORD	Ferrera Erbognone	PV	45.01	8.87	Fossil Gas
UP_NPWRFRRRRB_8	26WIMPI-S03FERRD	ENIPOWER FERRERA ERBOGNONE	1006	380	NORD	Ferrera Erbognone	PV	45.01	8.87	Fossil Gas
UP_NPWRFRRRRB_9	26WIMPI-S03FERRD	ENIPOWER FERRERA ERBOGNONE	1006	380	NORD	Ferrera Erbognone	PV	45.01	8.87	Fossil Gas
UP_NPWRLVORNO_7	26WIMPI-S09AGPP4	ENIPOWER LIVORNO	203	132	CNOR	Collesalvetti	LI	43.58	10.34	Fossil Gas
UP_NPWRMNTOVA_2	26WIMPI-S03EMC43	ENIPOWER MANTOVA	812	380	NORD	Mantova	MN	45.15	10.83	Fossil Gas
UP_NPWRMNTOVA_3	26WIMPI-S03EMC43	ENIPOWER MANTOVA	812	380	NORD	Mantova	MN	45.15	10.83	Fossil Gas
UP_NPWRRVENNA_10	26WIMPI-S08ERNPQ	ENIPOWER RAVENNA	961	380	NORD	Ravenna	RA	44.45	12.24	Fossil Gas
UP_NPWRRVENNA_11	26WIMPI-S08ERNPQ	ENIPOWER RAVENNA	961	380	NORD	Ravenna	RA	44.45	12.24	Fossil Gas
UP_NPWRRVENNA_9	26WIMPI-S08ERNPQ	ENIPOWER RAVENNA	961	380	NORD	Ravenna	RA	44.45	12.24	Fossil Gas
UP_NRGAMOLISE_1	26WIMPI-S14TERME	ENERGIA MOLISE	769	380	SUD	Termoli	CB	41.94	15	Fossil Gas
UP_ORTICA_1	26WIMPIORTICA-13	TIMPAGRANDE	395	150	CALA	Cotronei	KR	39.52	16.78	Hydro Run-of-river and poundage
UP_OSTIGLIA_12	26WIMPI-S03OSTG2	OSTIGLIA	1123	380	NORD	Ostiglia	MN	45.06	11.14	Fossil Gas
UP_OSTIGLIA_3	26WIMPI-S03OSTG2	OSTIGLIA	1123	380	NORD	Ostiglia	MN	45.06	11.14	Fossil Gas
UP_PALAZZO_2_1	26WIMPI-S18P2LZD	PALAZZO 2	46	150	CALA	Orsomarso	CS	39.8	15.87	Hydro Run-of-river and poundage
UP_PANTANO_D_1	26WIMPI-S03PDNTC	PANTANO D'AVIO	13	132	NORD	Edolo	BS	46.17	10.34	Hydro Water Reservoir
UP_PELOS_1	26WIMPI-S05PLSEK	PELOS	30	132	NORD	Vigo di Cadore	BL	46.49	12.45	Hydro Run-of-river and poundage
UP_PERRERES_1	26WIMPI-S02PRRRS	PERRERES	15	132	NORD	Valtournenche	AO	45.9	7.62	Hydro Water Reservoir
UP_PIACENZA_4	26WIMPI-S08PLCNW	PIACENZA	806	380	NORD	Piacenza	PC	45.06	9.71	Fossil Gas
UP_PIAN_DELL_1	26WIMPI-S09PDRND	PIAN DELLA ROCCA	23	132	CNOR	Borgo a Mozzano	LU	44	10.55	Hydro Run-of-river and poundage
UP_PIETRAFIT_5	26WIMPI-S10PTRFC	PIETRAFITTA	365	220	CSUD	Piegaro	PG	43	12.2	Fossil Gas
UP_PIZZONE_1	26WIMPI-S14PZZNZ	PIZZONE	19	150	SUD	Pizzone	IS	41.65	14.06	Hydro Water Reservoir
UP_PNTVENTOUX_3	26WIMPIENTOUX-1I	PONT VENTOUX	150	132	NORD	Venaus	TO	45.14	7.04	Hydro Pumped Storage

UP Name	Code	Power Plant Name	Capacity [MW]	Voltage Level [kV]	Market Zone	Municipality	Prov. Code	Lat.	Long.	Type
UP_PONTE_1		PONTE MORASCO	92	220	NORD	Formazza	VB	46.38	8.42	Hydro Run-of-river and poundage
UP_PONTVENTOUX_1	26WIMPIENTOUX-1I	PONT VENTOUX	150	132	NORD	Venaus	TO	45.14	7.04	Hydro Pumped Storage
UP_PORTO_COR_3	26WIMPI-S08PCRTB	PORTO CORSINI	704	380	NORD	Ravenna	RA	44.48	12.26	Fossil Gas
UP_PORTO_COR_4	26WIMPI-S08PCRTB	PORTO CORSINI	704	380	NORD	Ravenna	RA	44.48	12.26	Fossil Gas
UP_PORTOFERR_1	26WIMPI-S09PRTF4	PORTOFERRAIO	16	22	CNOR	Portoferraio	LI	42.8	10.3	Fossil Oil
UP_PRACOMUNE_1	26WIMPI-S04PRCMY	PRACOMUNE	35	220	NORD	Ultimo/Ulten	BZ	46.55	10.9	Hydro Pumped Storage
UP_PREM-GROSIO_1	26WIMPIGROSIO-11	GROSIO	737	220	NORD	Grosio	SO	46.29	10.27	Hydro Run-of-river and poundage
UP_PRESENZAN_1	26WIMPI-S15PRSN8	PRESENZANO	1005	380	CSUD	Presenzano	CE	41.38	14.09	Hydro Pumped Storage
UP_PRIOLO_C_1	26WIMPI-S19PCRLE	PRIOLO C.LE	700	220	SICI	Priolo Gargallo	SR	37.14	15.22	Fossil Gas
UP_PRIOLO_C_2	26WIMPI-S19PCRLE	PRIOLO C.LE	700	220	SICI	Priolo Gargallo	SR	37.14	15.22	Fossil Gas
UP_PROVVIDEN_1	26WIMPI-S13PRVVW	PROVVIDENZA	139	220	CSUD	L'Aquila	AQ	42.51	13.41	Hydro Pumped Storage
UP_PRTMPDCLCL_3	26WIMPI-S19PERTR	PORTO EMPEDOCLE C.LE	140	150	SICI	Porto Empedocle	AG	37.29	13.52	Fossil Gas
UP_RATINO_1	26WIMPI-S16CSSCB	RATINO	419	380	SUD	San Severo	FG	41.63	15.42	Fossil Gas
UP_RETE_2_1	26WIMPI-S08AGCA5	RETE 2	75	132	NORD	Reggio nell'Emilia	RE	44.71	10.61	Fossil Gas
UP_RIZZICONI_1	26WIMPI-S18RCZZW	RIZZICONI	760	380	CALA	Rizziconi	RC	38.44	15.99	Fossil Gas
UP_RIZZICONI_2	26WIMPI-S18RCZZW	RIZZICONI	760	380	CALA	Rizziconi	RC	38.44	15.99	Fossil Gas
UP_RONCOVALG_1	26WIMPI-S03RNCVS	RONCOVALGRANDE	1000	380	NORD	Maccagno con Pino e Veddasca	VA	46.07	8.73	Hydro Pumped Storage
UP_ROSELECTRA_1	26WIMPI-S09RSLCK	ROSELECTRA	380	380	CNOR	Rosignano Marittimo	LI	43.38	10.45	Fossil Gas
UP_ROSONE_1	26WIMPI-S01RASNN	ROSONE	135	220	NORD	Locana	TO	45.44	7.42	Hydro Water Reservoir
UP_ROSSANO_T_1	26WIMPI-S18RTSN9	ROSSANO TE	224	380	CALA	Corigliano-Rossano	CS	39.62	16.61	Fossil Gas
UP_ROSSANO_T_3	26WIMPI-S18RTSN9	ROSSANO TE	224	380	CALA	Corigliano-Rossano	CS	39.62	16.61	Fossil Gas
UP_ROVESCA_1	26WIMPIOVESCA-1G	ROVESCA	44	132	NORD	Antrona Schieranco	VB	46.06	8.12	Hydro Run-of-river and poundage
UP_S._ANGELO_1	26WIMPI-S13ASCNS	S. ANGELO	44	150	CSUD	Altino	CH	42.11	14.35	Hydro Water Reservoir
UP_S.F._DEL_1	26WIMPI-S19SDMCS	SAN FILIPPO DEL MELA	866	220	SICI	San Filippo del Mela	ME	38.2	15.28	Fossil Oil
UP_S.F._DEL_2	26WIMPI-S19SDMCS	SAN FILIPPO DEL MELA	866	220	SICI	San Filippo del Mela	ME	38.2	15.28	Fossil Oil
UP_S.F._DEL_5	26WIMPI-S19SDMCS	SAN FILIPPO DEL MELA	866	220	SICI	San Filippo del Mela	ME	38.2	15.28	Fossil Oil
UP_S.F._DEL_6	26WIMPI-S19SDMCS	SAN FILIPPO DEL MELA	866	220	SICI	San Filippo del Mela	ME	38.2	15.28	Fossil Oil
UP_S.FIORANO_1	26WIMPI-S03SFRNQ	S.FIORANO	272	380	NORD	Sellero	BS	46.05	10.35	Hydro Pumped Storage
UP_S.PANCRAZ_1	26WIMPI-S04SPNCE	S.PANCRAZIO	34	220	NORD	San Pancrazio/St. Pankraz	BZ	46.56	11.06	Hydro Water Reservoir
UP_SANGIACOMO_1	26WIMPI-S03SGNCJ	SAN GIACOMO	10	20	NORD	Valdidentro	SO	46.51	10.32	Hydro Water Reservoir
UP_SBARBARA_3	26WIMPI-S09SBRBU	S.BARBARA	391	380	CNOR	Cavriglia	AR	43.56	11.48	Fossil Gas

UP Name	Code	Power Plant Name	Capacity [MW]	Voltage Level [kV]	Market Zone	Municipality	Prov. Code	Lat.	Long.	Type
UP_SCTNPWPFRR_2	26WIMPI-S08EFNP0	S.E.F. SRL	761	380	NORD	Ferrara	FE	44.86	11.59	Fossil Gas
UP_SCTNPWPFRR_3	26WIMPI-S08EFNP0	S.E.F. SRL	761	380	NORD	Ferrara	FE	44.86	11.59	Fossil Gas
UP_SERMIDE_3	26WIMPI-S03SRMDD	SERMIDE	1151	380	NORD	Sermide e Felonica	MN	45.03	11.25	Fossil Gas
UP_SERMIDE_4	26WIMPI-S03SRMDD	SERMIDE	1151	380	NORD	Sermide e Felonica	MN	45.03	11.25	Fossil Gas
UP_SFLORIANO_2	26WIMPI-S04SFLVM	S.FLORIANO	180	220	NORD	Egna/Neumarkt	BZ	46.29	11.25	Hydro Run-of-river and poundage
UP_SGIACOMO_3	26WIMPI-S13S2GCF	S.GIACOMO	490	380	CSUD	Fano Adriano	TE	42.56	13.56	Hydro Pumped Storage
UP_SGTTRNUOVO_2	26WIMPI-S13SMSZ1	SAGITTARIO NUOVO	20	60	CSUD	Anversa degli Abruzzi	AQ	42.01	13.82	Hydro Run-of-river and poundage
UP_SIMERI_1	26WIMPISIMERI-15	MAGISANO	75	150	CALA	Magisano	CZ	39.01	16.62	Hydro Run-of-river and poundage
UP_SLDGLRENZA_1	26WIMPI-S04GLRNJ	SELED GLORENZA	102	220	NORD	Malles Venosta/Mals	BZ	46.67	10.58	Hydro Water Reservoir
UP_SLDGLRENZA_2	26WIMPI-S04GLRNJ	SELED GLORENZA	102	220	NORD	Malles Venosta/Mals	BZ	46.67	10.58	Hydro Water Reservoir
UP_SMRICRICHI_1	26WIMPI-S18SCMR8	SIMERI CRICHI	885	380	CALA	Simeri Crichi	CZ	38.88	16.66	Fossil Gas
UP_SND_ALBAN_1	26WIMPI-S03ALBAI	ALBANO	15	132	NORD	Dongo	CO	46.13	9.28	Hydro Run-of-river and poundage
UP_SND_CAMPO_1	26WIMPI-S03SCNDX	CAMPO	38	132	NORD	Novate Mezzola	SO	46.21	9.46	Hydro Run-of-river and poundage
UP_SONDEL_TE_1	26WIMPI-S09STYPK	TEGLIA	32	132	CNOR	Pontremoli	MS	44.34	9.89	Hydro Run-of-river and poundage
UP_SORA_2	26WIMPI-S12SDSY8	SORA	42	150	CSUD	Sora	FR	41.7	13.57	Fossil Gas
UP_SOSPIROLO_1	26WIMPI-S05SSPRY	SOSPIROLO	40	132	NORD	Sospirolo	BL	46.16	12.08	Hydro Water Reservoir
UP_SOVERZENE_1	26WIMPI-S05SVRZ0	SOVERZENE	214	220	NORD	Soverzene	BL	46.2	12.3	Hydro Water Reservoir
UP_SOVERZENE_2	26WIMPI-S05SVRZ0	SOVERZENE	214	220	NORD	Soverzene	BL	46.2	12.3	Hydro Water Reservoir
UP_SPARANISE_1	26WIMPI-S15SCPRH	SPARANISE	760	380	CSUD	Sparanise	CE	41.18	14.11	Fossil Gas
UP_SPARANISE_2	26WIMPI-S15SCPRH	SPARANISE	760	380	CSUD	Sparanise	CE	41.18	14.11	Fossil Gas
UP_SPEZIA_CE_3	26WIMPI-S07SCPZX	SPEZIA CENTR	520	380	NORD	La Spezia	SP	44.11	9.87	Fossil Hard coal
UP_SRGNPGLCNT_1	26WIMPI-S16CDMNU	SORGENIA PUGLIA CENTRALE DI MODUGNO	810	380	SUD	Modugno	BA	41.1	16.76	Fossil Gas
UP_SSTSNGVNN2_1	26WIMPI-S03SSSN8	SESTO SAN GIOVANNI	111	220	NORD	Sesto San Giovanni	MI	45.54	9.25	Fossil Gas
UP_SSTSNGVNNI_1	26WIMPI-S03SSSN8	SESTO SAN GIOVANNI	111	220	NORD	Sesto San Giovanni	MI	45.54	9.25	Fossil Gas
UP_SULCIS_CE_3	26WIMPI-S20SCLC8	SULCIS CENTR	432	220	SARD	Portoscuso	SU	39.2	8.4	Fossil Hard coal
UP_SULCIS_CEN_2	26WIMPI-S20SCLC8	SULCIS CENTR	432	220	SARD	Portoscuso	SU	39.2	8.4	Fossil Hard coal
UP_TAGLIAMENTO_1	26WIMPIAMENTO-1T	SOMPLAGO	220	220	NORD	Cavazzo Carnico	UD	46.34	13.01	Hydro Run-of-river and poundage
UP_TALAMONA_2	26WIMPI-S03TLMNC	TALAMONA	18	132	NORD	Talamona	SO	46.18	9.64	Hydro Run-of-river and poundage
UP_TALORO1_1	26WIMPI-T20TLRAJ	TALORO1	240	220	SARD	Ovodda	NU	40.13	9.14	Hydro Pumped Storage
UP_TAVAZZANO_5	26WIMPI-S03TVZZK	TAVAZZANO	1411	380	NORD	Montanaso Lombardo	LO	45.33	9.44	Fossil Gas
UP_TAVAZZANO_C_6	26WIMPI-S03TVZZK	TAVAZZANO	1411	380	NORD	Montanaso Lombardo	LO	45.33	9.44	Fossil Gas

UP Name	Code	Power Plant Name	Capacity [MW]	Voltage Level [kV]	Market Zone	Municipality	Prov. Code	Lat.	Long.	Type
UP_TELESSIO_1	26WIMPI-S01TLSSX	TELESSIO	35	132	NORD	Locana	TO	45.41	7.49	Hydro Pumped Storage
UP_TERMINI_I_4	26WIMPI-S19TCRMT	TERMINI IMERESE C.LE	1221	380	SICI	Termini Imerese	PA	37.97	13.75	Fossil Gas
UP_TERMINI_I_42	26WIMPI-S19TCRMT	TERMINI IMERESE C.LE	1221	380	SICI	Termini Imerese	PA	37.97	13.75	Fossil Gas
UP_TERMINI_I_5	26WIMPI-S19TCRMT	TERMINI IMERESE C.LE	1221	380	SICI	Termini Imerese	PA	37.97	13.75	Fossil Gas
UP_TERMINI_I_6	26WIMPI-S19TCRMT	TERMINI IMERESE C.LE	1221	380	SICI	Termini Imerese	PA	37.97	13.75	Fossil Gas
UP_TERNI_1	26WIMPI-S10ETDS9	TERNI	95	132	CSUD	Terni	TR	42.55	12.63	Fossil Gas
UP_TEVERE_1	26WIMPITEVERE-1I	BASCHI	80	132	CSUD	Baschi	TR	42.66	12.24	Hydro Run-of-river and poundage
UP_TOR_DI_VA_2	26WIMPI-08737107	Tor di Valle MCI	18	150	CSUD	Roma	RM	41.81	12.42	<undefined>
UP_TORBOLE_1	26WIMPI-S04TRBLJ	TORBOLE	110	220	NORD	Nago-Torbole	TN	41.81	12.42	Hydro Run-of-river and poundage
UP_TORINONORD_1	26WIMPI-0066050X	TORINO NORD	395	220	NORD	Torino	TO	45.1	7.61	Fossil Gas
UP_TORREVALD_4	26WIMPI-S12TRRVU	TORREVALDALIGA		380	CSUD	Civitavecchia	RM	42.12	11.76	<undefined>
UP_TORREVALN_2	26WIMPI-S12TRRLD	TORREVAL.NORD	1845	380	CSUD	Civitavecchia	RM	42.13	11.76	Fossil Hard coal
UP_TORREVALN_3	26WIMPI-S12TRRLD	TORREVAL.NORD	1845	380	CSUD	Civitavecchia	RM	42.13	11.76	Fossil Hard coal
UP_TORREVALN_4	26WIMPI-S12TRRLD	TORREVAL.NORD	1845	380	CSUD	Civitavecchia	RM	42.13	11.76	Fossil Hard coal
UP_TORRITE_1	26WIMYI-S09TRRTB	TORRITE	67	132	CNOR	Castelnuovo di Garfagnana	LU	44.1	10.38	Hydro Water Reservoir
UP_TORVISCOSA_1	26WIMPI-S06TRVC2	TORVISCOSA	830	380	NORD	Torviscosa	UD	45.82	13.29	Fossil Gas
UP_TRAPANI_C_1	26WIMPI-S19TCRPN	TRAPANI C.LE	212	150	SICI	Trapani	TP	37.88	12.59	Fossil Gas
UP_TRAPANI_C_2	26WIMPI-S19TCRPN	TRAPANI C.LE	212	150	SICI	Trapani	TP	37.88	12.59	Fossil Gas
UP_TROINAGRTT_1	26WIMPINAGRTT-1O	TROINA	24	150	SICI	Troina	EN	37.76	14.61	Hydro Run-of-river and poundage
UP_TRRVLDLIGA_5	26WIMPI-S12TRRVU	TORREVALDALIGA	1180	380	CSUD	Civitavecchia	RM	42.12	11.76	Fossil Gas
UP_TRRVLDLIGA_6	26WIMPI-S12TRRVU	TORREVALDALIGA	1180	380	CSUD	Civitavecchia	RM	42.12	11.76	Other
UP_TURBIGO_4	26WIMPI-S03TRBGZ	TURBIGO	800	380	NORD	Milano	MI	45.52	8.74	Fossil Gas
UP_VADOTERM_5	26WIMPI-S07VTDR2	VADO TERM.	760	380	NORD	Quiliano	SV	44.28	8.43	Fossil Gas
UP_VAL_NOANA_1	26WIMPI-S04VNLNS	VAL NOANA	55	132	NORD	Imer	TN	46.11	11.77	Hydro Water Reservoir
UP_VALMALENCO_1	26WIMPIALENCO-1B	LANZADA	350	220	NORD	Lanzada	SO	46.3	9.93	Hydro Run-of-river and poundage
UP_VALPELLIN_1	26WIMPI-S02VLPL3	VALPELLINE	130	220	NORD	Valpelline	AO	45.83	7.33	Hydro Water Reservoir
UP_VENAUS_1	26WIMPI-S01VNSE6	VENAUS	230	380	NORD	Venaus	TO	45.16	7.01	Hydro Water Reservoir
UP_VILLA_1	26WIMPI-S01VALLS	VILLA	40	220	NORD	Ceresole Reale	TO	45.44	7.21	Hydro Water Reservoir
UP_VINADIO_1	26WIMPI-S01VNDI6	VINADIO	60	132	NORD	Vinadio	CN	44.3	7.2	Hydro Run-of-river and poundage
UP_VOGHERA_1	26WIMPI-S03VEGHN	VOGHERA	381	380	NORD	Voghera	PV	45.03	8.97	Fossil Gas

Table A.2: Italian power-oriented Combined Cycle Gas Turbine power plants.

Power Plant	Operator	UP Name	Config.	Prov. Code	Zone	Capacity [MW]	VLE NO_x [mg/Nm^3]	VLE CO [mg/Nm^3]	SCR (YES/NO)	CO Catalyzer (YES/NO)	Gas Turbine Model
Cassano d'Adda	A2A SPA	UP_CASSANO_2	2+1	MI	NORD	748	30	30	NO	NO	MS 9001 FA
									NO	NO	MS 9001 FA
Chivasso	A2A SPA	UP_CHIVASSO_1	2+1	TO	NORD	790	30	30	NO		MS9001FA mod.PG9351FA
									NO		MS9001FA mod.PG9351FA
	A2A SPA	UP_CHIVASSO_2	1+1			387	30	30	NO		MS9001FA mod.PG9351FA
Scandale	A2A SPA	UP_CNTRLDSCND_1	1+1	KR	CALA	410	30	30	NO	YES	GT26B2.2
	A2A SPA	UP_CNTRLDSCND_2	1+1			410	30	30	NO		GT26B2.3
Ponti Sul Mincio	A2A SPA	UP_CTE_DEL_M_2	1+1	MN	NORD	381	30	50	NO	NO	PG9351(FA)
Gissi	A2A SPA	UP_GISSI_1	1+1	CH		420	30	50	NO	YES	GT26B
	A2A SPA	UP_GISSI_2	1+1	CH		420	30	30	NO	YES	GT26B
Sermide	A2A SPA	UP_SERMIDE_3	1+1	MN	NORD	385	30	30	NO	NO	PG9351(FA)
	A2A SPA	UP_SERMIDE_4	2+1			775	30	30	NO	NO	PG9351(FA)
									NO	NO	PG9351(FA)
San Severo	ALPIQ ENERGIA ITALIA S.p.A.	UP_RATINO_1	1+1	FG	SUD	419	30	30	NO	YES	V94.3A.4
Rizziconi	AXPO ITALIA SPA	UP_RIZZICONI_1	1+1	RC	CALA	380	30	30	NO	YES	V94.3A2
	AXPO ITALIA SPA	UP_RIZZICONI_2	1+1			380	30	30	NO	NO	V94.3A2
Sparanise	AXPO ITALIA SPA	UP_SPARANISE_1	1+1	CE	CSUD	380	30	24	NO	YES	V94.3A2
	AXPO ITALIA SPA	UP_SPARANISE_2	1+1			380	30	24	NO	NO	V94.3A2
Tamarete	BKW ENERGIE AG	UP_CTTAMARETE_1	2+1	CH	CSUD	115	50	30	NO		
									NO		
Altomonte	EDISON SPA	UP_ALTOMONTE_1	2+1	CS	CALA	808	40	30	NO		9FB
									NO		9FB
Candela	EDISON SPA	UP_CANDELA_1	1+1	FG	SUD	401	50	30	NO		
Simeri Crichi	EDISON SPA	UP_SMRICRICHI_1	2+1	CZ	CALA	885	40	30	NO		9FB
									NO		9FB
La Casella	ENEL PRODUZIONE S.P.A.	UP_LA_CASELL_1	1+1	PC	NORD	375	30	30	NO		
	ENEL PRODUZIONE S.P.A.	UP_LA_CASELL_2	1+1			367			NO		
	ENEL PRODUZIONE S.P.A.	UP_LA_CASELL_3	1+1			365			NO		
	ENEL PRODUZIONE S.P.A.	UP_LA_CASELL_4	1+1			300			NO		
Pietrafitta	ENEL PRODUZIONE S.P.A.	UP_PIETRAFIT_5	1+2	PG	CSUD	365	50	30	NO		

Power Plant	Operator	UP Name	Config.	Prov. Code	Zone	Capacity [MW]	VLE NO_x [mg/Nm^3]	VLE CO [mg/Nm^3]	SCR (YES/NO)	CO Catalyzer (YES/NO)	Gas Turbine Model
Porto Corsini	ENEL PRODUZIONE S.P.A.	UP_PORTO_COR_3	1+1	RA	NORD	370	40	30	NO		
	ENEL PRODUZIONE S.P.A.	UP_PORTO_COR_4	1+1			370	40	30	NO		
Santa Barbara	ENEL PRODUZIONE S.P.A.	UP_SBARBARA_3	1+1	AR	CNORD	391	50	30	NO		V94.3A
Termini Imerese	ENEL PRODUZIONE S.P.A.	UP_TERMINI_I_6	2+1	PA	SICI	780	40	30	NO		
									NO		
Livorno Ferraris	EP PRODUZIONE SPA	UP_NCTLVRNFRR_1	2+1	VC	NORD	778	30	30	NO		SGT5-4000F
									NO		SGT5-4000F
Ostiglia	EP PRODUZIONE SPA	UP_OSTIGLIA_12	2+2	MN	NORD	750.5	30	30	NO		MS9001FA+e (PG9351FA)
									NO		MS9001FA+e (PG9351FA)
	EP PRODUZIONE SPA	UP_OSTIGLIA_3	1+1	MN	NORD	375.5	30	30	NO		MS9001FA+e (PG9351FA)
Tavazzano	EP PRODUZIONE SPA	UP_TAVAZZANO_5	2+1	LO	NORD	760			NO		MS9001FA+e (PG9351FA)
									NO		MS9001FA+e (PG9351FA)
	EP PRODUZIONE SPA	UP_TAVAZZANO_C_6	1+1	LO	NORD	385			NO		MS9001FA+e (PG9351FA)
Turbigo	IREN ENERGIA SPA	UP_TURBIGO_4	2+1	MI	NORD	800	30	30	NO	NO	SGT5-4000F
									NO	NO	SGT5-4000F
Teverola	REPOWER ITALIA SPA	UP_CNTRLDTVRL_1	1+1	CE	CSUD	404	40	30	NO		PG9351(FA)
Aprilia	SORGENIA S.P.A.	UP_CCGTPRILIA_1	2+1	LT	CSUD	787	30	30	NO	NO	V94.3A
									NO	YES	V94.3A
Turano Lodigiano	SORGENIA S.P.A.	UP_CNTRLDTRNL_1	2+1	LO	NORD	800	30	30	NO	YES	V94.3A
									NO	YES	V94.3A
Termoli	SORGENIA S.P.A.	UP_NRGAMOLISE_1	2+1	CB	SUD	769	30	30	NO	NO	
									NO	NO	
Modugno	SORGENIA S.P.A.	UP_SRGNPGLCNT_1	2+1	BA	SUD	810	30	30	NO	YES	GT26
									NO	YES	GT26
Napoli Levante	TIRRENO POWER S.P.A.	UP_NAPOLIL_4	1+1	NA	CSUD	400	40	30	NO	NO	V94.3A2
Torre Valdiglia Sud	TIRRENO POWER S.P.A.	UP_TRRVLDLIGA_5	2+1	RO	CSUD	790	40	50	NO	NO	9FA
									NO	NO	9FA
		UP_TRRVLDLIGA_6	1+1			390	40	50	NO	NO	9FA
Vado Ligure	TIRRENO POWER S.P.A.	UP_VADOTERM_5	2+1	SV	NORD	760	40	50	NO	NO	V94.3 A2
									NO	NO	V94.3 A2